CONTRIBUTION OF TDAG51 IN ATHEROSCLEROSIS

CONTRIBUTION OF T CELL DEATH ASSOCIATED GENE 51 (TDAG51) TO THE DEVELOPMENT AND PROGRESSION OF ATHEROSCLEROSIS: CAUSAL ASSOCIATION AND POTENTIAL MECHANISMS

By

G.M. SHOWKAT HOSSAIN, M.Sc.

A Thesis

Submitted to the School of Graduate Studies

in Partial Fulfilment of the Requirements

for the Degree of

Doctor of Philosophy

McMaster University

DOCTOR OF PHILOSOPHY (2009) McMaster University

(Medical Sciences) Hamilton, Ontario

TITLE: Contribution of T Cell Death Associated Gene 51 (TDAG51) to the Development and Progression of Atherosclerosis: Causal Association and Potential Mechanisms

AUTHOR: G.M. Showkat Hossain, M.Sc. (McMaster University, Hamilton, Canada)

SUPERVISOR: Richard C. Austin, PhD.

NUMBER OF PAGES: XXVI, 314

ABSTRACT

Atherosclerosis is a multi-factorial disease and is the major cause of death in the western world. Numerous risk factors, including hyperlipidemia, obesity, diabetes, smoking, hypertension, and family history increase the risk of atherosclerosis and death from cardiovascular disease (CVD). Clinical and epidemiological studies have now shown that hyperhomocysteinemia (HHcy) is an independent risk factor for CVD. Further, we and others have demonstrated that HHcy accelerates atherosclerosis in apolipoprotein E-deficient ($apoE^{-/-}$) mice. Although several studies have reported that homocysteine-induced endoplasmic reticulum (ER) stress causes growth arrest and programmed cell death (PCD) in cultured vascular endothelial cells, the cellular factors responsible for this effect and their relevance to atherosclerosis have not been completely elucidated.

Previously, we have demonstrated that homocysteine induces the expression of T-cell death associated gene 51 (TDAG51), a member of the pleckstrin homology-related domain family, in cultured human vascular endothelial cells. Transient overexpression of TDAG51 elicited significant changes in cell morphology, decreased cell adhesion and promoted detachment-mediated PCD. In support of these *in vitro* findings, TDAG51 expression was increased and correlated with PCD in the atherosclerotic lesions from $apoE^{-/-}$ mice fed hyperhomocysteinemic diets, compared to mice fed control diet. To investigate the *in vivo* significance of TDAG51 on atherosclerotic lesion development and progression, knockout mice deficient in both TDAG51 and apoE genes were generated. Our findings show that $TDAG51^{-/-}/apoE^{-/-}$ double knockout (DKO) mice fed

control chow diet have significantly reduced atherosclerotic lesion size, compared to age- and sex-matched apoE$^{-/-}$ control mice. Atheroprotective function of TDAG51 deficiency may be explained in part by the observation that there is a significant upregulation of peroxisome proliferator-activated receptor γ (PPAR-γ) in TDAG51-deficient (TDAG51$^{-/-}$) cells including mouse embryonic fibroblasts (MEFs), compared to control wildtype MEFs. Given that PPAR-γ has both atheroprotective and anti-inflammatory properties, TDAG51 may represent a unique negative regulator of PPAR-γ and its downstream gene targets. Taken together, my findings demonstrate that TDAG51 is a novel cellular mediator involved in the development and progression of atherosclerosis.

In addition to its anti-atherogenic properties, I have demonstrated that TDAG51$^{-/-}$ MEFs have increased migratory properties following monolayer disruption or in response to chemotaxis on fibronectin-coated Boyden chambers, compared to wildtype control MEFs. Although TDAG51-induced cell migration could potentially affect atherosclerotic lesion development, our recent observations suggest that TDAG51 may also have a role in wound healing. Our studies have shown that dorsal skin wounds within TDAG51$^{-/-}$ mice healed slowly, compared to those in control mice through a mechanism involving impaired myofibroblast differentiation. Since the underlying mechanisms of wound healing and fibrosis are similar, it is conceivable that TDAG51 may have role in fibrosis.

In summary, this thesis provides novel evidence that TDAG51 is involved in the pathogenesis of atherosclerosis and wound healing. Furthermore, TDAG51 may represent a novel therapeutic target for attenuating atherosclerotic lesion development, thereby reducing the risk of cardiovascular disease and its complications.

DEDICATION

This thesis is dedicated with love and respect to my parents, AKM Rafiqul Islam and Mossammat Umme Hani Chowdhurani, whose unconditional supports have been an inspiration to me and have allowed me to become the person I am today.

ACKNOWLEDGEMENTS

During my academic career, I am indebted to number of individuals for their supports. First of all, I wish to thank my MSc and PhD supervisor, Dr. Richard C. Austin, for allowing me to work on such an excellent project. I would also like to express my sincere gratitude to Dr. Austin for his guidance and encouragement throughout the time I spent at his laboratory. Regardless of his busy schedule, he always made the time to discuss the progress on the project. Especially, I appreciate him very much for critical review of my thesis and his help for the preparation leading to thesis defense. Truly, it has been a great learning process for me. I am grateful for all the help I received from Dr. Austin. He has been a great mentor and it was a pleasure working for him.

I also wish to acknowledge my supervisory committee members, Dr. Janusz Rak and Dr. Damu Tang, for their suggestion and direction on this project. I would like to thank our collaborator Dr. Christopher McCulloch of University of Toronto for his advice to take the project into next level, especially associating TDAG51 with wound healing and fibrosis. I would also like to express my deepest respect to Dr. Jeff Dickhout, Dr. Ji Zhou and Dr. Geoff Werstuck for sharing thoughtful insights, help and advice related to my project. Herein, I would also like to take the opportunity to express my sincere appreciation for the supports I received from my mentors, Dr. Jeff Weitz of McMaster University, Dr. Sherman Garver of University of Arizona and Dr. Dale Bramlet of Advent Medical Reseach Inc.

I would also like to give special thanks to Dr. Sudesh Sood for her help over the time I was at Dr. Austin's laboratory. My acknowledgement also goes to all our collaborators, including Dr. J Rho of University of Pennsylvania, Dr. Ken Maclean of University of Colorado, Dr. Barnado Trigatti and Dr. John Capone of McMaster University, for their help and advice on this project. Further, I wish to thank to all other members of Dr. Austin's laboratory and the Henderson Research Centre, including Dr. Sarka Lothak, Dr. Hiam al-Bayati, Linda May and Lisa Tenbrinke. It was a great experience to have the opportunity to work with such a wonderful group of people.

I also wish to acknowledge my appreciation to Heart and Stroke Foundation of Canada for Doctoral Research Award, Canadian Institute of Health Research, McMaster University and Henderson Research Centre.

Finally, I am greatly indebted to family members for all the supports I received over the years. My parents have always been supportive and inspired me to perform the best. Without their encouragement and love I would not be where I am today. My appreciation also goes to my siblings, Suzan, Shuvo and Real, for their understanding and supports in my academic carrier. During the time in Hamilton, my causin Ponu apa and her family members were very supportive and I would like to thank them for all the love and care.

TABLE OF CONTENTS

CHAPTER 1: Introduction.....1-66

1.2 General overview.....1

1.2 Overview of atherosclerosis.....7

1.2.1 Stages of atherosclerosis: development and progression.....8

1.2.2 Mechanisms of atherosclerosis.....9

1.2.2.1 Response to endothelial cell injury hypothesis.....9

1.2.2.2 Defects in lipoprotein transport and metabolism.....13

1.2.2.3 Inflammatory response in atherosclerosis.....16

1.2.3 Animal models of atherosclerosis.....19

1.2.4 Risk factors and current management for atherosclerosis.....23

1.3 Overview on T Cell Death Associated Gene 51.....24

1.3.1 Structural analysis of the TDAG51 gene.....26

1.3.2 Function of TDAG51.....29

1.3.3 Elucidation of TDAG51 function by gene knockout in C57 mice.....31

1.3.4 Involvement of TDAG51 in atherosclerosis.....32

1.4 Overview of hyperhomocysteinemia and vascular disease.....33

1.4.1 Historical perspective on hyperhomocysteinemia.....35

1.4.2 Overview on homocysteine.....36

1.4.3 Studies on mouse models of hyperhomocysteinemia.....40

1.4.4 Potential mechanisms linking hyperhomocysteinemia to atherosclerosis.....44

1.4.4.1 Oxidative stress.....44

1.4.4.2 Inflammation.....45

1.4.4.3 The molecular targeting hypothesis.....46

1.4.4.4 Endoplasmic reticulum stress and the unfolded protein response.....47

1.5 Significance of apoptosis and ER stress in the development and progression of atherosclerosis.....49

1.5.1 Mechanism of endoplasmic reticulum stress.....50

1.5.2 Mechanism of apoptosis.....55

1.5.3 Apoptotic cell death in the development and progression of atherosclerosis.....59

1.6 Project hypothesis, rationale and experimental objectives.....61

CHAPTER 2: TDAG51 is an ER stress response pro-apoptotic gene and a mediator of atherosclerosis.....67-150

2.1 Introduction.....67

2.2 Materials and Methods.....69

2.2.1 Materials.....69

2.2.2 Methods.....72

2.2.2.1 PCR amplification of open reading frame (ORF) and functional domains in TDAG51.....72

2.2.2.2 DNA extraction and purification from agarose gels.....73

2.2.2.3 Subcloning of TDAG51 ORF and functional domains into pCR® Blunt vector.....76

2.2.2.4 Construction of mammalian expression plasmids encoding pEGFP and TDAG51 inserts.....78

2.2.2.5 Isolation of endotoxin-free plasmid DNA.....78

2.2.2.6 Generation of radiolabeled probes.....79

2.2.2.7 Northern blot analysis.....80

2.2.2.8 Immunoblot analysis.....82

2.2.2.9 Indirect immunofluorescence in cultured cell and tissue sections.....83

2.2.2.10 DAPI staining of nuclear DNA.....85

2.2.2.11 Transient transfection of cultured cells.....85

2.2.2.12 TdT-mediated dUTP Nick End Labeling (TUNEL) assay in cultured cells and tissue sections.....86

2.2.2.13 DNA fragmentation assay.....87

2.2.2.14 Flow cytometry analysis.....88

2.2.2.15 Generation of mouse embryonic fibroblasts (MEFs).....88

2.2.2.16 Cytotoxicity assay in cultured MEFs.....89

2.2.2.17 Mice and dietary conditions.....90

2.2.2.18 Statistical Analysis.....90

2.3 Results.....92

2.3.1 Characterization of TDAG51 as an ER stress-inducible gene.....92

2.3.2 Cellular Distribution of TDAG51.....104

2.3.3 Induction of detachment-mediated PCD following TDAG51 overexpression.....109

2.3.4 Characterization of TDAG51 functional domain(s) in detachment-induced PCD.....116

2.3.5 Protection from ER stress-induced cell death following functional deficiency of TDAG51.....124

2.3.6 Correlation between TDAG51 expression and PCD in atherosclerotic lesions from apoE$^{-/-}$ mice having diet-induced HHcy.....124

2.3.7 Overexpression of TDAG51 increases the expression of tissue factor....139

2.4 Discussion.....142

CHAPTER 3: Contribution of TDAG51 to atherosclerotic lesion development – studies using TDAG51/apoE double knockout mice.....151-220

3.1 Introduction.....151

3.2 Materials and Methods.....159

3.2.1 Materials.....159

3.2.2 Methods.....159

3.2.2.1 Mice and dietary conditions.....159

3.2.2.2 Isolation of DNA for mouse genotyping.....160

3.2.2.3 Mouse genotyping using polymerage chain reaction.....160

3.2.2.4 Approach to generate mouse model deficient in both apoE and TDAG51 genes.....161

3.2.2.5 Immunoblot analysis.....161

3.2.2.6 Tissue sample preparation.....164

3.2.2.7 Hematoxylin/Eosin staining.....164

3.2.2.8 Immunohistochemical analysis.....165

3.2.2.9 *En face* oil red O staining of mice aorta.....165

3.2.2.10 Measurement of total cholesterol, triglyceride and glucose in mice plasma.....166

3.2.2.11 Measurements of lipids in tissue samples.....166

3.2.2.12 Measurement of mice plasma lipid profiles using FPLC.....167

3.2.2.13 Statistical Analysis.....167

3.3 Results.....168

3.3.1 Generation of TDAG51/apoE double knockout mice.....168

3.3.2 Effect of TDAG51 deficiency on atherosclerotic lesion development in apoE$^{-/-}$ mice.....168

3.3.3 Effect on total plasma lipid and glucose levels in TDAG51/apoE double knockout mice.....192

3.3.4 Status of lipids in the liver of TDAG51/apoE double knockout mice....192

3.3.5 Status of PPAR-γ expression in TDAG51$^{-/-}$ MEFs.....201

3.4 Discussion.....213

CHAPTER 4: Role of TDAG51 in cell migration and its potential relevance to wound healing and atherosclerosis.....221-266

4.1 Introduction.....221

4.2 Materials and Methods.....225

4.2.1 Immunoblot analysis.....225

4.2.2 Indirect immunofluorescence: Cell culture.....225

4.2.3 Laser scanning confocal microscopy: Cell culture.....226

4.2.4 Calcium phosphate transfection and retroviral infection into MEFs.....226

4.2.5 Cell migration assays.....227

4.2.5.1 Wounding experiments.....227

4.2.5.2 Boyden chambers.....228

4.2.6 Cell proliferation assays.....229

4.2.6.1 Thymidine incorpation.....229

4.2.6.2 Quantitative assessment using a phosphorimager.....229

4.2.7 Flow cytometry analysis.....230

4.2.8 Statistical analysis.....231

4.3 Results.....233

4.3.1 Characterization of TDAG51 protein expression in MEFs.....233

4.3.2 Effect of TDAG51 deficiency on migration and proliferation of MEFs.....233

4.3.3 Effect of TDAG51 deficiency on the phenotype of migratory MEFs....245

4.3.4 Assessing the status of β_1 integrin in the MEFs.....250

4.3.5 Examing the expression of genes that are involved in cell migration and atherosclerosis from the loss of TDAG51.....250

4.3.6 Effect of fibroblast migration on wound healing ability in TDAG51$^{-/-}$ mice.....255

4.4 Discussion.....261

CHAPTER 5: Concluding discussion and future directions.....267-277

5.1 Concluding remarks.....267

5.2 Future directions.....271

CHAPTER 6: References.....278-314

6.0 References.....278

LIST OF FIGURES

Figure 1: Initiation and progression of atherosclerosis.....10

Figure 2: Sequence analysis of T Cell Death-Associated Gene 51 ORF.....27

Figure 3: Schematic representation of homocysteine metabolism.....38

Figure 4: Atherosclerotic plaques in apoE-deficient mice fed hyperhomocysteinemic diets.....42

Figure 5: Unfolded protein response pathways in response to ER stress in eukaryotes.....51

Figure 6: Working Model linking ER Stress, TDAG51, and Atherothrombosis.....65

Figure 7: Functional domains within the TDAG51 open reading frame (ORF).....74

Figure 8: Northern blot analysis of the steady-state levels of TDAG51 and GRP78 mRNA in HUVEC.....93

Figure 9: Induction in the steady-state mRNA levels of TDAG51 is selective for homocysteine and DTT.....95

Figure 10: Induction of TDAG51 and GRP78 protein expression in response to homocysteine treatments.....97

Figure 11: Requirement of eIF2α for TDAG51 expression in response to ER stress...100

Figure 12: ER stress is induced by Sin-1 in human aortic endothelial cells.....102

Figure 13: Co-localization of TDAG51 with intracellular vesicles.....105

Figure 14: Effect of homocysteine on the cellular distribution of TDAG51.....107

Figure 15: Induction of PCD by homocysteine in HUVEC.....110

Figure 16: Expression of GFP or GFP-TDAG51 fusion protein in HUVEC.....112

Figure 17: Promotion of detachment-mediated PCD from overexpression of TDAG51.....114

Figure 18: Induction of caspase 3 from overexpression of GFP-TDAG51 fusion protein in HUVEC or HAEC.....117

Figure 19: Cell detachment prior to activation of caspases from the overexpression of TDAG51.....119

Figure 20: Restriction digestion of plasmids encoding functional domains of TDAG51 ORF.....122

Figure 21: Characterization of Mouse Embryonic Fibroblasts (MEFs) from C57, $TDAG51^{+/-}$ and $TDAG51^{-/-}$ mice.....125

Figure 22: Resistance from ER stress-induced cell death in TDAG51-deficient MEFs.....127

Figure 23: Deficiency of TDAG51 does not alter unfolded protein response (UPR) activation.....129

Figure 24: Effect of TDAG51 overexpression on eIF2α phosphorylation.....131

Figure 25: TDAG51 expression in the aortic root of $apoE^{-/-}$ mice fed normal chow or hyperhomocysteinemic diets.....135

Figure 26: TDAG51 expression and PCD in atherosclerotic lesions from $apoE^{-/-}$ mice fed normal chow or hyperhomocysteinemic diets.....137

Figure 27: Effect of TDAG51 overexpression on TF expression.....140

Figure 28: Expression of TDAG51 in early and advanced atherosclerotic lesions in apoE$^{-/-}$ mice.....153

Figure 29: TDAG51 expression and DAPI staining in atherosclerotic lesions from a human carotid artery.....155

Figure 30: Schematic diagram showing generation of mice deficient in both TDAG51 and apoE genes.....162

Figure 31: Genotyping of TDAG51 and apoE genes in DKO mice.....169

Figure 32: Measurement of body weight in TDAG51/apoE-deficient and apoE$^{-/-}$ control mice.....171

Figure 33: Atherosclerotic lesion size in the aortic root of mice fed normal chow diet for 40 weeks.....174

Figure 34: Atherosclerotic lesion size in the aortic root of mice fed normal chow diet for 25 weeks.....176

Figure 35: Atherosclerotic lesion size in the aortic root of mice fed normal chow diet for 15 weeks.....178

Figure 36: Unopened aorta demonstrating decreased atherosclerotic lesion size in TDAG51/apoE-deficient mice compared to apoE$^{-/-}$ control mice.....180

Figure 37: *En face* analysis demonstrating decreased atherosclerotic lesion size in TDAG51/apoE-deficient mice compared to apoE$^{-/-}$ control mice.....182

Figure 38: Mean necrotic lipid core size is decreased in TDAG51/apoE-deficient mice compared to apoE$^{-/-}$ control mice.....185

Figure 39: Effect of TDAG51 deficiency on apoptotic cell death in advanced atherosclerotic lesions.....187

Figure 40: Identification of atherosclerotic lesion components in apoE$^{-/-}$ and TDAG51/apoE double knock out mice.....190

Figure 41: Total plasma cholesterol and triglyceride levels in TDAG51/apoE-deficient and apoE$^{-/-}$ control mice.....193

Figure 42: Status of lipoprotein distribution in TDAG51/apoE-deficient and apoE$^{-/-}$ control mice.....195

Figure 43: Total plasma glucose levels in TDAG51/apoE-deficient and apoE$^{-/-}$ control mice.....197

Figure 44: Status of hepatic steatosis in TDAG51/apoE-deficient and apoE$^{-/-}$ control mice.....199

Figure 45: Status of hepatic cholesterol and triglyceride levels in TDAG51/apoE-deficient and apoE$^{-/-}$ control mice.....202

Figure 46: Expression of PPAR-γ in wildtype C57/BL6 and TDAG51$^{-/-}$ MEFs.....205

Figure 47: Schematic diagram of the various roles played by the macrophage (Mϕ) within the early and late atherosclerotic lesions.....207

Figure 48: Effect of TDAG51 deficiency on the expression of peroxiredoxin 1 in early and advanced atherosclerotic lesions.....209

Figure 49: Effect of TDAG51 deficiency on the expression of PPAR-γ in early and advanced atherosclerotic lesions.....211

Figure 50: Re-introduction of TDAG51 protein into TDAG51$^{-/-}$ MEFs.....234

Figure 51: Time-dependent migration of TDAG51$^{-/-}$ MEFs following wounding.....236

Figure 52: Loss of TDAG51 gene increases rate of migration in MEFs.....239

Figure 53: Loss of TDAG51 gene promotes MEF proliferation.....241

Figure 54: Loss of TDAG51 gene increases rate of MEF proliferation.....243

Figure 55: Morphological differences in MEFs with or without TDAG51.....246

Figure 56: Co-localization of vinculin and F-actin in migratory MEFs.....248

Figure 57: TDAG51$^{-/-}$ MEFs express increased cell surface active β_1-integrin.....251

Figure 58: β_1-integrin antibody (9EG7) inhibits the proliferation of TDAG51$^{-/-}$ MEFs.....253

Figure 59: Loss of TDAG51 delays skin wound healing in mice.....256

Figure 60: Quantitative measurement of wound area in mice with or without TDAG51.....258

LIST OF TABLES

Table 1: Total plasma homocysteine levels and atherosclerotic lesion size in apoE-deficient mice fed normal chow or hyperhomocysteinemic diets.....134

Table 2: Analysis of necrotic lipid core in the aortic lesion of mice fed normal chow diet for 25 weeks.....189

Table 3: Upregulation of genes in TDAG51$^{-/-}$ MEFs compared to C57 control MEFs.....204

Table 4: Tandem mass spectrometry analysis of MEFs.....260

LIST OF ABBREVIATIONS

AARS	aminoacyl-tRNA synthetase
ABCA1	adenosine triphosphate-binding cassette transporter-1
AICD	activation-induced cell death
ApoE	apolipoprotein E
$ApoE^{-/-}$	apolipoprotein E-deficient
APS	ammonium persulfate
ASK1	apoptosis-signal-regulating kinase
ATF-6	activating transcription factor
BHMT	betaine-homocysteine methyltransferase
BSA	bovine serum albumin fraction V
CAD	caspase-activated DNase
Caspases	cysteine-dependent aspartate-specific proteases
CBS	cystathionine-β-synthase
CMV	cytomegalovirus
CPM	counts per minute
CVD	cardiovascular disease
DAPI	4', 6-diamidino-2-phenylinole
DEPC	diethyl pyrocarbonate
DKO	$TDAG51^{-/-}/apoE^{-/-}$ double knockout

DNA	Deoxyribonucleic acid
DTT	dithiothreitol
ECGF	endothelial cell growth factor
ECRF	endothelium-derived relaxing factor
ECM	extracellular matrix
EDCF	endothelium-derived contracting factor
EDTA	ethylenediaminetetraacetic acid disodium salt
eIF2α	eukaryotic initiation factor 2α
eNOS	endothelial NO synthase
ER	endoplasmic reticulum
ERSE	ER stress response element
EtBr	ethidium bromide
ETP	etoposide
FAC	focal adhesion complex
FAK	focal adhesion kinase
FBS	fetal bovine serum
FGF	fibroblast growth factor
FPLC	fast protein liquid chromatography
GAPDH	glyceraldehyde-3-phosphate dehydrogenase
GFP	green fluorescence protein
HAECs	human aortic endothelial cells
HDL	high-density lipoprotein

HRP	horseradish peroxidase
HSF1	heat shock transcription factor 1
Hsps	heat shock proteins
HUVECs	human umbilical vein endothelial cells
IDL	intermediate density lipoprotein
IFN-γR	interferon-γ receptor
IGF-I	insulin like growth factor I
ILK	integrin-dependent kinase
IRE 1	inositol-requiring enzyme 1
JNK/SAPK	c-Jun NH_2-terminal kinase/stress-activated protein kinase
LCAT	lecithin cholesterol acyltransferase
LDH	lactate dehydrogenase
LDL	low-density lipoprotein
LDLR	LDL receptor
Lp(a)	abnormal LDL known as lipoprotein(a)
MAPK	mitogen-activated protein
MCP-1	monocyte chemoattractant protein-1
MEFs	mouse embryonic fibroblasts
Met	methionine
MMP-9	matrix metalloproteinase-9
MOBIX	Institute for Molecular Biology
MOPS	3-(N-morpholinol)propanesulphonic acid

MS	methionine synthase
MTHFR	methyltetrahydrofolate reductase
NAFLD	non-alcholic fatty liver disease
NES	nuclear export signal
NLS	nuclear localization signal
NO	nitric oxide
O_2^-	superoxide anion
$OONO^-$	peroxynitrite
ORF	open reading frame
PAK2	p21 activated kinase 2
PARP	poly (ADP)-ribose polymerase
PBA	4-phenyl butyric acid
PCD	programmed cell death
PCR	polymerase chain reaction
PERK	pancreatic ER kinase (PKR) like ER kinase
PH	proline-histidine
PI3K	phosphoinositide-3 kinase
PKC	protein kinase C
PMA	phorbol myristate acetate
PPAR-α	peroxisome proliferator-activated receptor α
PPAR-β	peroxisome proliferator-activated receptor β
PPAR-γ	peroxisome proliferator-activated receptor γ

PQ	proline-glutamine
Prdx 1	peroxiredoxin 1
PS	phosphatidylserine
QQ	polyglutamine
Rb	retinoblastoma
RNA	Ribonucleic acid
ROS	reactive oxygen species
SDS	sodium dodecyl sulphate
SMA	smooth muscle actin
SMCs	smooth muscle cells
SR-B1	scavenger receptor B1
SREBP	sterol regulatory element-binding proteins
TDAG51	T cell death-associated gene 51
$TDAG51^{-/-}$	TDAG51-deficient
TdT	terminal deoxynucleotidyl transferase
TEMED	N,N,N',N'-tetramethylenediamine
TF	tissue factor
TGF-β	transforming growth factor β
Thap	thapsigargin
TIMP	tissue inhibitor of metalloproteinase
TM	tunicamycin
TNF-α	tumor necrosis factor-α

TNFR1	TNF receptor-1
Tris	tris(hydroxymethyl)aminomethane
Triton X-100	t-octylphenoxypolyethoxyethanol
Trypsin/EDTA	trypsin/ethylenediaminetetra-acetic acid
TUNEL	TdT-mediated dUTP Nick End Labeling
TWEEN-20	poloxyethylenesorbitan monolaurate
TZDs	thiazolidinediones
UA	uric acid
UPR	unfolded protein response
UPRE	unfolded protein response elements
VLDL	very low-density lipoprotein
XPB-1	X box-binding protein 1

CHAPTER 1: Introduction

1.1 General overview

Atherosclerosis is a progressive, inflammatory disease resulting from the interaction between modified lipoproteins, monocyte-derived macrophages, T cells and cellular elements of the arterial wall (Ross 1999; Lusis 2000; Glass and Witztum 2001). Early atherosclerotic lesions, termed fatty streaks, consist of lipid filled macrophages within the intima (Stary *et al.*, 1994). Pathological studies suggest that fatty streaks are the precursor to large or advanced lesions and that advanced lesions are observed where fatty streaks are most common (Davies and Woolf 1993). Studies on aortas and coronary arteries from adults show all stages of lesion formation, indicating that lesions develop throughout adult life (Stary 1989). Indications are that it takes 10-15 years for an advanced lesion to form. As lesions become larger and more complex, they tend to narrow the channel of the artery and may impede blood flow, contributing to blockage of the arteries. Atherosclerotic lesion rupture can result in formation of thrombi or blood clots, the underlying cause of myocardial infarction and stroke.

In addition to hyperlipidemia, obesity, smoking, hypertension and diabetes, numerous clinical studies have demonstrated that hyperhomocysteinemia (HHcy) is a risk factor for cardiovascular disease (CVD). Although earlier studies implicated HHcy as an independent risk factor for CVD (Boushey *et al.*, 1995; Refsum *et al.*, 1998; Eikelboom *et al.*, 1999; Malinow *et al.*, 1999; Ross 1999), several recent studies with homocysteine

lowering supplements, including folic acid and B vitamins, did not reduce the risk factor of established CVD (Lonn *et al.*, 2006; Ray *et al.*, 2007; Bonaa *et al.*, 2006). Nonetheless, high plasma levels of homocysteine are still considered an independent risk factor for CVD (Bostom *et al.*, 2006; Yang *et al.*, 2007). *In vivo* studies have also established a direct causal relationship between the induction of HHcy and the acceleration of atherosclerosis in apolipoprotein E-deficient ($apoE^{-/-}$) mice fed hyperhomocysteinemic diets (Hofmann *et al.*, 2001; Zhou *et al.*, 2001). Hyperhomocysteinemic $apoE^{-/-}$ mice showed increased expression of inflammatory markers in atherosclerotic lesions and enhanced atherosclerotic lesion area and complexity (Hofmann *et al.*, 2001). Furthermore, dietary enrichment in B vitamin co-factors essential for intracellular homocysteine metabolism attenuates atherosclerotic lesion development in HHcy (McCully 1996; Loscalzo 1996; Welch and Loscalzo 1998). Although diet-induced HHcy accelerates early plaque development and enhances plaque fibrosis in $apoE^{-/-}$ mice, no difference in plaque size between control and hyperhomocysteinemic mice was observed after long-term treatment (Zhou *et al.*, 2001). These findings imply that HHcy mediates the early stages of atherogenesis in $apoE^{-/-}$ mice. Interestingly, Zhou *et al.* (2008) have recently demonstrated that diet-induced HHcy does not contribute to atherosclerosis in C57BL/6 mice even in presence of increased plasma LDL (low density lipoprotein) from western diet. However, HHcy together with atherogenic diet can significantly accelerate atherosclerotic lesion development. The findings suggest that HHcy is not an independent risk factor in

C57BL/6 mice and additional risk factors such as elevated VLDL (very low density lipoprotein) or inflammatory cytokines are necessary for increased atherosclerosis.

Several hypotheses have been proposed to explain the mechanism by which homocysteine promotes atherogenesis. Because the thiol group of homocysteine readily undergoes auto-oxidation in plasma to generate reactive oxygen species (ROS), it has been suggested that homocysteine induces cell injury/dysfunction through a mechanism involving oxidative stress (Starkebaum and Harlan 1986; Loscalzo 1996). This hypothesis, however, fails to explain why cysteine, which is present in plasma at much higher concentrations than homocysteine and is also readily auto-oxidized, does not cause cell injury and is not considered a risk factor for CVD (Jacobsen 2000 & 2001).

We as well as others have reported that homocysteine disrupts protein folding in the endoplasmic reticulum (ER), thereby leading to activation of the unfolded protein response (UPR) and increased expression of several ER stress response genes, including GRP78, GRP94, GADD153, Herp and RTP (Outinen *et al.*, 1998 & 1999; Kokame *et al.*, 1996 & 2000). These findings suggest that homocysteine acts intracellularly to elicit cell dysfunction by adversely affecting ER homeostasis. This mechanism may result from reductive stress or disruption of disulfides linkage similar to DTT treatment but has been demonstrated not to be due to ER Ca^{2+} depletion (Dickhout *et al.*, 2007). Homocysteine-induced ER stress is believed to promote specific cellular responses, including lipid biosynthesis, programmed cell death (PCD), and inflammation. Studies have demonstrated that homocysteine-induced ER stress increases lipid biosynthesis by activating the sterol regulatory element-binding proteins (SREBP) (Werstuck *et al.*, 2001;

Colgan *et al.*, 2007; Kammoun *et al.*, 2009). It has also been shown that homocysteine induces PCD in cultured human vascular endothelial cells and that this effect involves activation of the UPR (Zhang *et al.*, 2001). Furthermore, the activation of caspase-3 or a caspase-like protease(s) was reported to be essential for this process, a result consistent with the ability of homocysteine thiolactone, a cyclic thioester of homocysteine synthesized by specific aminoacyl-tRNA synthetases (Jakubowski 1997), to induce PCD in HL-60 cells (Huang *et al.*, 2001). Although these studies provide *in vitro* evidence that homocysteine and its derivatives can promote PCD, the pro-apoptotic factors involved in this process as well as their *in vivo* relevance to atherogenesis have not been identified.

Our research group has previously used mRNA differential display to demonstrate that homocysteine alters gene expression in cultured human vascular endothelial cells (HUVECs) (Outinen *et al.*, 1998 & 1999). However, a number of these differentially expressed genes were not fully characterized. The purpose of my research project was to identify and characterize these homocysteine-responsive genes and to determine their role in atherogenesis. Among a number of differentially expressed cDNA fragments, a 114-bp fragment was up regulated in HUVECs exposed to homocysteine. Northern blot hybridization using this fragment as a probe identified a homocysteine-inducible transcript of ~ 7 kb in HUVECs (Hossain *et al.*, 2003). Sequence analysis in GenBank™ revealed an open reading frame (ORF) encoding T cell death associated gene 51 (TDAG51), a member of the pleckstrin homology-related domain family having pro-apoptotic characteristics (Park *et al.*, 1996; Frank *et al.*, 1999). Our studies have demonstrated that TDAG51 is induced by ER stress agents, including homocysteine,

tunicamycin, thapsigargin, dithiothreitol and peroxynitrite (Hossain *et al.*, 2003; Dickhout *et al.*, 2005). TDAG51 expression was attenuated in homozygous A/A mutant eukaryotic initiation factor 2α (eIF2α) mouse embryonic fibroblasts (MEFs) treated with homocysteine or tunicamycin, suggesting that phosphorylation of eIF2α is required for TDAG51 transcriptional activation. Further, we have shown that transient overexpression of TDAG51 elicited significant changes in cell morphology, decreased cell adhesion and promoted detachment-induced PCD (Hossain *et al.*, 2003). In support of these *in vitro* findings, TDAG51 expression was increased and correlated with PCD in the atherosclerotic lesions from apoE$^{-/-}$ mice fed hyperhomocysteinemic diets, compared to mice fed normal chow diet (Hossain *et al.*, 2003).

The overall objective of this project was to investigate the potential cellular function of TDAG51 and to determine its role in atherogenesis. We have examined whether loss of TDAG51 attenuates the development and progression of atherosclerosis in apoE$^{-/-}$ mice. Based on these findings, I have made several important observations. **First**, the ER stress-inducible TDAG51 protein is expressed in atherosclerotic lesion-resident macrophages and endothelial cells, as well as being associated with apoptotic cells within the lipid-rich necrotic core from apoE$^{-/-}$ mice fed normal chow or hyperhomocysteinemic diets. **Second**, loss of TDAG51 in apoE$^{-/-}$ mice attenuates atherogenesis compared to age- and sex-matched apoE$^{-/-}$ mice fed normal chow diet. These findings confirm our original hypothesis that TDAG51 is a mediator of atherosclerosis.

Interestingly, in addition to its atheroprotective effect, our recent findings have demonstrated that TDAG51 may have a role in wound healing. TDAG51$^{-/-}$ mice have decreased skin wound healing ability, compared with age- and sex-matched C57 control mice. Also, loss of TDAG51 promotes the migration and proliferation of MEFs. In earlier studies, we have reported that overexpression of TDAG51 promotes detachment-induced PCD and that TDAG51 co-localizes with focal adhesion kinase (FAK), a component of focal adhesion complex (FAC) (Hossain *et al.*, 2003). It is therefore conceivable that deficiency of TDAG51 may affect cell adhesion and FAC organization. In support of this, our investigations suggest that deficiency of TDAG51 disrupts the formation of mature FACs, thereby resulting in increased migration and proliferation of MEFs. In addition, since we have demonstrated that TDAG51 negatively regulates proliferator-activated receptor γ (PPAR-γ) expression, this may offer an explanation for TDAG51 effects on wound healing. Transforming growth factor-β_1 (TGF-β_1) signalling, a very important component of wound healing, is influenced by PPAR-γ expression or activation (Burgess *et al.*, 2005; Yokote *et al.*, 2006). Earlier studies have demonstrated that increased PPAR-γ expression interferes with TGF-β_1 signalling and thus can inhibit the differentiation of fibroblasts to myofibroblasts (Burgess *et al.*, 2005). Myofibroblasts are believed to be responsible for the contraction of wound and the lack of myofibroblasts can potentially delay the closure of wound (Hinz *et al.*, 2007). The underlying mechanism by which increased migration of fibroblasts contributes to decreased wound healing in TDAG51$^{-/-}$ mice remains to be explained. However, it is conceivable that

hyperproliferation of fibroblasts and their lack of differentiation may create the significant increased wound size we have observed in TDAG51$^{-/-}$ mice.

Furthermore, the atheroprotective effect from the loss of TDAG51 can also be explained by our observation that there is a significant increase in PPAR-γ expression and its downstream targets in cultured TDAG51$^{-/-}$ MEFs, compared to control wildtype MEFs. Previous studies have demonstrated that PPAR-γ can accelerate reverse cholesterol transport in lesion-resident macrophages (Chawla *et al.*, 2001; Chinetti *et al.*, 2001) and has both anti-inflammatory and atheroprotective properties (Lehrke and Lazar 2005). It is therefore possible that TDAG51 negatively regulates PPAR-γ expression, thus mediating foam cell formation and atherogenesis.

Collectively, my research findings provide unique evidence that TDAG51 is a novel mediator of atherosclerosis and plays a critical role in accelerating atherosclerotic lesion development by modulating PPAR-γ expression. Further, we have identified TDAG51 as a novel gene involved during skin wound healing process.

1.2 Overview of atherosclerosis

Atherosclerosis is a major cause of morbidity and mortality in the western world. The word "atherosclerosis" is derived from Greek word "athero," meaning porridge, and "sclerosis," meaning hardening. Mechanisms contributing to atherosclerosis are multiple and complex. A number of theories, including endothelial dysfunction, dyslipidemia, hypercoagulability and inflammation, have been implicated to explain the mechanisms for the development and progression of atherosclerosis (Ross 1999; Lusis 2000; Glass

and Witztum 2001; Hansson *et al.*, 2006). Major risk factors for the development of atherosclerosis include hyperlipidemia, hyperhomocysteinemia, smoking, hypertension, obesity and diabetes.

1.2.1 Stages of atherosclerosis: development and progression

The morphological term for early atherosclerotic lesions is "fatty streaks" which are mainly composed of monocyte-derived macrophages and T lymphocytes engorged with low-density lipoprotein (LDL)-derived cholesterol. Although LDL uptake is regulated, oxidized forms of LDL (oxLDL) are not. Endothelium dysfunction leads to the release of ROS species that can oxidize LDL (Yla-Herttuala *et al.*, 1989; Rosenfeld *et al.*, 1990; Steinbrecher *et al.*, 1990; Steinberg 1991). Scavenger receptors on macrophages can then recognize and engulf oxLDL resulting in the formation of foam cells (Navab *et al.*, 1996).

Manifestations of the initial response to endothelial injury generally include the appearance of specific adhesive glycoproteins, such as P- and E-selectins, on the surface of endothelial cells and recruitment of inflammatory cells, especially monocytes and T cells (Gerrity *et al.*, 1985; Davies 1986; Munro and Cotran 1988). Inflammatory cells are believed to migrate into the subendothelial space under the influence of growth regulatory molecules and chemoattractants released by injured endothelium. Although initial recruitment of monocytes and their subsequent differentiation into macrophages may initially serve as a protective measure to remove cytotoxic oxLDL particles or apoptotic cells from the subendothelial space (Faggiotto *et al.*, 1984; Masuda and Ross

1990; Rosenfeld *et al.*, 1987), the progressive accumulation of macrophages and their uptake of oxLDL ultimately lead to the development of atherosclerotic lesions.

The transition of fatty streaks to advanced lesions is normally characterized by the migration of smooth muscle cells toward the subendothelial space **(Figure 1)**. Cholesterol-laden macrophages and smooth muscle cells, morphologically recognized as foam cells, are observed at most stages of lesion development and are key cellular components of the atherosclerotic lesion. Overproduction of ECM proteins by proliferating smooth muscle cells results in the development of fibrous plaques. It is suggested that this phase of lesion development is influenced by interactions between monocytes/macrophages and T cells, which result in cellular and humoral responses from the chronic inflammation state (Steinberg and Witztum 1999). Interestingly, inflammatory cells are believed to release proteases that may degrade ECM and result in the formation of unstable plaques and the increase risk of development of a thrombus. In support of this, a recent study has demonstrated that overexpression of tissue inhibitor of metalloproteinase (TIMP)-2 inhibits atherosclerotic plaque development and destabilization, possibly through modulating macrophage migration and apoptosis (Johnson *et al.*, 2006).

1.2.2 Mechanisms of atherosclerosis

1.2.2.1 Response to endothelial cell injury hypothesis

Endothelial injury is an early feature of atherogenesis. Under normal conditions, the endothelium functions as a permeable, nonthrombogenic and nonleukocyte-adherent

Figure 1: Initiation and progression of atherosclerosis

Injury to the endothelium can lead to cell dysfunction. This can result in the exposure of endothelium, leading to the recruitment of monocytes. Differentiation of monocytes into macrophages and their subsequent uptake of lipids allow the formation of foam cells. Activated macrophages also release inflammatory molecules that can further propagate the lesion progression. Smooth muscle cells (SMC) migration and proliferation also take place during that period. The continuation of this process ultimately leads to the generation of advanced or complicated lesions having a distinct fibrous cap, lipid core and necrotic core.

(Obtained and modified from Ross (1993) Nature 362: 802)

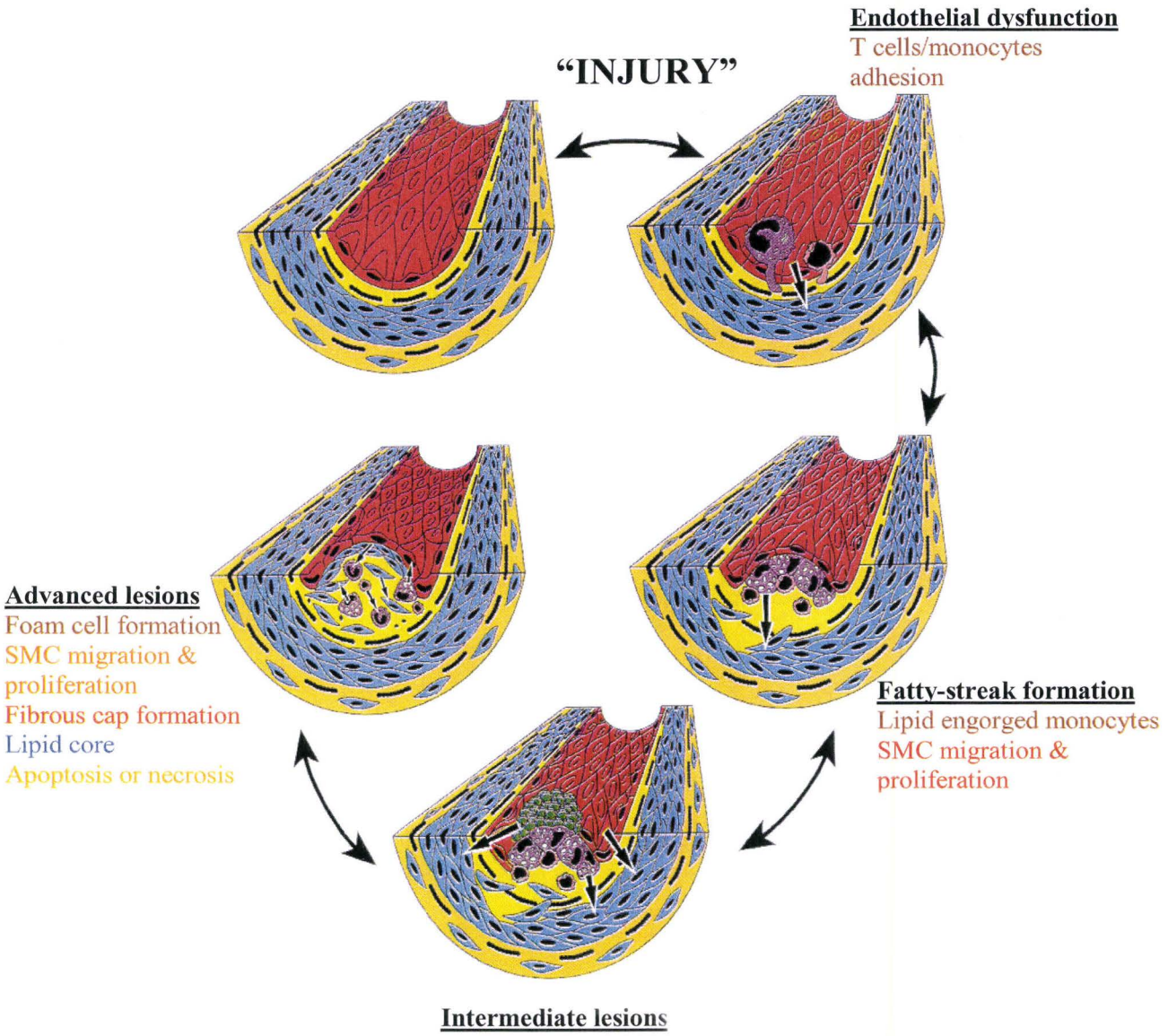
"INJURY"
Endothelial dysfunction
T cells/monocytes
adhesion
Fatty-streak formation
Lipid engorged monocytes
SMC migration &
proliferation
Intermediate lesions
Advanced lesions
Foam cell formation
SMC migration &
proliferation
Fibrous cap formation
Lipid core
Apoptosis or necrosis

barrier (Ross 1993). Atherosclerotic lesion prone areas, such as those in arterial bifurcations, are subject to continuous hemodynamic forces (Wissler and Vesselinovitch 1983; Glagov *et al.*, 1988; Stary *et al.*, 1992). Alterations in hemodynamic forces can damage arterial endothelium. It is believed that endothelial injury is repaired through maintaining the balance between vasodilation and vasoconstriction (Ross 1993). However, alterations of normal endothelium function by major cardiovascular risk factors, such as hyperlipidemia, hyperhomocysteinemia, smoking, hypertension, and diabetes, can cause endothelial dysfunction, leading to the formation of atherosclerotic lesions (Ross 1999).

The mechanism by which cardiovascular risk factors contribute to endothelial dysfunction is complex and heterogeneous (Davignon and Ganz 2004). In vascular endothelial cells, endothelium-dependent responses are mediated by the release of several diffusible substances, namely endothelium-derived relaxing factor (EDRF) and endothelium-derived contracting factor (EDCF). To maintain vascular tone, nitric oxide (NO) is synthesized by the endothelial NO synthase (eNOS) and is released from vascular endothelial cells in a calcium dependent manner (Busse *et al.*, 1993). Reduced NO bioavailability is a common feature in atherosclerosis (Sorescu *et al.*, 2002). It is believed that increased production of ROS, such as superoxide anions ($\cdot O_2^-$), within atherosclerotic lesions promotes the formation of peroxynitrite through a reaction between available NO and $\cdot O_2^-$ (Reiter *et al.*, 2000). In support of this, supplementation with L-arginine, a substrate for eNOS, attenuated atherosclerotic lesion development in $LDLR^{-/-}$ mice, an established animal model for hypercholesterolemia (Aji *et al.*, 1997).

Furthermore, inhibition of eNOS with L-NA (L-nitroarginine) abrogated the beneficial effects of L-arginine. In addition, accelerated atherosclerosis was observed in mice deficient in both eNOS and apoE, suggesting that endothelial NO may have anti-atherosclerotic properties (Kuhlencordt *et al.*, 2001).

To further explain this mechanism, several earlier studies have implicated the presence of oxygen radicals and the importance of oxidative stress in the pathogenesis of atherosclerosis (Azumi *et al.*, 1999; Kalinina *et al.*, 2002; Sorescu *et al.*, 2002). We have demonstrated an association between atherogenesis and peroxynitrite-induced ER stress, a cellular stress pathway induced by the accumulation of unfolded proteins in the ER (Dickhout *et al.*, 2005). Importantly, human atherosclerotic lesions have elevated levels of 3-nitrotyrosine (3-NT), a marker for *in vivo* peroxynitrite generation (Sucu *et al.*, 2003). Additional studies are however required to further understand the mechanism by which endothelial dysfunction contributes to the development and progression of atherosclerosis. It is conceivable that endothelial damage regulates the balance between vasoconstriction and vasodilation, thereby initiating a series of events that can promote or attenuate atherogenesis. However, earlier studies demonstrated that endothelial injury to rabbits, having low levels of plasma cholesterol, produced fibrotic lesions instead of atherosclerotic lesions similar to those in humans (Vanhoutte 1997; Helft *et al.*, 2001). These findings further support the concept that atherosclerosis involves more than just endothelial injury.

1.2.2.2 Defects in lipoprotein transport and metabolism

Lipid deposition in the arterial wall appears to be the major cause for atherosclerotic lesion development. Primarily, oxidation of LDL promotes the deposition of lipid within the subendothelial cell space. Lipid can also accumulate within the arterial wall as a result of defects in lipoprotein transport and metabolism, thus causing injury to the endothelium. The resulting endothelial dysfunction has been implicated in the formation of advanced or unstable atherosclerotic lesions.

Lipids, such as cholesterol and triglycerides, are transported in plasma by lipoprotein particles containing specific apolipoproteins (Brown and Goldstein 1986). Triglyceride-rich lipoproteins include chylomicrons and very low-density lipoprotein (VLDL), while cholesterol rich lipoproteins include low-density lipoprotein (LDL) and high-density lipoprotein (HDL). Studies suggest that one of the four following defects in lipoprotein metabolism can lead to coronary heart disease: (i) increased LDL, (ii) decreased HDL (normally with increased in VLDL), (iii) increased intermediate density lipoprotein (IDL) and chylomicron remnants, and (iv) high levels of abnormal LDL known as lipoprotein(a) [Lp(a)] (Breslow 1993).

ApoE, a constituent of chylomicrons, VLDL, and HDL, acts as a ligand in the receptor-mediated clearance of these particles (Mahley 1988). ApoE has a high affinity for the LDL receptor (LDLR) and normally dissociates from IDL. Studies show that genetic defects in apoE can cause the accumulation of IDL, leading to hypercholesterolemia (Mahley 1988). This has been associated with increased atherosclerosis in coronary and peripheral arteries. Plasma LDL is cleared from the circulation via the LDLR. Defects in the LDLR can result in the accumulation of plasma

LDL (Brown and Goldstein 1986; Stary *et al.*, 1992). Patients with familial hypercholesterolemia have dysfunctional LDLR (Goldstein and Brown 1977), thereby resulting in elevation of plasma LDL and subsequent deposition within the atherosclerotic lesion prone areas of arterial intima.

In contrast to LDL, HDL functions to remove cholesterol from peripheral tissues and atheromas of the artery wall and transfer them back to the liver through a mechanism involving reverse cholesterol transport (Anderson *et al.*, 1987; Bierman 1992). Cholesterol uptake is mediated through interaction between adenosine triphosphate-binding cassette transporter-1 (ABCA1) and apoA-1 (Klucken *et al.*, 2000). Maturation of HDL particles is modulated under the influence of enzymes, primarily lecithin cholesterol acyltransferase (LCAT) (Rye *et al.*, 1999). HDL cholesterol transfer into tissue is mediated by a specific receptor, namely scavenger receptor B1 (SR-B1) (Trigatti *et al.*, 2000). It is therefore conceivable that a low level of plasma HDL or a deficiency of either apoA or ABCA1 or LCAT may impair the removal of cholesterol from the arterial wall. Although clinical studies have linked low levels of HDL with coronary artery disease, experiments on transgenic animals have not conclusively demonstrated an association between efficient reverse cholesterol transport and plasma level HDL. For instance, SR-B1 deficient mice show increased plasma HDL but have severe atherosclerosis (Trigatti *et al.*, 2004). In contrast, overexpression of SR-B1 results in decreased plasma HDL levels due to increased uptake of HDL by the liver. This in turn appears to be protective from atherosclerosis as a result of improvement in reverse

cholesterol transport. Studies are now investigating the significance of the mutations in ABCA1 or SR-B1 in the development of atherosclerosis.

In summary, defects in cholesterol transport can cause the accumulation of lipids in the arterial wall and are considered as causative factors in the development of atherosclerosis. In addition, this concept has been supported by the findings that cholesterol lowering drug, such as statins, can reduce the morbidity and mortality from atherosclerosis in humans (Assmann *et al.*, 1999). The underlying mechanism behind the progression of this disease remains unclear and the cholesterol lowering drugs do not always reduce the risk of CVD in all the patients with atherosclerosis.

1.2.2.3 Inflammatory response in atherosclerosis

Inflammation plays a pivotal role in all stages of atherosclerosis, including initiation, progression, and the formation of the advanced lesion (Libby 2002; Stoll and Bendszus 2006). It is believed that the initial response to endothelial injury is the recruitment of phagocytic mononuclear cells in an attempt to remove noxious substances and repair damaged tissue. However, subsequent uptake of oxLDL by macrophages and smooth muscle cells leads to the formation of lipid engorged foam cells, which release a host of cytokines that influences the development of the atherosclerotic plaque.

Early human atherosclerotic lesions, termed "fatty streaks", are composed of monocyte-derived macrophages and T-lymphocytes (Munro *et al.*, 1987; Stary *et al.*, 1994). Although the initial inflammatory response is to repair EC injury, however, activation of macrophages promotes inflammation through release of cytokines and

growth factors. Inflammatory molecules, including interleukins, interferons, tumor necrosis factor-alpha (TNF)-α, growth factors and colony-stimulating factors have been found in all stages of human atherosclerotic lesions (Rajavashisth *et al.*, 1990; Nilsson 1993). The atherosclerotic lesions gradually increase in size through recruitment of inflammatory cells from the blood, leading to their subsequent differentiation. Studies have shown that endothelial-derived adhesive glycoproteins contribute to the adherence of mononuclear cells at the atherosclerotic lesion prone regions of the artery (Chappell *et al.*, 1998; Iiyama *et al.*, 1999). In support of this, apoE$^{-/-}$ mice lacking cell adhesion molecules such as E selectin, P selectin or ICAM-1, which are known to play a role in monocyte recruitment, do not develop significant atherosclerotic lesions (Dong *et al.*, 1998; Collins *et al.*, 2000). Further, disruption in the production of monocyte chemotactic protein 1 (MCP-1), which plays a major role in the recruitment of macrophages and is stimulated by hypercholesterolemia (Han *et al.*, 1999), significantly reduces atherosclerosis in apoE$^{-/-}$ mice (Smith *et al.*, 1995), LDL receptor-deficient (LDLR$^{-/-}$) mice (Gu *et al.*, 1998) or apoB overexpressing mice (Gosling *et al.*, 1999).

During progression from fatty streak to intermediate and advanced atherosclerotic lesions, secreted inflammatory molecules also promote the migration and proliferation of medial smooth muscle cells (SMC) (Lusis 2000; Libby *et al.*, 2002). In response to inflammatory stimulus, medial SMC express enzymes that can degrade elastin and collagen within the arterial ECM. This in turn allows the penetration of SMC through the internal elastic laminae, and subsequently, promotes the migration of cells into the subintimal spaces. Further, release of inflammatory molecules maintains the repetition of

the cycle, leading to intimal thickening and development of intermediate atherosclerotic lesions. Herein, activated inflammatory cells release inflammatory mediators, cytokines and interleukins. This also allows the adherence and infiltration of leukocytes into the atherosclerotic lesions (Ridker *et al.*, 1998). At this stage, the lesion is defined as being advanced having characteristic lipid and necrotic core covered by a fibrous cap. In support of the involvement of inflammatory pathways in atherosclerosis, $LDLR^{-/-}$ mice were treated with antibody against CD40L to interrupt the signaling of immunomodulatory molecule CD40 (Mach *et al.*, 1998). Studies have demonstrated a reduction in aortic atherosclerotic lesion size and its lipid content in hypercholesterolemic mice. To further establish the importance of CD40-CD154 interaction in atherosclerosis, $apoE^{-/-}$ mice that are deficient in CD154, a ligand for CD40, has been generated and the lesion development assessed (Lutgens *et al.*, 1999). Although there was no effect at the early lesion development, advanced plaques in these mice were collagen-rich and stable containing reduced lipid and macrophage content. CD154 is expressed by endothelial and smooth muscle cells, macrophages, and T cells within human atherosclerotic lesions. A similar finding was reported in $apoE^{-/-}$ mice lacking interferon-γ receptor (IFN-γR) (Gupta *et al.*, 1999).

Inflammation also plays a significant role during plaque destabilization or rupture. It is believed that plaque rupture occurs at the site of sustained inflammation, macrophage infiltration/accumulation and apoptosis (Davies 1990). Activated T-cells stimulate the production of proteolytic enzymes, including metalloproteinases and collagenases, from macrophages, resulting in degradation of the fibrous cap (Schonbeck *et al.*, 1997).

Activated T-cells can further produce interferon-γ that may inhibit collagen synthesis by SMC and may thus affect fibrous cap formation (Libby 2001). Collectively, inflammation is a key event not only during development and progression of atherosclerosis but also during plaque rupture.

1.2.3 Animal models of atherosclerosis

As early as 1908, Ignatowski reported evidence of intimal thickening and the development of large clear cells in the aorta of rabbits fed an animal protein diet. Although rabbits do not develop spontaneous atherosclerosis, they are highly responsive to dietary manipulation of cholesterol and develop atherosclerosis in a short period of time (Drobnik *et al.*, 2000). Further, atherosclerotic lesions in pigs, monkeys and apes have cellular composition similar to those in human. In addition, rats and dogs do not appear to develop spontaneous atherosclerotic lesions without extensive dietary modifications. Herein, it is important to mention that early insights regarding the mechanism of atherosclerosis came from research on larger animals. The pig models showed that infiltration of monocytes was one of the early events in atherogenesis (Gerrity 1981). The cellular events during initiation and development of atherosclerosis were further defined in monkey and rabbit models (Faggiotto *et al.*, 1984; Rosenfeld *et al.*, 1987).

To overcome the limitations in larger animals and to better understand the mechanism and etiology of atherosclerosis, the development of mouse models of atherosclerosis was initiated. Mice are primarily used since their genome is relatively

easy to manipulate to assess the *in vivo* importance of different gene products. Genetic predisposition to atherosclerosis however varies depending upon strain of mice (Shih *et al.*, 1995). The majority of mouse strains do not develop atherosclerosis since they present normal lipoprotein patterns. The only exception is the C57BL/6 strain of mice. Thompson (1969) first reported the development of atherosclerosis in C57BL/6 mice fed 50% fat-containing diet for 5 weeks compared to regular diets containing 5% fat. Since this diet causes high mortality, Paigen *et al.* (1985) modified the diet with 15% fat, 1.25% cholesterol and 0.5% cholic acid. Paigen diet not only reduces high mortality rate in C57BL/6 mice but also induces noticeable early atherosclerotic lesions, mainly fatty streaks, within 10 weeks (Paigen *et al.*, 1985 & 1994). However, atherosclerotic lesions in this mouse model are small and mainly visible within the aortic root.

In gene-targeted mouse models, genes involved in lipoprotein transport were either deleted by homologous recombination in embryonic stem cells or cloned into the mice germ line by transgenic techniques. These transgenic mouse models have allowed researchers to assess the significance of these genes in the development and progression of atherosclerosis as well in other human lipoprotein disorders. Targeted disruption of apoE or LDLR genes or overexpression of human apoB in mice has been shown to increase plasma VLDL and/or LDL cholesterol levels. The major transgenic mouse models for atherosclerosis include apoE$^{-/-}$, LDLR$^{-/-}$, SR-B1$^{-/-}$, and apoB overexpression (Plump *et al.*, 1992; Ishibashi *et al.*, 1993; Linton *et al.*, 1993; Trigatti *et al.*, 1999).

In 1992, mice deficient in apoE were first reported (Plump *et al.*, 1992). Mice had 4 to 5 times higher plasma cholesterol levels and shown to develop spontaneous

atherosclerosis when fed normal chow diet (4.5% fat-containing diet). The cellular composition (endothelial cells, macrophages, T cells, and smooth muscle cells) involved in atherosclerosis was found to be similar to human atherosclerotic lesions (Nakashima *et al.*, 1994; Reddick *et al.*, 1994). The lesion progression can also be defined over time from fatty streak formation to complicated lesions with fibrous cap. Contrary to the diet-induced C57BL/6 mouse model, apoE$^{-/-}$ mice presented with atherosclerotic disease throughout the aorta. Further, the progression of lesion development can be accelerated when apoE$^{-/-}$ mice are fed a western diet (high fat diet) instead of a normal chow diet (Nakashima *et al.*, 1994). However, the lipoprotein profiles in apoE$^{-/-}$ mice are not similar to those in human atherosclerotic patients. In human, LDL is the major plasma cholesterol-carrying molecule, but in apoE$^{-/-}$ mice, VLDL is the carrier.

LDLR plays a major role in the clearance of plasma LDL cholesterol. Deficiency of LDLR in humans contributes to hypercholesterolemia and accelerated atherosclerosis (Goldstein and Brown 1974). Patients with homozygous deficiency for LDLR present with myocardial infarctions during the second decade of life (Brown and Goldstein 1990). Interestingly, LDLR$^{-/-}$ mice have only a 2-fold increase in plasma cholesterol levels and do not develop atherosclerosis when fed a diet containing 10% fat (Ishibashi *et al.*, 1993). In contrast, accelerated atherosclerosis (aorta, aortic root and coronary arteries) is observed when these mice are fed a western diet (Masucci-Magoulas *et al.*, 1997). Morphological analysis suggests that the lesions consist of lipid-laden macrophages (Roselaar *et al.*, 1996). Advanced lesions are only observed when these

mice are fed high fat diets over long periods of time. Importantly, lipoprotein profiles are similar to those in human atherosclerotic patients.

ApoB is a structural constituent of several lipoprotein particles, including LDL, VLDL, and chylomicrons, and is a ligand for receptor-mediated removal of LDL particles from the circulation (Kane *et al.*, 1989). Increased apoB is an important risk factor for coronary artery disease (Young 1990). It is therefore expected that increased presence of apoB will result in atherosclerosis in mice. Transgenic mice overexpressing apoB do not develop atherosclerotic lesions (Linton *et al.*, 1993), however, these mice showed accelerated atherosclerosis when fed high cholesterol diets (Purcell-Huynh *et al.*, 1995). Morphological analysis has revealed that the atherosclerotic lesions in these mice consist of macrophage foam cells.

Although the above mentioned mouse models of atherosclerosis have limitations, $apoE^{-/-}$ and $LDLR^{-/-}$ mouse models are now regarded as essential tools for atherosclerosis research. It is important to mention that the progression of atherosclerosis is usually more marked in mouse models deficient in both apoE and LDLR, compared to $apoE^{-/-}$ or $LDLR^{-/-}$ (Ishibashi *et al.*, 1994; Witting *et al.*, 1999). Pathological findings from these animal studies suggest that increased hyperlipidemia can result in extensive atherosclerotic disease throughout the aorta. It has therefore been suggested that genetic and dietary manupulations are effective methods to study the promotion of atherosclerosis. Mouse models now provide a view of the development of atherosclerosis from early (fatty streaks) to more complex lesions (acellular lipid cores, necrotic cores, fibrous caps, and calcification).

1.2.4 Risk factors and current management for atherosclerosis

Over the last two decades, our understanding of risk factors for atherosclerosis has been changed significantly due to numerous clinical and epidemiological studies. The major risk factors for atherosclerosis include age, smoking, family history, high cholesterol, low HDL, diabetes, high blood pressure, and hyperhomocysteinemia (Frohlich *et al.*, 2001). Interestingly, a large worldwide case control study by Yusuf *et al.* (2004), representing 15152 cases and 14820 controls from 52 countries, has reported nine major risk factors (abnormal lipids, smoking, hypertension, diabetes, abnormal obesity, psychosocial factors, consumption of fruits, vegetables, and alcohol, and regular physical activity) for acute myocardial infarction. Importantly, this study has suggested that similar principles can be applied worldwide for the prevention of cardiovascular disease.

Based on the guidelines from the American Heart Association and the National Heart, Lung, and Blood Institute's National Cholesterol Education Program, patients can be placed into 3 risk categories, including low, intermediate and high. The management of the disease is based on the category in which the patients are placed. Low-risk patients are encouraged to maintain healthy lifestyle. Plasma lipid levels of intermediate patients are monitored over the time to assess the appropriateness of the therapy. However, most high-risk patients are normally placed on cholesterol lowering drugs.

Since atherosclerosis is heterogeneous, there is no standard pharmacological intervention available at present. Clinical studies however have suggested that blocking the progression of atherosclerosis can be achieved by lowering plasma lipid

concentrations, especially cholesterol. Lipid lowering drugs such as statins have been shown to decrease the level of atherogenic lipoproteins, clinical complications, and mortality from CVD (Assmann *et al.*, 1999). Interestingly, studies also demonstrate that statin therapy increases the lifespan of patients with CVD (Foody *et al.*, 2006; Mehta *et al.*, 2006). Increasing good cholesterol or plasma HDL levels can further reduce patients from atherosclerotic complications. In addition, lifestyle modifications have now been emphasized greatly in the management of atherosclerosis (Yusuf *et al.*, 2004). Consumption of dietary fish, vitamin C and E are correlated with a decrease in coronary artery disease (Ballard-Barbash and Callaway 1987; Frei *et al.*, 1988). However, prospective clinical trials with vitamins, such as vitamin E, showed no positive effect in patients with established atherosclerosis (Yusuf *et al.*, 2000; Lonn *et al.*, 2006).

1.3 Overview on T Cell Death Associated Gene 51

T cell hybridomas are widely used to study signalling processes during activation-induced apoptosis of T cells (Ashwell *et al.*, 1987; Ucker *et al.*, 1989; Shi *et al.*, 1992). Previous studies have implicated several genes in the regulation of anti-T cell receptor (TCR)-induced apoptosis. Primarily, anti-TCR-induced apoptosis of T cell hybridomas is mediated by the interaction of Fas-Fas ligand (Fas L) (Brunner *et al.*, 1995; Dhein *et al.*, 1995; Ju *et al.*, 1995; Nagata and Goldstein 1995; Yang *et al.*, 1995). In addition, inhibition of *c-myc* expression has been shown to block the anti-TCR-induced apoptosis of T cell hybridomas (Shi *et al.*, 1992; Green *et al.*, 1994). Studies have also demonstrated that *nur77* is essential for the induction of anti-TCR-induced apoptosis in T

cell hybridomas (Liu *et al.*, 1994; Woronicz *et al.*, 1994; Yazdanbakhsh *et al.*, 1995). However, these studies have not explained the underlying mechanisms as to how these gene products interact to regulate T cell apoptosis. Park *et al.* (1996) generated T cell hybridoma mutants resistant to anti-TCR-induced apoptosis using somatic cell genetics. Complementation studies, including screening cDNA library and transfection, facilitated the identification of TDAG51 as a novel gene associated with the anti-TCR-induced apoptosis of T cell hybridomas. Subsequent studies have also shown that functional TDAG51 is required for Fas-mediated apoptosis in T cells (Park *et al.*, 1996). In contrast to this original observation, several studies have suggested that TDAG51 promotes Fas-independent apoptosis in numerous cell lines, including neuronal, melanoma, and vascular endothelial cells (Gomes *et al.*, 1999; Neef *et al.*, 2002; Hossain *et al.*, 2003). Further, the association of TDAG51 in cell growth has been suggested by the observation that the expression of TDAG51 is decreased in metastatic tumors (Neef *et al.*, 2002; Nagai *et al.*, 2007). Interestingly, TDAG51 may have a role in cell survival (Toyoshima *et al.*, 2004). It has been demonstrated that TDAG51 mediates the anti-apoptotic effects of insulin like growth factor I (IGF-I) in NIH3T3 cells via p38 mitogen-activated protein kinase (MAPK) pathway. In addition, overexpression of TDAG51 inhibits protein biosynthesis *in vitro* and *in vivo* (Hinz *et al.*, 2001). Using the yeast two hybrid method, Hinz and colleagues showed the involvement of TDAG51 in the regulation of translation by the observation that human TDAG51 protein interacts with three proteins, namely the p66 subunit of translation initiation factor3 (eIF3-p66), the ribosomal protein L14, and the inducible poly(A)-binding protein (iPABP).

1.3.1 Structural analysis of the TDAG51 gene

Using immunohistochemical and confocal analysis using confocal microscope, previous studies have demonstrated that TDAG51 may be localized in the cytosol (Park *et al.*, 1996; Gomes *et al.*, 1999; Neef *et al.*, 2002; Hossain *et al.*, 2003). However, sequence analysis suggests that the N-terminus of TDAG51 has a potential nuclear export signal and a nuclear localization signal **(Figure 2)**. It is therefore possible that, like tumor suppressor protein p53 (Liang and Clerke 1998), TDAG51 is a nuclear protein that shuttles between the cytosol and nucleus. TDAG51 also contains several distinct motifs consisting of polyglutamine (QQ), proline-glutamine (PQ), or proline-histidine (PH) repeats (**Figure 2**). Long QQ stretches are located in the N terminal region of the TDAG51 protein. It has been suggested that proteins with polyglutamine repeats promote PCD in neurodegenerative diseases such as Huntington's disease (Li *et al.*, 1995). Previous findings also showed that proteins containing PQ repeats (McNabb and Courtney, 1992) or PH repeats (Han *et al.*, 1989; Cai *et al.*, 1994) can act as transcriptional activators. Therefore, it was originally suggested that TDAG51 may function as a transcriptional activator (Park *el al.*, 1996).

Immunoblot analysis using anti-TDAG51 antibody detected a protein of molecular mass ~ 40 kDa on SDS-PAGE gels (Hossain *et al.*, 2003), which is different from the predicted molecular mass of 29 kDa. This difference between the predicted and apparent molecular mass of the TDAG51 protein is likely due to secondary structure resulting from the high proline, glutamine, and histidine content in the protein. Previous

Figure 2: Sequence analysis of T Cell Death-Associated Gene 51 ORF

(A) The human TDAG51 gene encodes 260 amino acids, including a long stretch of glutamine (Q) residues near the N-terminus. Proline-glutamine (PQ) and proline-histidine (PH) repeats are located near the C-terminus. TDAG51 also contains an N-terminal pleckstrin homology-like domain. Further, there is a nuclear localization signal (NLS) and a nuclear export signal (NES) within the N-terminal domain of the protein. (B) The figure demonstrates the amino acid sequence of TDAG51 as color-coding, corresponding to figure 2A.

A

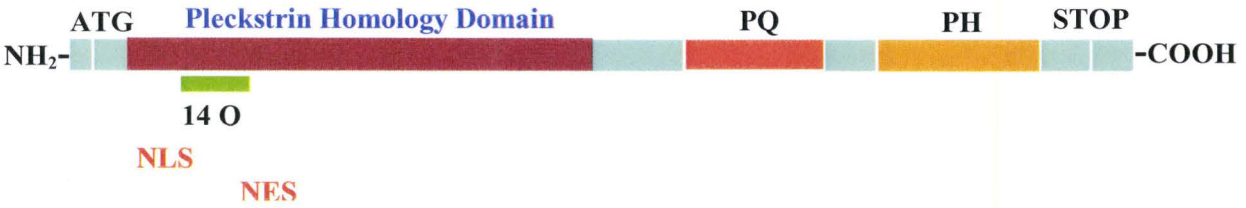

B

NH_2 - MLESSGCKALKEGVLEKRSDG LLQLWK
KKCCILTEEGLLLIPPKQLQHQQQQQQQQQQQ
QQQPGQGPAEPSQPSGPAVASLEPPVKLKELKFS
NMKTVDCVEKGKYMYFTVVMAEGKEIDFRCP
QDQGWNAEITLQMVQYKNRQAILAVKSTRQKQ
QHLVQQQPPSQPQPQPQLQPQPQPQPQPQPQP
QPQPQPQPQPKPQPQQLHPYPHPHPHPHSHPHS
HPHPHPHPHPHQIPHPHPQPHSQPHGHRLLRST
SNSA - COOH

studies have also reported that proline-rich regions alter the protein conformation in murine leukemia viruses (Lavillette *et al.*, 1998).

Sequence analysis has also revealed that TDAG51 has significant sequence homology to the tumor suppressor gene *Ipl/Tssc3*, which is located in the tumor suppressor region of human chromosome 11 (Qian *et al.*, 1997; Lee *et al.*, 1998; Schwienbacher *et al.*, 2000). Studies have reported that deletions in chromosome 11 containing this tumor suppressor gene promote tumorigenesis (Schwienbacher *et al.*, 1998; Lee *et al.*, 1998). Based on sequence homology, TDAG51 has been placed into a novel pleckstrin homology-related gene family that includes *Ipl/Tssc3* and *Tih1* (Frank *et al.*, 1999). Pleckstrin homology-related domains mediate protein-protein and protein-lipid vesicle interaction in cells and are believed to be involved in cytoskeleton organization in cells (Maffucci and Falasca 2001).

1.3.2 Function of TDAG51

TDAG51 was identified by its ability to complement a mouse T cell hybridoma resistant to activation-induced cell death (AICD) (Park *et al.*, 1996). Subsequent studies have demonstrated that TDAG51 is required for Fas (CD95) expression and AICD of T cells, indicating that TDAG51 may regulate apoptosis of T cells. Another report has shown that protein kinase C (PKC) inhibitors block activation-induced Fas expression and PCD in a murine T cell hybridoma (Wang *et al.*, 1998), suggesting that PKC may be responsible for TDAG51-dependent regulation of Fas. However, Gomes *et al.* (1999) demonstrated that TDAG51 promotes Fas-independent PCD in rat neuronal cells.

Consistent with this observation, TDAG51 is not essential for Fas induction and T-cell mediated PCD in TDAG51$^{-/-}$ mice (Rho *et al.*, 2001). Despite no difference in T cell apoptosis between TDAG51$^{-/-}$ mice and wild-type mice, it has been suggested that some known homologs of TDAG51 may substitute for TDAG51 in TDAG51$^{-/-}$ mice.

Since TDAG51 has significant sequence homology to the tumor suppressor gene *Ipl/Tssc3* (Schwienbacher *et al.*, 1998; Lee *et al.*, 1998), it has been suggested that TDAG51 may act as a tumor suppressor or regulator of cell growth. Studies have reported that decreased expression of TDAG51 in metastatic melanoma correlates with increased resistance to PCD and that constitutive overexpression of TDAG51 increases PCD sensitivity, thereby impairing melanoma cell proliferation (Neef *et al.*, 2002). Interestingly, recent findings have provided strong evidence that reduced TDAG51 expression is important in breast cancer progression (Nagai *et al.*, 2007).

Given that overexpression of TDAG51 leads to dramatic alterations in cell shape and increases detachment of cells from their appropriate matrix (Hossain *et al.*, 2003), a mechanism involving detachment-induced PCD or anoikis had been proposed. In addition, the observation that TDAG51-induced shape changes are independent of caspase activation and occur prior to activation of cell death program further supports this mechanism (Hossain *et al.*, 2003). Since TDAG51 colocalizes with FAK and alters the actin cytoskeleton (Hossain *et al.*, 2003), it is conceivable that TDAG51 overexpression disrupts FAC assembly and interrupts survival signaling from the extracellular matrix prior to activation of the cell death program. It is important to mention that TDAG51-induced PCD in endothelial cells is both concentration- and time-dependent (Hossain *et*

al., 2003). Also, overexpression of TDAG51 does not necessarily induce PCD in all cell lines, including melanoma cell lines and MEFs. Overexpression of TDAG51 may sensitize cells to PCD and additional cellular mediators or activation of cellular stress pathways are therefore necessary to induce cell death. The primary function of TDAG51 may be the regulation of cytoskeleton organization and cell adhesion foci. Gos *et al.* (2005) have reported through microarray analysis that TDAG51 was dramatically upregulated by contact inhibition in a mouse fetal fibroblast cell line, c3H10T1/2. Therefore, it is possible that loss of TDAG51 promotes cell proliferation.

Although all these studies provide convincing evidence that TDAG51 may have roles in cell growth, cytoskeletal organization and PCD, the exact cellular function of TDAG51 remains largely unknown.

1.3.3 Elucidation of TDAG51 function by gene knockout in C57 mice

TDAG51$^{-/-}$ mice were initially generated to investigate the role of TDAG51 in T cell apoptosis (Rho *et al.*, 2001). Contrary to *in vitro* findings, it was shown that TDAG51 is not essential for Fas expression and T cell apoptosis *in vivo*. The authors reported that there were no phenotypic differences between wildtype and TDAG51$^{-/-}$ mice. TDAG51$^{-/-}$ mice showed no differences in the lymphoid organs and also had no significant abnormalities in the lymph nodes or spleen, compared to wildtype mice. Importantly, white blood cell counts including T or B cells were similar. T or B cells derived from wildtype and TDAG51$^{-/-}$ mice did not show any differences in proliferation. Further, Fas transcript expression in liver and other tissues did not show any differences, suggesting

that TDAG51 is not required for Fas expression *in vivo*. In addition, TDAG51 did not appear to be important in activation-induced apoptosis of T cells given that there were no significant differences in apoptosis of T cells between wildtype and TDAG51$^{-/-}$ mice. These observations raised the possibility that other homologs of TDAG51 compensate for Fas expression and apoptosis *in vivo*.

Interestingly, TDAG51 can promote heat-induced germ cell death *in vivo* (Hayashida *et al.*, 2006). Earlier studies have demonstrated that cells express heat shock proteins (Hsps) to assist protein folding and to inhibit protein denaturation (Parsell and Lindquist 1993; Young *et al.*, 2004). This adaptive response is termed a "heat shock response" and is regulated by heat shock transcription factor 1 (HSF1) (Morimoto 1998). HSF1 also promotes apoptosis, given that heat-induced apoptosis of spermatocytes are inhibited in HSF1-deficient mice (Izu *et al.*, 2004). Hayashida *et al.* (2006) showed that TDAG51 is a target for HSF1. TDAG51 mRNA expression was markedly induced and correlated with PCD in wild-type germ cells including pachytene spermatocytes in response to heat shock. In support of this, a decrease in apoptotic germ cells was observed in TDAG51$^{-/-}$ mice. Further, overexpression of hsps blocked the pro-apoptotic effects of TDAG51 (Hayashida *et al.*, 2006). These findings imply that TDAG51 may have an important role in germ cell death *in vivo*.

1.3.4 Involvement of TDAG51 in atherosclerosis

We first reported the association of TDAG51 in the development of atherosclerosis (Hossain *et al.*, 2003). TDAG51 mRNA and protein were induced in response to

homocysteine, an independent risk factor for atherosclerosis. In addition, increased TDAG51 expression correlates with apoptosis within the advanced atherosclerotic lesions from apoE$^{-/-}$ mice fed hyperhomocysteinemic diets. In support of our findings, TDAG51 was defined as an atherosclerosis-susceptible gene (Dai *et al.*, 2004). In brief, using a high-throughput transcriptional profiling approach, Dai *et al.* (2004) reproduced arterial shear stress waveforms (athero-prone and athero-protective) on cultured human endothelial cells, representing the wall shear stresses within two distinct regions of the carotid artery. The involvement of TDAG51 in the development of atherogenesis is supported by the observation that the athero-prone waveform increases TDAG51 expression in cultured human endothelial cells. Furthermore, Zhou *et al.* (2005) demonstrated the expression of TDAG51 within early and advanced atherosclerotic lesions from apoE$^{-/-}$ mice fed normal chow diet. Additional studies are however needed to explain the underlying role of TDAG51 in the development and progression of atherosclerosis.

1.4 Overview of hyperhomocysteinemia and vascular disease

HHcy is defined as elevated levels of plasma homocysteine, a non-essential amino acid and an intermediate in the metabolism of methionine (Butz *et al.*, 1932; du Vigneaud *et al.*, 1952). Since McCully proposed a link between HHcy and vascular disease in 1969, numerous clinical studies have demonstrated that elevated level of plasma homocysteine is an independent risk factor for atherosclerotic disease such as ischemic heart disease, stroke, and peripheral vascular disease (Refsum *et al.*, 1998; Eikelboom *et al.*, 1999).

Various studies have also associated homocystinuria with arteriosclerosis (fibrotic thickening), narrowing of arteries, and thrombotic events (Mudd *et al.*, 1995). Homocystinuric patients develop intimal thickening and fibrous plaques rich in smooth muscle cells, collagen and deposited connective tissue (Wilcken and Dudman 1992; Refsum *et al.*, 1998). However, lipid rich atherosclerotic lesions are less frequently observed than arteriosclerotic fibrous lesions in the major arteries of patients suffering from homocystinuria. Furthermore, accelerated or increased thrombotic events are shown to cause infarction in various organs, resulting in death at very early age (Refsum *et al.*, 1998). Interestingly, homocysteine-induced thrombosis is linked to thrombogenesis from endothelial dysfunction rather than changes in platelet physiology (Welch and Loscalzo 1998). It is suggested that endothelial dysfunction alters the anti-thrombotic phenotype of the endothelium, resulting in pro-thrombotic environment that leads to the development of vascular injury (Welch and Loscalzo 1998).

Although severe HHcy (>100 μM) is rare, it is estimated that approximately 5-7% of the population are mildly hyperhomocysteinemic (15 to 30 μM), and develop premature atherosclerosis and thrombotic disease (Welch and Loscalzo 1998). Up to 40% of patients diagnosed with premature coronary artery disease, peripheral vascular disease or recurrent venous thrombosis are reported to have mild HHcy (Refsum *et al.*, 1998). It is also suggested that mild HHcy may have multiple effects when combined with other CVD risk factors, including hypercholesterolemia, hypertension, smoking, and diabetes (Ross 1993; McCully 1996; Welch and Loscalzo 1998). It was therefore believed that control of mild HHcy may be very important in preventing plaque

formation and thrombosis. However, recent studies have demonstrated that homocysteine lowering supplements combining folic acid and vitamins B6 and B12 did not reduce the risk of major cardiovascular events or symptomatic venous thromboembolism in patients with vascular disease (Lonn *et al.*, 2006; Ray *et al.*, 2007). Also, supplements containing B vitamins did not lower the recurrent CVD after acute myocardial infarction (Bonaa *et al.*, 2006). A harmful effect was suggested from combined B vitamin treatment, and therefore, such treatment should not be recommended. Interestingly, studies have also reported that decreasing total plasma homocysteine levels by folic acid supplementation reduces CVD risk (Bostom *et al.*, 2006). In addition, population-based cohort studies in USA and in Canada have demonstrated that folic acid fortification helps to reduce death from stroke, further implying a role of folate in the improvement of stroke mortality (Yang *et al.*, 2007). Although controversy still exists, studies have continued to support an independent role for high levels of plasma homocysteine in the development of premature vascular disease.

1.4.1 Historical perspective on hyperhomocysteinemia

In 1962, high concentrations of homocysteine were reported in the urine of two siblings, aged 4 and 6 years, with mental retardation (Carson and Neil 1962). In the same year, Gerritsen *et al.* (1962) identified increased homocysteine in the urine of a mentally retarded infant with congenital anomalies. This new inborn error of metabolism due to elevated homocysteine in urine was then termed homocystinuria. In 1964, deficiency of CBS was discovered in the liver biopsy specimen from a homocystinuric patient (Madd

et al., 1964). In the same year, widespread vascular changes and thrombosis were also observed in homocystinuric patients (Gibson *et al.*, 1964).

McCully, in 1969, was the first to demonstrate a link between increased levels of homocysteine and CVD (McCully 1969). He observed that an infant with homocystinuria who died of a different disorder of cobalamin metabolism exhibited widespread, severe arteriosclerosis similar to the lesions seen in CBS-deficient homocystinuric patients. He therefore proposed that elevated levels of homocysteine, designated hyperhomocysteinemia (HHcy), were responsible for the vascular changes observed in these two metabolic abnormalities.

In 1976, Wilcken and Wilcken reported that the concentration of plasma homocysteine was slightly higher in patients with coronary heart disease after a methionine-loading test, compared to age- and sex-matched controls. To further establish the relationship between increased homocysteine levels and CVD, patients with CBS-deficiency were given high doses of vitamin B_6. It was demonstrated that 50% of patients had a significant decrease in cardiovascular events (Mudd *et al.*, 1985). These pioneering studies by Wilcken and Wilcken (1976) and Mudd *et al.* (1985) led to experimental and clinical studies demonstrating the relationship between HHcy and CVD.

1.4.2 Overview on homocysteine

Homocysteine is normally found at relatively low concentrations within the cells, including endothelial cells and hepatocytes ($\leq$ 1 μmol/L), and in the plasma (5 to 15

μmol/L) (Ueland *et al.*, 1993). Homocysteine exists in several forms in plasma. Due to the oxidizing conditions in plasma, only a small fraction (<2%) of total circulating homocysteine exists in the reduced form. The remainder is a mixture of disulphide derivatives, including homocysteine-homocysteine (homocystine), homocysteine-cysteine mixed disulphide, and protein bound disulphides (Mudd *et al.*, 2000).

In most cell types, homocysteine is metabolized intracellularly to methionine by the remethylation pathway **(Figure 3)**. However, it can be metabolized to cysteine by the transsulphuration pathway in liver or kidney. Under conditions of low protein intake, the metabolism of homocysteine is primarily via the remethylation pathway. Homocysteine can be recycled to methionine by two distinct pathways. In the liver, homocysteine is remethylated by betaine-homocysteine methyltransferase (BHMT) with betaine as the methyl donor. In other tissues, remethylation of homocysteine is catalyzed by methionine synthase (MS) where N^5-methyltetrahydrofolate acts as a methyl donor and vitamin B_{12} is an essential cofactor. N^5-methyltetrahydrofolate is produced by N^5, N^{10}-methylenetetrahydrofolate reductase (MTHFR) from N^5, N^{10}-methylenetetrahydrofolate, which is derived from dietary folate. In the presence of excess methionine, homocysteine enters the transsulphuration pathway, where it irreversibly condenses with serine to form cystathionine in the presence of the vitamin B_6-dependent enzyme, cystathionine β-synthase (CBS). Cystathionine can be further metabolized to cysteine by another vitamin B_6-dependent enzyme, cystathionine-γ-lyase. Cysteine can then be converted to sulphate to be excreted in urine, incorporated into protein or used to generate glutathione. Studies have shown the importance of the transsulphuration pathway in maintaining the

Figure 3: Schematic representation of homocysteine metabolism

Homocysteine is an amino acid formed by the metabolism of methionine, an essential amino acid derived from the diet. Homocysteine is shunted through either the transsulphuration or remethylation pathway depending on the concentration of dietary methionine. The transsulphuration pathway converts homocysteine to cystathionine and cysteine which can be used in the generation of glutathione or sulphate or protein synthesis. Homocysteine can also be converted to homocysteine thiolactone by the editing function of aminoacyl-tRNA synthetase (AARS). Deficiencies of enzymes [cystathionine-β-synthase (CBS), methyltetrahydrofolate reductase (MTHFR), betaine-homocysteine methyltransferase (BHMT), methionine synthase (MS)] or cofactors (vitamin B_{12} or vitamin B_6) involved in homocysteine metabolism can lead to HHcy.

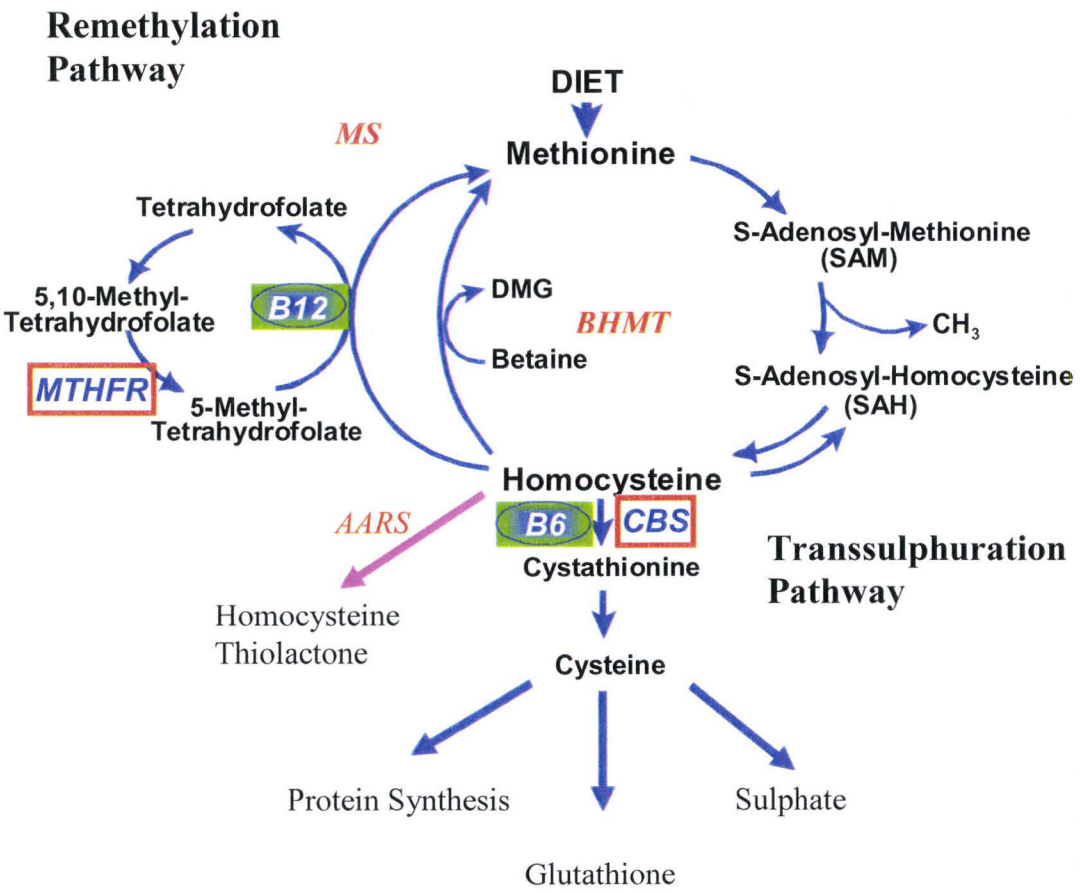
Remethylation Pathway
DIET
MS
Methionine
Tetrahydrofolate
S-Adenosyl-Methionine (SAM)
5,10-Methyl-Tetrahydrofolate
B12
DMG
BHMT
CH3
Betaine
MTHFR
5-Methyl-Tetrahydrofolate
S-Adenosyl-Homocysteine (SAH)
Homocysteine
AARS
B6
CBS
Transsulphuration Pathway
Cystathionine
Homocysteine Thiolactone
Cysteine
Protein Synthesis
Sulphate
Glutathione

intracellular glutathione pool under oxidative stress conditions (Mosharov *et al.*, 2000; Vitvitsky *et al.*, 2004).

1.4.3 Studies on mouse models of hyperhomocysteinemia

Mouse models for HHcy were generated by targeting genes involved in homocysteine metabolism and/or dietary modifications. Plasma homocysteine levels are generally increased by dietary addition of methionine and/or depletion of B vitamins and folate, or by targeted disruption of genes involved in homocysteine metabolism such as CBS or MTHFR. Earlier studies on CBS-deficient mice showed developmental abnormalities similar to those observed in human homocystinuric patients (Watanebe *et al.*, 1995). CBS heterozygotes have plasma homocysteine levels twice the normal levels but do not exhibit severe developmental defects (Watanebe *et al.*, 1995; Weiss 2002), making them an ideal candidate to study mild HHcy. Neither dietary nor transgenetic animal models of HHcy develop atherosclerosis (Lang *et al.*, 2000; Lentz *et al.*, 2001). Instead, mice exhibit endothelial dysfunction, which is believed to be an important factor for the initiation of atherosclerotic lesions (Lentz *et al.*, 2001). Studies have suggested that HHcy is atherogenic since mice deficient in both apoE and CBS demonstrate accelerated atherosclerosis without dietary modification (Wang *et al.*, 2003). Also, HHcy appears to alter hepatic and macrophage lipoprotein metabolism by enhancing uptake of modified LDL.

Chen *et al.* (2001) have reported that MTHFR-deficiency may predispose mice to accelerated atherosclerosis. These mice appear to share developmental abnormalities

with CBS-deficient mice. Mature homozygous and heterozygous MTHFR-deficient mice were shown to accumulate lipid in their proximal aorta, a sign of early atherosclerotic lesions (Chen *et al.*, 2001). These animals became the first animal model associating mild HHcy with atherosclerotic lesion development. The lesions developed in this model, however, were not as large as those observed in murine models of hyperlipidemic atherosclerosis, such as LDLR- and apoE-deficient mice. Interestingly, a study by Werstuck *et al.* (2001) has implicated ER stress-induced hepatic lipid accumulation (hepatic steatosis) with HHcy in wildtype or CBS-deficient heterozygote mice. Hepatic steatosis is a characteristic feature of homocystinuric patients as well as CBS- and MTHFR-deficient mice.

Last several years, *in vivo* studies of HHcy have focused on apoE-deficient mice, which are known to develop spontaneous atherosclerosis. Two reports by Hofmann *et al.* (2001) and Zhou *et al.* (2001) have established a direct causal relationship between induction of HHcy and accelerated atherosclerosis in apoE-deficient mice fed hyperhomocysteinemic diets. These mice developed enhanced and more complexed atherosclerotic lesions in the aorta, compared to those observed in apoE-deficient mice fed normal chow diet **(Figure 4)**. Interestingly, both studies used two different dietary approaches while demonstrating similar outcome. One study used a low-fat diet that was supplemented with methionine and deficient in folate, vitamin B_{12} and B_6 (Hofmann *et al.*, 2001), while the other used a high-fat diet supplemented with homocysteine or methionine (Zhou *et al.*, 2001). Hofmann *et al.* (2001) demonstrated that HHcy enhances inflammatory responses, resulting in increased expression of vascular cell adhesion

Figure 4: Atherosclerotic plaques in apoE-deficient mice fed hyperhomocysteinemic diets

Atherosclerotic plaques in the aortic root of $apoE^{-/-}$ mice fed normal chow (A), high homocysteine (B) or high methionine diet (C). Lesion sizes in the hyperhomocysteinemic mice (B,C) were significantly larger, compared with the control mice (A). Atrophy of the tunica media and rupture of elastic membranes were often observed (arrow in B). All sections were stained with Orcein to reveal the elastic lamina.

(Obtained and modified from Zhou et al. (2003) Atherosclerosis 168: 258)

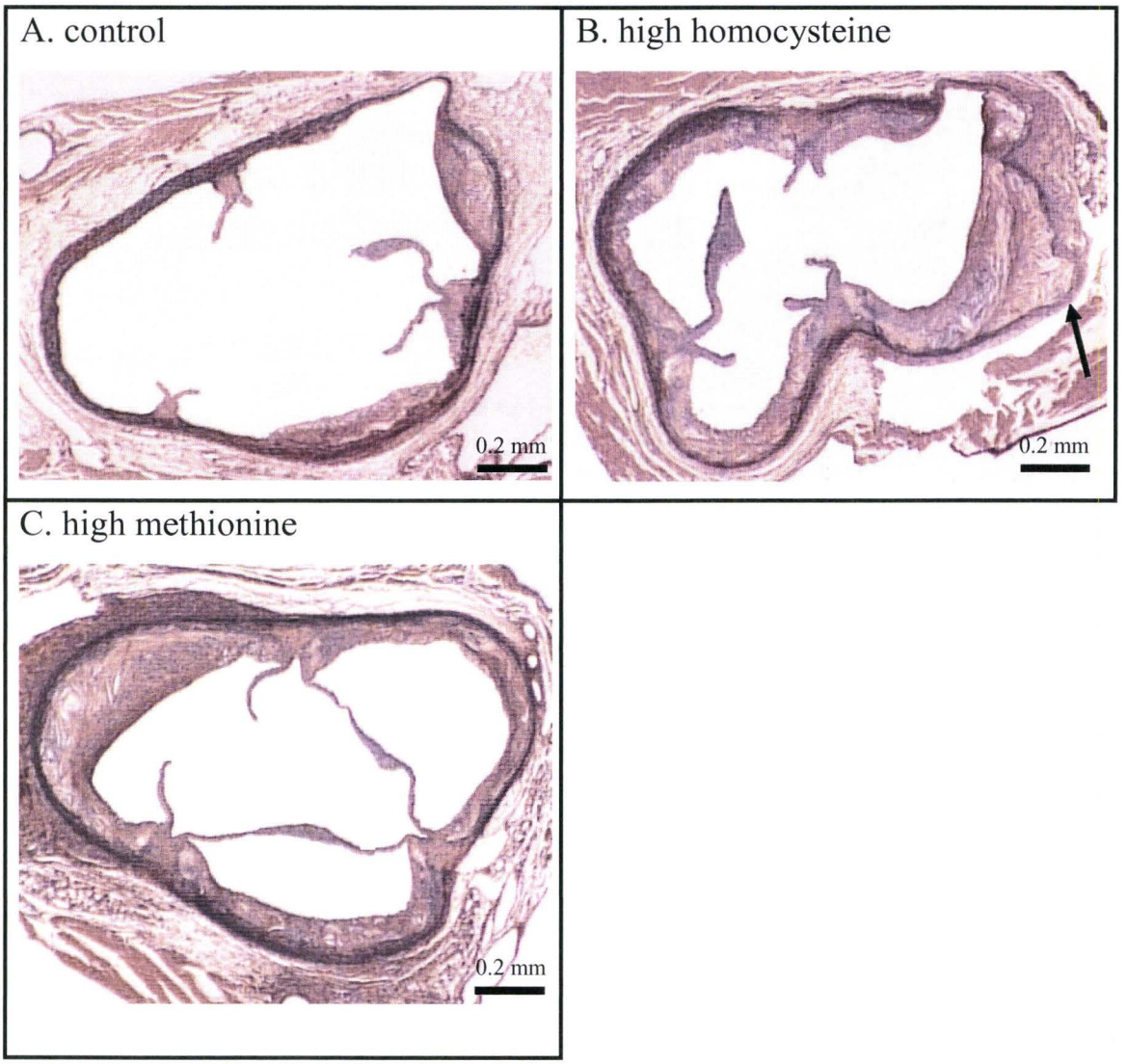
A. control
0.2 mm
B. high homocysteine
0.2 mm
C. high methionine
0.2 mm

molecule-1 and elevated levels of tumor necrosis factor-α (TNF-α). The authors also observed increased expression of procoagulant tissue factor and matrix metalloproteinase-9 (MMP-9), suggesting that HHcy might not only promote atherogenesis but also increase plaque rupture and thrombosis. In contrast, Zhou *et al.* (2001) have shown that these plaques are rich in collagen and are apparently stable. Homocysteine is believed to enhance smooth muscle cell proliferation (Majors *et al.*, 1997). It has been suggested that increased extracellular matrix deposition may enhance plaque stability. Furthermore, no differences in atherosclerotic plaque size between control and hyperhomocysteinemic mice were observed after long-term treatment (Zhou *et al.*, 2001). While these findings suggest that HHcy mediates early stages of atherogenesis, additional studies are needed to verify HHcy's role in long-term pathogenesis.

1.4.4 Potential mechanisms linking hyperhomocysteinemia to atherosclerosis

1.4.4.1 Oxidative stress

It has been suggested that homocysteine-induced cell injury involves oxidative damage because homocysteine is readily oxidized in plasma to generate ROS (Starkebaum and Harlan 1986; Loscalzo 1996). However, the oxidative stress theory fails to explain why cysteine, another thiol containing amino acid, which is present at approximately 25-fold higher concentrations in plasma than homocysteine and is also readily auto-oxidized, does not cause cell injury (Jacobsen 2000 & 2001). Findings have also shown that homocysteine does not significantly increase the production of ROS and is largely

involved in antioxidant and reductive cellular biochemistry (Zappacosta *et al.*, 2001). Based on these recent reports, this auto-oxidation mechanism has been challenged.

Studies have suggested that several types of ROS, including superoxide, hydrogen peroxide, and hydroxyl radical, may contribute to the oxidative inactivation of endothelium-derived nitric oxide (NO) in HHcy (Lentz 2005). Homocysteine alters the vasodilatory properties of normal endothelial cells by attenuating the production of nitric oxide (NO) (Stamler *et al.*, 1993). It is suggested that the protective action of NO is compromised due to chronic exposure of the endothelial cells to HHcy. Superoxide is a major mediator of endothelial dysfunction in hyperhomocysteinemic mice given that dilation of cerebral arterioles to acetylcholine in $Cbs^{+/+}$ and $Cbs^{+/-}$ mice fed a high methionine diet has been restored toward normal by the superoxide scavenger, trion (Dayal *et al.*, 2004). Studies have demonstrated that superoxide anion (O_2^-) can react with endothelial NO (Jia *et al.*, 1993; Duan *et al.*, 2000) to form peroxynitrite ($OONO^-$), a mediator for atherosclerosis (Dickhout *et al.*, 2005). Both O_2^- and $OONO^-$ have been shown to contribute to the oxidative modification of tissues. The observation that homocysteine decreases the expression of a wide range of antioxidant enzymes (Outinen *et al.*, 1999) and decreases NO bioavailability (Upchurch et al., 1997), raises the possibility that homocysteine may enhance the cytotoxic effect of agents or conditions known to generate ROS. Furthermore, homocysteine-induced oxidative stress may also contribute to atherogenesis by other mechanisms.

1.4.4.2 Inflammation

Since Russell Ross (1993) defined atherosclerosis as an inflammatory disease, numerous studies have suggested that HHcy-induced inflammation contributes to the development and progression of atherosclerosis. Expression of monocyte chemoattractant protein-1 (MCP-1) has shown to be increased in cultured human vascular endothelial cells, smooth muscle cells, and monocytes treated with homocysteine (Poddar *et al.*, 2001; Lusis 2001). Intravascular MCP-1 secretion is known to enhance intimal infiltration by monocytes, which is a critical step in the formation of foam cells and atherosclerotic plaques (Lusis 2001). Furthermore, homocysteine-induced release of MCP-1 in monocytes and endothelial cells occurs through activation of NF-κB, a transcription factor involved in the inflammatory process (Collins and Cybulsky 2001). Active NF-κB, which is found in atherosclerotic plaques, stimulates the production of cytokines, chemokines, interferons, leukocyte adhesion molecules, hematopoetic growth factors and major histocompatibility (MHC) class I molecules. These pro-inflammatory molecules are believed to influence vascular inflammation, and ultimately atherogenesis (Collins and Cybulsky 2001). Consistent with these findings, Hofmann *et al.* (2001) reported the *in vivo* activation of NF-κB and the expression of downstream markers in atherosclerotic lesions from apoE-deficient mice fed hyperhomocysteinemic diets, further supporting a theory that homocysteine promotes atherosclerosis through vascular inflammation.

1.4.4.3 The molecular targeting hypothesis

Given that homocysteine is generated intracellularly and can accumulate in cells, Jacobsen (2000 & 2001) proposed the molecular targeting hypothesis which states that

intracellular and extracellular homocysteine can directly interact and modulate the activity of both large (enzymes, receptors) and small molecular (NO, glutathionine) targets, thereby altering specific cellular processes and pathways. Nishio and Watanabe (1997) have shown that homocysteine can decrease glutathione peroxidase activity while increasing superoxide dismutase activity in a dose-dependent manner in cultured rat aortic smooth muscle cells. Other studies have also shown that homocysteine can form disulphide bonds with annexin II, resulting in the inhibition of tissue plasminogen activator, thus decreasing the conversion of plasminogen to plasmin (Hajjar *et al.*, 1998). Further, Barbato *et al.* (2007) recently demonstrated that L-homocysteine targets intracellular metallothionein in cultured endothelial cells by forming a mixed-disulphide conjugate and that loss of function happens after homocysteinylation. In this study, Barbato and colleagues provide significant evidence that intracellular targets of homocysteine may be the main cause for endothelial dysfunction that contributes to atherothrombotic disease. Importantly, the findings suggest that total plasma homocysteine levels may not be significant with regard to the pathophysiology of HHcy given that the cytotoxic effect of homocysteine are compartmentalized in cells and tissues (Colgan and Austin, 2007). Based on all these findings, it is believed that other cellular targets affected by homocysteine will be identified and may further explain the mechanisms responsible for endothelial cell cytotoxicity.

1.4.4.4 Endoplasmic reticulum stress and the unfolded protein response

Previous reports have demonstrated that homocysteine adversely affects ER function by disrupting protein folding in the ER, resulting in activation of the UPR and elevated expression of several ER stress response genes, including GRP78, GRP94, GADD153, Herp, RTP and TDAG51 (Outinen *et al.*, 1998 & 1999; Kokame *et al.*, 1996 & 2000; Hossain *et al.*, 2003). Several studies have also reported that homocysteine-induced ER stress promotes specific cellular responses, including lipid biosynthesis, PCD, and inflammation (Werstuck *et al.*, 2001; Zhang *et al.*, 2001; Huang *et al.*, 2001; Hossain *et al.*, 2003). Although these *in vitro* studies provide evidence that homocysteine has a role in lipid biosynthesis, PCD, and inflammation, additional studies are required to explain *in vivo* relevance of homocysteine in atherogenesis.

Interestingly, HHcy has been shown to accelerate atherogenesis in apoE-deficient mice (Hofmann *et al.*, 2001; Zhou *et al.*, 2001), possibly involving the induction of an inflammatory response. Previous studies have also reported NF-κB activation in cells undergoing ER stress (Pahl *et al.*, 1996). In addition, ER stress-mediated UPR induction sensitizes the activation of JNK protein kinases, which can potentially result in further inflammation and PCD (Urano *et al.*, 2000). Further, Zhou *et al.* (2004) have demonstrated an association of multiple stress pathways, including ER stress, in the development of atherosclerosis in apoE-deficient mice fed hyperhomocysteinemic diets. Based on all these findings, homocysteine-induced ER stress may prove to be an important mechanism that contributes to the development and progression of atherosclerosis.

1.5 Significance of apoptosis and ER stress in the development and progression of atherosclerosis

Apoptosis is well documented in both animal and human atherosclerotic lesions (Isner *et al.*, 1995; Kockx *et al.*, 1996; Hegyi *et al.*, 1996). The distribution of cell death is heterogeneous within the lesion, but is most prominent in the lipid-rich necrotic core that contains a high density of macrophages and smooth muscle cells. PCD is rare in early atherosclerotic lesions. However, PCD occurs as atherosclerosis progresses and increases the risk of lesion rupture by decreasing the stability of the atherosclerotic lesion. Further, PCD may enhance plaque thrombogenicity by increasing the number of TF-rich apoptotic microparticles within the atherosclerotic lesion (Tedgui and Mallat 2001).

Accumulation of free cholesterol (FC) in macrophage foam cells is believed to be an important process during atherosclerotic lesion progression (Ball *et al.*, 1995; Tabas 2002). Feng *et al.* (2003) have demonstrated that FC loading in the ER of cultured peritoneal macrophages can induce ER stress and activate the UPR, thereby resulting in PCD. The ER regulates protein synthesis, folding and trafficking of secretory and membrane resident proteins, as well as intracellular calcium homeostasis (Welihinda *et al.*, 1999). Therefore, disruption of ER function initiates a cellular stress response termed the unfolded protein response (UPR). Interestingly, Feng *et al.* (2003) demonstrated a correlation between FC accumulation and increased expression of the ER stress response gene CHOP in advanced atherosclerotic lesion from apoE$^{-/-}$ mice. In addition, Zhou *et al.* (2005) have reported UPR activation during all stages of atherosclerotic lesion development in apoE$^{-/-}$ mice fed normal chow diet. Recently, Thorp *et al.* (2009)

demonstrated reduced apoptosis and atherosclerotic lesion size in advanced atherosclerosis of apoE$^{-/-}$ and LDLR$^{-/-}$ mice lacking CHOP. Further, PCD and FC accumulation within lesion-resident macrophages were predominantly observed in the advanced atherosclerotic lesion, implying involvement of additional cellular mediators and/or pathways for macrophage PCD. Herein, it is important to mention that prolonged ER stress has been implicated with PCD observed in several other diseases, including diabetes, chronic liver disease, Parkinson's, and Alzheimer's disease (Kaufman 2002; Ron 2002).

1.5.1 Mechanism of endoplasmic reticulum stress

UPR is an integrated intracellular signaling pathway that responds to ER stress by increasing the expression of UPR responsive genes, attenuating global protein translation and degrading unfolded proteins (Shen *et al.*, 2004; Schroder and Kaufman 2005). ER stress activates three arms of the UPR, namely inositol-requiring enzyme 1 (IRE1), activating transcription factor 6 (ATF-6) and pancreatic ER kinase (PKR)-like ER kinase (PERK) **(Figure 5)**. In response to ER stress, UPR activation pathways normally facilitate the correct folding of misfolded proteins within the ER. However, if these adaptive responses fail to relieve ER stress, the damaged cells then undergo PCD.

When unfolded proteins accumulate in the ER, it signals the dissociation of GRP78 from these mediators, resulting in the binding of GRP78 to unfolded proteins. PERK is then activated via dimerization and autophosphorylation. Following activation, PERK catalyzes the phosphorylation of eukaryotic initiation factor 2α (eIF2α) (Shi *et al.*,

Figure 5 : Unfolded protein response pathways in response to ER stress in eukaryotes

Following ER stress, ER transmembrane protein IRE-1 dimerizes and autophosphorylates upon release of GRP78 to bind unfolded proteins. Endoribonuclease activity of IRE-1 cleaves mammalian XBP-1 mRNA to remove a 26-base intron. Translation of alternatively spliced XBP-1 mRNA yields XBP-1 protein containing a novel C-terminus that binds to ER stress response element (ERSE) promoters, increasing transcription of ER chaperone genes. In ATF-6 pathway, ATF-6 migrates to the Golgi following GRP78 release and is cleaved by site 1 and site 2 (S1/S2) proteases. The cleaved 50-60 kDa bZip-containing transcription factor migrates to the nucleus and binds to ERSE, increasing transcription of ER chaperones. In PERK pathway, PERK is activated via oligmerization and autophosphorylation following GRP78 release. PERK catalyzes the phosphorylation of eukaryotic initiation factor-2α (eIF-2α), which prevents eIF-2α from initiating translation, thereby limiting the unfolded protein load on the ER. Activation of the PERK pathway has also been shown to mediate transcription of UPR genes involved in the re-folding of unfolded proteins within the ER

(Obtained and modified from de Koning et al. (2003) Clinical Biochemistry 36: 434).

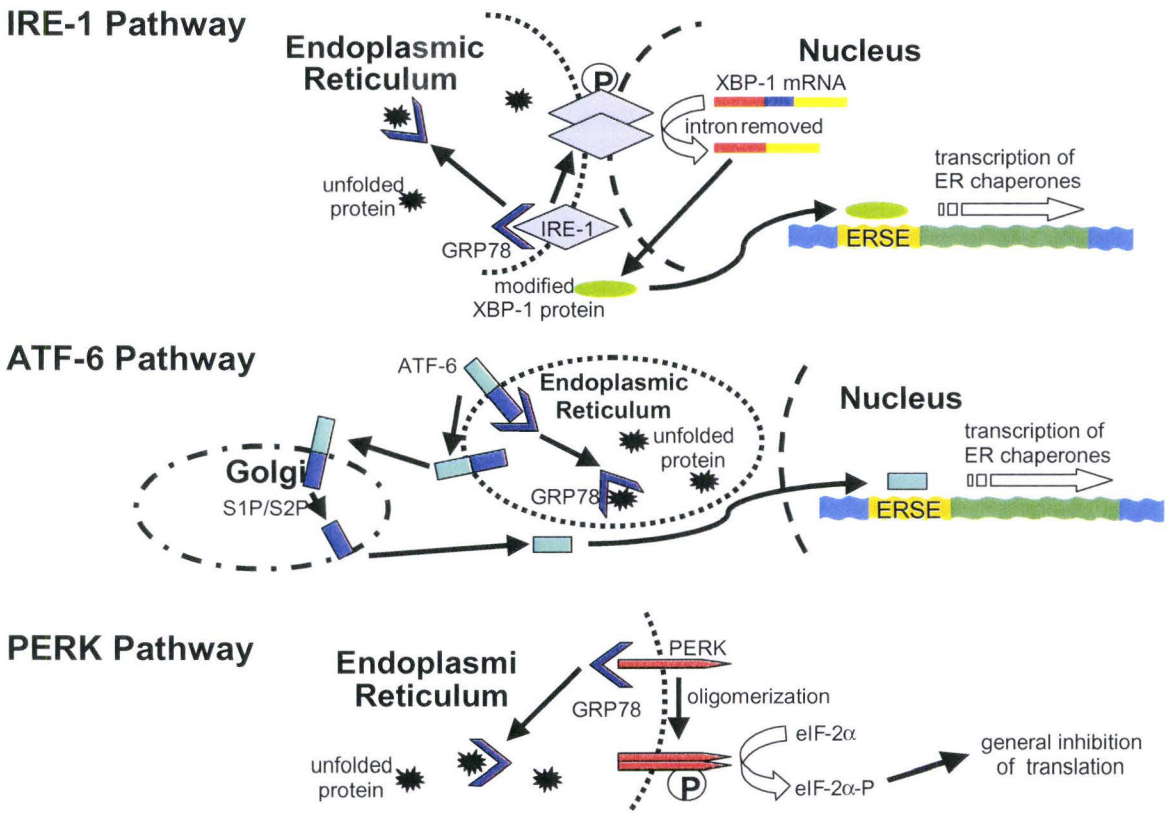
IRE-1 Pathway
Endoplasmic Reticulum
Nucleus
P
XBP-1 mRNA
intron removed
transcription of ER chaperones
unfolded protein
IRE-1
GRP78
ERSE
modified XBP-1 protein
ATF-6 Pathway
ATF-6
Endoplasmic Reticulum
Nucleus
unfolded protein
transcription of ER chaperones
Golgi
S1P/S2P
GRP78
ERSE
PERK Pathway
Endoplasmi Reticulum
PERK
GRP78
oligomerization
eIF-2α
unfolded protein
P
eIF-2α-P
general inhibition of translation

1998; Harding *et al.*, 1999), thereby preventing global protein translation. Inhibition of protein translation is initially considered to enhance cell survival since it decreases the load of nascent proteins into the ER. In support of this, *PERK*$^{-/-}$ MEFs both failed to inhibit protein translation and demonstrated increased cell death when challenged with ER stress agents (Harding *et al.*, 2000). In addition, reduced ER stress-induced cell death was observed when translation was blocked with cycloheximide. Significance of the PERK pathway was further demonstrated by the observation that MEFs expressing non-phosphorylatable eIF2α (S51A) were hypersensitive to ER stress-induced cell death (Scheuner *et al.*, 2001). However, mRNA encoding transcription factor ATF4 can be translated. ATF4 protein promotes cell survival by facilitating the induction of several genes involved in amino-acid metabolism, stress response and protein secretion (Harding *et al.*, 2003). It can therefore be suggested that activation of PERK is initially cytoprotective, but later on, it favors apoptosis due to the inhibition of global translation and the induction of the pro-apoptotic gene CHOP.

Similar to PERK, IRE1 has dual roles since it contains both a Ser/Thr kinase domain and an endoribonuclease domain. Autophosphorylation and dimerization of IRE1 are also initiated upon release of GRP78. Activated IRE1 cleaves the X box-binding protein 1 (XBP-1) mRNA and translates an alternatively spliced XBP-1 protein, a bZIP-family transcription factor (Yoshida *et al.*, 2001; Lee *et al.*, 2003). XBP-1 then activates the transcription of ER stress response genes by binding to ER stress enhancer (ERSE) and unfolded protein response elements (UPRE) (Yoshida *et al.*, 2001). An important target for spliced XBP-1 protein is the HSP40 family protein member, P58^{IPK}

(Lee *et al.*, 2003). $P58^{IPK}$ protein can relieve PERK-mediated inhibition of translation by binding to PERK, thereby terminating UPR activation (Yan *et al.*, 2002). It is important to note that upregulation of $P58^{IPK}$ protein is not an early event but it occurs following phosphorylation of PERK and eIF2α. It is not yet established whether $P58^{IPK}$ protein has a pro-apoptotic role following prolonged ER stress. Similar to *PERK*$^{-/-}$ mice, $P58^{IPK}$-deficient mice demonstrate increased apoptosis in pancreatic β-cells (Ladiges *et al.*, 2005). It is possible that deficiency of $P58^{IPK}$ may lead to increase activity of PERK, and subsequently, may result in the upregulation of both ATF4 and CHOP. However, studies have shown that IRE1 can activate apoptotic kinase pathways, including c-Jun N-terminal kinase (JNK) and apoptosis-signal-regulating kinase (ASK1) (Hatai *et al.*, 2000; Urano *et al.*, 2000; Nishitoh *et al.*, 2002). This pro-apoptotic condition contributes to ER stress-induced apoptosis.

In the presence of ER stress, ATF-6 migrates to the Golgi following release of GRP78 and is cleaved by site 1 and site 2 proteases. The activated domain of ATF-6 then migrates to the nucleus and induces the transcription of ER stress-induced genes, including GRP78, GRP94, protein disulphide isomerase, and XBP-1 (Schroder and Kaufman 2005). Although ATF-6 promotes increased transcription of XBP-1 mRNA, endonuclease activity of IRE1 however facilitates the generation of XBP-1 protein. Further, the ATF-6 pathway is believed to be pro-survival given that no studies show that ATF-6 causes ER stress-induced cell death.

In summary, the temporal induction of the UPR to ER stress is pro-survival or establishment of normal function of ER by reducing the accumulation of unfolded

proteins. However, chronic or severe ER stress triggers the activation of three signaling pathways, including PERK, ATF-6 and IRE1, leading to apoptotic cell death. Based on current knowledge, PERK is first activated upon UPR, followed by ATF-6. IRE1 is believed to be the last arm of UPR and holds the key for the initiation of pro-apoptotic signaling. Initiation phase may then lead to the activation of downstream pro-apoptotic molecules, including CHOP, JNK or Bcl-2 member proteins. This may lead to the activation of cysteine-dependent aspartate-specific proteases (caspases), thereby resulting in cell death. For instance, procaspase-12 in mice and -4 in human is localized to the cytosolic face of the ER membrane and is activated upon ER stress by IRE1-dependent mechanisms (Nakagawa *et al.*, 2000; Hitomi *et al.*, 2004).

1.5.2 Mechanism of apoptosis

Unlike necrosis, apoptosis or PCD is a well-regulated event (Wyllie *et al.*, 1980; Thronberry and Lazebnik 1998). PCD directs cells to self-destruction following the loss of survival signals. PCD is a genetically programmed event that is initiated by a variety of internal or external stimuli, such as ligation of specific death receptors, radiation, chemotherapeutic drugs, ER stress, withdrawal of growth factors or loss of matrix attachment (Hengartner 2000; Rao *et al.*, 2001; Frisch and Screaton 2001). Despite differences in the initiation of PCD, the morphological and biochemical changes are very similar: cell shrinkage and separation from neighbouring cells, change in phospholipid content of the plasma membrane or bubble-like formations on the membrane surface, chromatin condensation in the nucleus and protein fragmentation (Hengartner 2000). In

the final stage, DNA is fragmented into small, membrane-wrapped "apoptotic bodies" which are promptly endocytosed by phagocytic cells.

Caspases are implicated in the process of PCD (Alnemri *et al.*, 1996). In humans, at least 14 caspases have been identified (Thronberry and Lazebnik 1998). Caspase-2, -3, -6, -7, -8, -9, -10, and -12 play major roles in PCD, and are classified as initiators and effectors based on their location in the protease cascade and their roles in PCD (Earnshaw *et al.*, 1999). Initiator caspases are activated by autocatalysis or self-cleavage and act upstream at a "point of no return". Effector caspases are activated by initiator caspases and are involved downstream of the "point of no return" and cleave cellular substrates, including DNA repair enzyme PARP (poly (ADP)-ribose polymerase) (Lazebnik *et al.*, 1994), caspase-activated DNase (ICAD), gelsolin and p21 activated kinase 2 (PAK2) (Hengartner 2000).

Recruitment of caspases and their activators involves two major pathways. The first involves the ligation of death receptors such as Fas (Fas R or CD95) and the TNF receptor-1 (TNFR1), leading to recruitment and oligomerization of adaptor proteins such as pro-caspase-8. Activated caspase-8 is believed to play an essential role in promoting the caspase cascade. The second involves the release of cytochrome c from the mitochondria into the cytoplasm. This allows the formation of a caspase-9 activating complex. It is believed that mitochondria undergo major changes in membrane integrity, which involve both the inner and outer mitochondrial membrane, resulting in the dissipation of the inner transmembrane potential ($\Delta\psi_m$) and/or the release of intermembrane proteins such as cytochrome c (Liu *et al.*, 1996). Cytoplasmic

cytochrome c forms an essential part of the apoptosome, which is composed of cytochrome c, Apaf-1, and pro-caspase-9. Assembly of the apoptosome leads to the proteolytic self-activation of caspase-9, which then processes and activates caspase-3 (Li *et al.*, 1997). Caspase-3 cleaves effector substrates and results in PCD. It is also suggested that pro-apoptotic Bcl-2 family member Bax may be involved in decreasing inner transmembrane potential-allowing cytochrome c release (Jurgensmeier *et al.*, 1998). It is reported that some pro-apoptotic Bcl-2 family proteins, including Bax, have the ability to form ion channels and thus open pores or produce breaks in the outer membrane, resulting in the efflux of cytochrome c (Wolter *et al.*, 1997). However, this process can be prevented by pro-survival Bcl-2 family proteins, such as Bcl-2, Bcl-x_L, which are predominantly located in the outer mitochondrial membrane (Antonsson *et al.*, 1997). Interestingly, the death receptor pathway and mitochondrial pathway are not strictly separated. They are thought to communicate through Bid, a pro-apoptotic Bcl-2 family protein (Li *et al.*, 1998; Luo *et al.*, 1998). It has been demonstrated that activated caspase-8 can cleave Bid, and that fragmented Bid can act on mitochondria to trigger cytochrome c release and activate the apoptotic cascade.

In addition to the death receptor and mitochondrial pathways, anchorage-dependent PCD [termed "anoikis" (Greek for "homelessness")] was reported in endothelial (Meredith *et al.*, 1993) and epithelial cells (Frisch and Francis 1994) that were experimentally dissociated from their ECM. Although anoikis mediates activation of a cascade of caspases (Frisch and Screaton 2001), the underlying mechanism by which the caspase cascade is initiated after ECM detachment is unknown. Studies have

implicated death receptors or proteins associated with death domain in triggering anoikis. Caspase-8 and its substrate Bid are activated by cell-matrix detachment, and that fragmented Bids are believed to play roles in cytochrome c release from mitochondria (Ashkenazi and Dixit 1998; Muzio *et al.*, 1998; Li *et al.*, 1998). It has been demonstrated that in the presence of adequate growth factors, phosphoinositide-3 kinase (PI3K) becomes activated and phosphorylates Akt kinase, which then phosphorylates pro-apoptotic Bcl-2 family protein BAD and sequesters it to the cytosol via protein 14-3-3 (Gross *et al.*, 1999). However, loss of cell adhesion promotes loss of Akt function and dephosphorylates BAD. Dephosphorylated BAD then translocates to mitochondria and neutralizes the pro-survival activity of Bcl-2 or Bcl-x_L protein by binding to it, resulting in release of cytochrome c and thereby activating the apoptotic cascade (Fujio and Walsh 1999; Attwell *et al.*, 2000; Bachelder *et al.*, 2001).

ER stress-induced PCD has also been implicated in the pathophysiology of neurodegenerative and cardiovascular diseases (Sherman and Goldberg 2001; Kaufman 2002). Chronic or severe ER stress can contribute to the protein aggregation in the ER, thereby signaling from pro-survival to caspase-mediated pro-apoptotic conditions. Several molecules, including GADD153, Bax/Bak, caspase-12, and IRE1 are reported to be associated in the ER stress-induced cell death, indicating that the ER may also regulate apoptosis by sensitizing the mitochondria to a variety of extrinsic and intrinsic stimuli (Rao *et al.*, 2002; Yamaguchi *et al.*, 2004). In response to chronic ER stress, the damaged cells are committed to cell death and this process is mediated by ATF4 and ATF-6, as well as the activation of JNK/AP-1/GADD153 pathway (Kim *et al.*, 2006).

GADD153-deficient MEFs are resistant to ER stress-induced cell death (Zinszner *et al.*, 1998). GADD153 sensitizes ER stress-induced cell death through down regulation of Bcl2 (McCullough *et al.*, 2001). The balance between GRP78 and GADD153 expression regulates the UPR-mediated cell survival or cell death. Furthermore, earlier studies by Nakagawa *et al.* (2000) have shown that caspase-12 is involved in ER stress-mediated PCD given that mice-deficient in caspase-12 were resistant to ER stressors. It is suggested that ER stress causes translocation of cytosolic caspase-7 to the ER surface, resulting in the activation of caspase-12 (Rao *et al.*, 2001). Prolonged ER stress facilitates the movement of active caspase-12 to the cytoplasm, where it interacts with pro-caspase-9. Activated caspase-9 cleaves caspase-3 and activates the apoptotic cascade. It is reported that overexpression of caspase-12 promotes PCD, which can be blocked by a general caspase inhibitor and can also be partially inhibited by overexpression of anti-apoptotic Bcl-2 member protein Bcl-x_L (Nakagawa *et al.*, 2000). Interestingly, Saleh *et al.* (2006) demonstrated that caspase $12^{-/-}$ MEFs were not resistant to ER stressors, including thapsigargin, indicating that caspase 12 may not be involved in the ER stress-induced apoptosis. It is important to mention that the human homolog of caspase 12 is silenced by several mutations. Additional studies are still required to explain which caspases are involved in the ER stress-induced PCD.

1.5.3 Apoptotic cell death in the development and progression of atherosclerosis

Studies have identified apoptotic cells in animal and human atherosclerotic lesions (Tedgui and Mallat 2001; Zhou *et al.*, 2005). PCD plays an important role in the

formation of the necrotic core (Bennet 1999), and it is proposed that apoptotic macrophages and smooth muscle cells influence plaque stability. Extracellular lipid within the necrotic core may determine the progression of plaque towards thrombosis. SMC death weakens the fibrous cap and can result in plaque rupture. On the other hand, apoptosis of T-lymphocytes and macrophages might be beneficial to plaque stability because it attenuates the inflammatory response (Tedgui and Mallat 2001). The observation that heterogeneous apoptosis of macrophages occurs within the plaque further supports the hypothesis that some regions may be predisposed to rupture (Kolodgie *et al.*, 2000). Interestingly, tissue factor (TF), a key initiator of the coagulation cascade, is highly expressed in human atherosclerotic plaques (Toschi *et al.*, 1997). Atherosclerotic plaques from patients with unstable angina were shown to express increased TF activity, compared to patients with stable angina (Ardissino *et al.*, 1997). It is known that TF activity is dependent on phosphatidylserine (PS), a phospholipid involved in PCD (Pei *et al.*, 1993). Several studies have shown that PCD can contribute to the redistribution of PS (Martin *et al.*, 1997), thereby promoting a procoagulant environment (Casciola-Rosen *et al.*, 1996).

Although it is believed that PCD increases atherosclerotic lesion development, studies on pro-apoptotic mice models provide contradictory results. The absence of cell cycle (p53 or Rb) or proapoptotic (Bax) genes surprisingly accelerates atherosclerotic lesion development in apoE$^{-/-}$ mice (Guevara *et al.*, 1999; Liu *et al.*, 2004; Boesten *et al.*, 2006). Mice lacking both apoE and p53 show accelerated aortic atherosclerosis but no difference in apoptotic cell death (Guevara *et al.*, 1999). Subsequent studies by van

Vlijmen *et al.* (2001) have demonstrated that macrophages deficient in p53 contribute to enhanced aortic atherosclerosis. Herein, authors have reconstituted apoE*3-leiden mice with *p53*$^{-/-}$ bone marrow and have shown increased atherosclerotic lesion size with increased necrosis and decreased apoptosis, indicating a suppressing role for macrophage p53 in atherosclerotic lesion progression. In addition, deficiency of Bax, an important pro-apoptotic protein of the Bcl-2 family, resulted in accelerated atherosclerosis in apoE$^{-/-}$ mice (Liu *et al.*, 2004). Similar to the findings of Vlijmen *et al.* (2001), authors have reported reduced macrophage apoptosis following reconstitution of LDLR$^{-/-}$ mice with Bax$^{-/-}$ bone marrow, supporting a protective role of macrophage apoptosis in the atherosclerotic lesion progression. Consistent with the findings from apoE$^{-/-}$ or Bax$^{-/-}$ mice, deficiency of macrophage retinoblastoma (Rb), a pro-apoptotic protein, also promotes increased atherosclerosis in apoE$^{-/-}$ mice with increased lesional macrophage proliferation (Boesten *et al.*, 2006). It is conceivable that deficiency of pro-apoptotic factors, including p53, Bax or Rb, may contribute to reduced apoptotic activity in macrophages, thus resulting in an increased atherosclerotic lesion size. Further, macrophage apoptosis may be a mechanism to suppress lesion size. However, the role for PCD is still unknown in atherosclerotic lesion stability and thrombogenicity.

1.6 Project hypothesis, rationale and experimental objectives

In vitro and *in vivo* studies have suggested that HHcy promotes endothelial cell injury and/or dysfunction, smooth muscle cell proliferation and collagen synthesis, decreased availability of nitric oxide production, oxidation of LDL particles, and increased

expression of inflammatory molecules - all of which may contribute to atherosclerotic lesion development (de Koning *et al.*, 2003). This project was initiated in an attempt to identify genes whose expression levels were significantly changed in cultured human vascular endothelial cells treated with homocysteine. It was hypothesized that the identification of such genes would greatly facilitate the investigation of how HHcy promotes endothelial cell dysfunction and potentially atherosclerosis. While earlier studies have identified several homocysteine-responsive genes involved in the development and progression of atherosclerosis, none of these studies have identified homocysteine-responsive pro-apoptotic genes that modulate atherogenesis. The discovery of such genes would be important given that the presence of apoptotic cells within atherosclerotic lesions increases the risk of lesion rupture.

Following identification of TDAG51 as a homocysteine-inducible, pro-apoptotic gene, we speculated that this discovery would allow us to further explain the significance of apoptosis in atherosclerotic lesion progression. Thus, it was hypothesized that TDAG51 contributes to the development and progression of atherosclerosis through its pro-apoptotic characteristics. The overall objective of this project was to investigate the role of TDAG51 in the development and progression of atherosclerosis. Specific objectives include **(i)** assessing the relationship between ER stress and TDAG51 expression **(ii)** examing the cellular function of TDAG51 and **(iii)** investigating the significance of TDAG51 in atherosclerosis.

We have provided novel evidence that overexpression of TDAG51 induces PCD by impairing cell adhesion and contributes to the development of atherosclerosis in apoE-

deficient mice with diet-induced HHcy (Hossain *et al.*, 2003). Furthermore, our findings demonstrate that TDAG51 **(i)** is induced by homocysteine through a mechanism involving ER stress, **(ii)** promotes detachment-induced PCD in cells relevant to atherosclerosis, and **(iii)** is increased and correlates with PCD in atherosclerotic lesions from apoE$^{-/-}$ mice with diet-induced HHcy. In addition, we have generated mice deficient in both TDAG51 and apoE genes to investigate the causal relationship between TDAG51 and the atherosclerotic lesion development. We demonstrated that the loss of TDAG51 attenuates the development and progression of atherosclerosis in apoE$^{-/-}$ mice fed normal chow diet. As well, deficiency of TDAG51 promotes migration and proliferation of MEFs. Furthermore, TDAG51 overexpression in cultured endothelial cells increases the expression of TF, an initiator for blood coagulation. Given that apoptotic cells from atherosclerotic lesions have increased TF activity (Toschi *et al.*, 1997), further studies will be necessary to address whether there is any association between increased TF activity and/or expression and elevated TDAG51 expression within the atherosclerotic plaque. Taken together, our studies provide evidence that TDAG51 may have a role in plaque growth and/or stability, thereby contributing to the development and progression of atherosclerosis.

Despite several studies, the underlying mechanism by which TDAG51 contributes to atherosclerosis remains to be elucidated. It is possible that loss of TDAG51-decreasing PCD may reduce chemotaxis of monocytes to the atherosclerotic lesions. Further, since deficiency of TDAG51 attenuates atherogenesis, one would speculate that the primary function of TDAG51 is to regulate apoptosis of cells relevant to

atherosclerosis. However, this concept was contradicted by several studies demonstrating enhanced atherosclerotic lesions in mice following loss of cell cycle or pro-apoptotic genes, including p53, Bax or Rb in macrophages (Guevara *et al.*, 1999; Liu *et al.*, 2004; Boesten *et al.*, 2006). Interestingly, the atheroprotective role of TDAG51 can in part be explained by the observation that PPAR-γ expression is upregulated in TDAG51$^{-/-}$ MEFs and within atherosclerotic lesion from DKO mice. Earlier studies reported that PPAR-γ has both anti-inflammatory and atheroprotective properties (Lehrke and Lazar 2005). Further, PPARγ can enhance reverse cholesterol transport in lesion-resident macrophages (Chawla *et al.*, 2001; Chinetti *et al.*, 2001) and activation of PPAR-γ by pioglitazone and rosiglitazone increases macrophage cell death in advanced atherosclerosis (Thorp *et al.*, 2007). It is therefore conceivable that TDAG51 is a unique negative regulator of PPAR-γ and its downstream gene targets.

In our working model, we propose that cardiovascular risk factors contribute to ER stress. ER stress can then promote increased TDAG51 expression that may lead to increased plaque growth, decreased plaque stability and/or increased plaque thrombogenicity - all of which may ultimately result in atherothrombosis (**Figure 6**).

In brief, our findings demonstrate that TDAG51 mediates PCD, is involved in cell migration and proliferation, and contributes to the development of atherosclerosis. This thesis will provide further insight into the molecular mechanisms by which TDAG51 may promote the development of atherosclerosis, thereby providing opportunities for the development of therapeutic modalities useful in the treatment of cardiovascular disease.

Figure 6: Working Model linking ER Stress, TDAG51, and Atherothrombosis

Cardiovascular risk factors can cause ER stress. Increased ER stress may induce the expression of the pro-apoptotic gene, TDAG51, which has been shown to promote detachment-induced programmed cell death (PCD) in cell lines relevant to atherothrombosis. Based on our current findings, we have postulated that TDAG51-induced PCD may decrease plaque stability and may increase plaque thrombogenicity. Further, TDAG51 could potentially increase plaque growth by decreasing the expression of PPAR-γ, a transcription factor having anti-inflammatory and atheroprotective properties. Together, all these may lead to atherothrombotic disease.

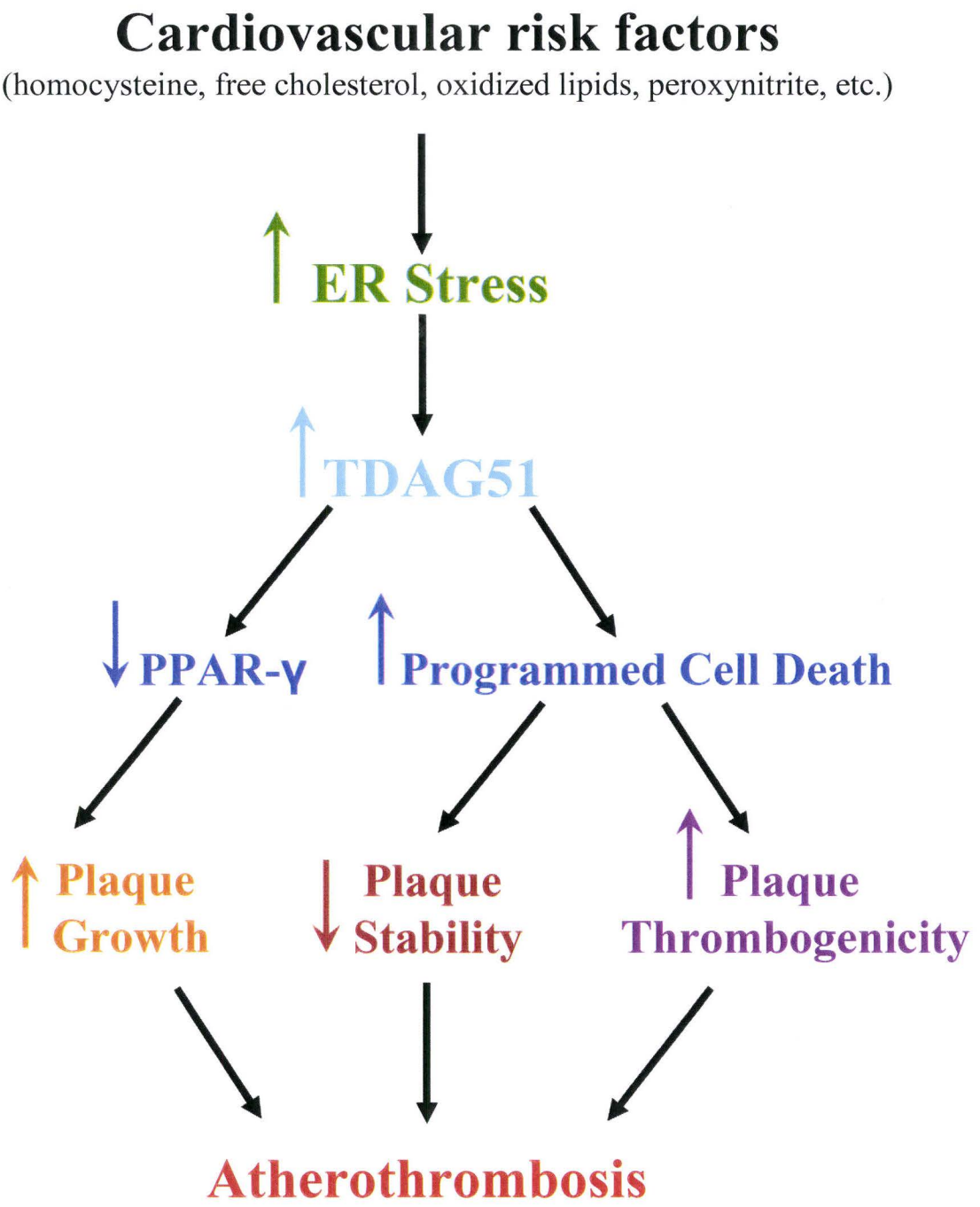
Cardiovascular risk factors
(homocysteine, free cholesterol, oxidized lipids, peroxynitrite, etc.)
ER Stress
TDAG51
PPAR-γ
Programmed Cell Death
Plaque Growth
Plaque Stability
Plaque Thrombogenicity
Atherothrombosis

CHAPTER 2: TDAG51 is an ER stress response pro-apoptotic gene and a mediator of atherosclerosis

2.1 Introduction

Studies using apoE$^{-/-}$ mouse model have established a causal association between HHcy and accelerated atherosclerosis (Hofmann *et al.*, 2001; Zhou *et al.*, 2001). In earlier studies, it was suggested that the thiol group of homocysteine may undergo auto-oxidation to generate ROS and thus may cause cell injury or dysfunction through a mechanism involving oxidative stress (Starkebaum and Harlan 1986; Loscalzo 1996). This auto-oxidation hypothesis, however, fails to explain why cysteine, another thiol containing amino acid, does not cause cell injury and is not a risk factor for CVD. Cysteine is present in plasma at much higher concentrations than homocysteine (Jacobsen 2000 & 2001). We as well as others have demonstrated that homocysteine acts intracellularly to disrupt protein folding in the ER, thereby resulting in the activation of UPR and increased expression of several ER stress response genes, including GRP78, GRP94, GADD153, Herp and RTP (Outinen *et al.*, 1998 & 1999; Kokame *et al.*, 1996 & 2000). In addition, studies have reported that homocysteine-induced ER stress promotes PCD in cultured human vascular endothelial cells through a mechanism involving activation of the UPR and that this process requires activation of caspase 3 (Cai *et al.*, 2000; Zhang *et al.*, 2001). Although these studies suggest an association between

homocysteine and PCD, additional studies are required to identify pro-apoptotic factors involved in this process and their importance in the development of atherosclerosis.

Herein, we have demonstrated that homocysteine induces the expression of TDAG51, a member of the pleckstrin homology-related domain family (Park *et al.*, 1996; Frank *et al.*, 1999). Further, TDAG51 expression was upregulated by ER stress agents, including homocysteine, tunicamycin, thapsigargin, dithiothreitol and peroxynitrite. Overexpression of TDAG51 caused morphological changes, decreased cell adherence and promoted detachment-mediated PCD. MEFs deficient in TDAG51 demonstrated significant resistant from ER stress-induced cell death. Consistant with these *in vitro* findings, TDAG51 expression and PCD were increased and co-localized in the atherosclerotic lesions from apoE$^{-/-}$ mice having diet-induced HHcy. These observations support our hypothesis that the ER stress-inducible gene, TDAG51, is associated with the development of atherosclerosis. In summary, these studies provide novel evidence that TDAG51 is induced by homocysteine, promotes detachment-mediated PCD, and is associated with atherosclerotic lesion development observed in HHcy (Hossain *et al.*, 2003).

2.2 Materials and Methods

2.2.1 Materials

Tissue culture flasks and dishes, 6-, 12- and 96-well tissue culture plates, plastic tubes, disposable pipettes, needles and syringes were obtained from Becton Dickinson (Franklin Lakes, NJ). Acrodisc® syringe filters were purchased from Pall Gelman Laboratory (Ann Arbor, MI). Cryogenic vials were purchased from NalgeNunc International (Rochester, NY). Microcentrifuge tubes, thin-walled PCR tubes and pipette tips were purchased from DiaMed Lab Supplies (Mississauga, ON). Dulbecco's modified eagle medium (DMEM), Hank's balanced buffered saline, trypsin/ethylenediaminetetra-acetic acid (trypsin/EDTA) and penicillin/streptomycin were obtained from GIBCO BRL (Burlington, ON). EGM-2 medium supplemented with FBS, hydrocortisone, hFGF, VEGF, R^3-IGF-1, ascorbic acid, hEGF, GA-100 and heparin were purchased from Clonetics (Walkersville, MD).

DL-Homocysteine, L-cysteine, L-methionine, dithiothreitol (DTT), thapsigargin, ampicillin, kanamycin, diethyl pyrocarbonate (DEPC), β-mercaptoethanol, hydrogen peroxide, xylene, hexane, Na-uric acid, dimethyl sulfoxide, Ponceau s solution, 3-(N-morpholinol) propanesulphonic acid (MOPS), 4', 6-diamidino-2-phenylinole (DAPI), xylene cyanol FF, collagenase type IA from *Clostridium histolyticum*, gelatin type B bovine skin, bovine serum albumin fraction V (BSA), fetal bovine serum (FBS), ethidium bromide (EtBr) and β-actin antibody were purchased from Sigma (St. Louis, MO). The NO donor DETA-NoNoate was from Cayman, peroxynitrite donor 3-morpholino-sydnonimine hydrochloride (Sin-1) from Dojindo (Gaithersburg, MD). Peroxynitrite was

obtained from Calbiochem (Darmstadt, Germany). Nitrocellulose and Zeta-Probe GT nylon membranes, bromophenol blue, Coomassie brilliant blue G-250, ammonium persulfate (APS), prestained SDS-PAGE standards, t-octylphenoxypolyethoxyethanol (Triton X-100), poloxyethylenesorbitan monolaurate (TWEEN-20), 30% acrylamide solution, 1.5 M Tris-HCl buffer (pH 8.8), 0.5 M Tris-HCl buffer (pH 6.8), 10% (w/v) SDS solution and N,N,N',N'-tetramethylenediamine (TEMED) were obtained from Bio-Rad Laboratories (Mississauga, ON).

Acetone, diethlylether, propan-2-ol, hydrochloric acid, glycerol, potassium chloride, paraformaldehyde, potassium dihydrogen orthophosphate, dipotassium hydrogen orthophosphate, potassium acetate, potassium chloride, sodium dihydrogen orthophosphate, disodium hydrogen orthophosphate, ethylenediaminetetraacetic acid disodium salt (EDTA), and formamide were purchased from BDH (Toronto, ON). Chloroform, methanol and glacial acetic acid were obtained from Caledon Laboratories (Georgetown, ON). Sodium citrate, glycine, urea, sodium dodecyl sulphate (SDS), tris(hydroxymethyl)aminomethane (Tris) and sodium chloride were purchased from Bioshop Canada (Burlington, ON). Formaldehyde solution (37%) and iso-propyl alcohol were obtained from ACP Chemicals (Montreal, PQ). Buffer-saturated phenol was obtained from GIBCO BRL. Anhydrous ethanol was purchased from Commercial Alcohols (Brampton, ON). Sodium acetate trihydrate was obtained from EM Industries (Darmstadt, Germany).

Restriction endonucleases, one kb DNA Ladder, T4 DNA ligase, 10X DNA ligase buffer, DH5α^{TM} competent cells, DM1^{TM} competent cells, PCR SuperMix, and agarose

were purchased from GIBCO BRL. One shot™ TOP10 cells and zeocin™ were purchased from Invitrogen (Burlington, ON). Bacto-yeast extract, bacto-tryptone, and bacto-agar were obtained from Difco Laboratories (Detroit, MI). [α^{35}P] dCTP (specific activity > 3000 Ci/mmol), [α^{35}S] dATP (specific activity > 1318.0 Ci/mmol), Renaissance Chemiluminescence Reagents, and Kodak X-OMAT film were obtained from Dupont/NEN (Mississauga, ON). Liquid scintillation cocktail was purchased from Beckman Instruments (Fullerton, CA). RNase Zap was purchased from Ambion (Austin, TX).

RNeasy total RNA Kit, QIAquick nucleotide extraction kit, QIAEX II agarose gel extraction kit, QIAprep spin plasmid kit, QIAGEN endo-free plasmid medi kit, and Superfect™ transfection reagent kit were purchased from QIAGEN (Valencia, CA). Random primed DNA labeling kit was obtained from Boehinger Mannheim (Montreal, PQ). pCR®-Blunt vector was purchased from Invitrogen (Burlington, ON). pEGFP-C1 vector was obtained from CLONTECH Laboratories (Palo Alto, CA). *In situ* cell death detection kit (Fluorescein and TMR red) and cytotoxicity detection kit were obtained from Roche Diagnostics (Indianapolis, IN).

A polyclonal antibody to TDAG51 (anti-TDAG51) was obtained from Santa Cruz Biotechnology (Santa Cruz, CA). Monoclonal antibody to Grp78/94 (anti-KDEL) was purchased from StressGen Biotechnologies (Victoria, BC). Horseradish peroxidase (HRP)-conjugated rabbit anti-goat, sheep anti-rabbit or goat anti-mouse IgG were obtained from DakoCytomation (Glostrup, Denmark). Alexa™ 488- or 594-conjugated donkey anti-mouse, donkey anti-goat and donkey anti-rabbit were obtained from

Molecular Probes (Eugene, Oregon). PermaFluor mountant medium was obtained from Thermo electron corporation (Pittsburgh, USA).

Primers AB19652 (5'-CTT AAG CTT CTT ATG CTG GGA GGA TGC TG-3'), AB19653 (5'-GAA TTC TAG ATC AGG CAG AGT TGG AGG TGC T-3'), L1F (5'-CT TAA GCT TCT GCC ACC ATG GCT CTG GAG AGT AGC GGC TGC AAA-3'), L1R (5'-G AAT TCT AGA TCA CCC CTG CCC GGG CTG TTG TTG CTG CTG-3'), L2R (5'-G AAT TCT AGA TCA CAT CTG CAG CGT GAT CTC GGC GTT CCA-3'), L3F (5'-CT TAA GCT TCT GCC ACC ATG GCT CCG GCC GAG CCG TCC CAA CCC-3'), L3R (5'-G AAT TCT AGA TCA CTG CTG GGG CTG AGG CTT GGG TTG GGG-3'), L4F (5'-CT TAA GCT TCT GCC ACC ATG GCT CAG CAC CTG GTC CAG CAG CAG-3'), L5R (5'-G AAT TCT AGA TCA GGC AGA GTT GGA GGT GCT GCG GAG AAG-3'), L7F (5'-CT TAA GCT TCT GCC ACC ATG GCT CAC CCG TAT CCG CAT CCA CAT-3'), WT 1 (5'-CCG CAG CAC CTC CAA CTC TGC CTG-3'), WT 2 (5'-GTC TTC AAA TAC AAT GAA AGA GTC G-3'), TDAG51 KO 1 (5'-AAA TGG AAG TAG CAC GTC TCA CTA GTC TCG-3') and TDAG51 KO 2 (5'-AGA GCA GCC GAT TGT CTG TTG TGC CCA GTC-3') were synthesized at the MOBIX, McMaster Institute for Molecular Biology and Biotechnology (Hamilton, ON).

All other chemicals, reagents, and materials were of the highest quality available.

2.2.2 Methods

2.2.2.1 PCR amplification of open reading frame (ORF) and functional domains in TDAG51

The cDNA encoding the ORF of human TDAG51 was amplified from the EST cDNA clone, AI589460, by polymerase chain reaction (PCR) using Vent DNA polymerase (New England Biolabs, Mississauga, ON). The forward primer AB19652 (5'-CTT AAG CTT CTT ATG CTG GGA GGA **TGC** TG-3') contained a terminal *Hind*III restriction site (underlined) prior to the initiating ATG (bold). The reverse primer AB19653 (5'-GAA TTC TAG A**TC** AGG CAG AGT TGG AGG TGC T-3') contained a terminal *Xba*I restriction site (underlined) adjacent to the termination codon (bold). Parameters for the 35 cycles of PCR after denaturing once at 94°C for 3 min were as follows: denaturation at 94°C for 1 min, annealing at 55°C for 1 min, and extension at 72°C for 1 min.

The functional domains of TDAG51 **(Figure 7)** were PCR amplified using SolGent Tag DNA polymerase kit (Taejeon, South Korea). Seven fragments containing *Hind*III and *Xba*I restriction sites were generated using the following primers: L1F, L2R, L3F, L3R, L4F, L5R, L7F. Parameters for the 40 cycles of PCR following one cycle of denaturation at 94°C for 5 min were as follows: denaturation at 94°C for 20 sec, annealing at 68°C for 40 sec, and extension at 72°C for 2 min.

2.2.2.2 DNA extraction and purification from agarose gels

Following PCR, 5 µl of 6X loading dye [25% (w/v) bromophenol blue, 25% (w/v) xylene cyanol FF, 30% (w/v) glycerol in ddH_2O] was added to 25 µl of PCR amplified DNA samples, loaded onto 0.8% (w/v) agarose in TAE buffer [40 mM Tris-acetate, 1.0 mM EDTA] containing ethidium bromide (0.5 µg/ml), and run for 1 h at 45-65V. After visualizing the gel using an ultraviolet transilluminator (Ultra-Violet Products, Upland,

Figure 7: Functional domains within the TDAG51 open reading frame (ORF)

The TDAG51 gene encodes 260 amino acids, including a long stretch of glutamine (Q) residues near the N-terminus, proline-glutamine (PQ) and proline-histidine (PH) repeats are located near the C-terminus. TDAG51 also contains a N-terminal pleckstrin homology-like domain. Further, there is a nuclear localization signal (NLS) and a nuclear export signal (NES) toward N-terminal of the protein. L1-L7, regions within TDAG51 that will be expressed to define the functional domain(s) responsible for detachment-induced PCD.

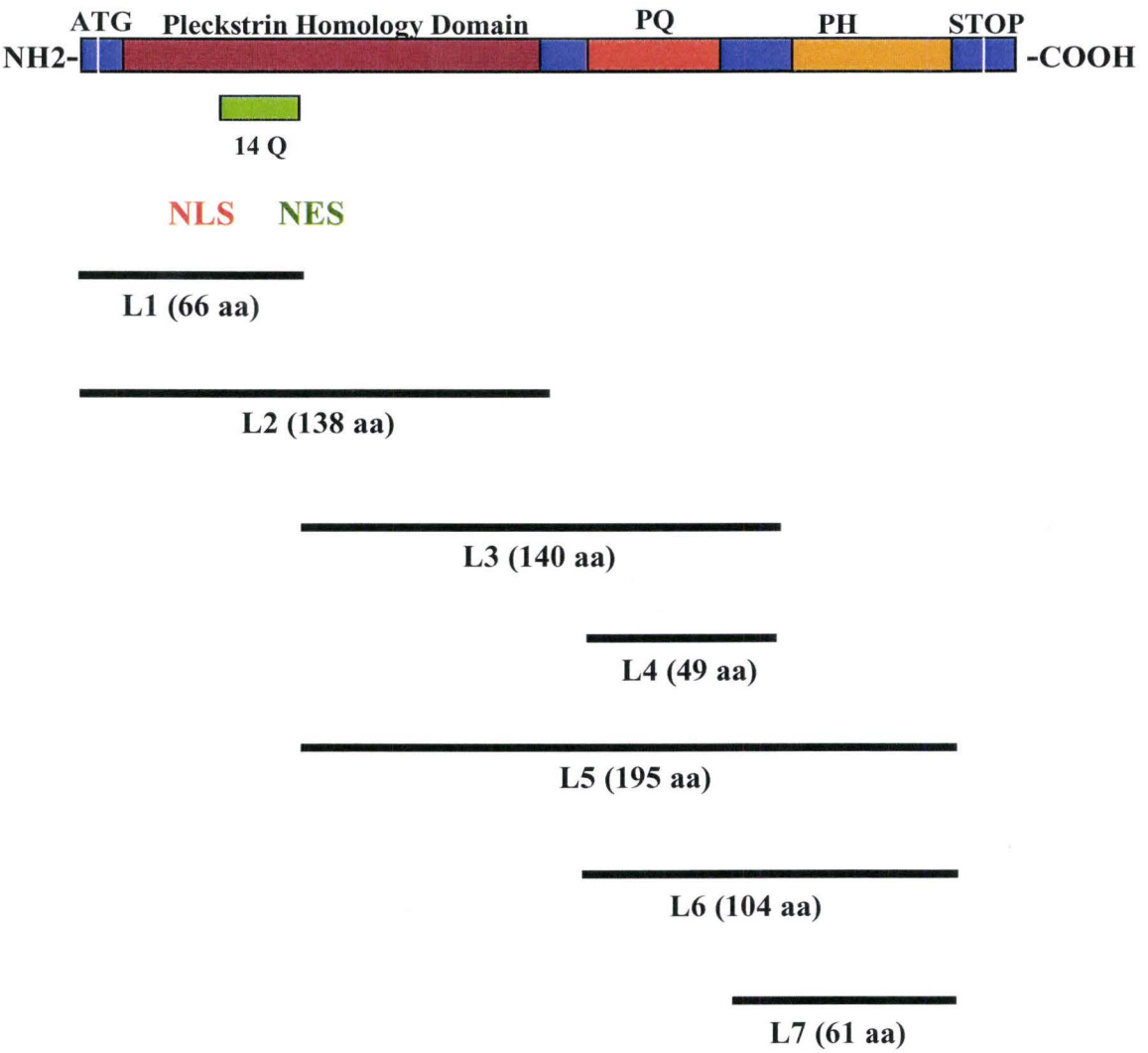
ATG
Pleckstrin Homology Domain
PQ
PH
STOP
NH2-
-COOH
14 Q
NLS
NES
L1 (66 aa)
L2 (138 aa)
L3 (140 aa)
L4 (49 aa)
L5 (195 aa)
L6 (104 aa)
L7 (61 aa)

CA), an image of the gel was captured using a Pharmacia gel documentation system and VDS ImageMaster software (Pharmacia Biotech, Baie d'Urfe', PQ). The PCR band of expected size was cut from the agarose gel and purified using the QIAEX II agarose gel extraction kit (QIAGEN, Valencia, CA). Briefly, the DNA was excised from the gel, weighed, and mixed with three volumes of solublization QX1 buffer and 20 µl of QIAEX II (silica-gel beads). Following solublization of the agarose gel slice, DNA absorbed to the beads was pelleted by centrifugation, and washed once in a high salt buffer and twice in an ethanol solution to remove all the non-nucleic acid impurities. DNA was then eluted from the beads by adding 20 µl of ddH_2O. The supernatant containing the purified DNA was collected following centrifugation, analyzed by agarose gel electrophoresis, and cloned into PCR Blunt vector, as described in section 2.2.2.3.

2.2.2.3 Subcloning of TDAG51 ORF and functional domains into pCR® Blunt vector

Gel purified TDAG51 ORF and functional domain fragments were subcloned into pCR® Blunt vector (Invitrogen, Burlington, ON). The ligation reaction was performed by incubating 1 µg of pCR® Blunt vector and 5 µg of blunt ended gel purified TDAG51 fragments in 1 µl of 10X ligation buffer and in 1 µl of T4 DNA ligase at a final volume of 10 µl at 16°C for 1 h. One shot™ TOP10 cells were transformed with the ligation mixture and screened for colonies containing the recombinant plasmid. Briefly, 2 µl ligation reaction mixture was mixed with 50 µl of One shot™ TOP10 cells and incubated on ice for 30 min. The cells were heat-shocked for 45 sec at 42°C, placed on ice for 10

min, and incubated in 250 µl of SOC medium [2% (w/v) tryptone, 0.5% (w/v) yeast extract, 0.05% (w/v) NaCl, 2.5 mM KCl, 10 mM $MgCl_2$, 20 mM glucose] for 1 h at 37°C with constant shaking. Bacterial cells (20-50 µl) were plated onto low salt LB media plates [1% (w/v) bacto-tryptone, 0.5% (w/v) bacto-yeast extract, 0.5% (w/v) NaCl, pH 7.5] containing 1.5% (w/v) bacto-agar supplemented with zeocin™ (25 µg/ml) and incubated overnight at 37°C. Plates were stored at 4°C and zeocin™ resistant bacterial colonies containing recombinant plasmid DNA were isolated. Five to 10 single clear colonies were grown overnight in 3 ml of LB media [1% (w/v) bacto-tryptone, 0.5% (w/v) bacto-yeast extract, 1% (w/v) NaCl, pH 7.5] supplemented with zeocin™ (25 µg/ml) at 37°C shaker.

Plasmid DNA was extracted and purified from bacterial cells using the QIAprep spin plasmid kit (QIAGEN) according to manufacturer's instruction. Briefly, bacterial cells from 3 ml overnight cultures were pelleted by centrifugation, resuspended in P1 buffer, lysed in P2 buffer under alkaline condition and neutralized in N3 buffer. Following centrifugation, the supernatant was applied to a QIAprep spin column. The spin column was then washed in PB buffer and PE buffer. Plasmid DNA absorbed to the silica-gel membrane was eluted in 50 µl of ddH_2O.

DNA isolated from minipreps was digested with *Hind*III and *Xba*I to confirm the size of TDAG51 inserts. Three µg of purified pCR® Blunt vector-TDAG51 insert plasmid DNA was incubated with 1 U of *Hind*III and *Xba*I restriction enzymes in 1 µl of 10X REact2 with a final volume of 10 µl at 37°C for 2 h. DNA was separated on 0.8%

agarose gels containing ethidium bromide and analyzed. Clones demonstrating the presence of appropriate size TDAG51 ORF or functional domain inserts were sequenced.

2.2.2.4 Construction of mammalian expression plasmids encoding pEGFP and TDAG51 inserts

The pCR® Blunt-TDAG51 insert vectors were digested with *Hind*III and *Xba*I. The TDAG51 inserts were then gel-purified and cloned in frame into the *Hind*III/*Xba*I sites of pEGFP-C1 (CLONTECH Laboratories) generating a fusion protein of mammalian codon-optimized enhanced GFP protein with TDAG51 inserts linked to its C-terminus. In brief, the ligation reaction was performed after incubating 5 μg of TDAG51 inserts, 1 μg of pEGFP-C1 vector, 1 μl of 10X DNA ligase buffer, and 1 μl of T4 DNA ligase at 16°C for 1 h. Following ligation, 2 μl of recombinant plasmid DNA was added with 50 μl of DM1™ competent cells, incubated on ice for 30 min, heat-shocked for 45 sec at 37°C, placed on ice for 10 min, and mixed with 950 μl of LB media. After 3 h of shaking at 37°C, bacterial cells were plated onto LB media plates containing 1.5% (w/v) bacto-agar supplemented with kanamycin (50 μg/ml) and incubated overnight at 37°C. Kanamycin resistant colonies were cultured and plasmid purified as described in section 2.2.2.3. Authenticity of the plasmid containing appropriate insert was confirmed by restriction digestion and sequencing as described in sections 2.2.2.3.

2.2.2.5 Isolation of endotoxin-free plasmid DNA

Endotoxin-free plasmid DNA was isolated using the QIAGEN EndoFree Plasmid Midi Kit (QIAGEN, Valencia, CA). Single colony transformed with pEGFP-C1 (designated GFP) or pEGFP-C1-TDAG51 insert plasmids were cultured overnight at 37°C in 4 ml of LB media containing kanamycin (50 μg/ml) with constant shaking. One hundred μl of the culture was added to 100 ml of fresh LB media supplemented with kanamycin and incubated overnight at 37°C shaker. Cultures were harvested by centrifugation at 3000 x *g* for 25 min. The bacterial pellet was resuspended in P1 buffer, lysed in P2 buffer at room temperature for 5 min, neutralized in P3 buffer, and immediately centrifuged. The supernatant was then mixed with ER buffer and incubated on ice for 30 min. The solution was then applied to QIAGEN-tip 100 column equilibrated in QBT buffer and allowed to flow through by gravity. Following washing the column in QC buffer, DNA absorbed to the column was eluted in QN buffer. DNA was precipitated in 0.7 volume of isopropanol, washed in endotoxin-free 70% ethanol, dried for 5-10 min, and dissolved in endotoxin-free TE buffer. Authenticity of the insert was reconfirmed by restriction digestion and sequencing as stated in section 2.2.2.3.

2.2.2.6 Generation of radiolabeled probes

Following gel purification, probes were labeled to high specific activity with [α-^{32}P] dCTP (NEN) using a Random primed DNA labeling kit (Boehringer Mannheim, Montreal, PQ). Briefly, ddH_20 was added to 2 μg of purified DNA to make the final volume of 9 μl, heated at 100°C for 10 min, cooled down on ice, mixed with 5 μl of 4X reaction mixture (3 μl of a 1:1:1 mixture of dATP, dGTP, dTTP along with 2 μl of

hexanucleotide mixture), 5 µl of [α-^{32}P] dCTP, 1 µl of Klenow enzyme, and incubated the mixture for 1 h at 37°C. The unincorporated nucleotides were removed using the QIAquick nucleotide removal kit (QIAGEN, Valencia, CA). Ten volumes of PN buffer were mixed with the labeled probe mixture, applied to the QIAquick spin column, and centrifuged at 6000 x *g* for 1 min. Following washing twice in PE buffer, DNA was eluted in 50 µl of ddH_2O. Specific activity of the probe was measured using a Beckman LS 6000LL β-counter (Beckman Instruments, Fullerton, CA).

2.2.2.7 Northern blot analysis

Preparation of total RNA

Total RNA was isolated using the RNeasy total RNA kit (QIAGEN, Valencia, CA) according to the manufacturer's protocol. Briefly, following treatment, cells were washed with 1X PBS and lysed in RLT lysis buffer containing β-mercaptoethanol (14.5 M). Cell lysates were removed from the culture flasks using a rubber policeman and homogenized with a plastic syringe fitted with a 20 gauge needle. An equal volume of 70% ethanol was added to the homogenized lysates, and the samples were applied to a RNeasy spin column. Following a brief centrifugation (15 sec at 8,000 x *g*), total RNA bound to the spin column was washed in RW1 buffer. RPE buffer was then applied to the spin column, and centrifuged for 15 sec at 8,000 x *g*. After a final wash in RPE buffer for 2 min at full speed, total RNA was eluted by pipetting 30-50 µl of diethyl pyrocarbonate-treated water directly onto the spin column membrane and centrifuging the samples for 1 min at 8,000 x *g*. Quantification and purity of the RNA was assessed by

A_{260}/A_{280} absorbance, and the RNA samples with ratios above 1.6 were stored at -70°C for further analysis.

Fractionation of total RNA and northern transfer

Total RNA (10 μg per lane) was size fractionated on 2.2 M formaldehyde/1.2% agarose gels, transferred overnight onto Zeta-Probe GT nylon membranes in 10X SSC as previously described (Outinen *et al.*, 1998 & 1999). The RNA was cross-linked to the membranes using a stratagene UV Stratalinker™ 2400 (La Jolla, CA) before hybridization.

Prehybridization and hybridization

Prehybridization and hybridization buffer consisted of 40% formamide, 0.12 M di-sodium hydrogen orthophosphate, 0.25 M sodium chloride, 5% SDS, and 1 mM EDTA in DEPC water. The Techne Hybridizer HB-1D rotisserie style hybridization oven (MANDEL Scientific Company, Guelph, ON) was used for all hybridization and washing procedures. Prehybridization was performed by incubating membranes with prehybridization buffer at room temperature for 10 min. Probes were labeled as described in section 2.2.2.6, heated at 100°C for 10 min, cooled on ice, and mixed with 10 to 15 ml of hybridization solution to obtain at least 1-3 X 10^6 cpm/ml. Overnight hybridization was carried out at 43°C. The membranes were then rinsed in 2X SSC, followed by three 15 min washes in: (i) 2X SSC/0.1% SDS, (ii) 0.5X SSC/0.1% SDS at room temperature, and (iii) 0.1X SSC/0.1% SDS at 43°C. Membranes were exposed to

Kodak X-OMAT film at -70°C for 1-10 days. Following autoradiography, the membranes were stripped by washing twice for 20 min at 100°C in a large volume of dehybridization solution (0.1X SSC, 0.5% SDS). Membranes were then hybridized with a cDNA fragment of human glyceraldehyde-3-phosphate dehydrogenase (GAPDH), using the same buffer and conditions as described above, to verify equal RNA loading in each lane.

2.2.2.8 Immunoblot analysis

Total cell lysates were solublized in 4X SDS-PAGE sample buffer [0.0625 M Tris-HCl, pH 6.8; 10% (w/v) glycerol; 20% (w/v) 10% SDS; 5% (w/v) β-mercaptoethanol; 5% (w/v) 1% bromophenol blue]. An equivalent amount of protein lysates were separated by electrophoresis on SDS-polyacrylamide gels under reducing conditions as described previously (Laemmli 1970). Separated proteins were then transferred electrophoretically onto nitrocellulose membranes using a Trans-Blot® Semi-Dry Transfer Cell apparatus (Bio-Rad Laboratories, Mississauga, ON) at 15 V for 1 h. Nonspecific protein binding sites were blocked overnight with TBST blocking buffer containing 5% milk [25 mM Tris, 0.05% (w/v) Tween-20, 5% (w/v) fat free skim milk powder] in a shaker at 4°C. After rinsing the membranes three times (15 min each) in TBST buffer containing 1% milk, the membranes were incubated with the primary antibody (in 1X TBST buffer) for 1 h at room temperature. Following washing three times in TBST buffer containing 1% milk, the membranes were incubated with horse radish peroxidase (HRP) conjugated secondary antibody (in 1X TBST buffer) for 1 h. The membranes were then washed

three times (15 min each) with 1X TBST buffer containing 1% milk. The membranes were developed with the Renaissance Chemiluminescence Reagents as directed by the manufacturer before exposing to the Kodak X-OMAT film.

2.2.2.9 Indirect immunofluorescence in cultured cell and tissue sections

After appropriate treatments, cells grown on coverslips were washed in 1X PBS and fixed in cold 4% paraformaldehyde [4% (w/v) paraformaldehyde, 0.2 M NaH_2PO_4, 0.2 M Na_2HPO_4]. Cells were then washed in 1X PBS, permeablized in 0.025% Triton X-100 (1X PBS) for 10 min on ice. Following 30 min of incubation with blocking buffer (3% BSA in 1X PBS), primary antibodies diluted in blocking buffer (1:50) were added to the coverslips for 1 h at 4°C. The coverslips were then washed in 1X PBS and incubated with Alexa^{TM} 488- or 594-conjugated secondary antibody diluted in blocking buffer (1:200) to detect primary antibody binding sites. Cells stained with normal serum or secondary only were used to normalize for non-specific immunofluorescence and considered as a negative control. The coverslips were allowed to dry after washing in 1X PBS and mounted onto slides using PermaFluor mountant medium. Immunofluorescence was examined by epifluorescence microscopy using a Zeiss Axioskop 2 microscope. Images were captured using CCD color video camera (Sony, Tokyo, Japan) and Northern Exposure Image Analysis/Archival Software (Empix, Mississauga, ON). For co-immunofluorescence studies, both primary antibodies were incubated together to specific coverslips for 1 h following blocking the cells. After washing the coverslips in 1X PBS, primary antibody binding sites were detected using appropriate Alexa^{TM} 488- or 594-

conjugated to secondary antibodies. Images were captured from mounted coverslips and analyzed as described earlier.

A Carl Zeiss LSM510 laser-scanning confocal microscope was used to examine immunofluorescently labeled HUVEC and HAEC to localize endogenously expressed TDAG51 and determine its co-localization with catalase, GRP78 and/or focal adhesion kinase. Optical sectioning was performed throughout the depth of the cells at 1.5 μm intervals, providing adequate special resolution to determine protein localization within regions of the cell and co-localization with other marker proteins.

Indirect immunofluorescence was further performed on paraffin-embedded aortic tissue sections from apoE-deficient mice fed control or hyperhomocysteinemic diets. Tissue sections were heated at 56°C to deparaffinize and dehydrated through a graded series of ethanol treatment (100%, 10 min; 95%, 10 min; 90%, 10 min; 80%, 10 min; 70%, 10 min). Sections were then treated in 0.3% H_2O_2 for 30 min to inactivate endogenous peroxidase. Following washing in 1X PBS, sections were incubated in proteinase K (20 μg/ml) for 30 min at 37°C, rinsed in 1X PBS, and placed in blocking buffer for 30 min. A goat polyclonal antibody to TDAG51 diluted in blocking buffer (1:12.5) was incubated with tissue sections for 1 h, and washed in 1X PBS. Primary antibody binding sites were detected using Alexa^{TM} 488-conjugated to donkey anti-goat diluted in blocking buffer (1:400). Normal goat IgG or secondary only was used to normalize for non-specific immunoflurescence. Sections were mounted with coverslips using PermaFluor mounting medium. Images were captured and analyzed as described above.

2.2.2.10 DAPI staining of nuclear DNA

Cells grown on coverslips were washed in 1X PBS, fixed in 4% paraformaldehyde overnight at 4°C, washed in ice cold 1X PBS, and incubated in the dark with DAPI (0.2 μg/ml) on ice for 5-10 min. The coverslips were then washed in 1X PBS, mounted onto slides using PermaFluor aqueous mounting medium. Images were captured and analyzed as described in section 2.2.2.9.

2.2.2.11 Transient transfection of cultured cells

Primary HUVECs or HAECs were cultured in EGM-2 medium supplemented with 2% FBS, 50 μg/ml gentamycin, 50 ng/ml amphotericin and a mixture of growth factors as described by the manufacturer. Transient transfections were performed using Superfect transfection reagent (QIAGEN, Valencia, CA) according to manufacturer's protocol. Superfect reagent assembles DNA into compact positively charged structures and ensures the entry of DNA into the nucleus of the cell. In short, a routine transient transfection experiment involved the addition of purified plasmid DNA and superfect transfection reagent mixture to 100 μl of incomplete medium (only EBM-2 medium). Following incubation for 10 min, 700 μl of complete medium (EGM-2 medium) was added, mixed and added to the cells previously washed in 1X PBS, and incubated at 37°C in a humidifier with 5% CO_2 for 2-3 h. Complete media was then added to the cells and incubated for time periods up to 48 h. Following transfections, coverslips were washed in 1X PBS, fixed in 4% paraformaldehyde, dried for 10 min, and mounted onto slides

using PermaFluor aqueous mounting medium. GFP or GFP-TDAG51 fusion protein expression was examined by epifluorescence microscopy using a Zeiss Axioskop 2 microscope. Images were captured and analyzed as described in section 2.2.2.9.

2.2.2.12 TdT-mediated dUTP Nick End Labeling (TUNEL) assay in cultured cells and tissue sections

HUVECs or HAECs (4 X 10^5 cells per well) were grown on gelatin-coated coverslips and transient transfections were performed as described in section 2.2.2.11 for periods up to 48 h using GFP or GFP-TDAG51 expression vectors. Both adherent and non-adherent cells were fixed in 4% paraformaldehyde in 1X PBS at 4°C on ice, washed in 1X PBS, and permeablized in 0.1% Triton X-100 in 0.1% sodium citrate. The TUNEL assay was then performed using *In situ* cell death detection kit (Roche Diagnostics, Indianapolis, IN) to identify DNA strand breaks (nicks) in apoptotic cells. In short, the 3'-nick ends were labeled by incubating for 1 h with 50 µl of reaction mixture having tetramethyl-rhodamine-dUTP and terminal deoxynucleotidyl transferase. As a result, terminal deoxynucleotidyl transferase (TdT) catalyzes the incorporation of labeled nucleotides to free 3'-OH DNA ends in a template-independent manner. Fixed cells in which terminal deoxynucleotidyl transferase was omitted served as a negative control. After washing in 1X PBS, the coverslips were mounted onto slides using PermaFluor aqueous mounting medium. Images were captured and analyzed as described in section 2.2.2.9.

Paraffin embedded apoE$^{-/-}$ mouse tissue sections were deparaffinized as described in section 2.2.2.9, followed by treatment with 0.3% H_2O_2, and washed in 1X PBS.

Sections were then incubated in proteinase K (20 μg/ml), washed in 1X PBS, permeablized in 0.1% Triton X-100 in 0.1% sodium citrate, and rinsed in 1X PBS. TUNEL assay was next performed as described above to identify apoptotic cells in tissue sections. The 3'-nick ends were labeled by incubating fluorescence-dUTP with terminal deoxynucleotidyl transferase. Following TUNEL staining, tissue sections were blocked with 3% BSA (in 1X PBS) and indirect immunofluorescence for TDAG51 was also performed as described in section 2.2.2.9 using Alexa^{TM} 594-conjugated to a donkey anti-goat secondary antibody. After rinsing in 1X PBS, sections were mounted with coverslips using PermaFluor aqueous mounting medium. Images were captured and analyzed as described in section 2.2.2.9.

2.2.2.13 DNA fragmentation assay

HUVECs or HAECs were treated for 24 h in the absence or presence of various concentrations of homocysteine (0.5-10 mM), 0.5 mM methionine, 0.5 mM cysteine, or 0.5 mM homocysteine. The cells (floating and adherent) were harvested by scraping, pelleted, lysed in 20 mM Tris-HCL, 10 mM EDTA, 0.5% Triton X-100, pH 8.0, on ice for 45 min. The nuclear pellet was collected by centrifugation and resuspended in 0.1 M Tris-HCl, pH 8.5, 5 mM EDTA, 0.2 M NaCl, 0.2% SDS (w/v), and 0.2 mg/ml proteinase K, at 37°C overnight. NaCl was added to a final concentration of 1.5 M, and the DNA was ethanol-precipitated and resuspended in Tris-EDTA, pH 8.0, containing 200 mg/ml DNase-free RNase A. Following overnight incubation at 37°C, the DNA was separated on a 2% agarose gel and visualized under UV light after staining with ethidium bromide.

2.2.2.14 Flow cytometry analysis

HAECs grown in 6-well plates were transiently transfected for up to 24 h with or without pEGFP-C1 plasmids encoding regions of TDAG51 ORF as described in section 2.2.2.11. Without fixation, adherent and non-adherent cells were collected. Following centrifugation, cell pellets were diluted in 1 ml of 1X PBS. The samples were then examined using flow cytometry to detect green fluorescence. During gating, cells transfected with pEGFP-C1 and superfect transfection reagent were considered as positive and negative control, respectively. Non-adherent transfected cells with green fluorescence were considered as the cells that were in process of apoptosis. Flow cytometry analysis was performed with a FACScan or FACSCalibur flow cytometer with CellQuest software from BD Immunocytometry Systems (Mississauga, ON).

2.2.2.15 Generation of mouse embryonic fibroblasts (MEFs)

MEFs were prepared from C57/Bl6, TDAG51$^{+/-}$ and TDAG51$^{-/-}$ mice using the method described by Abboondanzo *et al.* (1993). Briefly, after appropriate pairing to obtain the desired genotype, the copulatory plug was used as a marker of impregnation. Thirteen and a half days later, the pregnant females were sacrificed to collect C57/Bl6 wildtype (wt), TDAG51$^{+/-}$ or TDAG51$^{-/-}$ embryos. The minced embryos were cultured in fibroblast growth media (DMEM) and were selected for MEFs. Immunobloting was then performed as described in section 2.2.2.8 using TDAG51 polyclonal antibody to confirm the genotype of the MEFs.

PCR was also performed using DNA collected from MEFs to further confirm the aauthenticity of the generated MEFs. In short, MEFs grown in T25 flask were washed with 1X PBS and dissolved in lysis buffer [1M Tris-HCl pH 8.5, 0.5M EDTA, 10% SDS, 5M NaCl]. The supernatant was then collected in a microcentrifuge tube. Following overnight incubation at 55°C with proteinase K (10 mg/ml), the samples were vortexed and centrifuged at 1400 rpm for 20 min. To precipitate DNA, equal volumes of supernatant and isopropanol were mixed. After drying, DNA was dissolved in TE buffer [1M Tris-HCl pH 8.0, 0.5M EDTA pH 8.0]. PCR was next performed to show the presence of wildtype and/or disrupted TDAG51 alleles using following primers: WT 1, WT 2, TDAG51 KO 1, TDAG51 KO 2. Parameters for the 40 cycles of PCR after denaturing once at 94°C for 2 min were as follows: denaturation at 94°C for 30 sec, annealing at 58°C for 30 sec, and extension at 68°C for 1 min. PCR amplified products were further analyzed by agarose gel electrophoresis.

2.2.2.16 Cytotoxicity assay in cultured MEFs

The cytotoxicity detection kit (Roche Diagnostics, Indianapolis, IN) was used to measure cell death by assaying for lactate dehydrogenase (LDH) activity. MEFs (1 X 10^5 cells per well) were seeded onto 12-well plates. Following treatment with or without ER stress agents, the supernatant was collected from each sample. Cells were then washed in 1X PBS, lysed in 2% Triton X-100 (in H_2O), and collected into a new microcentrifuge tube. Media from untreated cells was used as a low control, while supernatant from untreated lysed cells was used as a high control. After several titrations, 50 µl of aliquots from

each condition was diluted to a final volume of 100 µl in 1X PBS. The LDH activity was measured at 492 nm using a $VERSA_{max}$ tunable microplate reader (Molecular Devices, Sunnyvale, CA) after incubating for 1 h with equal volume (100 µl) of working solution (catalyst diaphorase and tetrazolium salt INT dye solution). In the first step, LDH catalyzes lactate to pyruvate, where NAD^+ is reduced to $NADH/H^+$. In the second step, tetrazolium salt INT is reduced to red colored formazan, where diaphorase transfers H/H^+ from $NADH/H^+$. The amount of enzyme activity correlates to the formazan formation and is proportional to the number of lysed or dead cells. Percent cytotoxicity, which corresponds to the percent cell death, is measured using the following formula:

Cytotoxicity (%) = ((Experimental Value – Low Control) / (High Control – Low Control)) X 100

2.2.2.17 Mice and dietary conditions

Female $apoE^{-/-}$ mice (Transgenic Alliance, Lyon, France) were backcrossed 9 generations onto a C57BL/6 background. At 6 weeks of age, mice were divided into control groups fed a low fat/vitamin-defined purified diet (Special Diet Services, Witham, UK) or hyperhomocysteinemic groups fed the same diet but supplemented with either 0.09% (w/v) D,L-homocysteine in the drinking water or 1.4% (w/v) L-methionine in the diet. The mice were sacrificed after 18 week on the diets.

2.2.2.18 Statistical Analysis

All experiments were performed at least 3 times in triplicate. Values are presented as mean ± standard deviation. Comparison between the means was performed using the

unpaired Student's *t*-test. ANOVA was used for multiple comparisons among the means. For all analyses, $P<0.05$ was considered statistically significant.

2.3 Results

2.3.1 Characterization of TDAG51 as an ER stress-inducible gene

To examine the effect of homocysteine on TDAG51 expression, Northern blot analysis was performed and revealed that the steady-state mRNA levels of TDAG51 were increased in HUVECs by homocysteine in both a concentration- **(Figure 8a)** and time-dependent **(Figure 8b)** manner. Induction of TDAG51 mRNA levels correlated with an increase in the steady-state mRNA levels of GRP78, an ER-resident chaperone responsive to ER stress. This effect was specific for homocysteine because other structurally similar amino acids such as methionine, cysteine and homoserine failed to induce TDAG51 expression **(Figure 9)**. The ability of other ER stress inducing agents such as DTT **(Figure 9)** to increase the expression of TDAG51 supports a mechanism involving ER stress and UPR activation.

To determine whether transcriptional induction of TDAG51 corresponds to an increase in TDAG51 protein, HUVECs were cultured in the absence or presence of homocysteine and total cell lysates examined by immunoblot analysis using a polyclonal antibody directed against TDAG51 **(Figure 10a)**. TDAG51 protein was increased in HUVECs following exposure to homocysteine and correlated with an increase in GRP78 protein. Consistent with these findings, TDAG51 and GRP78 protein were increased in HAECs in a dose-dependent (50 μM to 5 mM) manner following treatment with increasing concentrations of homocysteine for 18 hr **(Figure 10b)**. The observation that TDAG51 and GRP78 protein levels were increased at physiological concentrations of 50

Figure 8: Northern blot analysis of the steady-state levels of TDAG51 and GRP78 mRNA in HUVEC.

(**a**) Dose-dependent induction in the steady-state mRNA levels of TDAG51 and GRP78. Total RNA isolated from HUVEC cultured in the absence or presence of increasing concentrations of homocysteine for 4 h. (**b**) Time-dependent induction in the steady-state mRNA levels of TDAG51 and GRP78. Total RNA (10 μg/lane) isolated from HUVECs cultured in the absence or presence of 1 mM homocysteine for the indicated time periods up to 18 h.

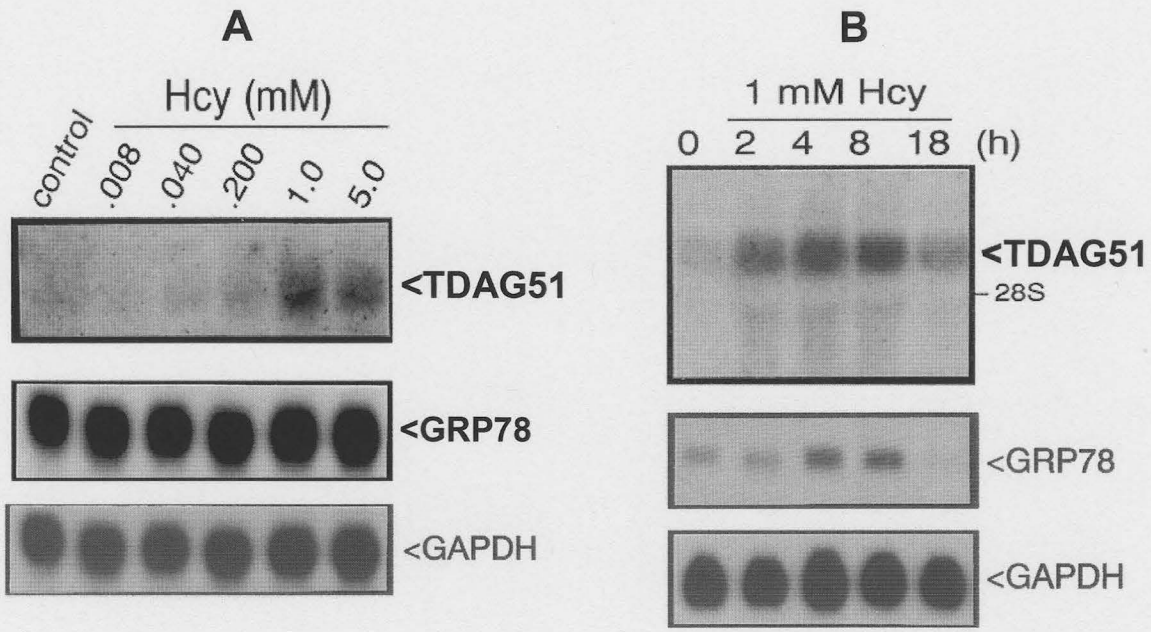
A
Hcy (mM)
control
.008
.040
.200
1.0
5.0
<TDAG51
<GRP78
<GAPDH
B
1 mM Hcy
0 2 4 8 18 (h)
<TDAG51
28S
<GRP78
<GAPDH

Figure 9: Induction in the steady-state mRNA levels of TDAG51 is selective for homocysteine and DTT.

Total RNA (10 μg/lane), isolated from HUVEC cultured for 4 h in the absence (control) or presence of either 1 mM homocysteine, cysteine, methionine, homoserine or DTT. Steady-state mRNA levels of TDAG51 were detected using a radiolabelled 6-2 cDNA probe, followed by autoradiography. The arrow indicates the migration position of TDAG51 mRNA transcripts. Hybridization to a GAPDH cDNA probe was used to normalize RNA loading.

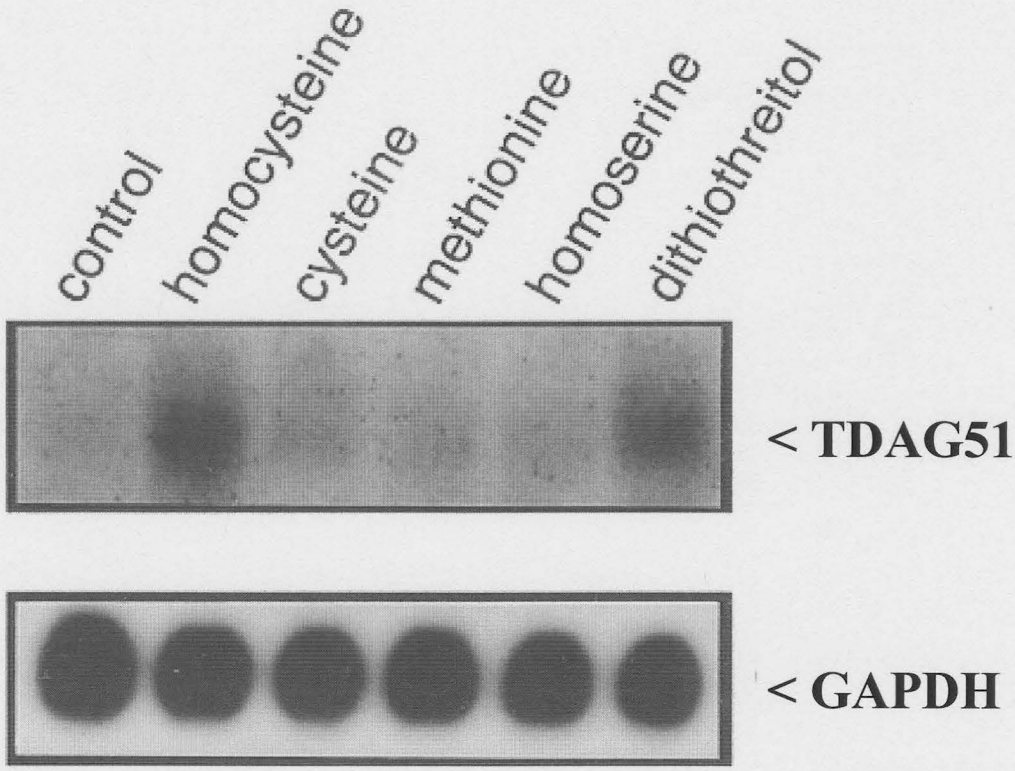
control
homocysteine
cysteine
methionine
homoserine
dithiothreitol
< TDAG51
< GAPDH

Figure 10: Induction of TDAG51 and GRP78 protein expression in response to homocysteine treatments

Homocysteine increases TDAG51 and GRP78 protein levels in HUVEC or HAEC. (A) Total protein lysates (40 μg/lane) from HUVEC cultured in the absence or presence of 1 mM homocysteine for the indicated time periods were examined by immunoblot analysis using antibodies to either TDAG51 or GRP78. (B) Total protein lysates (40 μg/lane) from HAEC cultured in the absence (control) or presence of increasing concentrations of homocysteine for 18 h were examined by immunoblot analysis using antibodies to either TDAG51 or GRP78.

A

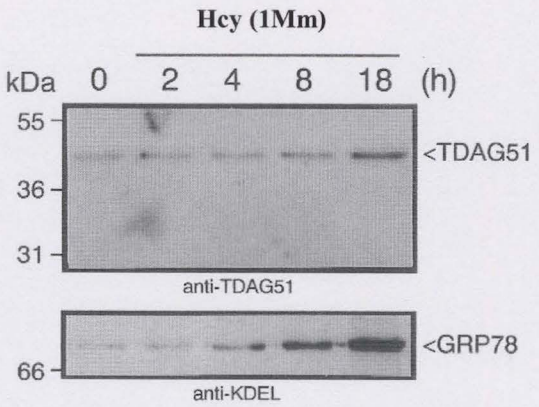

HUVEC

B

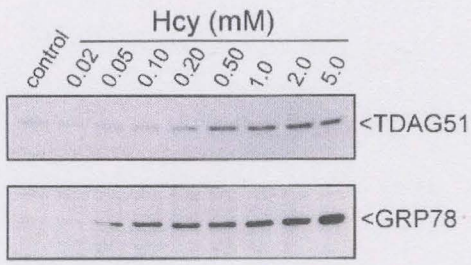

HAEC

to 200 μM homocysteine suggests that HAECs are more sensitive to exogenous levels of homocysteine then are HUVECs (Outinen *et al.*, 1998 & 1999).

Furthermore, studies have demonstrated that UPR activation of PERK causes phosphorylation of eIF2α, which is required for the inhibition of cellular mRNA translation and transcriptional induction of the majority of ER stress response genes, including GRP78, GRP94 and GADD153 (Harding *et al.*, 2000; Scheuner *et al.*, 2001). To provide insight into whether TDAG51 expression is mediated by eIF2α phosphorylation, we assessed the steady-state mRNA levels of TDAG51 upon activation of ER stress by homocysteine or tunicamycin in wild-type and homozygous A/A eIF2α mutant MEFs **(Figure 11)**. Upon treatment with homocysteine and tunicamycin, steady-state mRNA levels of both TDAG51 and GRP78 in wild-type MEFs were attenuated in the homozygous mutant MEFs. Furthermore, the ER-stress agent peroxynitrite in HAECs induced ER stress/UPR activation, as indicated by increased GRP78/GRP94 and TDAG51 protein levels at 18 hr **(Figure 12)**. Peroxynitrite treatment also induced the phosphorylation of eIF2α from 4 to 18 hr. These effects were inhibited by coincubation with uric acid (UA), a scavenger for peroxynitrite. Further, coincubation of thapsigargin with uric acid (UA) failed to inhibit ER stress induction in HAECs, indicating that UA is not a general inhibitor of ER stress. Collectively, these findings provide evidence that TDAG51 transcriptional activation is dependent on eIF2α phosphorylation and that TDAG51 can be classified as an ER stress response gene.

Figure 11: Requirement of eIF2α for TDAG51 expression in response to ER stress

Northern blot analysis of total RNA from wildtype or homozygous A/A mutant eIF2α mouse embryonic fibroblasts treated with 5 mM homocysteine (Hcy) or 10 μg/ml tunicamycin (Tm) for the indicated time periods. TDAG51 or GRP78 mRNA transcripts were detected using the appropriate radiolabeled cDNA probe. Hybridization to a glyceraldehyde-3-phosphate dehydrogenase (GAPDH) cDNA probe was used to normalized RNA loading.

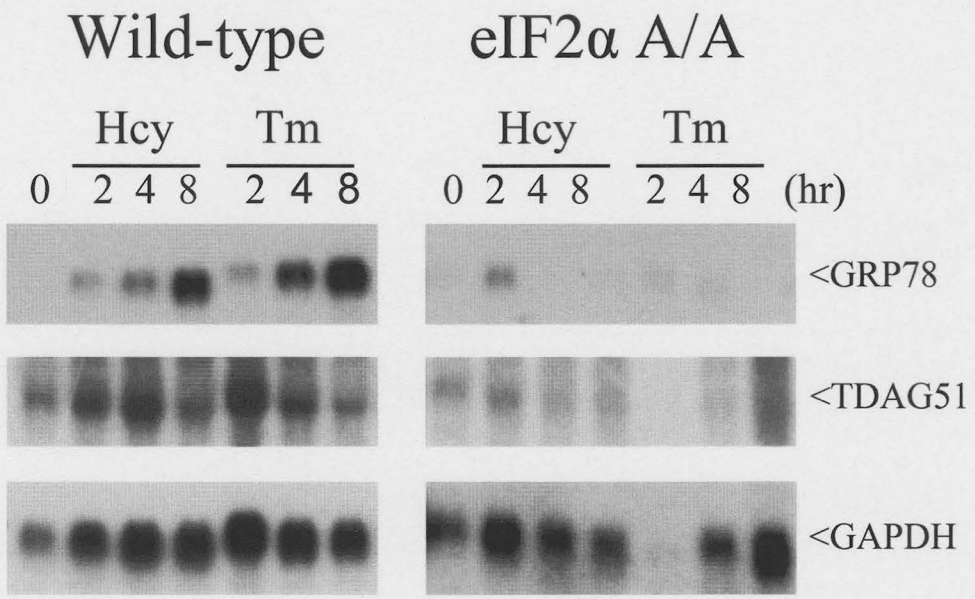
Wild-type
eIF2α A/A
Hcy
Tm
Hcy
Tm
0 2 4 8 2 4 8 0 2 4 8 2 4 8 (hr)
<GRP78
<TDAG51
<GAPDH

Figure 12: ER stress is induced by Sin-1 in human aortic endothelial cells.

Total protein lysates (40 μg/lane) from HAECs cultured in indicated agents for the indicated time periods were examined by immunoblot analysis. (A) Sin-1, an inducer of peroxynitrite synthesis, caused ER stress/UPR activation in HAECs as indicated by GRP78/GRP94, TDAG51 upregulation at 18 hours and eIF2α phosphorylation from 4 to 18 hours. These effects were inhibited by uric acid (UA). (B) Incubation of HAECs with thapsigargin (200 nmol/L) caused upregulation of GRP78/GRP94, TDAG51, and eIF2α phosphorylation. Coincubation of thapsigargin with uric acid (UA) failed to inhibit ER stress induction. Blots were probed for ß-actin to control for protein loading.

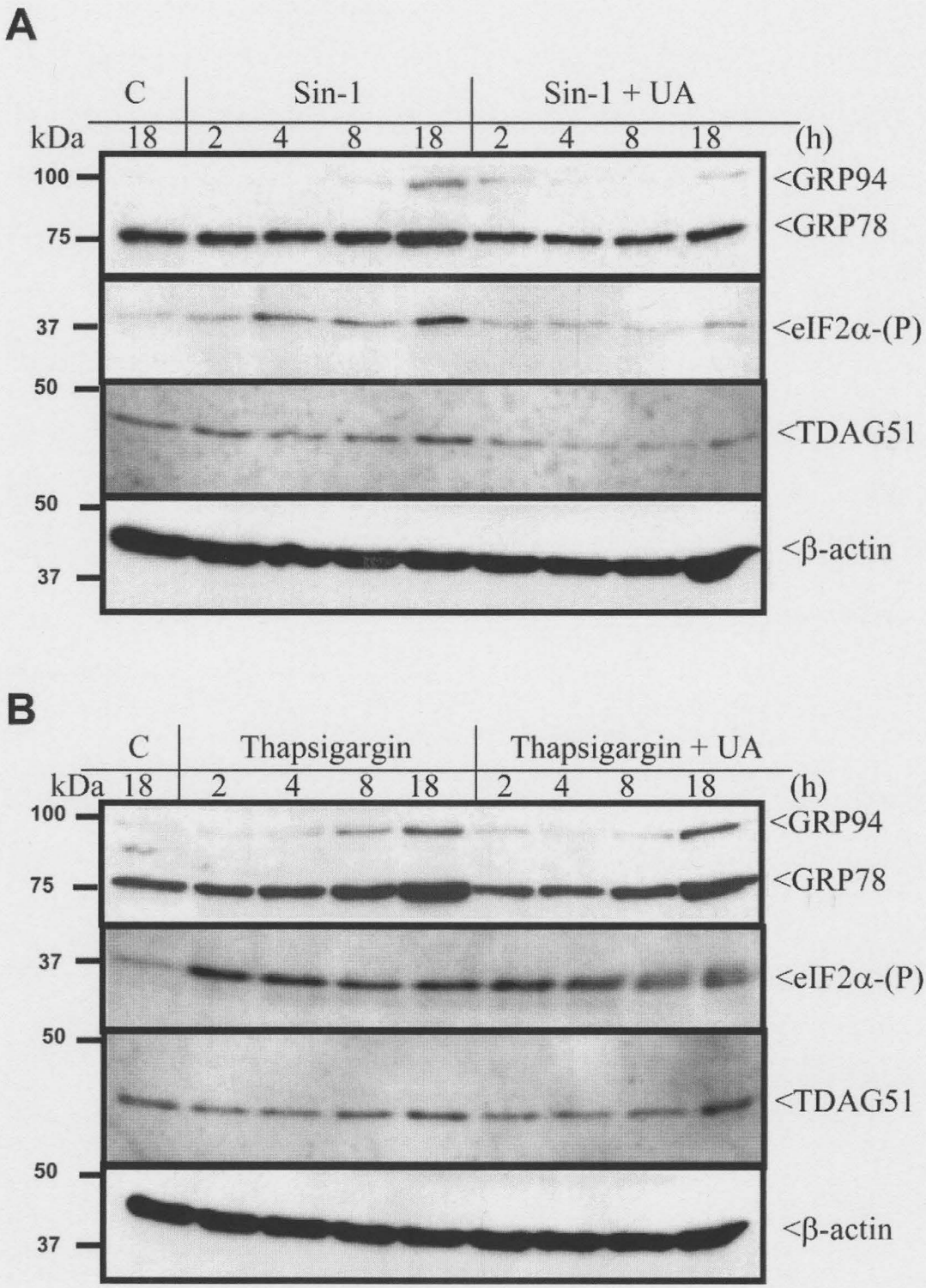
A
C
Sin-1
Sin-1 + UA
kDa
18
2
4
8
18
2
4
8
18
(h)
100
75
37
50
50
37
<GRP94
<GRP78
<eIF2α-(P)
<TDAG51
<β-actin
B
C
Thapsigargin
Thapsigargin + UA
kDa
18
2
4
8
18
2
4
8
18
(h)
100
75
37
50
50
37
<GRP94
<GRP78
<eIF2α-(P)
<TDAG51
<β-actin

2.3.2 Cellular Distribution of TDAG51

To elucidate the cellular localization of TDAG51, indirect immunofluorescence confocal microscopy was performed using anti-TDAG51 antibodies **(Figure 13a-d)**. TDAG51 was primarily localized in the cytoplasm of HUVECs in vesicles of two types; large perinuclear vesicles **(Figure 13a)** and smaller vesicles at the periphery of the cell **(Figure 13b)**. Similar TDAG51 immunostaining was observed for HAECs (data not shown). Co-localization studies in HUVECs using antibodies to TDAG51 and to specific cellular marker proteins, including GRP78 (ER), catalase (peroxisomes) and FAK (focal adhesion complex), revealed that TDAG51 associated with the large perinuclear vesicles co-localized with peroxisomes **(Figure 13c)** and with the smaller vesicles co-localized with focal adhesion complexes **(Figure 13d)**. Treatment of HUVECs with homocysteine affected TDAG51 distribution **(Figure 14a-c)**. A 30 min treatment of HUVECs with 1 mM homocysteine resulted in reduced density of the smaller peripheral TDAG51-positive vesicles with the larger vesicles remaining perinuclear in distribution **(Figure 14b)**, compared to untreated controls **(Figure 14a)**. The typical distribution of TDAG51 positive vesicles returned after 24 hr treatment, however, the intensity of TDAG51 staining appeared to increase in both small and large vesicles **(Figure 14c)**, a finding consistent with our immunoblot analysis. No specific immunostaining was observed when non-immune goat IgG was used as the primary antibody (data not shown).

Figure 13: Co-localization of TDAG51 with intracellular vesicles.

HUVEC grown on gelatin coated glass coverslips were fixed, permeabilized, and immunostained with antibodies to TDAG51, catalase, or focal adhesion kinase. Cells were optically sectioned throughout their depth at 1.5 μm intervals using laser-scanning confocal microscopy. Endogenously expressed TDAG51 protein was found to be associated with cytoplasmic vesicles of two types: large vesicles found predominately in the perinuclear region centrally located in the depth of the cell (*A, large arrows*) and smaller vesicles that were adjacent to the cytoplasmic membrane at the periphery of the cell (*B, small arrows*). C, TDAG51 (*green*) in the large perinuclear vesicles co-localized (*yellow regions*) with catalase (*red*), a peroxisome marker (*large arrowheads*). TDAG51 associated with the smaller vesicles did not co-localize with catalase (*small arrows*). D, the small cytoplasmic vesicles of TDAG51 (*red*) co-localized with focal adhesion kinase (*green*) at the cell membrane periphery (*arrows*). Original magnification was X630.

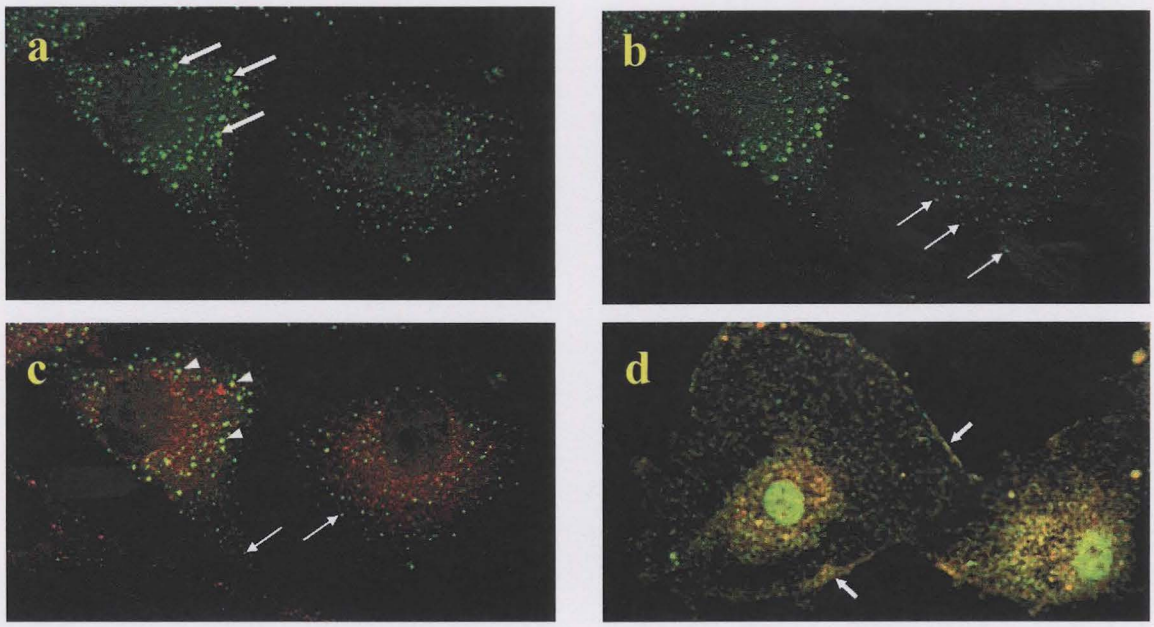
a
b
c
d

Figure 14: Effect of homocysteine on the cellular distribution of TDAG51

HUVEC grown on gelatin coated glass coverslips were treated in the absence (*a*) or presence of 1 mM homocysteine for 30 min (*b, asterisks*) or 24 h (*c*). Cells were then fixed, permeabilized, and immunostained with goat polyclonal antibody against TDAG51. Cells were optically sectioned throughout their depth at 1.5-μm intervals using laser-scanning confocal microscopy and these images were captured in the middle plain of the cell. Original magnification was X630.

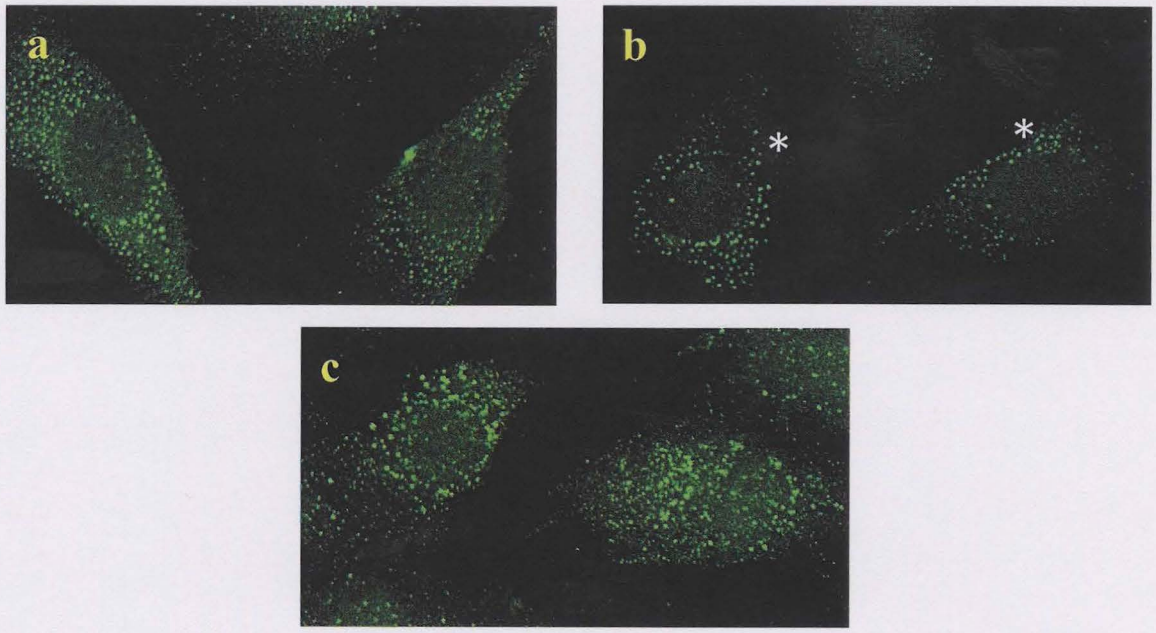
a
b
*
*
c

2.3.3 Induction of detachment-mediated PCD following TDAG51 overexpression

Previous studies have demonstated that homocysteine induces PCD in HUVECs through activation of the UPR (Zhang *et al.*, 2001). In support of these findings, homocysteine induced a dose-dependent (50 μM to 10 mM) increase in PCD in HAECs, as measured by DNA fragmentation **(Figure 15)**. As a positive control, TNFα in the presence of actinomycin D also increased DNA fragmentation. However, cysteine, methionine and homocystine did not promote PCD in HAECs.

Given that homocysteine induces the expression of TDAG51 and promotes PCD, we assessed the effect of TDAG51 overexpression on cell viability and integrity. Expression plasmids encoding GFP or a GFP-TDAG51 fusion protein were transiently transfected into cultured vascular endothelial cells. To verify expression of the recombinant proteins, immunoblot analysis was performed using antibodies specific to TDAG51 or GFP **(Figure 16)**. HUVECs and HAECs (data not shown) transfected with the GFP-TDAG51 expression plasmid produced a fusion protein with an apparent molecular mass of 67 kDa which was immunoreactive for both anti-TDAG51 and anti-GFP antibodies, a finding consistent with the predicted fusion between TDAG51 (40 kDa) and GFP (27 kDa). Cells transfected with the GFP expression plasmid contained the expected 27 kDa GFP protein.

Overexpression of the GFP-TDAG51 fusion protein caused dramatic changes in cell morphology, including rounding up, membrane ruffling and long pseudopodial extensions **(Figure 17a, b, d)**, compared to cells overexpressing GFP **(Figure 17c)**. Disruption of the actin cytoskeleton was also observed in the GFP-TDAG51

Figure 15: Induction of PCD by homocysteine in HUVEC

Homocysteine induces PCD in HAEC. HAEC were cultured in the absence (*0* and *C*) or presence of 0.05–10 mM homocysteine (*Hcy*), 0.5 mM methionine (*Met*), 0.5 mM cysteine (*Cys*), or 0.5 mM homocystine (*HH*) for 24 h. As a positive control for PCD, HAEC were treated with tumor necrosis factor-α in the presence of actinomycin D (*T*). Following treatment, chromosomal DNA was isolated and separated on a 2% agarose gel, as described under experimental procedures.

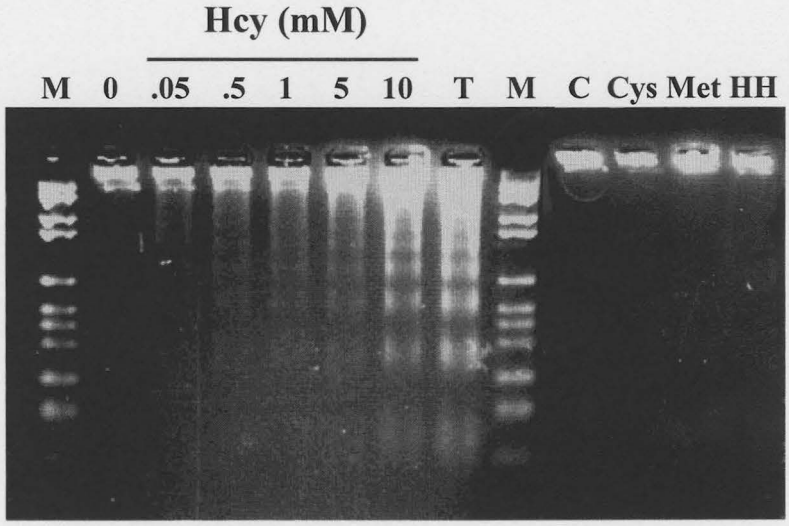
Hcy (mM)
M 0 .05 .5 1 5 10 T M C Cys Met HH

Figure 16: Expression of GFP or GFP-TDAG51 fusion protein in HUVEC

Total protein lysates (40 μg/lane) from cells transiently transfected for 24 h with transfection reagent alone (*control*) or transfection reagent containing 2 μg of the pEGFP-C1 (*GFP*) or pEGFP-C1-TDAG51 (*GFP-TDAG51*) expression plasmids were subjected to immunoblot analysis using antibodies against GFP or TDAG51. The *arrowheads* indicate the migration position of GFP or GFP-TDAG51 fusion protein. The *asterisk* indicates the migration position of endogenous TDAG51.

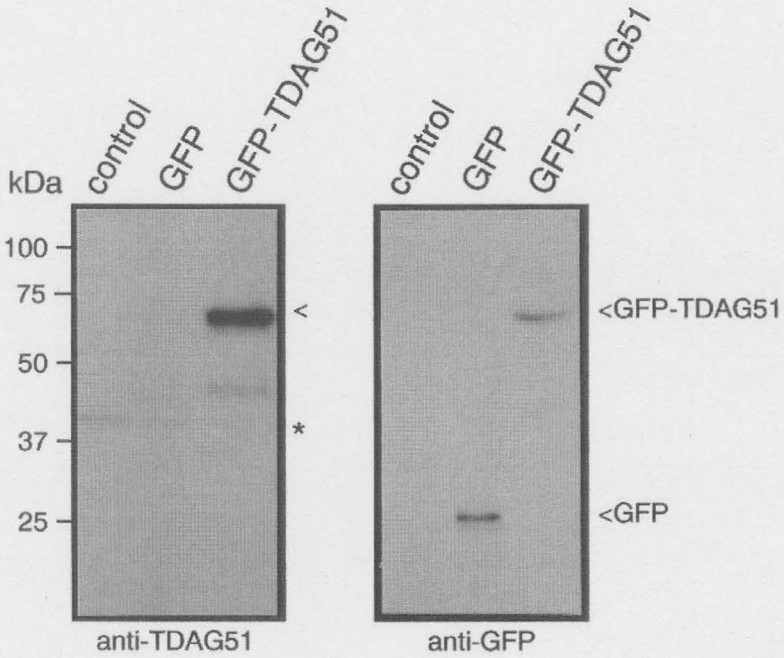
kDa
control
GFP
GFP-TDAG51
100
75
50
37
25
<
*
anti-TDAG51
control
GFP
GFP-TDAG51
<GFP-TDAG51
<GFP
anti-GFP

Figure 17: Promotion of detachment-mediated PCD from overexpression of TDAG51

HUVEC plated on gelatin-coated coverslips were transiently transfected with 2 μg of the pEGFP or pEGFP-TDAG51 expression plasmids, and cells showing nuclear DNA fragmentation were identified by TUNEL staining (TUNEL-positive cells are red in color). *A* and *B*, GFP-TDAG51-overexpressing HUVEC, 12 or 24 h post-transfection, respectively. *C*, GFP-positive HUVEC, 24 h post-transfection. Also shown are adherent GFP-TDAG51-positive HUVEC (*D*) demonstrating TUNEL-positive staining (*E*), 12 h post-transfection. *F*, merged image of *D* and *E*. Nonadherent GFP-TDAG51 positive HUVEC (*G*) demonstrating TUNEL-positive staining (*H*), 24 h post-transfection, are shown. *I*, merged image of *G* and *H*. Adherent GFP positive HUVEC (*J*) demonstrating TUNEL-negative staining (*K*), 24 h post-transfection, are shown. *L*, merged image of *J* and *K*. Original magnification was x630.

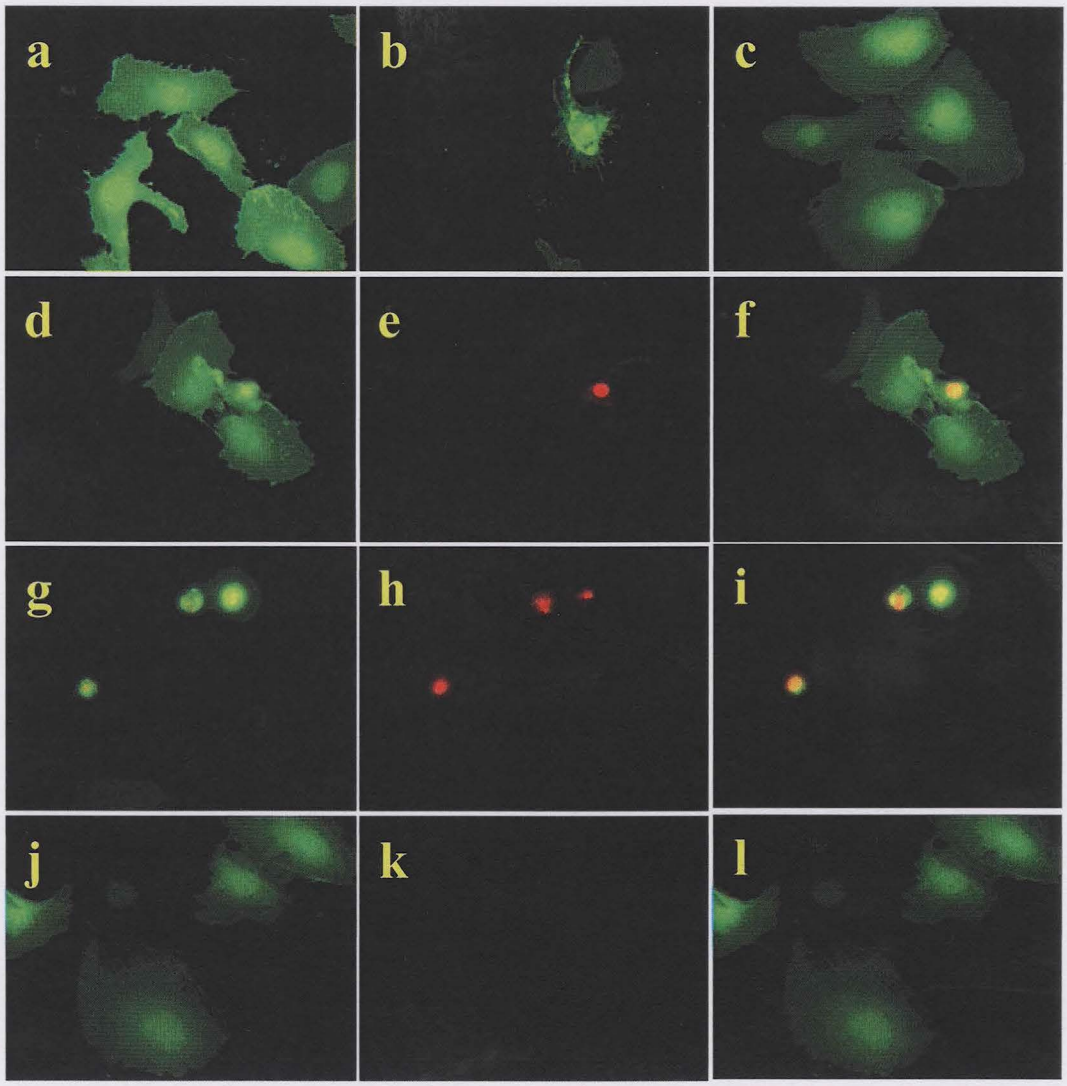
a
b
c
d
e
f
g
h
i
j
k
l

overexpressing cells (data not shown). Following these changes in cell morphology, there was clear evidence of PCD **(Figure 17e, f)** with a significant number of cells ($P<0.001$) becoming detached from the tissue culture dishes. Virtually all of the non-adherent cells expressing GFP-TDAG51 **(Figure 17g)** were TUNEL positive **(Figure 17h, i)**. Furthermore, GFP-TDAG51 overexpression induced the cleavage of both procaspase-3 and PARP in HUVECs and HAECs **(Figure 18)**. In contrast, cells overexpressing GFP were morphologically normal **(Figure 17c, j)**, remained adherent, and did not undergo PCD, as measured by TUNEL staining **(Figure 17k, l)**, caspase-3 activation and PARP cleavage **(Figure 18)**.

To determine whether the changes in cell morphology and adherence induced by TDAG51 were dependent on the activation of caspases, HUVECs were pretreated with the pan-caspase inhibitor, ZVAD, prior to transiently transfection with the GFP-TDAG51 expression plasmid **(Figure 19a-c)**. ZVAD pretreatment did not prevent changes in either cell morphology or loss in cell adherence. However, it inhibited TUNEL staining. These findings indicate that TDAG51-mediated changes in cell morphology and adherence are not dependent on caspase activation and suggest that TDAG51 promotes detachment-induced PCD or anoikis.

2.3.4 Characterization of TDAG51 functional domain(s) in detachment-induced PCD

Sequence analysis revealed that the C-terminal region of TDAG51 contains PQ and PH repeats while the N-terminal region has a polyglutamine (QQ) stretch and a pleckstrin

Figure 18: Induction of caspase 3 from overexpression of GFP-TDAG51 fusion protein in HUVEC or HAEC

Total protein lysates (40 μg/lane) from untreated cells (*untreated*) or cells transiently transfected for 24 h with transfection reagent alone (*control*) or transfection reagent containing 2 μg of the pEGFP (*GFP*) or pEGFP-TDAG51 (*GFP-TDAG51*) expression plasmids were subjected to immunoblot analysis using antibodies directed against procaspase-3 or PARP. To control for protein loading, immunoblots were reprobed with anti-β-actin monoclonal antibody.

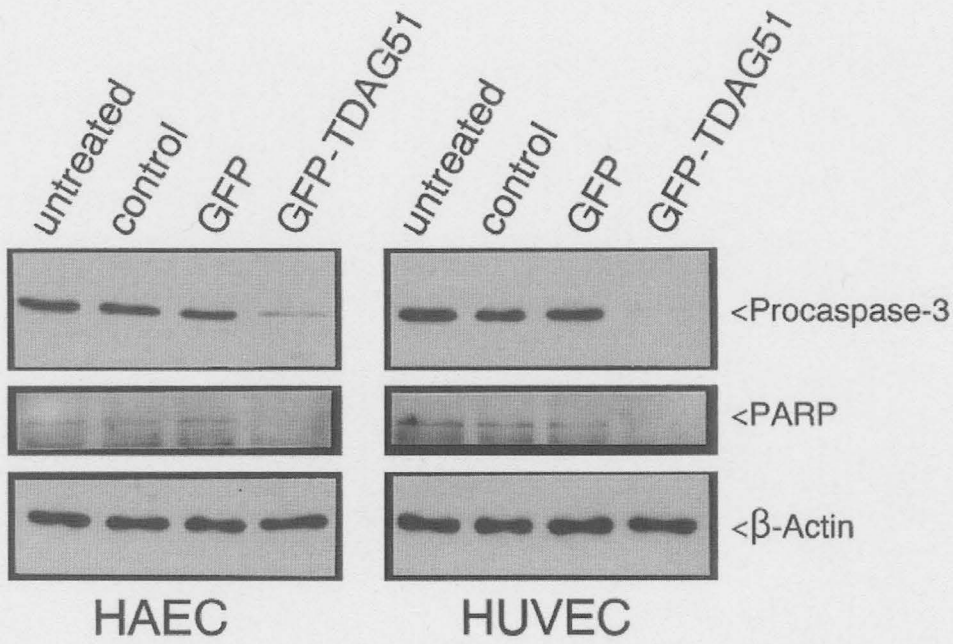
untreated
control
GFP
GFP-TDAG51
untreated
control
GFP
GFP-TDAG51
<Procaspase-3
<PARP
<β-Actin
HAEC
HUVEC

Figure 19: Cell detachment prior to activation of caspases from the overexpression of TDAG51

HUVEC plated on gelatin-coated coverslips were transiently transfected with 2 μg of the pEGFP or pEGFP-TDAG51 expression plasmids, and cells showing nuclear DNA fragmentation were identified by TUNEL staining. Pretreatment with pan-caspase inhibitor, ZVAD, decreases TUNEL staining but does not prevent morphological changes and loss of adherence in HUVEC overexpressing GFP-TDAG51. Nonadherent GFP-TDAG51 positive HUVEC pretreated for 18 h with 20 μM ZVAD (*A*) demonstrating TUNEL-negative staining (*B*), 24 h post-transfection, are shown. *C*, merged image of *M* and *N*. Original magnification was x630.

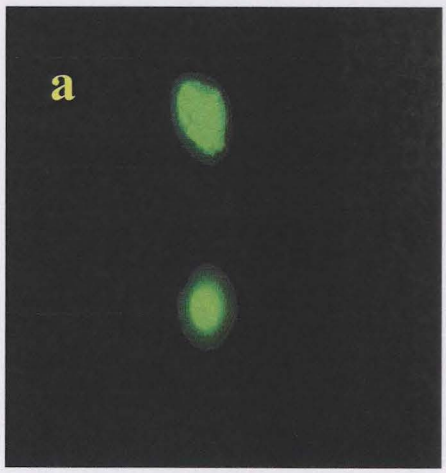

GFP-TDAG51

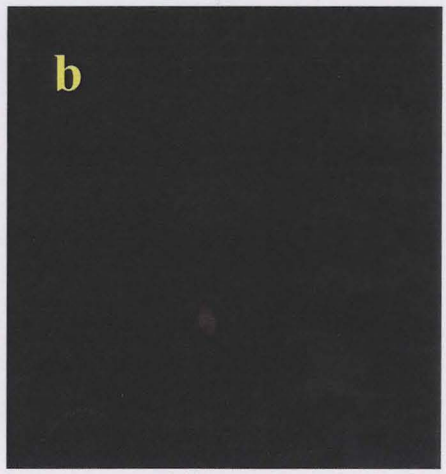

TUNEL

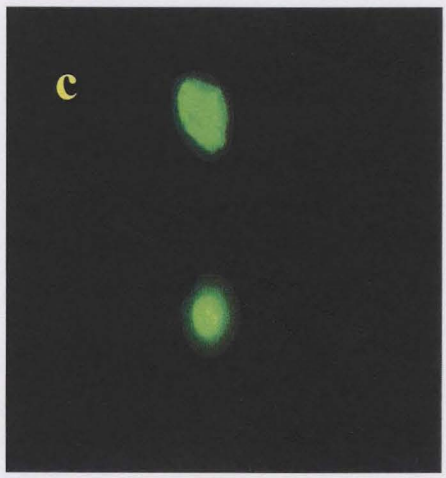

GFP-TDAG51/TUNEL

homology related domain. Previous studies have implicated that proteins with QQ, PQ or PH repeats are important for transcriptional regulation and PCD (McNabb and Courtney 1992; Cai *et al.*, 1994; Li *et al.*, 1995). Further, pleckstrin homology related domains are involved in cytoskeletal organization and PCD (Maffucci and Falasca 2001). To identify the functional domain(s) of TDAG51 that contribute to detachment-induced PCD, seven deletion mutants of TDAG51 were generated by PCR and were cloned in frame into the *Hind*III/*Xba*I sites of pEGFP-C1. Authenticity of the insert sizes was confirmed by restriction digestions **(Figure 20)**.

Furthermore, following 24 hr of transient transfection, flow cytometry was then used to identify potential functional domain(s) of TDAG51 that contribute to detachment-induced PCD in endothelial cells (Data not shown: preliminary observation). Based on the number of non-adherent green fluorescent HAECs in FACs analysis, inserts containing QQ or pleckstrin homology related domain independently did not promote detachment-induced PCD. Herein, fluorescence intensity was similar to GFP control non-adherent cells. The requirement for PH domain was insignificant since the insert L3 (pleckstrin homology domain plus PQ repeats) or L5 (pleckstrin homology domain plus PQ and PH repeats) demonstrated similar fluorescence intensity, compared to full length TDAG51 ORF. These preliminary findings suggest that the PQ domain is the important domain of TDAG51 for detachment-induced PCD from TDAG51 overexpression in HAEC.

Figure 20 : Restriction digestion of plasmids encoding functional domains of TDAG51 ORF.

(A) The TDAG51 gene encodes 260 amino acids, including a long stretch of glutamine (Q) residues near the N-terminus, proline-glutamine (PQ) and proline-histidine (PH) repeats are located near the C-terminus. Further, TDAG51 contains pleckstrin homology-like domain, nuclear localization signal (NLS) and a nuclear export signal (NES) toward N-terminal of the protein. L1-L7, regions within TDAG51 that are generated for functional analysis of TDAG51.

(B) PCR amplified regions (L1-L7) of TDAG51 ORF were subcloned into the C terminus of mammalian expression vector having green fluorescent protein. After purification of plasmids, restriction digestion of vectors was performed with restriction enzymes, *Hind*III and *Xba*I. Representation of the lanes in the agarose gel is as follows: Lane 1 (Kb ladder), Lane 2 (pEGFP-C1), Lane 3-9 (vectors with insert L1-L7), Lane 10 (vector with TDAG51 ORF).

A

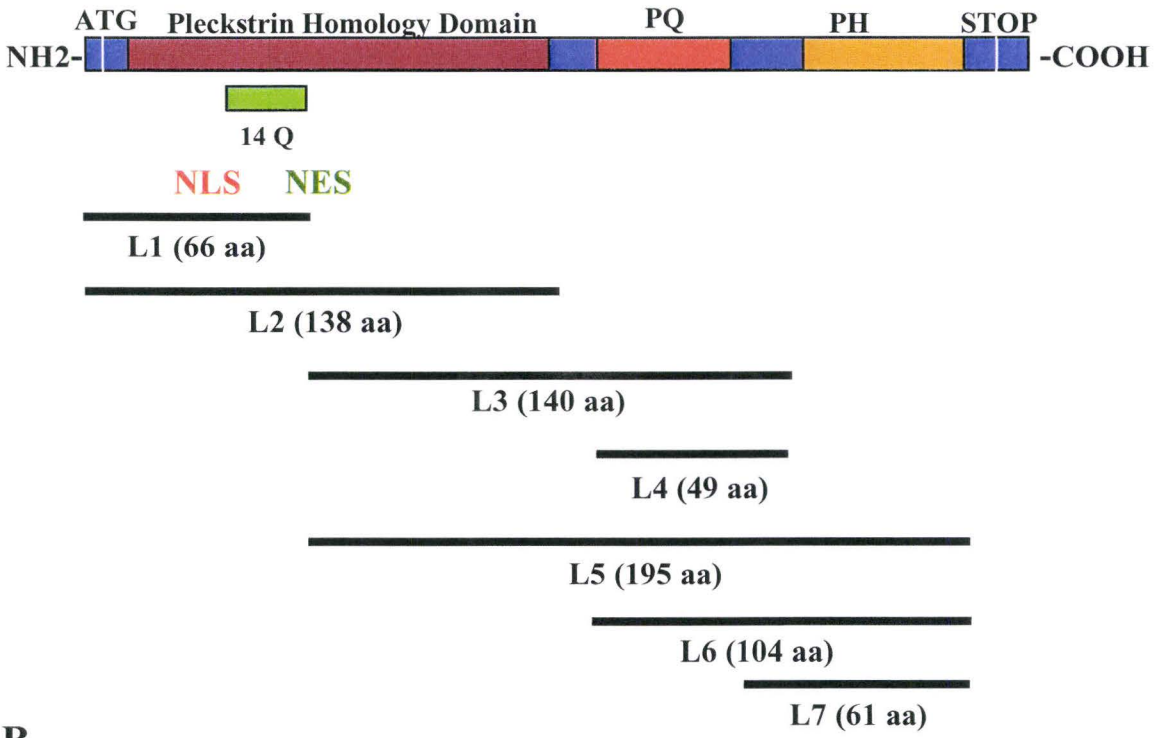
ATG
Pleckstrin Homology Domain
PQ
PH
STOP
NH2-
-COOH
14 Q
NLS
NES
L1 (66 aa)
L2 (138 aa)
L3 (140 aa)
L4 (49 aa)
L5 (195 aa)
L6 (104 aa)
L7 (61 aa)

B

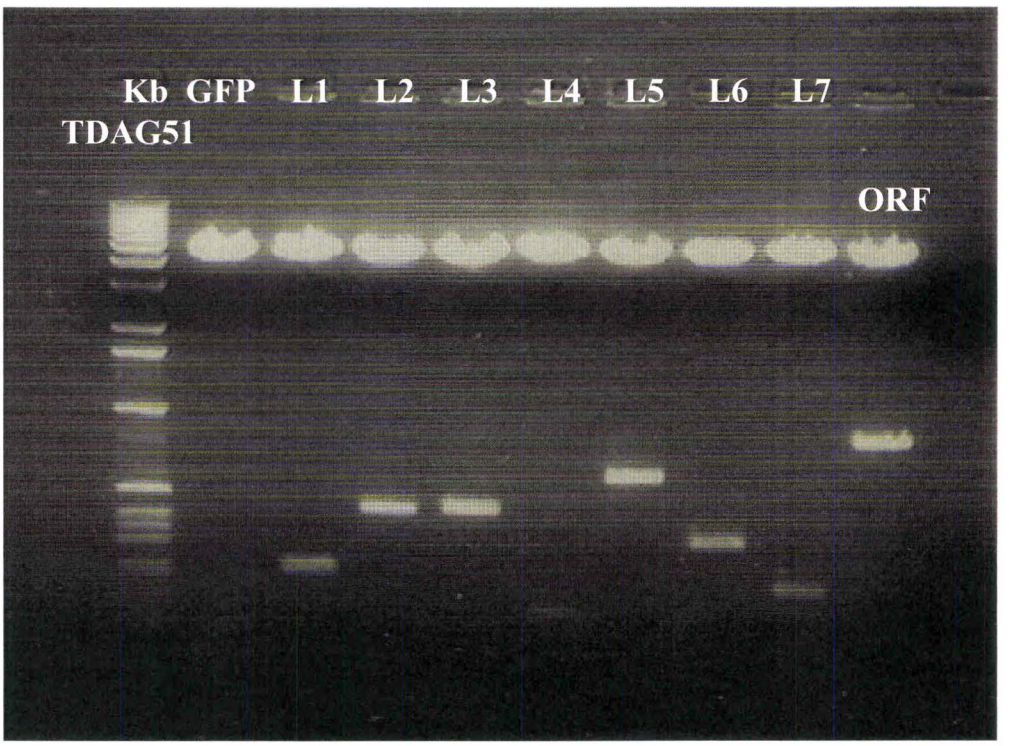
Kb
GFP
L1
L2
L3
L4
L5
L6
L7
TDAG51
ORF

2.3.5 Protection from ER stress-induced cell death following functional deficiency of TDAG51

We have demonstrated that TDAG51 is responsive to ER stress and overexpression of TDAG51 promotes detachment-induced PCD. To further address the role of TDAG51 in ER stress, wildtype and TDAG51$^{-/-}$ MEFs were generated as described in section 2.2.2.15 and characterized by western blotting and PCR **(Figure 21)**.

Loss of TDAG51 in MEFs demonstrated protection from ER stress-induced cell death **(Figure 22)**, as measured by LDH release, following 24 hr treatments with thapsigargin (500 nM) or tunicamycin (2 μM) in TDAG51$^{-/-}$ MEFs, compared to wildtype MEFs. However, deficiency of TDAG51 did not appear to block UPR activation since there was no difference in Grp78 protein expression in TDAG51$^{-/-}$ MEFs compared to wildtype MEFs **(Figure 23)**. Further, loss of TDAG51 appeared to have an effect on GADD153 by the observation that TDAG51$^{-/-}$ MEFs had reduced GADD153 expression following thapsigargin or tunicamycin treatment. It is possible that TDAG51 is upstream of GADD153 in the PERK pathway. Interestingly, overexpression of TDAG51 in HUVECs or HAECs promoted phosphorylation of eIF2α, a downstream target for PERK, by an unexplained mechanism **(Figure 24)**.

2.3.6 Correlation between TDAG51 expression and PCD in atherosclerotic lesions from apoE$^{-/-}$ mice having diet-induced HHcy

Consistent with our previous findings (Zhou *et al.*, 2001), mice fed diets supplemented with methionine or homocysteine for 18 weeks became hyperhomocysteinemic and had

Figure 21: Characterization of Mouse Embryonic Fibroblasts (MEFs) from C57, TDAG51$^{+/-}$ and TDAG51$^{-/-}$ mice

MEFs derived from wildtype, TDAG51$^{-/+}$ or TDAG51$^{-/-}$ mice were cultured in DMEM media. Following collection of cell lysates, immunoblot was performed to confirm the genotypes. In brief, total protein lysates (40 μg/lane) were subjected to immunoblot analysis using antibodies against TDAG51 or β-actin. Results indicate that there is a complete loss of TDAG51 expression in TDAG51$^{-/-}$ MEFs and a 50% loss of TDAG51 expression in TDAG51$^{+/-}$ MEFs.

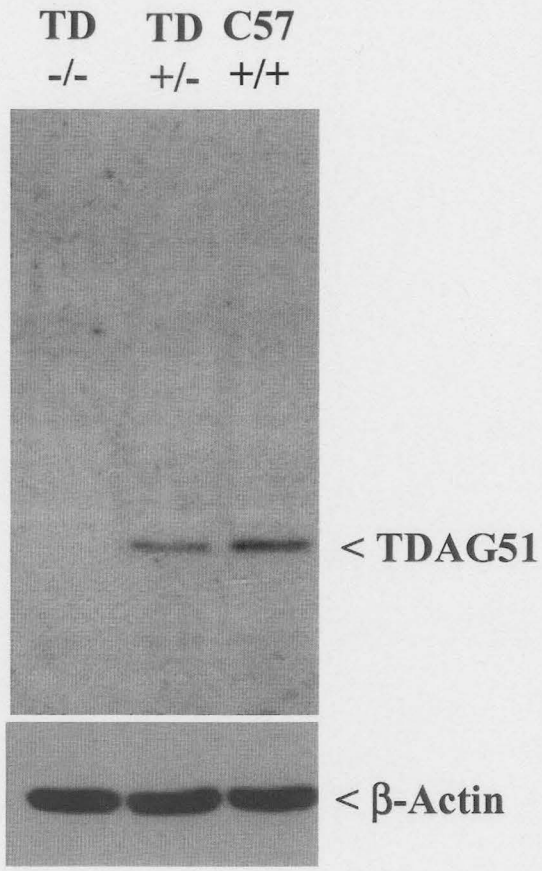
TD
-/-
TD
+/-
C57
+/+
< TDAG51
< β-Actin

Figure 22: Resistance from ER stress-induced cell death in TDAG51-deficient MEFs

C57 control and TDAG51$^{-/-}$ MEFs grown on 12 well plates were treated for 24 hr in the presence of thapsigargin (Thap), tunicamycin (TM) or etoposide (ETP). Media was collected and cell death was then assessed by measuring the release of lactate dehydrogenase (*LDH*) into the media using the Cytotoxicity Detection Kit (Roche). Data are presented as percent cytotoxicity that corresponds to percent cell death at a given treatment. * $p < 0.001$ *versus* TDAG51$^{-/-}$ MEFs.

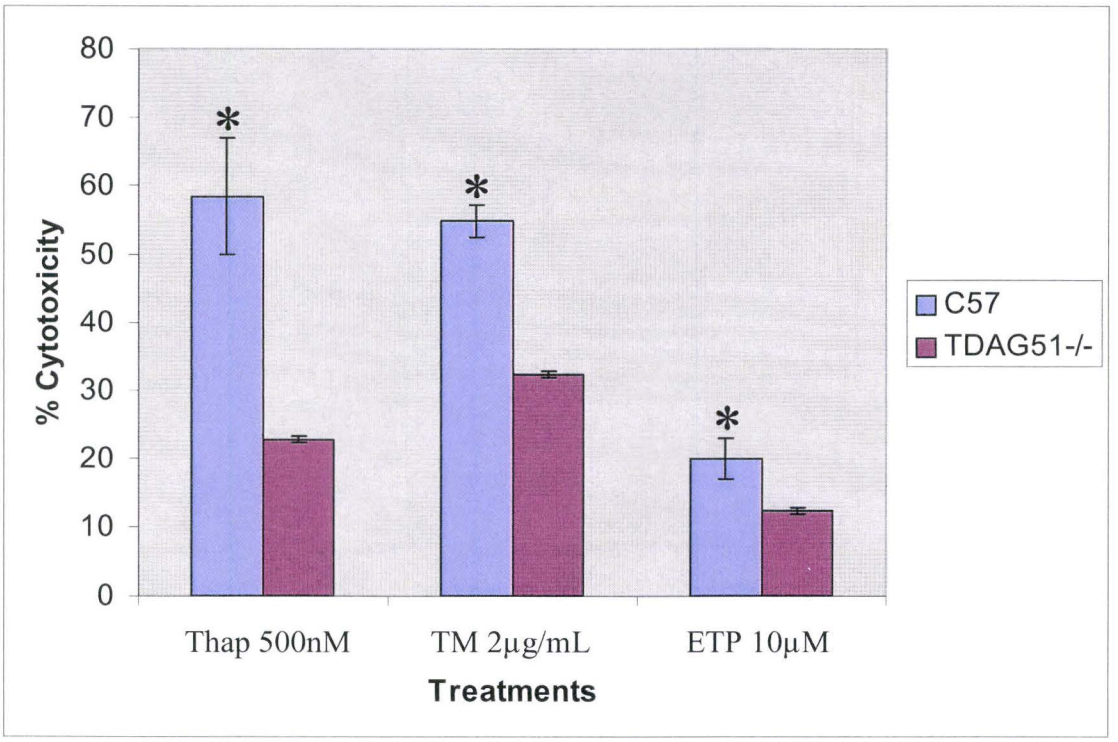
80
70
60
50
40
30
20
10
0
% Cytotoxicity
*
*
*
C57
TDAG51-/-
Thap 500nM
TM 2µg/mL
ETP 10µM
Treatments

Figure 23: Deficiency of TDAG51 does not alter unfolded protein response (UPR) activation.

Wild type ($TDAG51^{+/+}$) and TDAG51-deficient ($TDAG51^{-/-}$) MEFs were treated for time periods up to 18 hr in presence or absence of tunicamycin or thapsigargin. Total protein lysates (40 μg/ml) were subjected to immunoblot analysis using antibodies against GRP78 and GRP94 (anti-KDEL) or CHOP. Immunoblots were reprobed with anti-β-actin antibodies to control for protein loading.

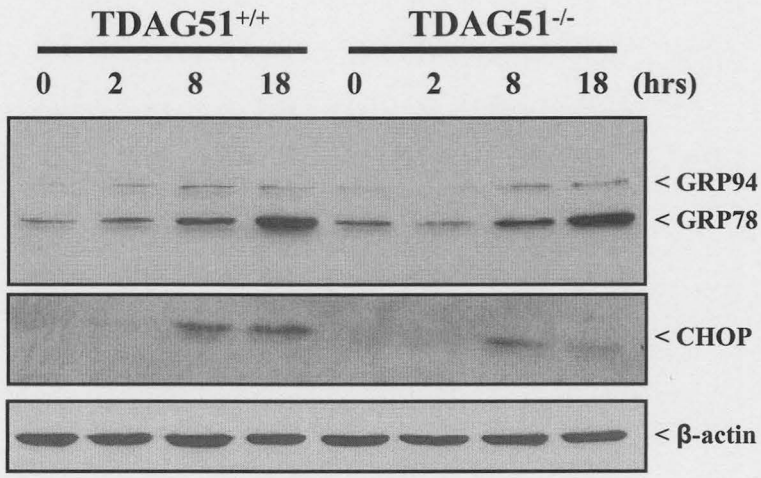

tunicamycin

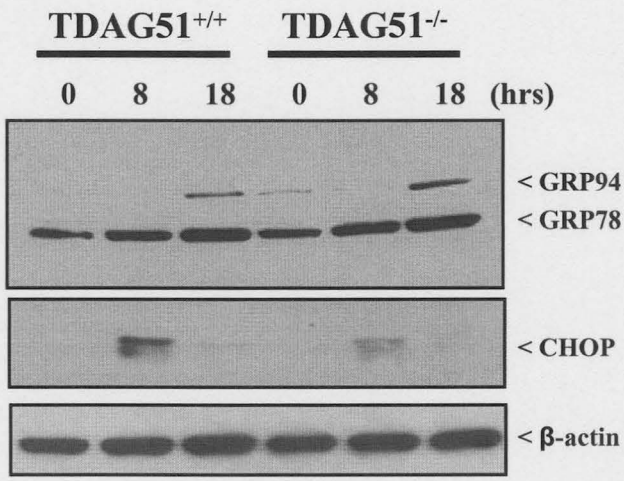

thapsigargin

Figure 24: Effect of TDAG51 overexpression on eIF2α phosphorylation

HUVEC or HAEC were transiently transfected with GFP or GFP-TDAG51 expression plasmids for 24 h. Total protein lysates (40 μg/ml) were subjected to immunoblot analysis using antibodies against eIF2α-P or β-actin. Results indicate that TDAG51 overexpression induces the phosphorylation of eIF2α compared to GFP control. Untreated, cells that were not transfected. Control, cells that were transfected with Superfect transfection reagent only.

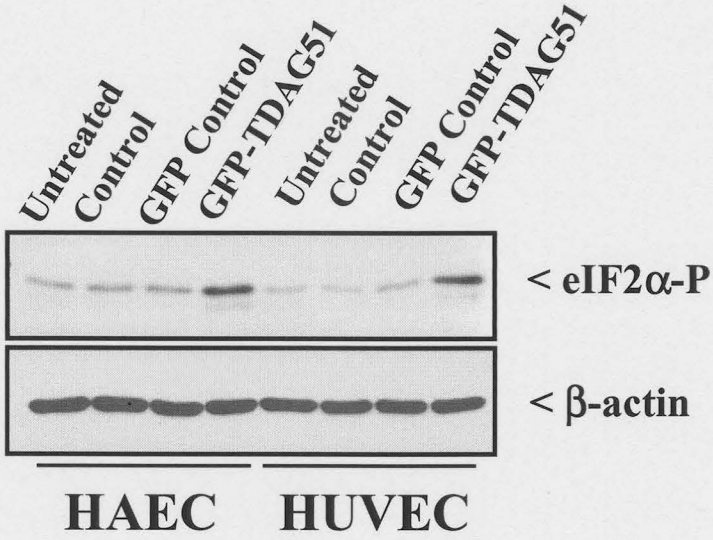
Untreated
Control
GFP Control
GFP-TDAG51
Untreated
Control
GFP Control
GFP-TDAG51
< eIF2α-P
< β-actin
HAEC
HUVEC

significant increases in aortic root lesion size **(Table 1)**. To examine the effect of HHcy on TDAG51 expression in atherosclerotic lesions, sections from the aortic root of apoE$^{-/-}$ mice fed normal chow, high methionine or high homocysteine diets were immunostained for TDAG51. In mice fed normal chow diet, immunohistochemical staining of the aortic wall showed that TDAG51 was confined to the atherosclerotic lesions **(Figure 25a)**. However, TDAG51 immunostaining was much more intense and widely distributed throughout the lesion and aortic wall of mice fed hyperhomocysteinemic diets **(Figure 25b, c)**. Aortic root sections immunostained with non-immune goat IgG as the primary antibody showed no detectable immunofluorescence signal within the aortic wall **(Figure 25d)**. Increased aortic root lesion size were also observed in mice fed a high methionine diet for 4 weeks, compared to mice fed normal chow diet **(Figure 25e, f)**. TDAG51 immunostaining was found predominantly within these early lesions but was increased in mice fed high methionine diet **(Figure 25f)**, compared to mice fed normal chow diet **(Figure 25e)**.

To determine whether TDAG51 expression correlated with PCD, atherosclerotic lesions from mice fed normal chow or hyperhomocysteinemic diets for 4 **(Figure 26b)** or 18 weeks **(Figure 26a)** were immunostained for TDAG51 and assayed by the TUNEL method. Compared to mice fed normal chow diet, TDAG51 expression and PCD were increased and co-localized to the necrotic core of lesions from mice fed high methionine or high homocysteine diet for 18 weeks **(Figure 26a)**. Immunocytochemical studies suggested that the majority of TDAG51/TUNEL positive cells within the necrotic core were macrophages and smooth muscle cells (data not shown). However, endothelial cells

Table 1: Total plasma homocysteine levels and atherosclerotic lesion size in apoE-deficient mice fed normal chow or hyperhomocysteinemic diets.

	Plasma homocysteine	Lesion size in aortic root
Group (n)	μmol/L	mm^2
Control (36)	9.46±0.28	0.18±0.01
High methionine (15)	53.6±8.7*	0.28±0.03*
High homocysteine (15)	51.4±2.9*	0.27±0.02*

Female apoE-deficient mice at 6 weeks of age were fed the indicated diet for 18 weeks. Values are the mean±SEM.

*$P<0.01$ vs control group.

Figure 25: TDAG51 expression in the aortic root of apoE$^{-/-}$ mice fed normal chow or hyperhomocysteinemic diets

Indirect immunofluorescence was performed to detect TDAG51 in aortic root sections of apoE$^{-/-}$ mice fed normal chow (*A*), high methionine (*B*), or high homocysteine (*C*) diet for 18 weeks. *D*, control section in which nonimmune goat IgG was used as the primary antibody. Indirect immunofluorescence for TDAG51 was performed in aortic root sections of apoE$^{-/-}$ mice fed normal chow (*E*) or high methionine (*F*) diet for 4 weeks. Increased areas of TDAG51 immunostaining are indicated by the *arrows*. Original magnification was x100.

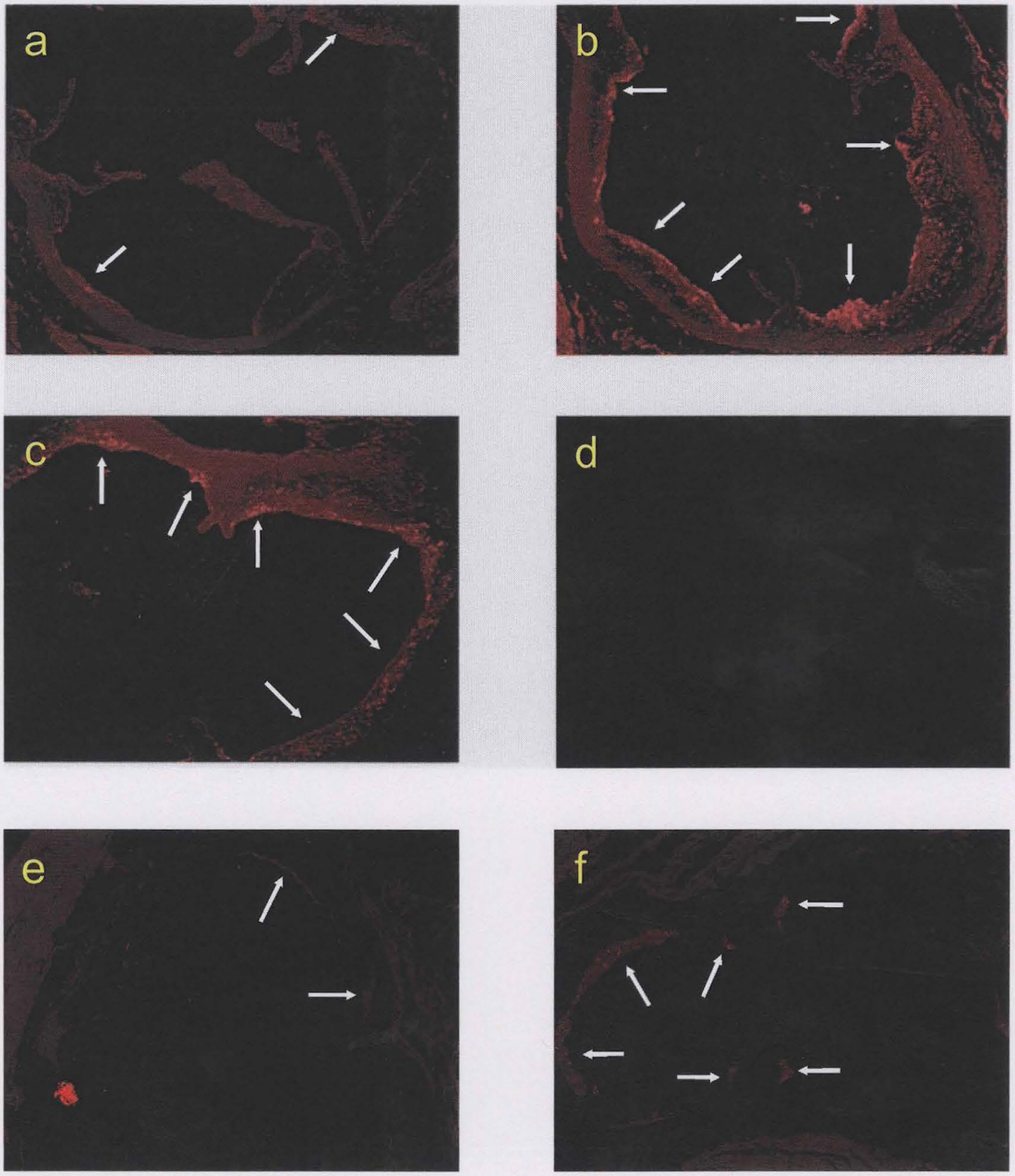
a
b
c
d
e
f

Figure 26: TDAG51 expression and PCD in atherosclerotic lesions from apoE$^{-/-}$ mice fed normal chow or hyperhomocysteinemic diets

A, identification of TDAG51 immunostaining and TUNEL-positive cells in sections from atherosclerotic lesions of apoE$^{-/-}$ mice fed normal chow, high methionine (*Met*), or high homocysteine (*Hcy*) diet for 18 weeks. *B*, TDAG51 immunostaining and TUNEL-positive cells in sections from atherosclerotic lesions of apoE$^{-/-}$ mice fed normal chow or high methionine (*Met*) diet for 4 weeks. TUNEL-positive cells are indicated by the *asterisks*. Original magnification was x200.

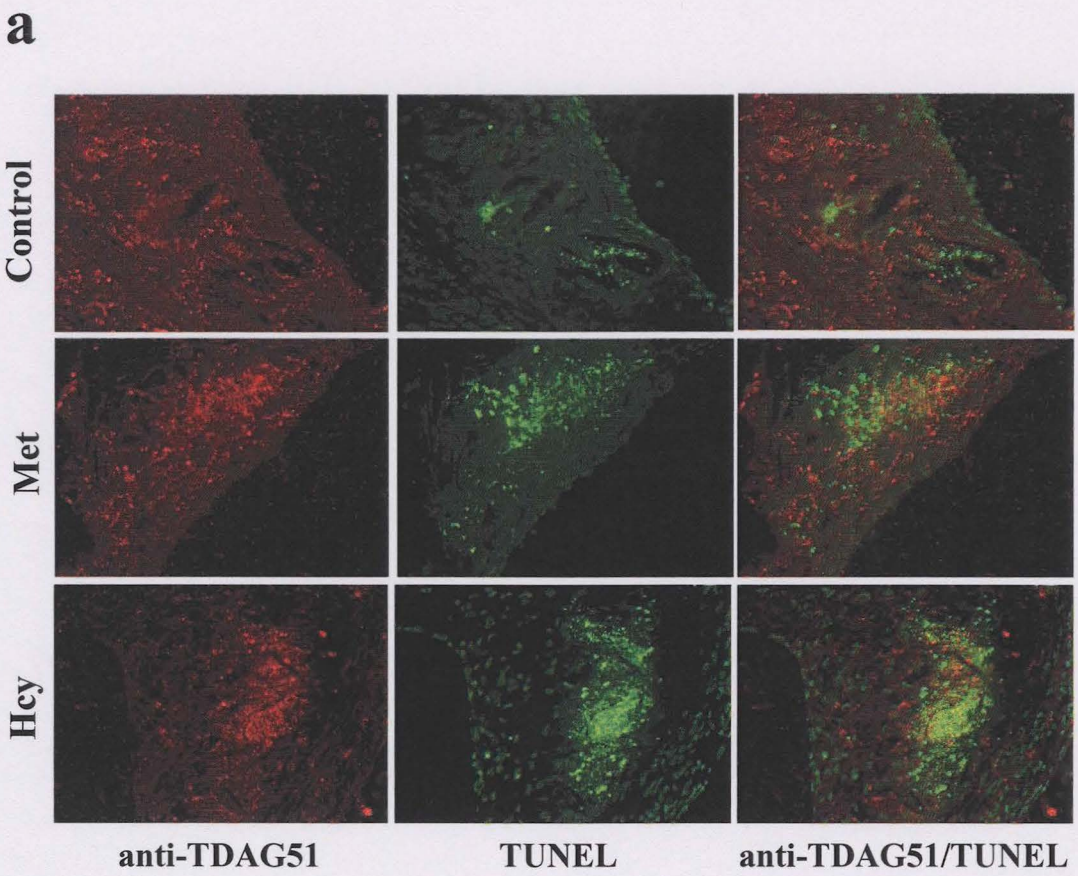
a
Control
Met
Hcy
anti-TDAG51
TUNEL
anti-TDAG51/TUNEL
b
Control
Met
anti-TDAG51
TUNEL

positive for both TDAG51 and TUNEL were rarely observed in the aortic root wall. Although few TDAG51/TUNEL positive cells were identified within the early lesions of mice fed normal chow diet for 4 weeks **(Figure 26b)**, there appeared to be more positive cells in the early lesions from hyperhomocysteinemic mice.

2.3.7 Overexpression of TDAG51 increases the expression of tissue factor

PCD plays a major role in atherosclerotic lesion development and increases the risk of plaque rupture by reducing the stability of atherosclerotic lesions. PCD also enhances plaque thrombogenicity since it increases the number of tissue factor-rich apoptotic microparticles within the atherosclerotic lesions (Tedgui and Mallat 2001). Since TDAG51 is a pro-apoptotic gene, we therefore assessed whether overexpression of TDAG51 affected the expression of TF, the major initiator of thrombosis. We have demonstrated that overexpression of TDAG51 increases TF expression in HUVECs or HAECs **(Figure 27)**. However, future studies are necessary to better define the association between TDAG51 expression and TF expression/activity to further explain potential pro-thrombotic effects of TDAG51.

Figure 27: Effect of TDAG51 overexpression on TF expression

HUVEC or HAEC were transiently transfected with GFP or GFP-TDAG51 expression plasmids for 24 h. Total protein lysates (40 μg/ml) were subjected to immunoblot analysis using antibodies against TF or β-actin. Results indicate that TDAG51 overexpression increases TF protein levels in HAEC or HUVEC compared to GFP control. Untreated, cells that were not transfected. Control, cells that were transfected with Superfect transfection reagent only.

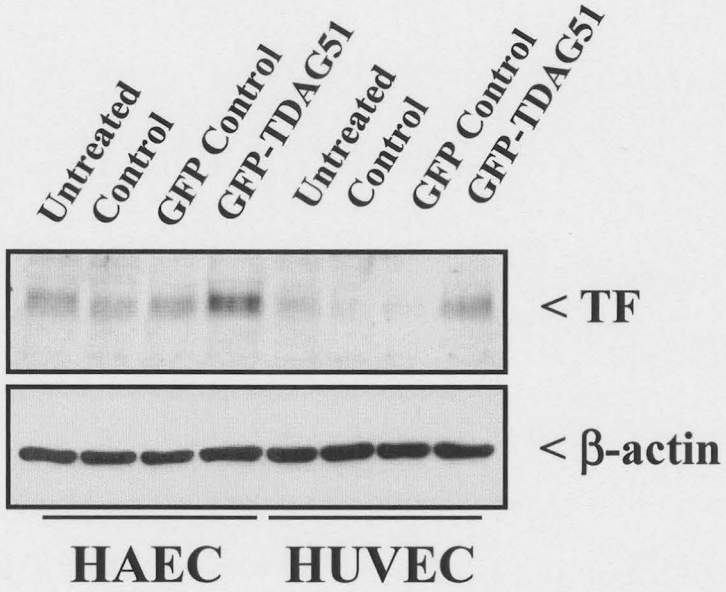
Untreated
Control
GFP Control
GFP-TDAG51
Untreated
Control
GFP Control
GFP-TDAG51
< TF
< β-actin
HAEC
HUVEC

2.4 Discussion

HHcy is an important and independent risk factor for the development of CVD (Boushey *et al.*, 1995; Refsum *et al.*, 1998; Eikelboom *et al.*, 1999; Malinow *et al.*, 1999). Previous studies have demonstrated that HHcy accelerates the development of atherosclerosis (Hofmann *et al.*, 2001; Zhou *et al.*, 2001) and that homocysteine causes ER stress, leading to growth arrest and PCD in cultured vascular endothelial cells (Outinen *et al.*, 1999; Huang *et al.*, 2001; Zhang *et al.*, 2001). Despite these findings, the pro-apoptotic factors implicated in this process and their *in vivo* relevance to atherogenesis have yet to be identified.

We now provide evidence that TDAG51, a member of the pleckstrin homology-related domain family (Park *et al.*, 1996; Frank *et al.*, 1999; Gomes *et al.*, 1999), is an ER stress response gene, promotes PCD and contributes to the development of atherosclerosis in apoE$^{-/-}$ mice having diet-induced HHcy. These findings are based on several lines of evidence presented here. First, homocysteine induces the expression of TDAG51 in cultured vascular endothelial cells in a time- and dose-dependent manner. The induction of TDAG51 by homocysteine involves ER stress and is dependent on eIF2α phosphorylation. Second, transient overexpression of TDAG51 causes dramatic changes in cell morphology, decreases cell adhesion and promotes detachment-mediated PCD. Furthermore, deficiency of TDAG51 protects MEFs from ER stress-induced cell death. Third, TDAG51 expression is increased in early and mature atherosclerotic lesions from apoE$^{-/-}$ mice fed hyperhomocysteinemic diets, compared to mice fed a normal chow diet. Fourth, a direct correlation between increased TDAG51 expression

and PCD was observed in the atherosclerotic lesions from apoE$^{-/-}$ mice having diet-induced HHcy. The additional observation that early and mature atherosclerotic lesions from apoE$^{-/-}$ mice fed hyperhomocysteinemic diets showed increased evidence of ER stress, as measured by GRP78/94 immunostaining (Zhou *et al.*, 2004), suggests that TDAG51 contributes to the development of atherosclerosis through a mechanism involving ER stress.

HUVECs were exposed to different concentrations of homocysteine for different durations to investigate the expression of TDAG51. TDAG51 expression was induced in a dose- and time-dependent manner by homocysteine. These observations indicated that relatively high concentrations of extracellular homocysteine (1.0 mM or greater) were required to induce TDAG51 mRNA levels in HUVEC, suggesting that homocysteine-induced TDAG51 expression requires internalization of sufficient amounts of extracellular homocysteine to overcome the pathways through which it is metabolized and/or excreted. While the exogenous homocysteine concentrations used are higher than typical plasma levels, Outinen *et al.* (1998 & 1999) demonstrated that intracellular levels of homocysteine are more important than plasma levels in inducing changes in gene expression in cultured human vascular endothelial cells. Outinen *et al.* (1998) showed that 1 mM extracellular homocysteine causes a 2-fold increase in intracellular levels of homocysteine. Interestingly, cell viability was not greatly affected when endothelial cells were exposed to high concentrations ($\geq$ 1 mM) of homocysteine, a result consistent with previous findings (Lentz and Sadler 1991; Hajjar *et al.*, 1993; Outinen *et al.*, 1998). Time-dependent induction of TDAG51 mRNA with 1 mM homocysteine further supports

the importance of intracellular homocysteine concentrations on gene expression. An initial increase in intracellular homocysteine concentrations at 8 hr resulted in maximum transcript expression that was decreased by 18 hr. This decrease is likely due to the clearance of intracellular homocysteine through metabolism and/or secretion. The observation that 8, 40, 200 μM homocysteine did not induce TDAG51 expression, suggests that > 200 μM concentration of extracellular homocysteine is required to facilitate the transport of extracellular homocysteine that could overcome intracellular homocysteine metabolism in HUVECs. However, TDAG51 protein expression was upregulated in HAECs at a much lower concentration (50 to 200 μM), suggesting that some cell lines are more sensitive to extracellular homocysteine.

Expression of TDAG51 in HUVECs was specific to homocysteine since TDAG51 mRNA levels did not significantly change when HUVECs were exposed to the structurally similar thiol containing amino acids cysteine and methionine. As a control, when HUVECs were exposed to the structurally similar non-thiol containing amino acid, homoserine, TDAG51 transcript expression remained unchanged. The findings that other structurally similar thiol and non-thiol containing amino acids such as cysteine, methionine, and homoserine, also failed to induce TDAG51 mRNA expression, clearly supports the selectivity of TDAG51 transcript expression for homocysteine. These observations can be explained as follows: (i) HUVEC are more sensitive to homocysteine than other thiol and non-thiol containing amino acid, (ii) there may be preferential accumulation of intracellular homocysteine compared to other amino acids, and/or (iii) HUVECs may have the ability to metabolize, utilize or eliminate cysteine, methionine

and homoserine more efficiently than homocysteine. For example, methionine can be incorporated into protein in addition to being metabolized to homocysteine and cysteine (Welch and Loscalzo 1998). Therefore, under certain conditions, methionine could potentially cause similar cellular effects as those observed with homocysteine. In addition, the finding that the TDAG51 transcripts were not induced by cysteine, further supports the observation that cysteine is not an atherogenic agent even though it is structurally similar and exists at 20-25 fold higher concentrations in plasma, compared to homocysteine (Welch and Loscalzo 1998).

Like homocysteine, the ER stress-inducing agent DTT increased TDAG51 mRNA levels. This observation suggests a mechanism involving ER stress, and supports our previous findings that homocysteine can alter the expression of genes involved in ER stress (Outinen *et al.*, 1998 & 1999; Werstuck *et al.*, 2001). These findings are also consistent with other previous reports (Park *et al.*, 1996; Gomes *et al.*, 1999) demonstrating that TDAG51 expression is induced in T cell hybridomas and neuronal cells by other additional ER stress agents, including ionomycin and thapsigargin. Interestingly, the finding that elevated TDAG51 protein expression correlates with increased GRP78 protein levels further supports a mechanism related to ER stress. In addition, the ER stress agent peroxynitrite increases the expression of TDAG51 and this effect can be prevented by coincubation of peroxynitrite with uric acid, a scavenger for peroxynitrite (Dickhout *et al.*, 2005). Also, TDAG51 expression is highly upregulated by farnesol, a pro-apoptotic and ER-stress inducible agent (Joo *et al.*, 2007). Collectively, these findings provide evidence that TDAG51 is an ER stress-induced gene.

TDAG51 is a member of a novel pleckstrin homology-related gene family that consists of Ipl/Tssc and Tih (Frank *et al.*, 1999). Sequence analysis has revealed that TDAG51 contains a central motif resembling a pleckstrin homology domain and several distinctive C-terminal proline-glutamine and proline-histidine repeats, suggesting a role in transcriptional regulation and/or PCD (Park *et al.*, 1996; Gomes *et al.*, 1999). Studies have now demonstrated that decreased expression of TDAG51 occurs in metastatic melanoma and that overexpression of TDAG51 sensitizes PCD and impairs melanoma cell proliferation (Neef *et al.*, 2002). However, the precise mechanism by which TDAG51 mediates PCD is not known. TDAG51 has been shown *in vitro* to play critical roles in the upregulation of Fas gene expression and activation-induced PCD of T cells (Park *et al.*, 1996). However, TDAG51$^{-/-}$ mice express normal levels of Fas with no impairment in T-cell PCD (Rho *et al.*, 2001). Furthermore, TDAG51 promotes Fas-independent apoptosis in numerous cell lines, including neuronal, melanoma, vascular endothelial cells (Gomes *et al.*, 1999; Neef *et al.*, 2002; Hossain *et al.*, 2003). In support of Fas-independent mechanism of apoptosis, we have proposed that TDAG51 promotes detachment-mediated PCD or anoikis. This is based on several lines of evidence. **First**, overexpression of TDAG51 promotes dramatic alterations in cell shape and increases detachment of endothelial cells from their appropriate matrix. **Second**, TDAG51-mediated shape changes are independent of caspase activation and occur prior to activation of the cell death program. Previous studies have reported that caspase-mediated cytoskeletal/shape changes are a rather rapid process (Kothakota *et al.*, 1997).

Currently, the underlying mechanism by which TDAG51 overexpression induces detachment-mediated PCD is unknown.

Based on our preliminary studies, it appears that the PQ rich domain of TDAG51 plays dominant role in promoting detachment-mediated PCD. Our finding is consistent with a study where it has been demonstrated that PQ rich domain of TDAG51 induces PCD in 293 cells while pleckstrin-homology domain suppresses cell death (Hayashida *et al.*, 2006). Previous reports have suggested that proteins containing PQ repeats can act as transcriptional activators (McNabb and Courtney, 1992; Park *el al.*, 1996). This is supported by our observation that overexpression of TDAG51 does not promote PCD following mutation of nuclear import signal of TDAG51 (al-Bayati and Austin; unpublished results). It is possible that TDAG51 may have a role in transcriptional regulation and may shuttle between the cytosol and nucleus.

Furthermore, experiments have shown that expression of active integrin-dependent kinase (ILK) or Akt prevents anoikis and cell detachment down-regulates survival functions of ILK (Fuji and walsh 1999; Atwell *et al.*, 2000; Frisch and Screaton 2001; Bachelder *et al.*, 2001). In addition, disruption of cell-extracellular matrix interaction also liberates Bfm from the cytoskeleton, which subsequently binds to and neutralizes the survival function of Bcl-2 (Puthalakath *et al.*, 2001). Since TDAG51 colocalizes with FAK and alters the actin cytoskeleton, it is conceivable that TDAG51 overexpression disrupts focal adhesion complex assembly and thus interrupts survival signalling from the extracellular matrix prior to activation of the cell death program.

In addition to its ability to decrease cell growth and to promote PCD, TDAG51 has been reported to inhibit protein synthesis, possibly by interacting with cellular factors involved in the regulation of protein translation (Hinz *et al.*, 2001). It is well established that activation of the UPR by ER stress leads to decreased rates of protein synthesis (Wong *et al.*, 1993) and that this cellular process is mediated by the ER-resident kinase, PERK (Harding *et al.*, 1999). Once activated by ER stress signals, PERK phosphorylates Ser51 of eIF2α, thereby inhibiting cellular mRNA translation and inducing transcriptional activation of a wide range of ER stress-inducible genes, including GRP78, GADD153 and TDAG51 (Scheuner *et al.*, 2001). Given that homocysteine causes ER stress, the ability of homocysteine to increase TDAG51 expression, activate PERK (Nonaka *et al.*, 2001; Ma *et al.*, 2002) and induce eIF2α phosphorylation (Ma *et al.*, 2002) is not surprising. In support of this, we have demonstrated that TDAG51 overexpression induces phosphorylation of eIF2α. However, the underlying mechanism by which TDAG51 phosphorylates eIF2α however remains to be explained.

Previous studies have proposed that acute clinical manifestations of atherosclerosis result from atherosclerotic lesion rupture, thereby triggering thrombus formation and vessel occlusion (Fuster 1994; Lee and Libby 1997). PCD has been well documented to occur in animal and human atherosclerotic lesions (Isner *et al.*, 1995; Kockx *et al.*, 1996; Hegyi *et al.*, 1996). The distribution of cell death is heterogeneous within the lesion, being more concentrated in regions containing a high density of macrophages and smooth muscle cells. Based on these findings, it has been suggested that PCD increases the risk of rupture by decreasing the stability of the atherosclerotic

lesions. Furthermore, PCD enhances thrombogenicity by increasing the number of tissue factor-rich apoptotic microparticles within the atherosclerotic lesions (Tedgui and Mallat 2001). Given our findings that TDAG51 expression and PCD are increased and co-localized in the atherosclerotic lesions from apoE$^{-/-}$ mice having diet-induced HHcy, TDAG51 could potentially alter plaque stability and/or thrombogenicity. Indeed, although a rare event in mice, we have documented spontaneous rupture of a coronary plaque in mice having diet-induced HHcy (Zhou *et al.*, 2001).

Our findings clearly demonstrate that TDAG51 overexpression in culture vascular endothelial cells causes dramatic changes in cell morphology, decreases cell adhesion and promotes PCD. However, very few TDAG51/TUNEL positive endothelial cells were observed in early or mature atherosclerotic lesions from apoE$^{-/-}$ mice having diet-induced HHcy. Because endothelial cells are increased in the circulation of patients with vascular disease following methionine load (Hladovec *et al.*, 1997), it is possible that the majority of TDAG51/TUNEL positive endothelial cells may have lost their adhesive properties and were shed into the circulation. This would be consistent with our finding that TDAG51 overexpression induces a loss in cell adhesion prior to PCD.

Although our studies implicate TDAG51 as an important pro-apoptotic factor that contributes to the development of atherosclerosis, additional cellular factors are likely to be involved. We as well as others have demonstrated that homocysteine induces the expression of GADD153 (Outinen *et al.*, 1998; Kokame *et al.*, 1996 & 2000; Werstuck *et al.*, 2001), a basic region leucine zipper transcription factor which is markedly induced in response to a variety of cellular stresses (Ron and Habener 1992). GADD153 correlates

with ER stress-induced cell death (Zinszner *et al.*, 1998) and overexpression of GADD153 sensitizes cells to ER stress by down-regulating Bcl-2 expression and enhancing oxidant injury (McCullough *et al.*, 2001). In addition, overexpression of GADD153 has been linked to the induction of PCD in 3T3 fibroblasts, keratinocytes and HeLa cells (Maytin *et al.*, 2001). In support of this, Feng *et al.* (2003) has demonstrated increased expression of GADD153 in advanced atherosclerotic lesions from $apoE^{-/-}$ mice fed a normal chow diet. Also, Zhou *et al.* (2004 & 2005) have demonstrated association of ER stress, TDAG51 and atherosclerotic lesion development in $apoE^{-/-}$ mice fed normal chow or hyperhomocysteinemic diets. Further experimentation is needed to better elucidate the contributions of both TDAG51 and GADD153 to ER stress-induced PCD and in the development of atherosclerosis.

In summary, we have established that TDAG51 is an ER stress-induced pro-apoptotic gene by the observation that loss of TDAG51 protects $TDAG51^{-/-}$ MEFs from ER stress-induced cell death. Furthermore, TDAG51 is a novel mediator of atherosclerosis. Our findings support an important role for TDAG51 in promoting detachment-mediated PCD *in vitro* and *in vivo*, and in contributing to the development of atherosclerosis in HHcy.

CHAPTER 3: Contribution of TDAG51 to atherosclerotic lesion development – studies using TDAG51/apoE double knockout mice

3.1 Introduction

PCD is a well defined feature in animal and human atherosclerotic lesions and may play an important role in the formation of the necrotic core (Isner *et al.*, 1995; Kockx *et al.*, 1996; Hegyi *et al.*, 1996; Bennet 1999; Tedgui and Mallat 2001). It is proposed that apoptotic macrophages and smooth muscle cells can influence plaque stability. Further, it is believed that PCD increases the risk of lesion rupture by decreasing the number of viable smooth muscle cells required for collagen production (Lusis 2000; Corti *et al.*, 2004). The observation that heterogeneous apoptosis of macrophages occurs within atherosclerotic lesions supports the hypothesis that some regions are predisposed to rupture (Kolodgie *et al.*, 2000). In addition, plaque thrombogenicity can increase since the lesion-resident apoptotic cells express cell surface tissue factor (TF), the major physiological initiator for blood coagulation (Tedgui and Mallat 2001). However, apoptosis of T-lymphocytes and macrophages might be beneficial to plaque stability because this process attenuates the inflammatory responses and the release of MMPs (Corti *et al.*, 2004; Tedgui and Mallat 2001). Although these studies provide evidence that PCD influences lesion growth, stability and/or thrombogenicity, the cellular mechanisms that mediate apoptotic cell death and their relevance to atherosclerosis are not completely understood.

Our earlier studies have demonstrated that TDAG51 promotes detachment-mediated PCD and is associated with the development of atherosclerosis in HHcy (Hossain *et al.*, 2003). We have further demonstrated that increased TDAG51 expression was correlated with PCD in the advanced atherosclerotic lesions from apoE$^{-/-}$ mice fed hyperhomocysteinemic diets, compared to mice fed normal chow diet. In addition, Dai *et al.* (2004) reported that TDAG51 is an atherosclerotic susceptible gene given that athero-prone waveform increases TDAG51 expression in endothelial cells. Our earlier studies have shown that TDAG51 is expressed in both early and advanced atherosclerotic lesions in apoE$^{-/-}$ mice fed normal chow diet **(Figure 28)**. We have also detected the presence of TDAG51 within the shoulder region of the plaque from human carotid arteries **(Figure 29)**. The current study was designed to investigate the effect of TDAG51 deficiency on the development and progression of atherosclerosis. To assess whether TDAG51 is a contributory factor to the development of atherosclerosis, TDAG51$^{-/-}$ mice were crossed with apoE$^{-/-}$ mice, an established hyperlipidemic mouse model of atherosclerosis, to obtain double knockout mice. Our findings have demonstrated that TDAG51$^{-/-}$/apoE$^{-/-}$ double knockout (DKO) mice fed normal chow diet have a significant reduction in atherosclerotic lesion size, compared to age- and sex-matched apoE$^{-/-}$ controls. This observation supports our hypothesis that the deficiency of a functional TDAG51 gene attenuates the development and progression of atherosclerotic lesions in apoE$^{-/-}$ mice fed normal chow diet. Thus, we have found that TDAG51 is a contributory factor to atherosclerotic lesion development in apoE$^{-/-}$ hyperlipidemic mice model. Furthermore, support for this hypothesis is drawn from the significant decrease in necrotic lipid core in

Figure 28: Expression of TDAG51 in early and advanced atherosclerotic lesions in apoE$^{-/-}$ mice.

Paraffin sections from the aortic root of apoE$^{-/-}$ mice either 9 (early-lesion group) or 23 (advanced-lesion group) weeks fed a normal chow diet were stained with goat polyclonal antibody against TDAG51. TDAG51 expression was observed in intimal macrophages (arrowhead, left panel, A) as well as macrophage foam cells in fatty streaks within the neointima of advanced lesions (right panel, B). Staining of TDAG51 was absent from acellular necrotic areas. I indicates intima; M, media; and L, lumen. Bar=50 μm.

(Obtained and modified from Zhou *et al.* (2005) Circulation 111: 1817)

Early lesion

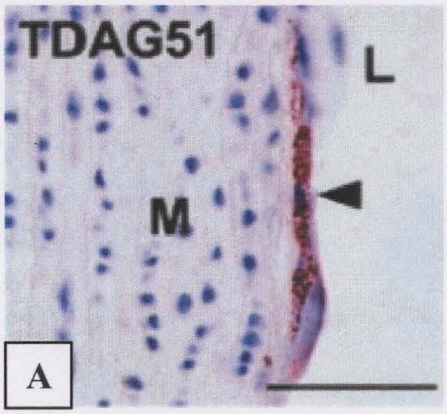

Advanced lesion

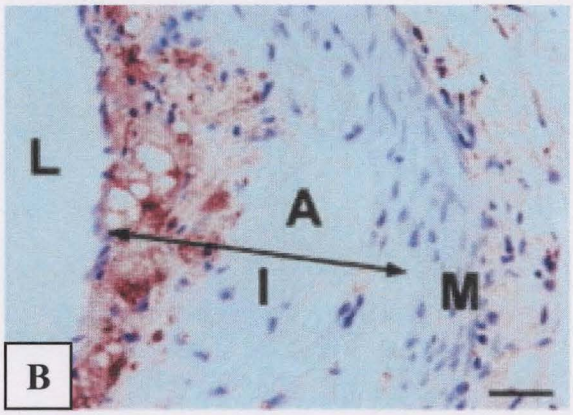

Figure 29: TDAG51 expression and DAPI staining in atherosclerotic lesions from a human carotid artery.

Carotid artery specimens were acquired at the time of endarterectomy for symptomatic or asymptomatic carotid artery disease (in collaboration with Dr. Claudio Cina of McMaster University). Following processing, the specimens were sectioned and placed onto slides. The tissue sections were then immunostained using antibody against TDAG51 to detect the presence of TDAG51 within the cellular portion of the lesions. DAPI staining further confirmed the nuclear staining of cellular portion of the lesions.

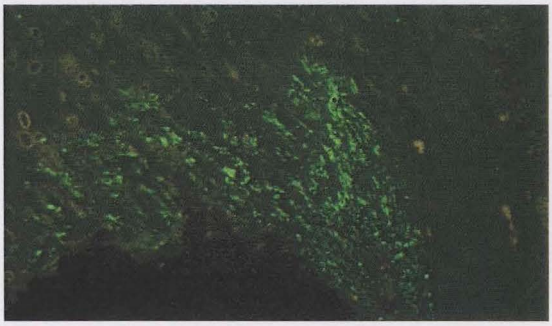

anti-TDAG51

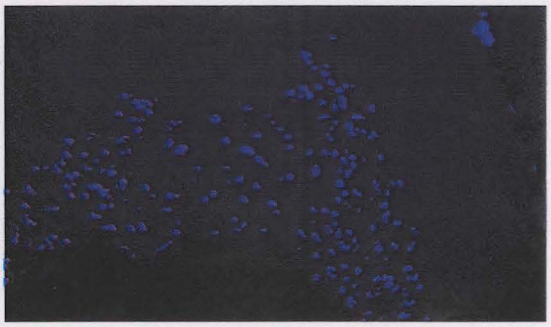

DAP

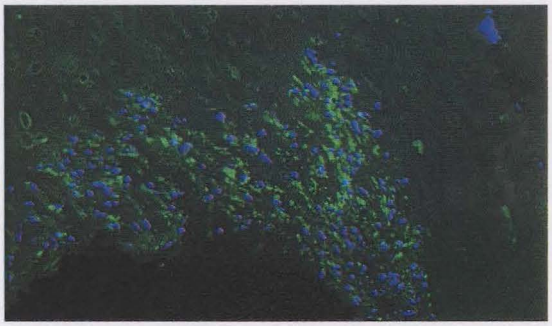

anti-TDAG51 / DAPI

sections from the aortic root and total atherosclerotic lesion area by *en face* lipid staining observed in the aortas of DKO mice, compared to apoE$^{-/-}$ controls. Given that TDAG51 is an ER stress-induced pro-apoptotic gene (Hossain *et al.*, 2003), it is conceivable that reduced atherosclerotic lesion size in DKO mice may be due to decreased apoptosis from the deficiency of TDAG51. However, necrotic lipid core size of DKO mice does not account for the attenuated lesion size, suggesting that additional factor(s) may be involved for the reduction of lesion size observed in DKO mice.

Furthermore, epidemiological studies in humans have reported an association between hepatic steatosis or fatty liver and cardiovascular risk factors such as dyslipidemia, insulin resistance, and type 2 diabetes mellitus (Laakso and Lehto 1998; Arad *et al.*, 2001; Völzke *et al.*, 2005; Targher and Arcaro 2007; Loria *et al.*, 2008; Sookoian and Pirola 2008). Hepatic steatosis is generally caused by increased influx of fatty acid to the liver or increased *de novo* synthesis of liver fatty acid, leading to the esterification of fatty acids into triglycerides. Interestingly, DKO mice fed normal chow diet presented with increased hepatic steatosis. In addition, we have observed a significant upregulation of peroxisome proliferators-activated receptor γ (PPAR-γ) in TDAG51$^{-/-}$ mouse embryonic fibroblasts (MEFs), compared to control wildtype MEFs. Earlier studies have shown the involvement of PPAR-γ in the development of obesity, diabetes, and cardiovascular disease (Lehrke and Lazar 2005). It is believed that the activity of PPAR-γ is modulated by direct binding of small molecules, namely PPAR-γ ligands. Anti-diabetic drugs, thiazolidinediones (TZDs), can activate PPAR-γ by mimicking the actions of PPAR-γ ligands. Clinical studies have reported the effect of

TZDs in diabetic patients and have suggested its vascular protective effects from improved insulin-sensitivity, decreased vascular and systemic inflammatory markers, and reduced atherosclerosis (Verges 2004; Zhang and Chawla 2004). Additionally, studies in mice have demonstrated that the overexpression of PPAR-γ decreases atherosclerotic lesion development and increases hepatic steatosis (Lehrke and Lazar 2005) - a phenotype similar to that observed in mice deficient for both apoE and TDAG51 genes.

It is therefore conceivable that the ability of TDAG51 deficiency to decrease atherosclerotic lesion development in $apoE^{-/-}$ mice may not be all due to its pro-apoptotic characteristic. It is possible that TDAG51 influences the transcription/translation of other genes, including PPAR-γ. Given that PPAR-γ activates reverse cholesterol transport in lesion-resident macrophages and is considered atheroprotective (Chawla *et al.*, 2001; Chinetti *et al.*, 2001; Lehrke and Lazar 2005), our findings suggest that TDAG51 is a contributory factor to the development of atherosclerosis through a mechanism involving PPAR-γ.

3.2 Materials and Methods

3.2.1 Materials

Mayer's hematoxylin and eosin and Oil red O were obtained from Sigma Aldrich. Primers WT 1 (5'-CCG CAG CAC CTC CAA CTC TGC CTG-3'), WT 2 (5'-GTC TTC AAA TAC AAT GAA AGA GTC G-3'), TDAG51 KO 1 (5'-AAA TGG AAG TAG CAC GTC TCA CTA GTC TCG-3'), TDAG51 KO 2 (5'-AGA GCA GCC GAT TGT CTG TTG TGC CCA GTC-3'), ApoE 1 (5'-GCC TAG CCG AGG GAG AGC CG-3'), ApoE 2 (5'-TGT GAC TTG GGA GCT CTG CAG C-3') and ApoE 3 (5'-GCC GCC CCG ACT GCA TCT-3') were synthesized at the MOBIX, McMaster Institute for Molecular Biology and Biotechnology (Hamilton, ON).

All other chemicals, reagents, and materials were of the highest quality available.

3.2.2 Methods

3.2.2.1 Mice and dietary conditions

$ApoE^{-/-}$ mice were obtained from the Jackson Laboratory (Bar Harbor, Maine). Two pairs of TDAG51 heterozygous ($TDAG51^{+/-}$) mice were a generous gift from Dr. Y. Choi, University of Pennsylvania. $ApoE^{-/-}$, $TDAG51^{-/-}$ or DKO mice for these studies were generated at the Henderson Research Centre Animal facilities. After 15-, 25- or 40-weeks on the normal chow diet, the mice were sacrificed and the tissue samples were collected. All experimental procedures were approved by the McMaster University Animal Research Ethics Board.

3.2.2.2 Isolation of DNA for mouse genotyping

Small pieces of tail or ear were collected from mice and placed in 500 µl DNA lysis buffer (1M Tris HCl pH8.5; 0.5M EDTA; 10% SDS; 5M NaCl). Five microliters of proteinase K (10 mg/ml) was added to each microcentrifuge tube and incubated overnight at 55°C. The samples were then allowed to cool down at room temperature, vortexed and centrifuged at 1400 rpm for 20 min. Four hundred microlitres of sample were removed and placed into designated tubes containing 400 µl of isopropanol. After votexing, DNA was precipitated and the supernatant was discarded. TE buffer (1M Tris-HCl, 0.5M EDTA) was then added to the dried DNA. The DNA samples were stored at 4°C before using for PCR.

3.2.2.3 Mouse genotyping using polymerage chain reaction

PCR was performed using collected mouse DNA to confirm the genotypes of the mice. The following primers were used to assess the presence of wildtype and/or disrupted TDAG51 alleles: WT 1, WT 2, TDAG51 KO 1 and TDAG51 KO 2. Parameters for the 44 cycles of PCR after denaturing once at 94°C for 2 min were as follows: denaturation at 94°C for 30 sec, annealing at 58°C for 30 sec, and extension at 68°C for 1 min. Additional extension at 68°C for 5 min was performed before storing at 4°C. PCR amplified products (1 kilobase pair band for wildtype TDAG51 gene and a 400 base pair band for disrupted TDAG51 gene) were analyzed by agarose gel electrophoresis.

ApoE genotyping was confirmed by using the following primers: ApoE 1, ApoE 2 and ApoE 3. Parameters for the 40 cycles of PCR after denaturing DNA once at 94°C

for 5 min were as follows: denaturation at 94°C for 20 sec, annealing at 68°C for 40 sec, and extension at 72°C for 2 min. PCR amplified products (155 base pair band for wildtype apoE gene and a 245 base pairs band for disrupted apoE gene) were analyzed by agarose gel electrophoresis.

3.2.2.4 Approach to generate mouse model deficient in both apoE and TDAG51 genes

Mice deficient in both TDAG51 and apoE were generated as described in **Figure 30**. In brief, TDAG51$^{+/-}$ mice, having C57BL/6 background, were crossed to generate TDAG51$^{-/-}$ mice. ApoE$^{-/-}$ mice (C57BL/6 background) were then crossed with TDAG51$^{-/-}$ mice to obtain mice that were deficient in both apoE and TDAG51 genes as described in Figure 30. In each step, genotypes of the offsprings were determined by PCR analysis. To further confirm the lack of TDAG51 expression in DKO mice, immunoblot analysis for TDAG51 was performed on tissue samples. Since female DKO mice failed to breed, male DKO mice were crossed with female apoE-deficient mice heterozygous for TDAG51 to obtain the desired numbers of DKO mice.

3.2.2.5 Immunoblot analysis

Tissue samples were homogenized and total cell lysates solublized in 4X SDS-PAGE sample buffer. An equivalent amount of protein lysate was separated by electrophoresis on SDS-polyacrylamide gels under reducing conditions, as described previously

Figure 30: Schematic diagram showing generation of mice deficient in both TDAG51 and apoE genes.

TDAG51$^{+/-}$ mice having C57BL/6 background were first paired to generated TDAG51$^{-/-}$ mice (step 1). Male TDAG51$^{-/-}$ mice were then crossed with female apoE$^{-/-}$ mice (C57BL/6 background) to obtain TDAG51$^{+/-}$/apoE$^{+/-}$ mice. Male and female TDAG51$^{+/-}$ /apoE$^{+/-}$ mice were next paired to generate mice deficient in both apoE and TDAG51 genes (step 3 & 4). In each step, genotype of the mice was confirmed by PCR analysis as described in the experimental procedures.

Step 1:

$TDAG51^{+/-}$ (M) X $TDAG51^{+/-}$ (F)

↓

$TDAG51^{-/-}$; $TDAG51^{+/-}$; $TDAG51^{+/+}$

Step 2:

$TDAG51^{-/-}$ (M) X $apoE^{-/-}$ (F)

↓

$TDAG51^{+/-}/apoE^{+/-}$

Step 3:

$TDAG51^{+/-}/apoE^{+/-}$ (M) X $TDAG51^{+/-}/apoE^{+/-}$ (F)

↓

$TDAG51^{+/+}/apoE^{+/+}$; $TDAG51^{+/-}/apoE^{+/+}$; $TDAG51^{-/-}/apoE^{+/+}$;
$TDAG51^{+/+}/apoE^{+/-}$; $TDAG51^{+/-}/apoE^{+/-}$; $TDAG51^{-/-}/apoE^{+/-}$;
$TDAG51^{+/+}/apoE^{-/-}$; $TDAG51^{+/-}/apoE^{-/-}$; $TDAG51^{-/-}/apoE^{-/-}$

Step 4:

$TDAG51^{-/-}/apoE^{-/-}$ (M) X $TDAG51^{+/-}/apoE^{-/-}$ (F)

↓

$TDAG51^{+/-}/apoE^{-/-}$; $TDAG51^{-/-}/apoE^{-/-}$

(Laemmli *et al.*, 1971) and the immunoblot analysis was then performed as described in section 2.2.2.8.

3.2.2.6 Tissue sample preparation

Following euthanization, hearts were flushed with 1X PBS and perfusion-fixed with 10% neutral buffered formalin (Zhou *et al.*, 2001). After removal, the hearts (including the aortic root) were cut transversely and embedded in paraffin (Paigen *et al.*, 1987). The aortic root was cross-sectioned serially at 4 μm intervals and collected on glass slides for the measurement of lesion size (hematoxylin/eosin staining) and immunohistochemical analysis. Atherosclerotic lesion area was measured using computer-assisted image analysis equipment (Zeiss Axioskop 2 microscope, Sony 3CCD color video camera and SigmaScan Pro from Jandel Scientific Software) and the mean plaque size was then calculated.

3.2.2.7 Hematoxylin/Eosin staining

Following deparaffinization in xylenes, the tissue sections were treated in ethanols (100%, 70%) and in water. The sections were stained with hematoxylin for 30 sec to 3 min, followed by rinsing in tap water and 1X PBS. After staining of the tissue sections with working solution of eosin, the sections were dehydrated in ethanols (95%, 100%) and in xylene, and the slides were mounted with coverslips using Permount mounting medium (Fisher Scientific).

3.2.2.8 Immunohistochemical analysis

Tissue sections were deparaffinized as described in section 3.2.2.7 and the endogenous peroxidase activity was blocked with 0.5% H_2O_2 in methanol for 10 min. For some antibodies, antigen retrieval was performed if necessary. After blocking with appropriate blocking serum, the tissue sections were incubated with appropriate primary antibodies for 1 hr. The sections were then washed in TBS buffer and incubated with appropriate biotinylated secondary antibodies (Vector Laboratories) and streptavidin-peroxidase (Zymed Laboratories). The sections were then washed in TBS buffer, developed in Nova Red peroxidase substrate (Vector Laboratories) and counterstained with hematoxylin. The sections were rinsed in tap water, dehydrated in ethanols (70%, 100%) and transferred to xylene before mounting the slides with coverslips. Nonspecific immunostaining was not detected in control sections. Controls consist of nonimmune IgG as the primary antibody or the secondary antibody alone.

3.2.2.9 *En face* oil red O staining of mice aorta

The unopened aorta was evaluated under a dissection microscope and the atherosclerotic plaques were easily identified in the transparent aortas. The unopened aorta was then stained in Oil red O solution for 1 hr, followed by rinsing in 50% ethanol and distilled water. Images of the unopened aortas were captured using a Zeiss Axioskop 2 microscope and a Sony 3CCD color video camera. Aortas were then opened longitudinally, mounted onto slides with coverslips and the image was again captured.

For both unopened and opened aorta, the stained area was measured as described in section 3.2.2.6 and compared as the percentage of the total aorta.

3.2.2.10 Measurement of total cholesterol, triglyceride and glucose in mice plasma

For the measurement of total cholesterol, concentrations of cholesterol standard (mg/dl) were first prepared by a series of dilutions according to Infinity^{TM} cholesterol measurement kit (Thermo Electron Corporation, Melbourne, Australia). Duplicate, 5 µl serum samples were then plated in a 96 well plate. After appropriate dilutions of the serum in ddH_2O, 200µl of cholesterol reagent was added to each well. Following 15 min of incubation at room temperature, the absorbance of the wells was read at 500 nm using a microplate reader (Molecular Devices, Union City, CA). SoftMax 3.1 program was then used to determine the cholesterol levels of the unknown samples.

The approach to measure triglyceride or glucose levels in mice plasma was also similar to the above described cholesterol assay (Thermo Electron Corporation). Herein, triglyceride or glucose standard curve (mg/dl) was prepared by a series of dilutions. Further, the absorbance of the wells was read at 500 nm or 340 nm to measure the concentrations of triglyceride or glucose, respectively.

3.2.2.11 Measurements of lipids in tissue samples

After weighing the tissue samples, 500 µl of homogenization buffer (10 mM Hepes, 20 mM MgCl, 10 mM 2-Mercaptoethanol, 0.5% Triton X-100) was added and the samples

were homogenized on ice. The lysates were then transferred to glass tubes and the lipids were extracted with hexane:isopropanol (3:2). The lipids were next placed into new glass tubes, dried down overnight in speed vacuum and resuspended in 200 µl of isopropanol. For the measurement of protein concentration, 150 µl of aqueous phase was transferred to an eppendorf tube. The remaining 50 µl of organic phase was dried in a glass tube and later used for the measurement of cholesterol and triglyceride, as described in section 3.2.2.10.

3.2.2.12 Measurement of mice plasma lipid profiles using FPLC

Mouse plasma was fractionated using gel Filtration-fast Protein Liquid Chromatography (FPLC) as described by Rigotti *et al.* (1997). In brief, plasma (150 µl) was diluted with an equal volume of elution buffer (154 mM NaCl/1 mM EDTA, pH 8) and subjected to FPLC using two Superose 6 columns (Pharmacia) connected in series. Forty seven fractions (0.5 ml each) were collected after the first 14 ml were eluted and the total cholesterol in each fraction was measured as described in section 3.2.2.10.

3.2.2.13 Statistical Analysis

All experimental values are presented as mean ± standard deviation. Comparison between the means was performed using the unpaired Student's *t*-test. ANOVA was used for multiple comparisons among the means. For all analyses, $P<0.05$ was considered statistically significant.

3.3 Results

3.3.1 Generation of TDAG51/apoE double knockout mice

In our earlier studies, we demonstrated that TDAG51 is associated with the development of atherosclerosis in apoE$^{-/-}$ mice (Hossain *et al.*, 2003). Furthermore, TDAG51 is expressed in early and advanced atherosclerotic lesions from apoE$^{-/-}$ mice fed normal chow diet (Zhou *et al.*, 2005). To further address the significance of TDAG51 deficiency in the development and progression of atherosclerosis, TDAG51$^{-/-}$ mice were crossed with apoE$^{-/-}$ mice to generate DKO mice, as described in section 3.2.2.4. Authenticity of the generated DKO mice was confirmed by PCR and immunoblot analysis **(Figure 31)**. It is important to mention that TDAG51$^{-/-}$ or DKO mice did not demonstrate any developmental abnormalities. Since male or female apoE$^{-/-}$ mice are established model for atherosclerosis (Daugherty 2002; Ohashi *et al.*, 2004), the studies were performed using male apoE$^{-/-}$ and male DKO mice. Interestingly, mean body weight of DKO mice was significantly increased at 40 weeks of age, compared to apoE$^{-/-}$ mice (39.2 ± 9.02 versus 32.6 ± 2.56 gm, $P<0.05$) **(Figure 32)**.

3.3.2 Effect of TDAG51 deficiency on atherosclerotic lesion development in apoE$^{-/-}$ mice

Apoptosis plays a significant role in the development and progression of atherosclerotic lesions. Earlier studies have demonstrated that the functional deficiency of pro-apoptotic genes (p53, Bax or Rb) contributes to enhanced atherosclerosis (Guevara *et al.*, 1999; Liu *et al.*, 2004; Boesten *et al.*, 2006). Since TDAG51 is a pro-apoptotic gene and is

Figure 31: Genotyping of TDAG51 and apoE genes in DKO mice.

Mouse genomic DNA was used for PCR amplification and identification of the wildtype TDAG51 allele (1 kilo base pairs; **panel A, lanes 2-5**) or the disrupted TDAG51 allele (400 base pairs; **panel B, lanes 4-7**) allowing the identification of mice homozygote for the disrupted TDAG51 allele (**panel B, lanes 6-7**). PCR amplification and identification were also used to determine if mice homozygote for the disrupted TDAG51 allele were homozygotic for the disrupted apoE allele (245 base pairs; **panel C, lanes 6-7**). Lanes 8 and 9 represent negative controls for PCR reactions (**panels A-C**). To reconfirm the genotyping results obtained by PCR, immunoblot analysis was performed on mice liver samples (40 week; **panel D**). Liver from DKO mice was homogenized to prepare cell lysates, immunoblotted with anti-TDAG51 antibodies (**panel D, lanes 1-5**), and compared to apoE$^{-/-}$ mice liver samples (**panel D, lanes 6-8**). Results indicate the lack of TDAG51 protein (40 kDa) in the livers of DKO mice fed normal chow diet for 40 weeks.

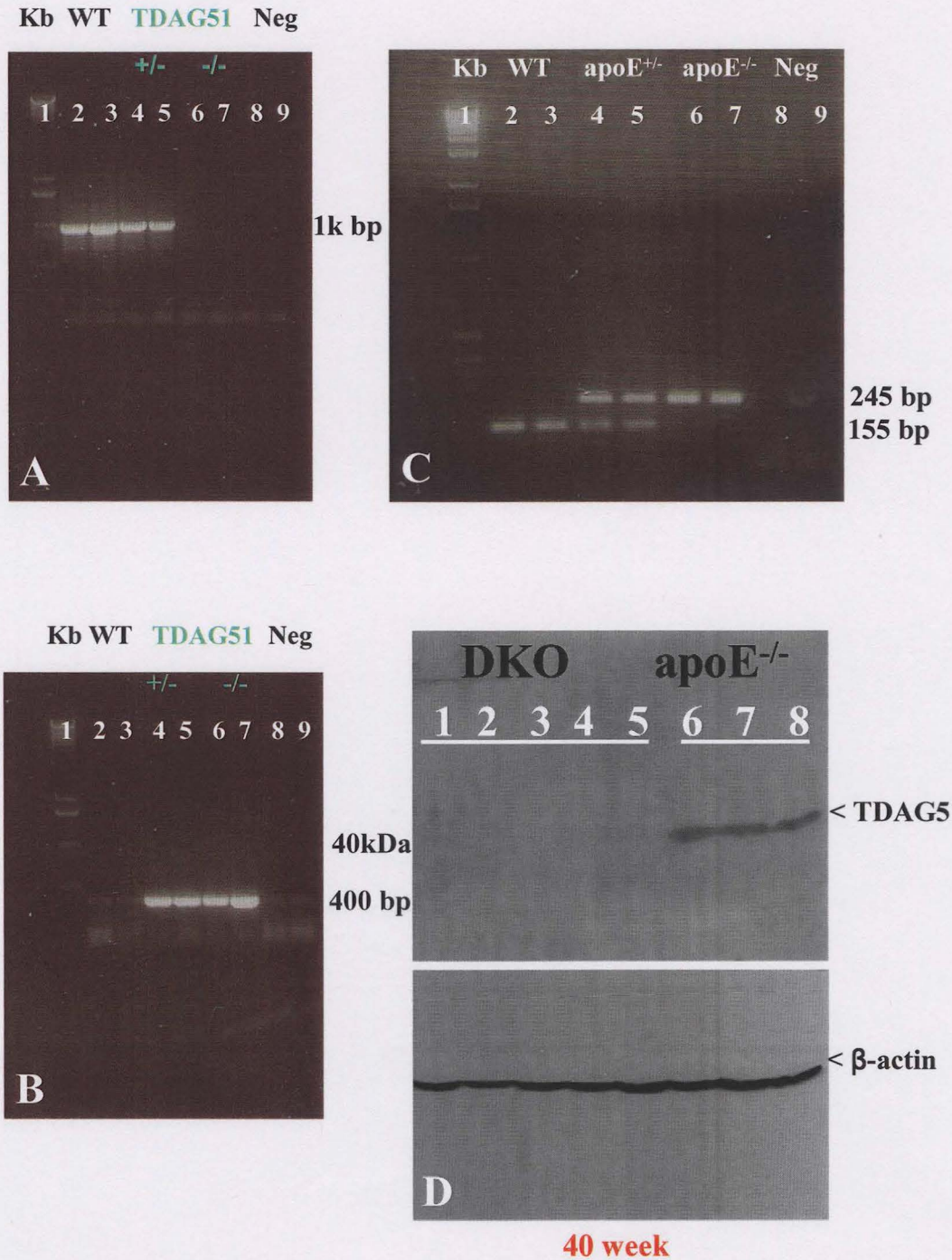
Kb WT TDAG51 Neg
+/- -/-
1 2 3 4 5 6 7 8 9
1k bp
A
Kb WT apoE+/- apoE-/- Neg
1 2 3 4 5 6 7 8 9
245 bp
155 bp
C
Kb WT TDAG51 Neg
+/- -/-
1 2 3 4 5 6 7 8 9
40kDa
400 bp
B
DKO apoE-/-
1 2 3 4 5 6 7 8
< TDAG51
< β-actin
D
40 week

Figure 32: Measurement of body weight in TDAG51/apoE-deficient and apoE$^{-/-}$ control mice.

Following genotyping, DKO or apoE$^{-/-}$ control mice were fed normal chow diet for 25 or 40 weeks. Before sacrificing, mice were weighed using TL-420 weighing machine (Denver Instrument Company). The results indicate that body weight of DKO mice were significantly ($P<0.05$) increased, compared to apoE$^{-/-}$ control mice at 40 week of age.

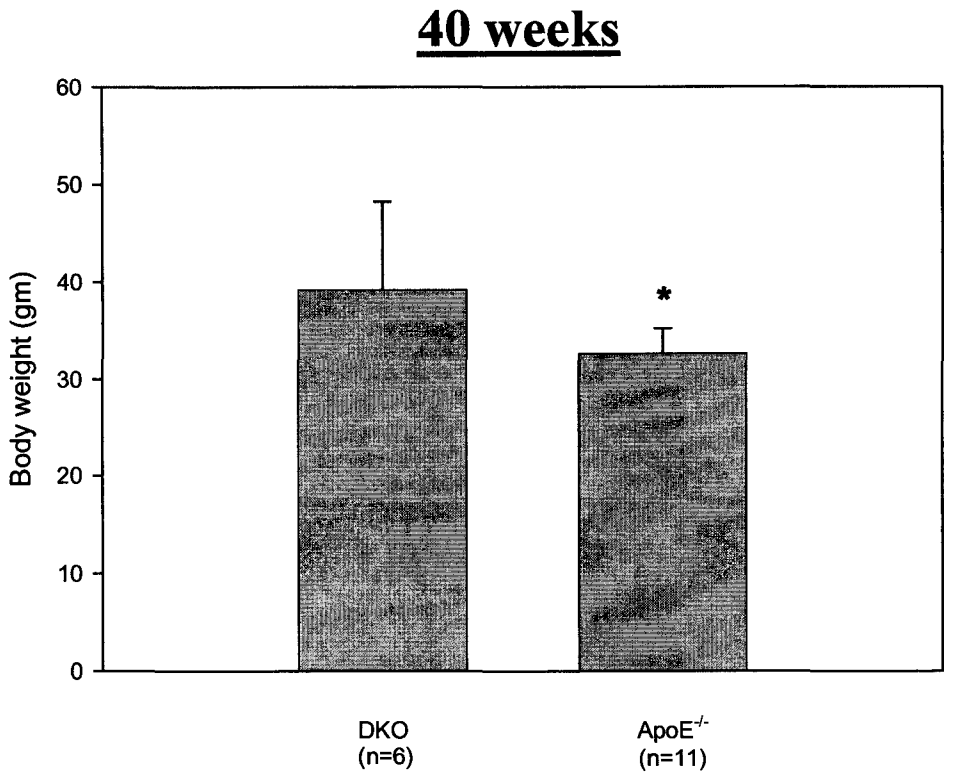
40 weeks
Body weight (gm)
60
50
40
30
20
10
0
*
DKO
(n=6)
ApoE-/-
(n=11)

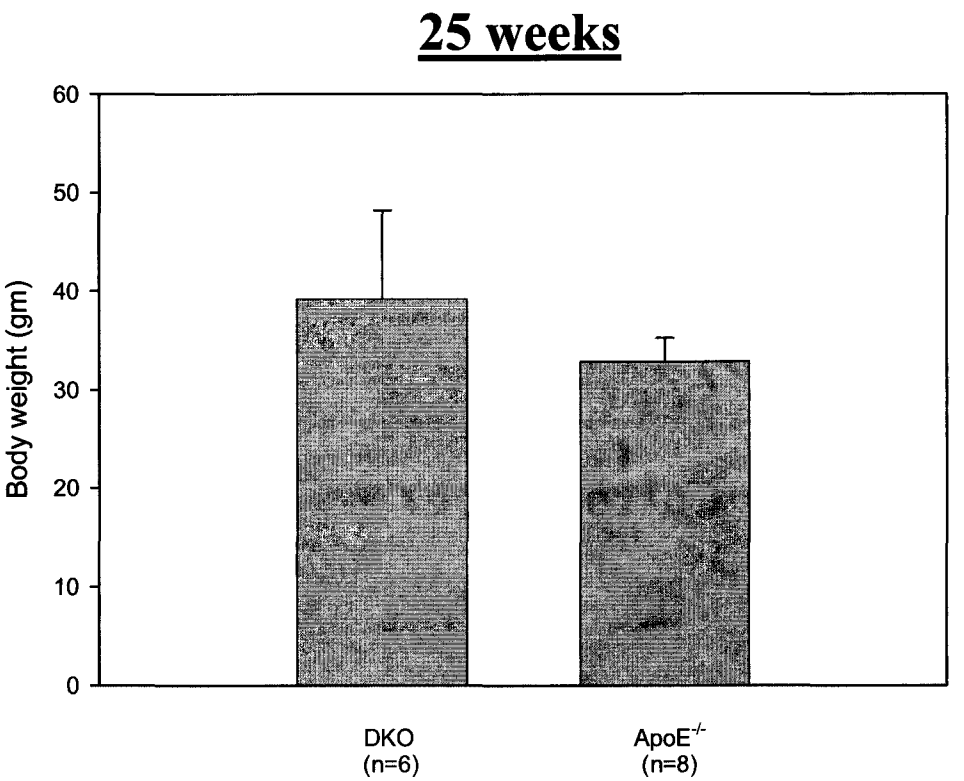
25 weeks
Body weight (gm)
60
50
40
30
20
10
0
DKO
(n=6)
ApoE-/-
(n=8)

expressed within cells relevant to atherosclerosis (Hossain *et al.*, 2003; Zhou *et al.*, 2005), it is conceivable that the deficiency of TDAG51 would enhance atherosclerosis. To examine the role of TDAG51 in atherosclerotic lesion development, apoE$^{-/-}$ control male mice and DKO male mice were fed normal chow diet for 15, 25 or 40 weeks and the aortic lesion development was then analyzed.

Hematoxylin/Eosin staining of the aortic root demonstrated that atherosclerotic lesions in 40 week old DKO mice were significantly decreased, compared to apoE$^{-/-}$ control mice **(Figure 33)**. The mean atherosclerotic lesion size in the aortic root of 40 week DKO group was significantly smaller (1.2 ± 0.34 versus 3.2 ± 0.61 μm^2 X 10^6, $P<0.05$). Consistent with these findings, atherosclerotic lesions in 25 week old DKO mice were also significantly reduced, compared to apoE$^{-/-}$ control mice **(Figure 34)**. Statistical analysis demonstrated that the mean atherosclerotic lesion size in the aortic root of 25 week DKO group was markedly smaller (0.36 ± 0.13 versus 0.77 ± 0.25 μm^2 X 10^6, $P<0.05$). No statistical difference was found in the mean atherosclerotic lesion size between DKO and apoE$^{-/-}$ mice at 15 weeks of age (0.32 ± 0.25 versus 0.73 ± 0.75 μm^2 X 10^5) **(Figure 35)**.

To further assess the role of TDAG51 deficiency in atherosclerosis, the total atherosclerotic lesion size was measured by unopened and *en face* oil red O lipid staining. The atherosclerotic lesion area within the whole aorta was significantly decreased in 40 week old DKO mice, compared to apoE$^{-/-}$ control mice **(Figures 36 and 37)**. Statistical analysis further confirmed the reduced mean atherosclerotic lesion area (unopened aorta:

Figure 33: Atherosclerotic lesion size in the aortic root of mice fed normal chow diet for 40 weeks.

TDAG51/apoE double knockout (DKO) mice or apoE$^{-/-}$ control mice were sacrificed after 40 week on normal chow diet. Aortic root sections were stained with hematoxylin/eosin and the images were captured as described in experimental procedures. The representative figure demonstrates a reduction in atherosclerosis from mice that are deficient in both apoE and TDAG51 genes (a), compared to apoE$^{-/-}$ control mice (b). In addition, lesion size was measured as described in experimental procedures (c). The results demonstrate that atherosclerotic lesion size is significantly smaller ($P<0.05$) in DKO mice, compared to apoE$^{-/-}$ control mice at 40 week of age.

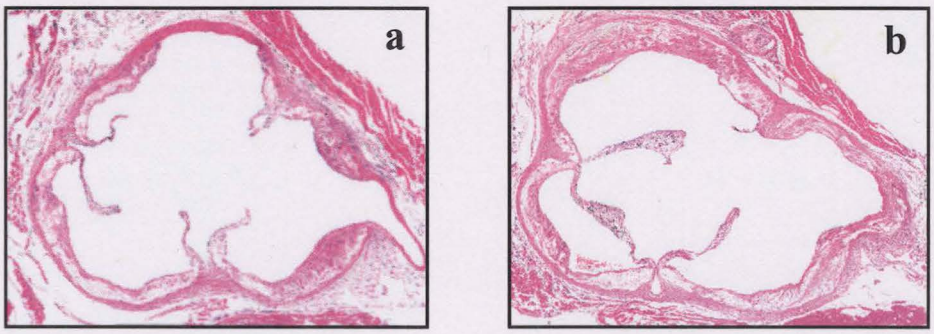
a
b
DKO
ApoE-/-

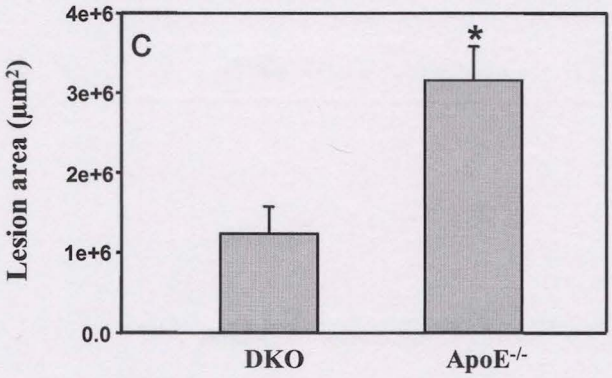
C
*
4e+6
3e+6
2e+6
1e+6
0.0
Lesion area (µm²)
DKO
ApoE-/-

Figure 34: Atherosclerotic lesion size in the aortic root of mice fed normal chow diet for 25 weeks.

DKO mice or apoE$^{-/-}$ control mice were sacrificed after 25 week on normal chow diet. Aortic root sections were stained with hematoxylin/eosin and the images were then captured as described in experimental procedures. The representative figure demonstrates that atherosclerotic lesion size is significantly smaller in DKO mice (a), compared to apoE$^{-/-}$ mice (b). In addition, lesion size was measured as described in experimental procedures (c). The results demonstrate that atherosclerotic lesion size is significantly smaller ($P<0.05$) in DKO mice, compared to apoE$^{-/-}$ control mice at 25 week of age.

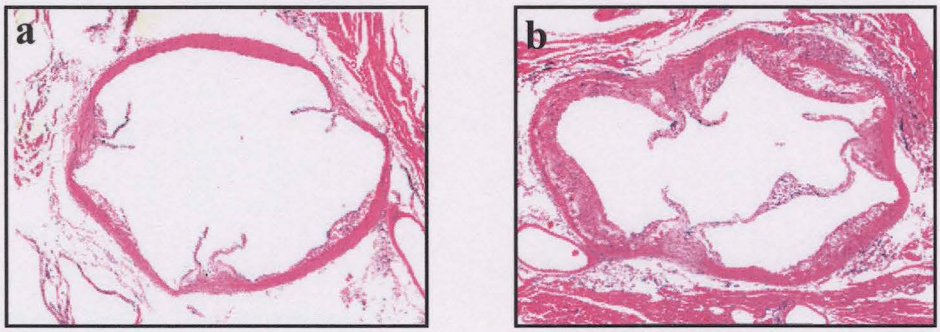
a
b
DKO
ApoE-/-

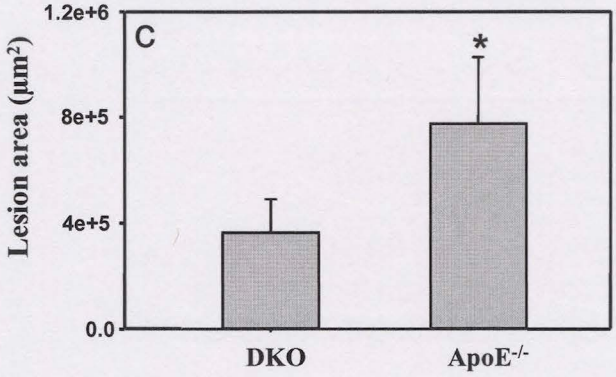
C
1.2e+6
8e+5
4e+5
0.0
Lesion area (µm²)
*
DKO
ApoE-/-

Figure 35: Atherosclerotic lesion size in the aortic root of mice fed normal chow diet for 15 weeks.

DKO or apoE$^{-/-}$ control mice were sacrificed after 15 week on normal chow diet. Aortic root sections were then stained with hematoxylin/eosin and the lesion size was measured as described in experimental procedures. The representative figure demonstrates no significant difference in atherosclerotic lesion size between DKO (a) and apoE$^{-/-}$ mice (b). In addition, lesion size was measured as described in experimental procedures (c). The results demonstrate that mean atherosclerotic lesion size is not significant at 15 week of age between DKO mice and apoE$^{-/-}$ control mice.

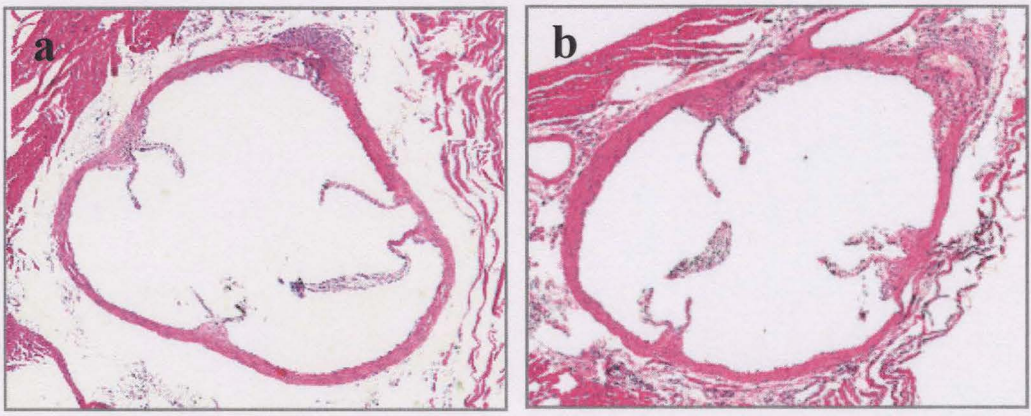
a
b
DKO
ApoE-/-

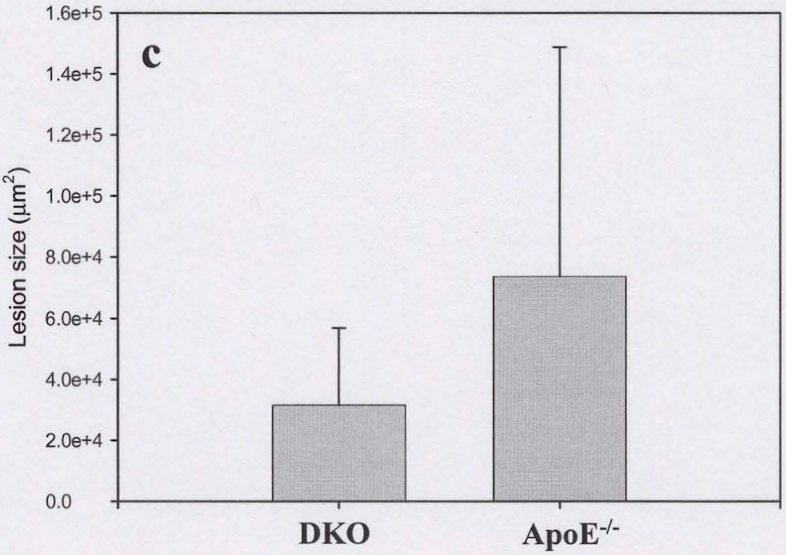
c
1.6e+5
1.4e+5
1.2e+5
1.0e+5
8.0e+4
6.0e+4
4.0e+4
2.0e+4
0.0
Lesion size (μm2)
DKO
ApoE-/-

Figure 36: Unopened aorta demonstrating decreased atherosclerotic lesion size in TDAG51/apoE-deficient mice compared to apoE$^{-/-}$ control mice.

Following genotyping, DKO or apoE$^{-/-}$ control mice were fed normal chow diet for 40 weeks. **Panel A**, representative oil red O stained aortas from DKO and apoE$^{-/-}$ control mice. **Panel B**, quantitative data on lesion size from the whole aortas. The results indicate that mean atherosclerotic lesion size from the whole aortas was significantly smaller ($P<0.005$) in the DKO mice, compared to apoE$^{-/-}$ control mice.

A

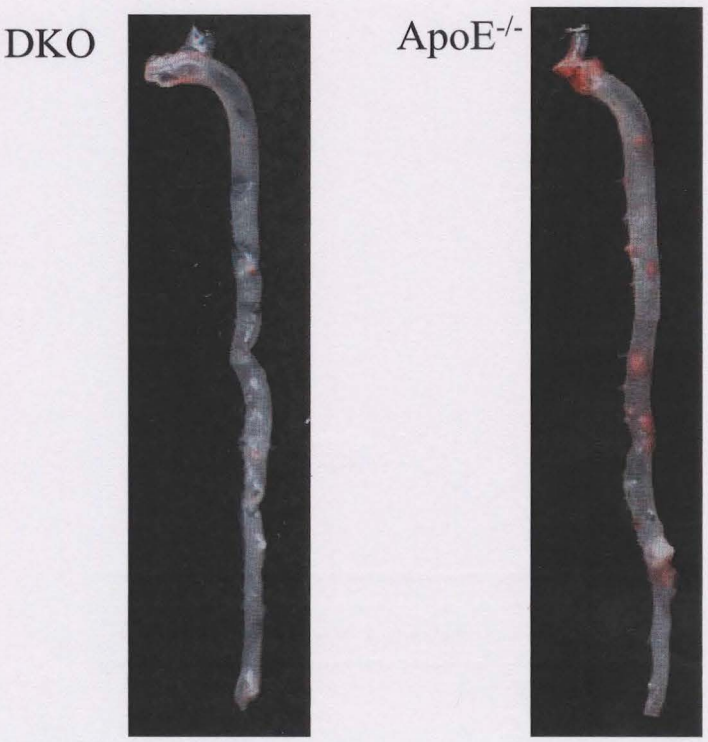

B

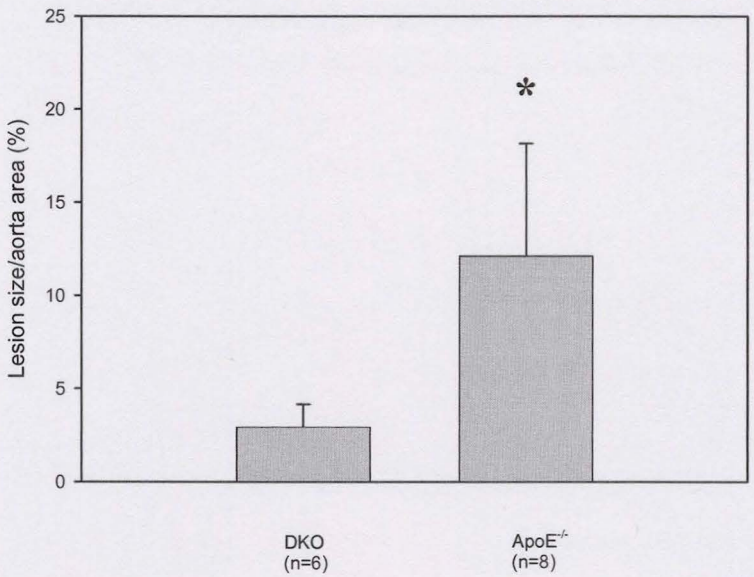

Figure 37: *En face* analysis demonstrating decreased atherosclerotic lesion size in TDAG51/apoE-deficient mice compared to apoE$^{-/-}$ control mice.

Following genotyping, DKO mice or apoE$^{-/-}$ control mice were fed normal chow diet for 40 weeks. Aortas were opened as described in the experimental protocols. **Panel A**, representative Oil red O stained opened aortas from DKO and apoE$^{-/-}$ control mice. **Panel B**, quantitative data on lesion size from the whole opened aortas. The results indicate that atherosclerotic lesion size from the whole opened aortas was significantly smaller ($P<0.005$) in the DKO mice, compared to apoE$^{-/-}$ control mice.

A

DKO

ApoE$^{-/-}$

B

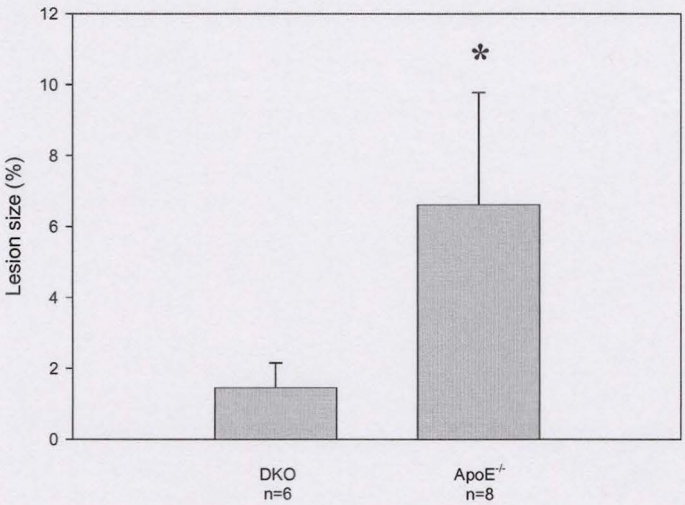

2.9 ± 1.2 versus 12 ± 6.0 %, $P<0.005$; *en face* aorta: 2.0 ± 0.96 versus 8.9 ± 4.4 %, $P<0.005$) in the aortas of 40 week old DKO mice **(Figures 36 and 37)**.

The effect of TDAG51 deficiency on the necrotic lipid core size was also investigated to explain the reduced atherosclerotic lesion size in DKO mice. The mean necrotic lipid core size in the atherosclerotic lesions of 25 week old DKO mice was markedly decreased, compared to apoE$^{-/-}$ mice (0.37 ± 0.20 versus 1.8 ± 0.10 μm^2 X 10^5, $P<0.05$) **(Figure 38)**. In support of this, reduced apoptosis is observed in the atherosclerotic lesions of DKO mice as shown by TUNEL staining, compared to those in apoE$^{-/-}$ mice **(Figure 39)**. However, the significant reduction in necrotic core size does not account for all the reduction in atherosclerotic lesion size for DKO mice **(Table 2)**. Statistical analysis demonstrates that only 35% of the reduction in atherosclerotic lesion size is associated with the reduction of necrotic core. It is therefore possible that other anti-atherogenic factor(s) may contribute to the remaining 65% reduction of lesion size in DKO mice.

Furthermore, to examine the morphology or cellular components, the atherosclerotic lesions from apoE$^{-/-}$ and DKO mice were stained with the cell marker proteins (antibodies against active caspase 3 (apoptotic cells), CD3 (lymphocytes), smooth muscle actin (smooth muscle cells) or MAC-3 (macrophages) **(Figure 40)**). Our results show that all the cells relevant to atherosclerosis (lymphocytes, macrophages, and smooth muscle cells) are present within the atherosclerotic lesions of both apoE$^{-/-}$ and DKO mice.

Figure 38: Mean necrotic lipid core size is decreased in TDAG51/apoE-deficient mice compared to apoE$^{-/-}$ control mice.

Following genotyping, DKO mice or apoE$^{-/-}$ control mice were fed normal chow diet for 25 weeks. Necrotic lipid core was calculated from the cross sections of aortic root that were stained with hematoxylin/eosin. Acellular region within atherosclerotic lesions where no cells were identified was considered as the necrotic core. The graph demonstrates that necrotic lipid core size is significantly smaller ($P<0.05$) at 25 weeks in DKO mice, compared to apoE$^{-/-}$ control mice.

Necrotic lipid core size in the lesion from the aortic root (DKO vs ApoE$^{-/-}$, 25 wk study)

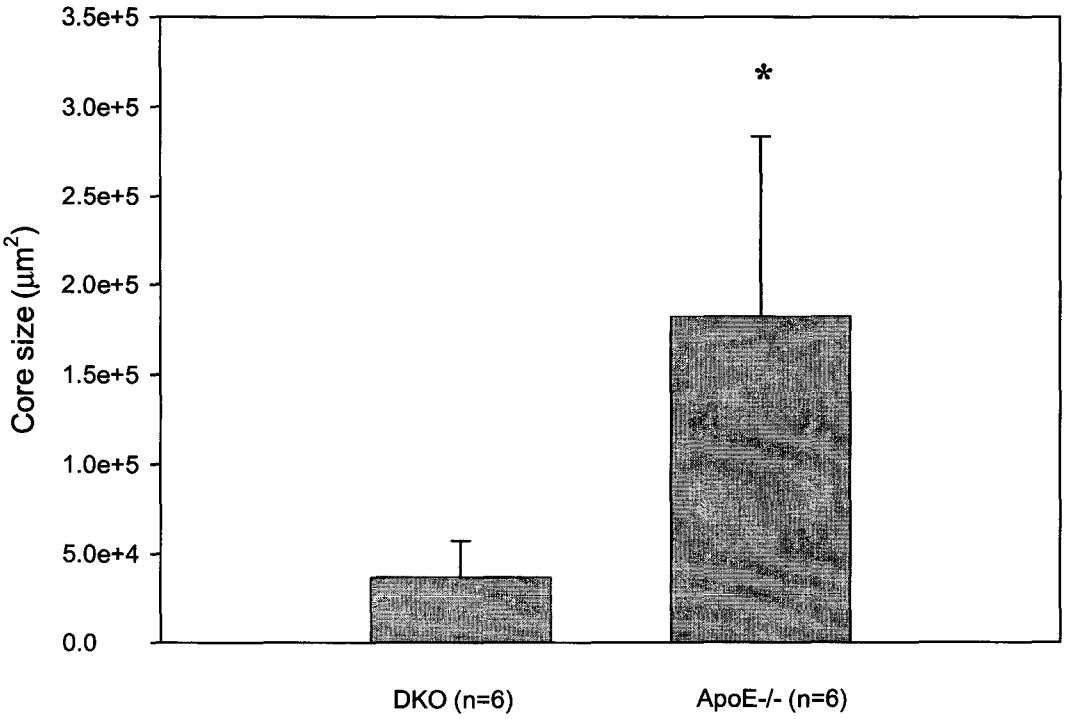

Figure 39: Effect of TDAG51 deficiency on apoptotic cell death in advanced atherosclerotic lesions.

Six week old DKO or apoE$^{-/-}$ mice were place on control chow diet for 40 weeks. TUNEL and cleaved caspase-3 staining were observed in the necrotic core of advanced lesions in DKO or apoE$^{-/-}$ mice. The figure demonstrates decreased TUNEL staining in the atherosclerotic lesions of DKO mice, compared to apoE$^{-/-}$ mice.

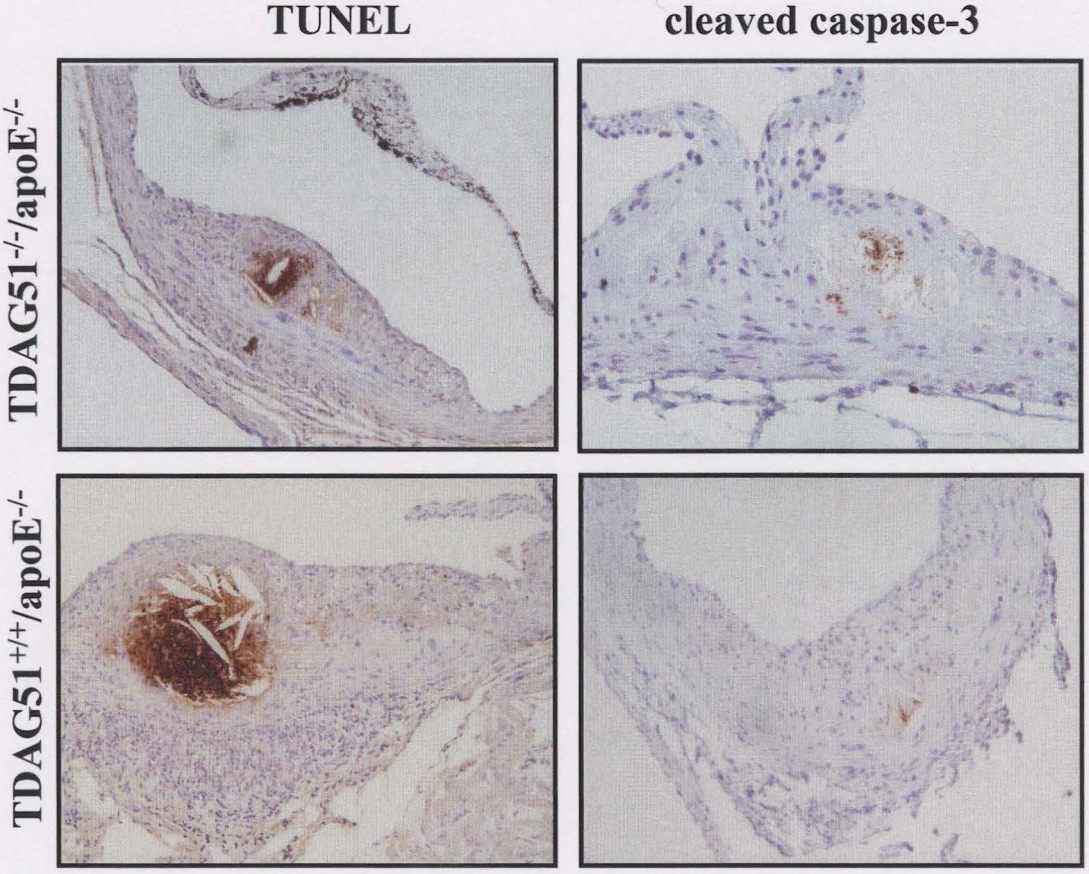
TUNEL
cleaved caspase-3
TDAG51-/-/apoE-/-
TDAG51+/+/apoE-/-

Table 2: Analysis of necrotic lipid core in the aortic lesion of mice fed normal chow diet for 25 weeks .

	ApoE$^{-/-}$ mice	DKO mice	Difference	% Reduction
Mean lesion (μm^2)	7.7 X 10^5	3.6 X 10^5	4.1 X 10^5	53.2%
Necrotic core (μm^2)	1.8 X 10^5	0.37 X 10^5	1.43 X 10^5	79.4%

Difference in mean lesion size (μm^2) = Mean lesion size (apoE$^{-/-}$) - Mean lesion size (DKO)

$= 7.7 \text{ X } 10^5 - 3.6 \text{ X } 10^5$
$= 4.1 \text{ X } 10^5$

Difference in necrotic core size (ΔNC, μm^2) = Mean NC size (apoE$^{-/-}$) - Mean NC size (DKO)

$= 1.8 \text{ X } 10^5 - 0.37 \text{ X } 10^5$
$= 1.43 \text{ X } 10^5$

% reduction in lesion size = $(4.1 \text{ X } 10^5/7.7 \text{ X } 10^5) \text{ X } 100\%$
$= 53.2\%$

% reduction in necrotic core size = $(1.43 \text{ X } 10^5/1.8 \text{ X } 10^5) \text{ X } 100\%$
$= 79.4\%$

% of reduction in lesion size accounted for by the reduction in necrotic core size
= **(Δ Necrotic core size/Δ Lesion size)** X 100% = $(1.43 \text{ X } 10^5/4.1 \text{ X } 10^5) \text{ X } 100\%$
= **34.8%**

Figure 40: Identification of atherosclerotic lesion components in apoE$^{-/-}$ and TDAG51/apoE double knockout mice.

Identification of macrophages (Mac-3), smooth muscle cells (SMA) and lymphocytes (CD3) in atherosclerotic lesions from the aortic root of TDAG51$^{-/-}$/apoE$^{-/-}$ or TDAG51$^{+/+}$/apoE$^{-/-}$ mice fed control chow diet for 15, 25 or 40 weeks. The representative stained sections from DKO or apoE$^{-/-}$ mice demonstrate the components of cells relevant to atherosclerosis.

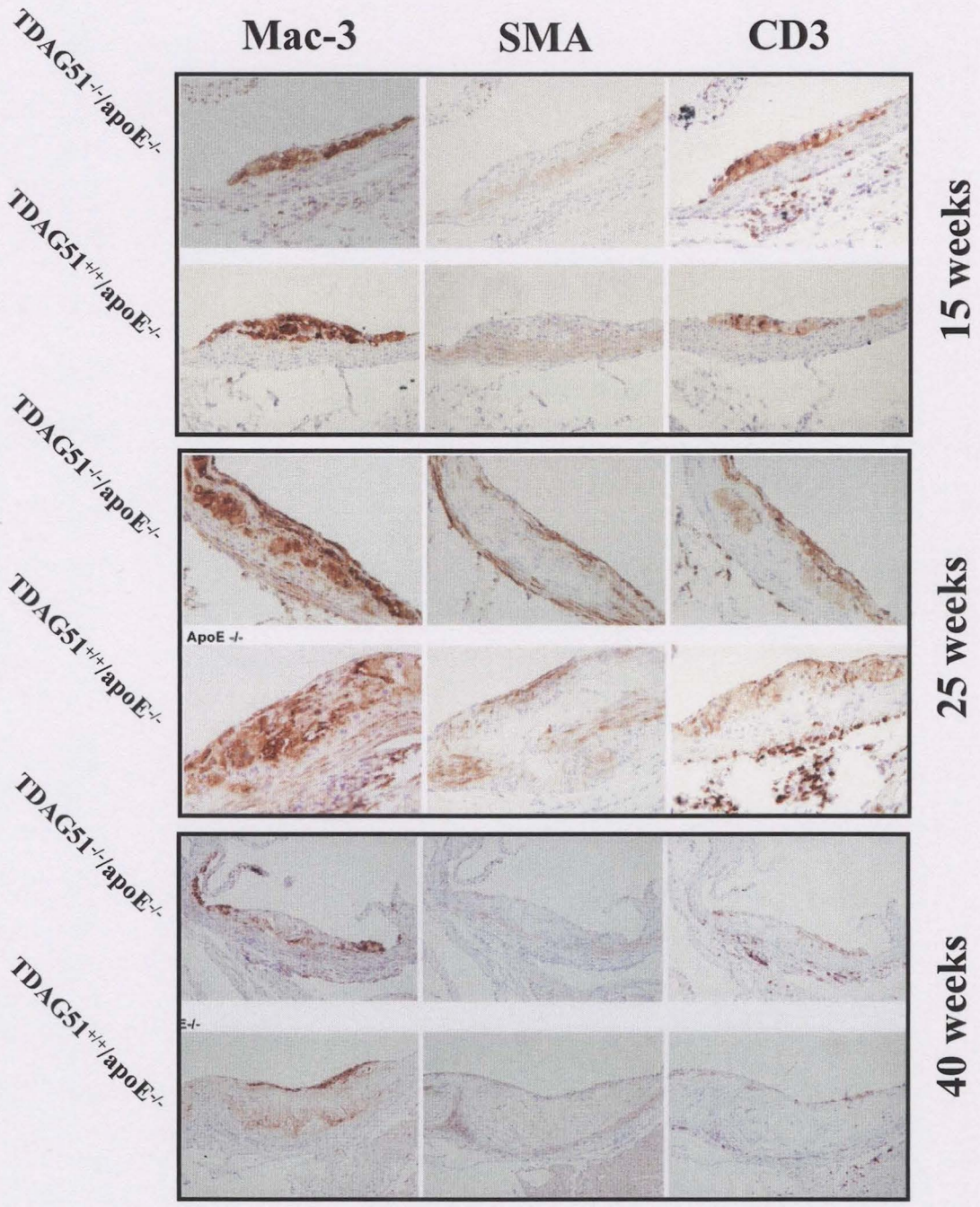
Mac-3
SMA
CD3
TDAG51-/-/apoE-/-
TDAG51+/+/apoE-/-
TDAG51-/-/apoE-/-
TDAG51+/+/apoE-/-
TDAG51-/-/apoE-/-
TDAG51+/+/apoE-/-
ApoE -/-
15 weeks
25 weeks
40 weeks

3.3.3 Effect on total plasma lipid and glucose levels in TDAG51/apoE double knockout mice

Numerous studies have demonstrated that hyperlipidemia contributes to the development of atherosclerotic lesions. The status of plasma lipids was therefore investigated using enzymatic assays to account for the decreased atherosclerotic lesion size in DKO mice. No difference in total plasma cholesterol and triglyceride levels was observed between DKO and apoE$^{-/-}$ control mice at 25 or 40 week of age **(Figure 41)**. In addition, lipoprotein profiles were measured using FPLC. Distribution of lipoproteins at 15 week old apoE$^{-/-}$ control and DKO mice was also indistinguishable **(Figure 42)**. However, mean plasma glucose levels in DKO mice were significantly decreased (40.0 ± 8.78 versus 29.6 ± 4.37 X 10^1 mg/dL, $P<0.05$) at 40 week of age **(Figure 43)**.

3.3.4 Status of lipids in the liver of TDAG51/apoE double knockout mice

Since apoE$^{-/-}$ control and DKO mice did not demonstrate any difference in total plasma cholesterol and triglyceride levels, hepatic lipid levels were assessed to explain whether there is any difference in the uptake or synthesis of lipids. At first, mouse liver sections were stained with hematoxylin/eosin (H&E) to examine the status of lipids in hepatocytes. Interestingly, hepatic steatosis was observed in the livers of DKO mice at 25 or 40 week **(Figure 44)**. To further investigate the role of TDAG51 in lipogenesis, the levels of cholesterol or triglycerides were measured in the liver tissue samples. The results support the findings from H&E staining. The mean hepatic triglyceride levels were markedly increased in DKO mice at 40 week of age, compared to that in apoE$^{-/-}$ mice (8.1 ± 3.8

Figure 41: Total plasma cholesterol and triglyceride levels in TDAG51/apoE-deficient and apoE$^{-/-}$ control mice.

Following genotyping, DKO or apoE$^{-/-}$ control mice were fed normal chow diet for 25 or 40 weeks. Total plasma cholesterol and triglyceride levels were measured as described in the experimental procedures. The results indicate no significant changes in total cholesterol or triglyceride levels between DKO and apoE$^{-/-}$ control mice.

Plasma total cholesterol

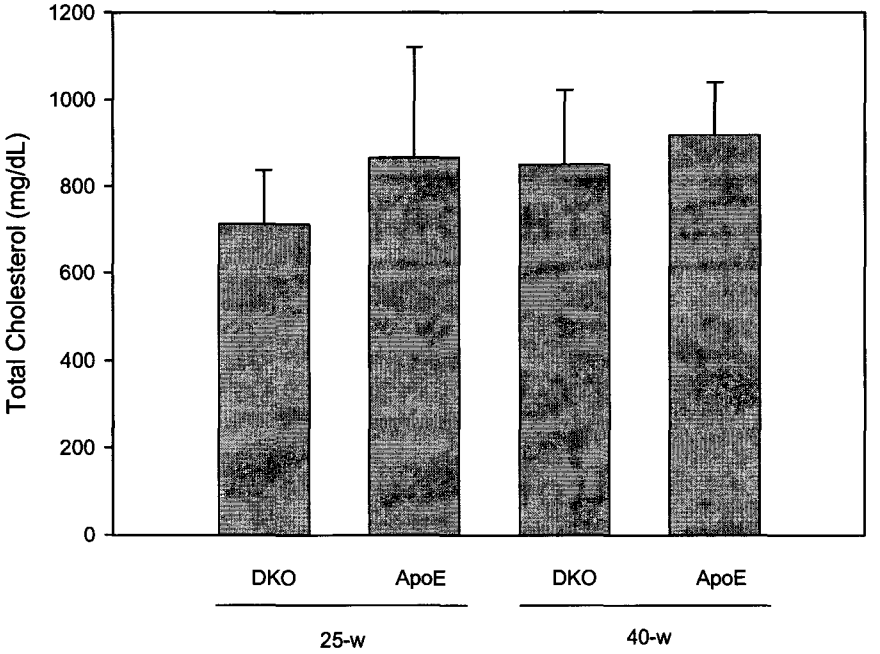

Plasma TG level

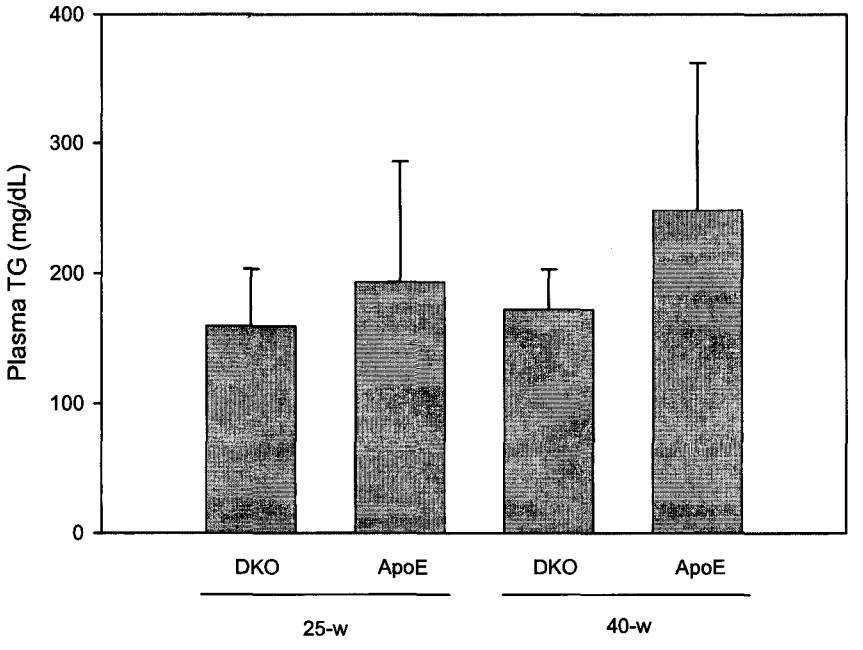

Figure 42: Status of lipoprotein distribution in TDAG51/apoE-deficient and apoE$^{-/-}$ control mice.

Following genotyping, DKO or apoE$^{-/-}$ control mice were fed normal chow diet for 15 weeks. Lipoprotein profiles were obtained by fast protein liquid chromatography (FPLC) as described in the experimental procedures. The results indicate no significant changes in lipoprotein distribution between DKO and apoE$^{-/-}$ control mice.

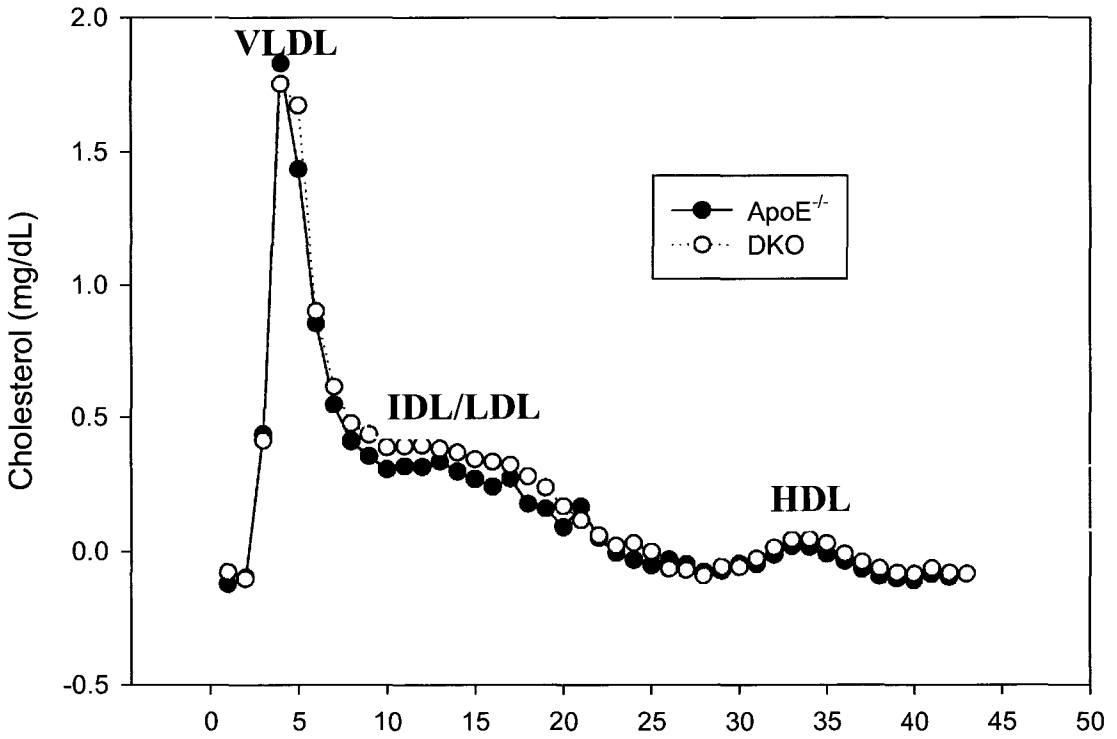
VLDL
IDL/LDL
HDL
ApoE-/-
DKO
Cholesterol (mg/dL)
2.0
1.5
1.0
0.5
0.0
-0.5
0
5
10
15
20
25
30
35
40
45
50

Figure 43: Total plasma glucose levels in TDAG51/apoE-deficient and apoE$^{-/-}$ control mice.

Following genotyping, DKO or apoE$^{-/-}$ control mice were fed normal chow diet for 25 or 40 weeks. Total glucose levels were measured as described in the experimental procedures. The results indicate that glucose levels were significantly decreased ($P<0.05$) in DKO mice, compared to apoE$^{-/-}$ control mice, at 40 week of age.

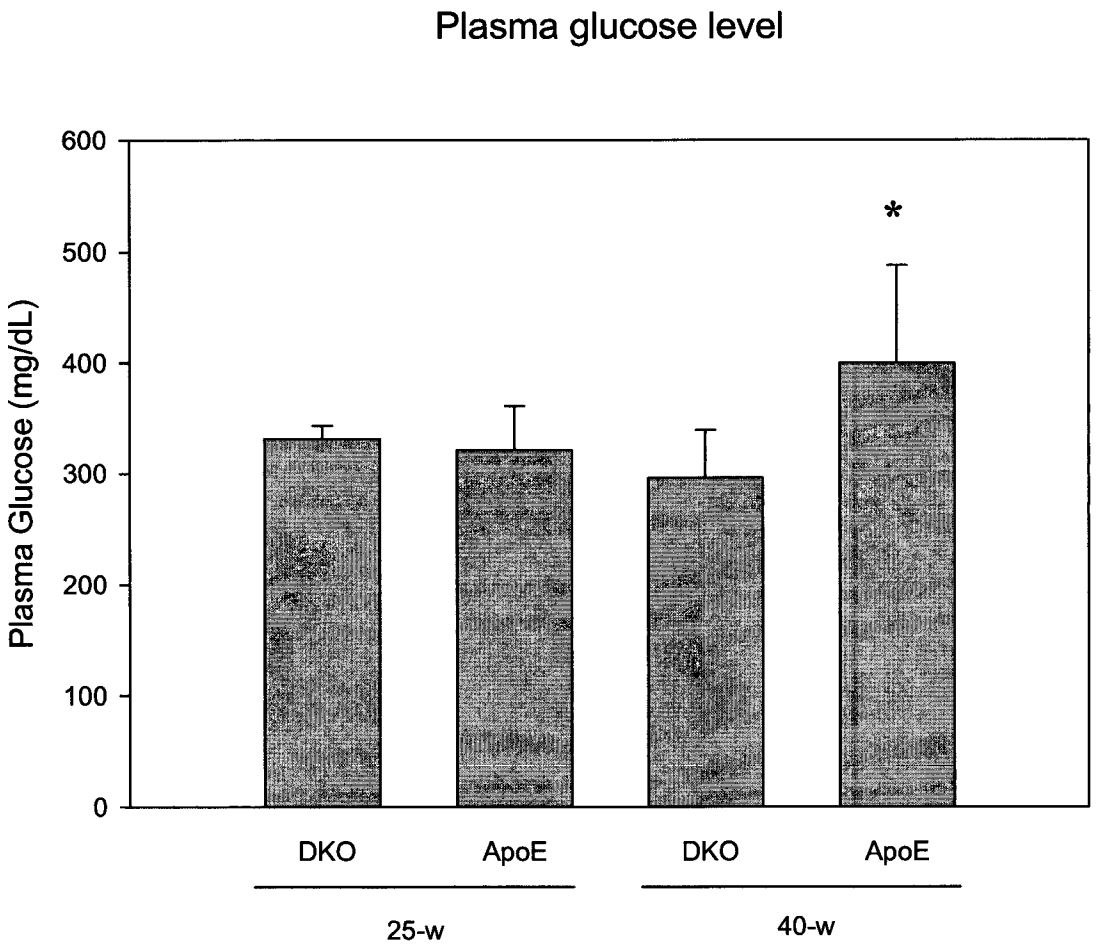
Plasma glucose level
Plasma Glucose (mg/dL)
600
500
400
300
200
100
0
*
DKO
ApoE
DKO
ApoE
25-w
40-w

Figure 44: Status of hepatic steatosis in TDAG51/apoE-deficient and apoE$^{-/-}$ control mice.

DKO or apoE$^{-/-}$ control mice were sacrificed after 15, 25 or 40 weeks in normal chow diet. Liver sections were then stained with hematoxylin/eosin and the image of hepatic lipid accumulation was captured as described in the experimental procedures. The results demonstrate hepatic steatosis in DKO mice fed normal chow diet for 25 or 40 weeks, compared to apoE$^{-/-}$ mice. Red arrows represent hepatocytes with accumulated lipids. Qualitative observation suggests an increased steatosis in DKO mice at 40 week of age.

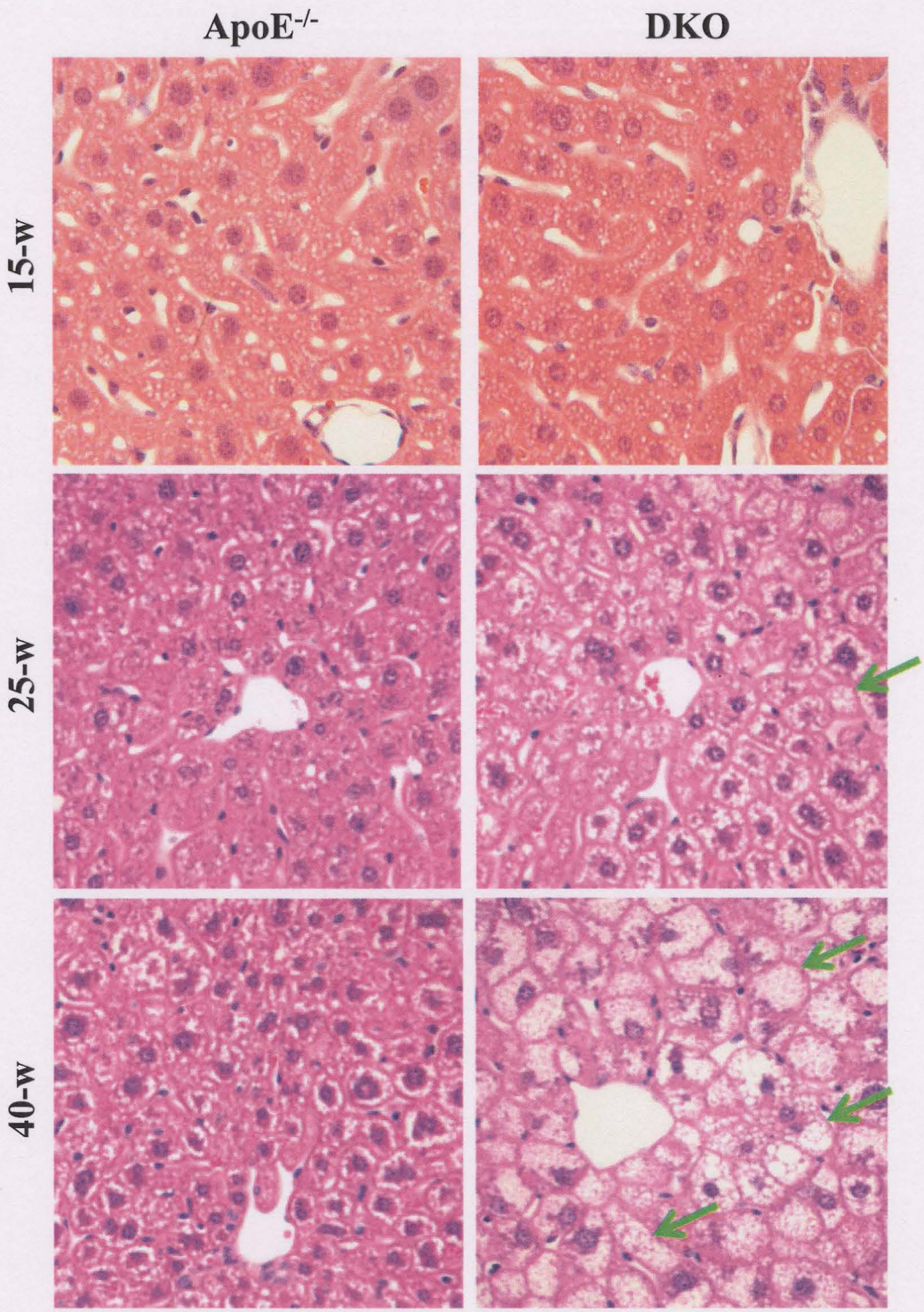
ApoE-/-
DKO
15-w
25-w
40-w

versus 3.6 ± 0.9 mg/mg protein, $P<0.05$) **(Figure 45)**. However, the hepatic cholesterol levels were indistinguishable between DKO and apoE$^{-/-}$ control mice.

3.3.5 Status of PPAR-γ expression in TDAG51$^{-/-}$ MEFs

To understand the effect from the loss of TDAG51 on gene expression, MEFs were generated from C57 control and TDAG51$^{-/-}$ mice as described in the experimental procedures. Affymetrix microarray analysis was performed in C57 control and TDAG51$^{-/-}$ MEFs (in collaboration with Dr. Ken Maclean of University of Colorado). Microarray analysis demonstrated a significant increased expression of PPAR-γ and its downstream gene targets in TDAG51$^{-/-}$ MEFs **(Table 3;** genes with 4-fold or greater induction were included only**)**. Furthermore, our microarray data on the expression of PPAR-γ was confirmed by Real Time PCR analysis (in collaboration with Dr. John Capone of McMaster University; **Figure 46**). Importantly, reintroduction of TDAG51 into TDAG51$^{-/-}$ MEFs blocked PPAR-γ expression. Also, the effect from the loss of TDAG51 is specific to PPAR-γ, since no significant difference was observed at the levels of PPAR-α or PPAR-δ between TDAG51$^{-/-}$ and wildtype MEFs. Previous studies have reported that overexpression of PPAR-γ in hyperlipidemic mice promotes hepatic steatosis and also contributes to reduced atherosclerotic lesions (Lehrke and Lazar 2005).

Figure 45: Status of hepatic cholesterol and triglyceride levels in TDAG51/apoE-deficient and apoE$^{-/-}$ control mice.

Following genotyping, DKO or apoE$^{-/-}$ control mice were fed normal chow diet for 15, 25 or 40 weeks. Liver samples were homogenized and the lipids were extracted as described in the experimental procedures. Hepatic cholesterol and triglyceride levels were then measured. The results indicate that triglyceride levels were significantly ($^{*}P<0.05$) increased in DKO mice, compared to apoE$^{-/-}$ control mice at 40 week of age.

A

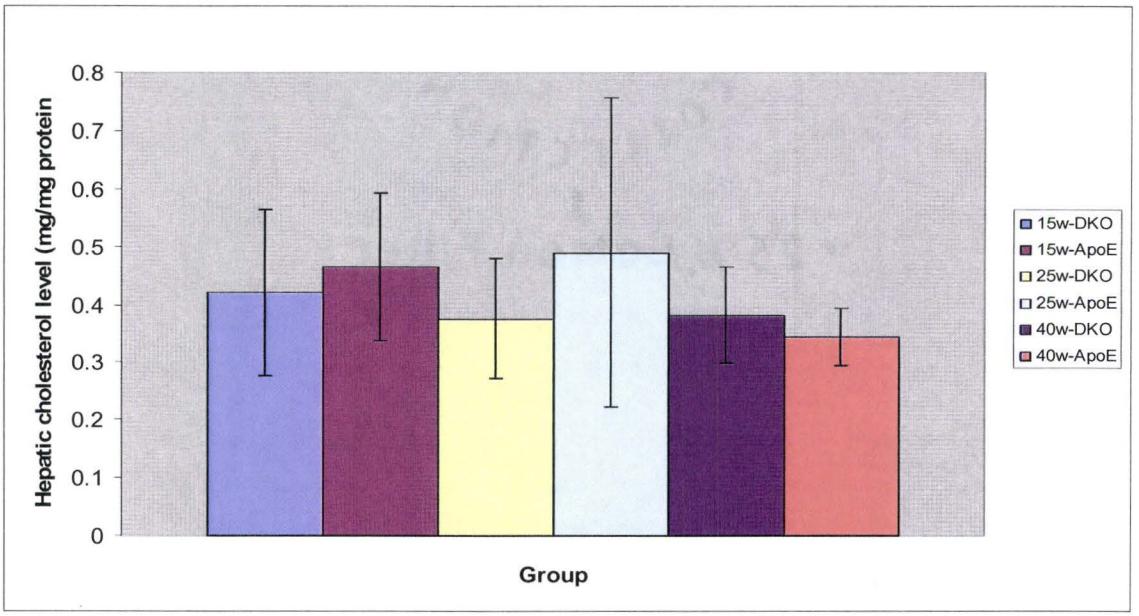
Hepatic cholesterol level (mg/mg protein
0.8
0.7
0.6
0.5
0.4
0.3
0.2
0.1
0
Group
15w-DKO
15w-ApoE
25w-DKO
25w-ApoE
40w-DKO
40w-ApoE

B

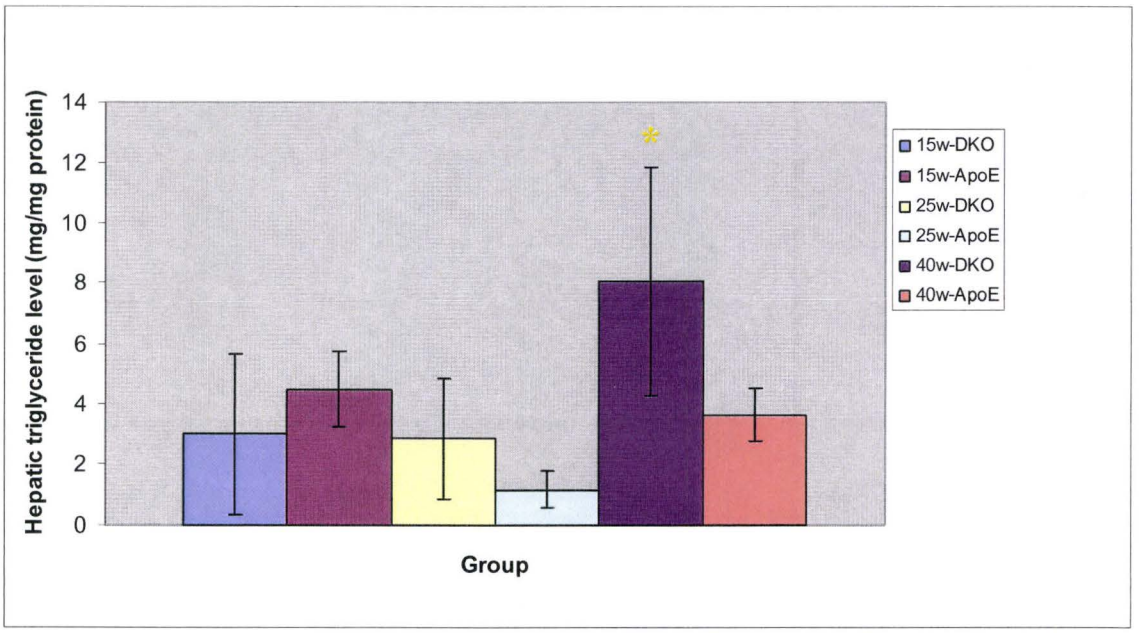
Hepatic triglyceride level (mg/mg protein)
14
12
10
8
6
4
2
0
*
Group
15w-DKO
15w-ApoE
25w-DKO
25w-ApoE
40w-DKO
40w-ApoE

Table 3: Upregulation of genes in TDAG51$^{-/-}$ MEFs compared to C57 control MEFs.
TDAG51$^{-/-}$ and C57 control MEFs were grown in fibroblast growth media. Following isolation of total RNA from both cell types, the microarray was performed on Affymetrix Mouse genome 430 2.0 chips to profile the relative expression levels of over 39,000 transcripts in TDAG51$^{-/-}$ MEFs compared to C57 control MEFs. Approximately 1000 genes were found to be either repressed or induced at the arbitrary cut-off level of 3-fold. Herein, the table demonstrates the genes that are induced 4-fold or greater. Results are represented as duplicate analysis, that is, the average of two separate experiments. Also, as a control, TDAG51 expression was greater than 500-fold in C57 control MEFs, compared to TDAG51$^{-/-}$ MEFs.

Genes	Fold induction
PPAR-γ	29
PPAR-γ targets	
Pyruvate carboxylase	15
Sterol regulatory element binding factor-2	6
prostaglandin E synthase	12
cytosolic acyl-CoA thioesterase 1	5
mitochondrial acyl-CoA thioesterase 1	5
serine protease inhibitor 6	9.5
fatty acid binding protein	10
Very LDL receptor	5
Bcl-2	78
Hepatocyte growth factor	13
Growth and apoptosis	
GAS2	6.5
melanoma inhibitory activity protein 2	22.6
Connective tissue and Osteogenesis	
phosphodiesterase 10A	5
matrilin 2 (ECM component)	4.3
thymosin, beta 10	4.28
asporin (ECM component)	9.18
procollagen, type VI, alpha 1	5
decorin	34.2
proteoglycan 4	8.5
procollagen, type VII, alpha 1	22.6
procollagen, type VI, alpha 2	6.4
procollagen, type VI, alpha 1	4.9
cathepsin k	9.2
Cytoskeleton, cellular adhesion and cell surface proteins	
Photoreceptor cadherin	5.2
protocadherin beta 20	4
astrotactin 2	57
neurofilament, medium polypeptide	16
myosin, heavy polypeptide 8, skeletal muscle, perinatal	64
Transport	
solute carrier family 7 (cationic amino acid transporter, y+ system), member 3	5.6
solute carrier family 39 (iron-regulated transporter), member 1	9.9
solute carrier family 7 (cationic amino acid transporter, y+ system), member 11	4.3
solute carrier family 21 (prostaglandin transporter), member 2	12
plasmacytoma variant translocation 1	8
claudin 1	26

Figure 46: Expression of PPAR-γ in wildtype C57/BL6 and TDAG51$^{-/-}$ MEFs.

Total RNA from MEFs was isolated by Qiagen RNEasy Kit according to the manufacturer's protocol. 2 μ of total RNA was reverse transcribed with random hexamers using M-MLV reverse transcriptase (Invitrogen). The cDNA were then used as templates for individual PCR reactions using gene specific primer sets designed by the Genescript Primer Design Program (www.genescriipt.com) for mouse PPARα, γ, and δ. PCR reaction was carried out using Platinum SYBR Green PCR supermix (Invitrogen) in an AB7900 HT Fast Real Time PCR System. Data was analyzed by standard curve method and normalized to β-actin. Results indicate that reintroduction of TDAG51 (pBabe/TDAG51) into TDAG51$^{-/-}$ MEFs reduces the expression of PPAR to wildtype levels.

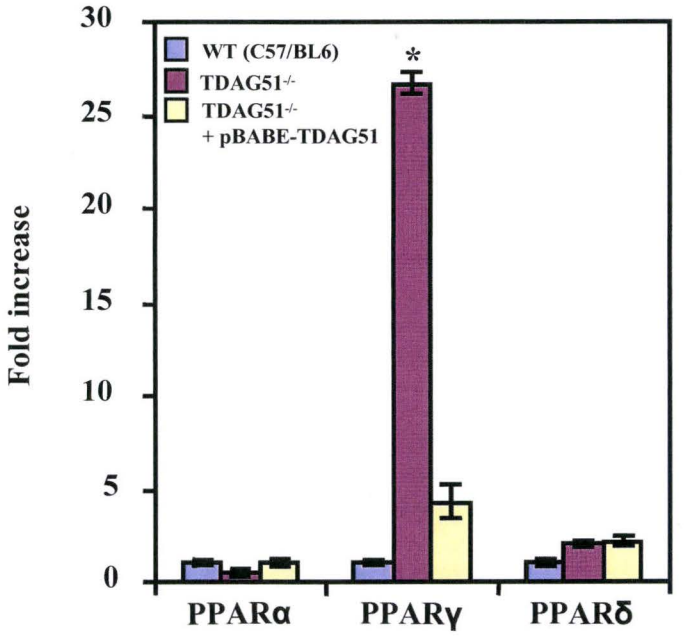
30
25
20
15
10
5
0
Fold increase
WT (C57/BL6)
TDAG51-/-
TDAG51-/-
+ pBABE-TDAG51
*
PPARα
PPARγ
PPARδ

Figure 47: Schematic diagram of the various roles played by the macrophage (Mϕ) within the early and late atherosclerotic lesions.

In early atherosclerosis, macrophage apoptosis attenuates lesion progression by reducing inflammatory responses. However, lesion development can be augmented by the macrophage through the unregulated uptake of oxidized LDL (oxLDL) via the scavenger receptor pathway, leading to foam cell formation. Macrophage activation leads to the secretion of proinflammatory cytokines and cytotoxic substance such as TNF-α and peroxynitrite ($ONOO^-$), respectively. The accumulation of free cholesterol or oxidatively modified cholesterol loading of macrophages, including 7-ketocholesterol, also produces cytotoxicity. As lesions progress, apoptosis generated by these processes contributes to necrotic core formation. Further, the macrophage also counters this process of lesion expansion through Mertk-mediated efferocytosis of apoptotic bodies (AB). This can prevent their secondary necrosis and release of lipids and MMPs which may accelerate the breakdown of collagen that maintains the structural integrity of the vessel wall. In short, although macrophage apoptosis is beneficial in early lesion development but it can be harmful in advanced lesions since this can contribute to the expansion of necrotic core, thereby facilitating the lesions to become unstable.

(Obtained and modified from Dickhout et al. (2008) ATVB 28: 1414.)

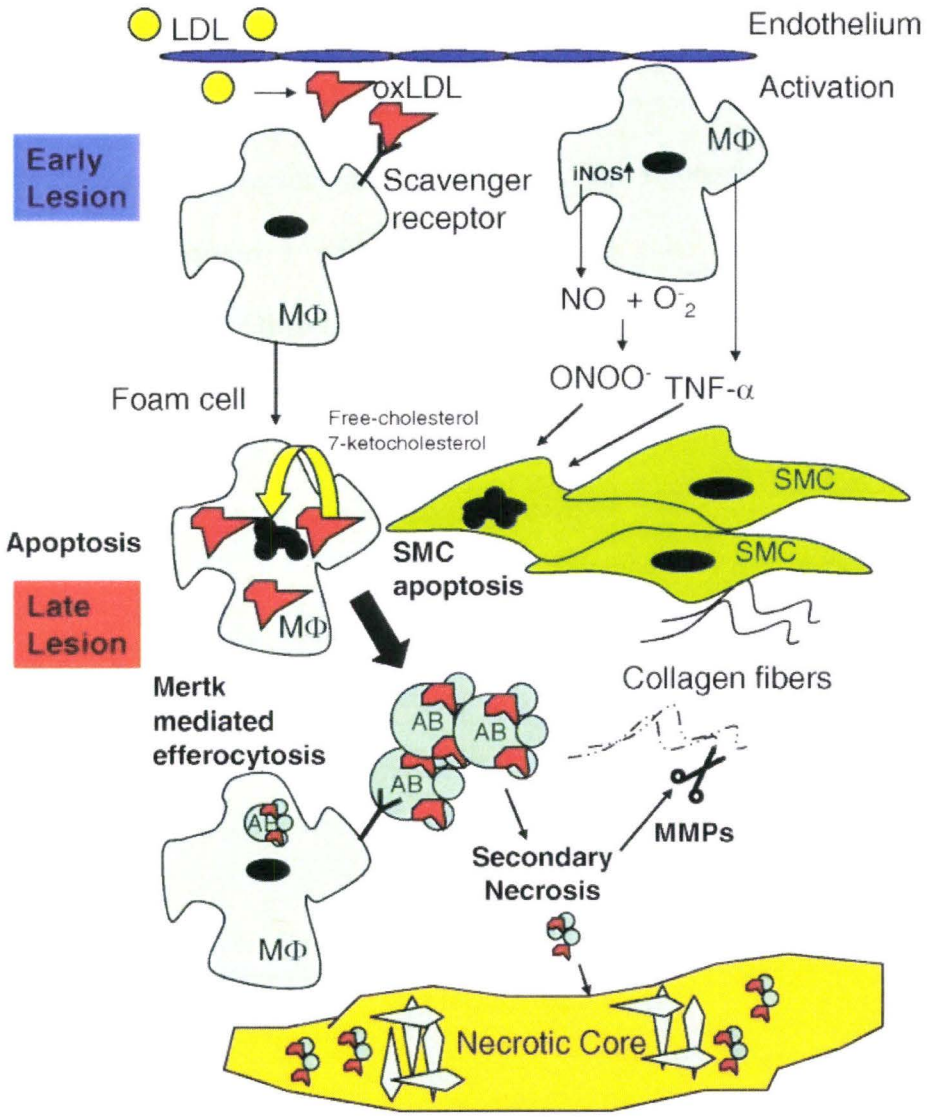
LDL
Endothelium
oxLDL
Activation
Early Lesion
Scavenger receptor
MΦ
iNOS↑
NO + O2-
ONOO-
TNF-α
Foam cell
Free-cholesterol
7-ketocholesterol
SMC
SMC
Apoptosis
Late Lesion
SMC apoptosis
MΦ
Collagen fibers
Mertk mediated efferocytosis
AB
AB
AB
AB
MMPs
Secondary Necrosis
MΦ
Necrotic Core

Figure 48: Effect of TDAG51 deficiency on the expression of peroxiredoxin 1 in early and advanced atherosclerotic lesions.

Six week old DKO or apoE$^{-/-}$ mice were placed on control chow diet for 25 (early) or 40 (advanced) weeks. Atherosclerotic lesions from the aortic root of DKO or apoE$^{-/-}$ mice were stained with antibody against peroxiredoxin 1. The figure demonstrates increased expression of peroxiredoxin 1 within the endothelial cells of early and advanced atherosclerotic lesions from DKO mice, compared to apoE$^{-/-}$ mice.

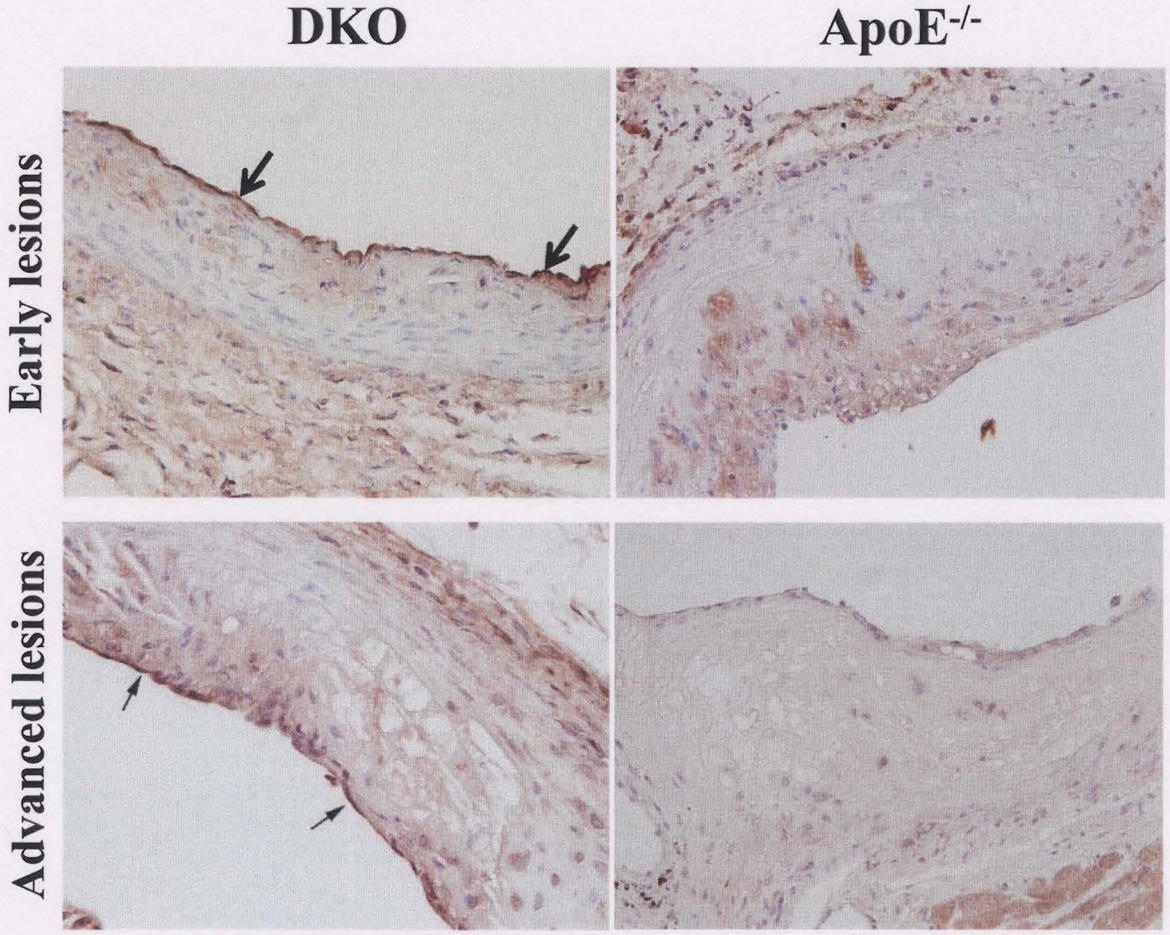
DKO
ApoE-/-
Early lesions
Advanced lesions

Figure 49: Effect of TDAG51 deficiency on the expression of PPAR-γ in early and advanced atherosclerotic lesions.

Six week old DKO or apoE$^{-/-}$ mice were placed on control chow diet for 25 (early) or 40 (advanced) weeks. Atherosclerotic lesions from the aortic root of DKO or apoE$^{-/-}$ mice were stained with antibody against PPAR-γ. The figure demonstrates nuclear localization of PPAR-γ within early and advanced atherosclerotic lesions from DKO mice, compared to apoE$^{-/-}$ mice.

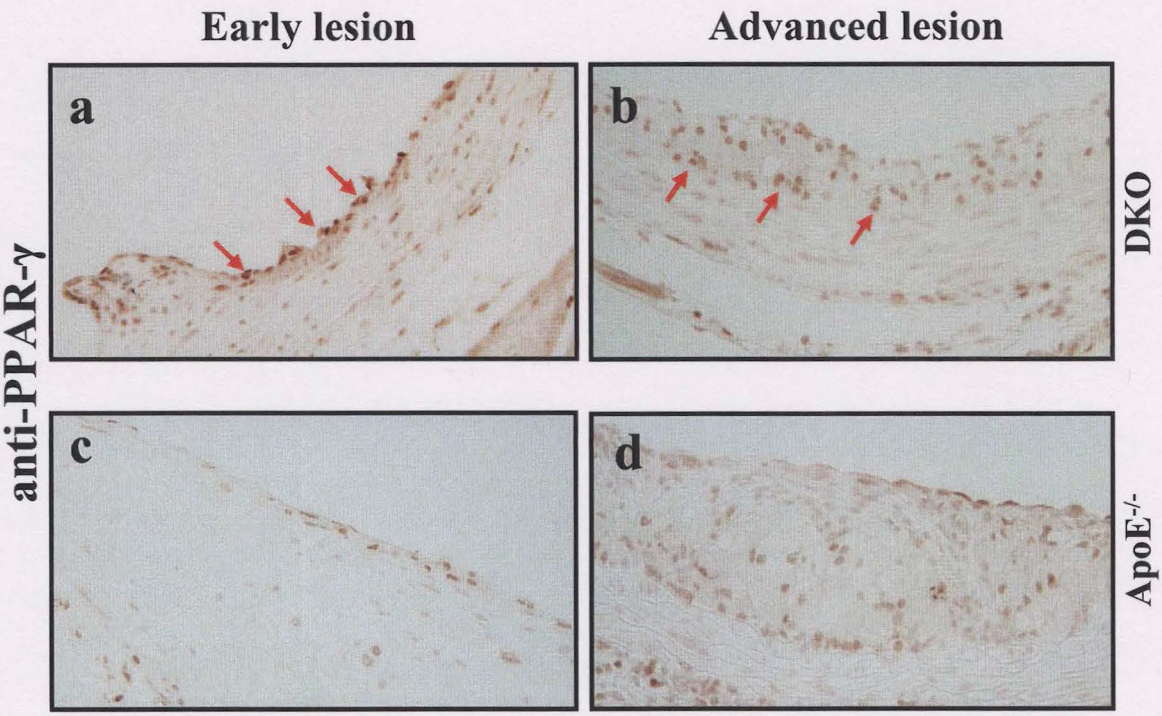
Early lesion
Advanced lesion
anti-PPAR-γ
a
b
c
d
DKO
ApoE-/-

3.4 Discussion

PCD plays an important role in atherosclerotic lesion stability and thrombogenicity (Tedgui and Mallat 2001). We first reported that TDAG51 is associated with the development of atherosclerosis in HHcy (Hossain *et al.*, 2003). To elucidate the significance of TDAG51 in atherosclerosis, we generated mice that were deficient in both the apoE and TDAG51 genes. Our findings can be explained in few lines. **First**, loss of TDAG51 attenuates the progression of atherosclerosis in apoE$^{-/-}$ mice fed normal chow diet, compared to apoE$^{-/-}$ control mice. **Second**, necrotic lipid core size was significantly decreased in DKO mice, compared to apoE$^{-/-}$ control mice. **Third**, plasma lipid levels and lipoprotein profiles were indistinguishable between apoE$^{-/-}$ and DKO mice. **Fourth**, atheroprotection from the loss of TDAG51 can in part be explained by our findings that the expression of transcription factor PPAR-γ and its downstream targets were increased in the TDAG51$^{-/-}$ MEFs, compared to wildtype control MEFs. Further, reintroduction of TDAG51 into TDAG51$^{-/-}$ MEFs inhibits PPAR-γ expression. Previous studies have suggested that PPAR-γ has both atheroprotective and anti-inflammatory properties (Lehrke and Lazar 2005). It is therefore possible that the reduced atherosclerotic lesion size in DKO mice may be due to a mechanism involving PPAR-γ.

Earlier studies on the cell cycle (p53 or Rb) and pro-apoptotic (Bax) genes have demonstrated that the functional deficiency of these genes contributes to the enhanced atherosclerosis (Guevara *et al.*, 1999; Liu *et al.*, 2004; Boesten *et al.*, 2006). Since macrophages are found in all stages of atherosclerosis, these studies have exclusively focused on the role of these genes in macrophage apoptosis and their significance in

atherosclerotic lesion progression. Interestingly, decreased macrophage apoptosis was observed within atherosclerotic lesions of these mice from the loss of these genes. Further, the authors have reported an increased cellular proliferation within atherosclerotic lesions of these mice. It is possible that the deficiency of p53, Bax or Rb may affect macrophage apoptosis during early stages of lesion development. Since macrophage apoptosis is believed to be beneficial in early stages of atherosclerosis (Dickhout *et al.*, 2008; review **Figure 47**), the functional loss of these genes in macrophages may enhance the progression of atherosclerosis. Upon activation, macrophages are believed to produce a large number of cytokines and growth factors that can promote lesion development in both autocrine and paracrine manners (Frostegard *et al.*, 1999; Seshiah et *al.*, 2002; Linton amd Fazio 2003). In addition, the loss of macrophages in early stages of atherosclerosis can promote the generation of pro-atherogenic factors, such as less production of apoE and reduced scavenging of toxic substances (oxidized LDL). Overall, these studies suggest that macrophage apoptosis in early atherosclerosis provides a self-defense mechanism by suppressing atherosclerosis, and therefore, the deficiency of macrophage specific genes enhances atherosclerosis. Further, it is possible that these genes may regulate macrophage turnover.

Contrary to early macrophage apoptosis, the late stages of macrophage apoptosis can be harmful (Dickhout *et al.*, 2008; review **Figure 47**), since macrophage apoptosis can reduce the production of growth factors and inflammatory cytokines. Although this process can lead to the attenuation of atherosclerosis, late macrophage apoptosis may facilitate the development of the necrotic core, thereby making the lesions more

vulnerable to rupture. The majority of apoptotic cells in advanced lesions are macrophages localized near the necrotic lipid core. Seimon *et al.* (2009) have recently demonstrated that the deficiency of macrophage specific p38α MAPK promotes apoptosis and necrosis in advanced lesions. This leads to an increase in necrotic core size, however, deficiency of macrophage specific p38α MAPK did not change overall lesion size in apoE$^{-/-}$ mice, compared to apoE$^{-/-}$ control mice. It is possible that p38α MAPK plays a critical role in suppressing macrophage apoptosis in advanced lesion. Also, activation of p38α MAPK can have both pro- or antiapoptotic effects depending on the cellular environments (Park *et al.*, 2002; Devries-Seimon *et al.*, 2005; Jinlian *et al.*, 2007). Taken together, these studies suggest that macrophage apoptosis in early or late stages of atherosclerosis may not influence the size of atherosclerotic lesions, since influencing necrotic core did not affect the overall lesion size. Further, Seimon and Tabas (2009) have recently suggested that macrophage apoptosis limits lesion cellularity and suppresses plaque progression in early lesions, while it promotes the development of necrotic core in advanced lesions. The authors have also proposed involvement of "multifactorial hits", including ER stress, oxidative stress and apoptotic inducers, to trigger apoptosis in advanced lesions. It has been suggested that macrophage apoptosis is coupled with phagocytic clearance (efferocytosis) in earlier lesions. However, macrophage apoptosis is not properly coupled with phagocytic clearance in advanced lesions, resulting in the development of necrotic core that may ultimately contribute to plaque rupture or thrombosis.

Like earlier discussed genes (p53, Bax or Rb), we expected the same effect on the lesion size of DKO mice if the effects of TDAG51 were sorely based on its' pro-apoptotic characteristics. Instead, the DKO mice showed reduced atherosclerosis. It is important to mention that we generated DKO mice that expressed functional deficiency of TDAG51 in all tissues not just macrophages. It is therefore conceivable that the loss of pro-apoptotic gene TDAG51 may reduce apoptotic cell death in lesion-resident cells, including macrophages, smooth muscle cells and lymphocytes. Less apoptosis may thus decrease inflammatory response, resulting in a slower progressing atherosclerotic lesion. In support of this, DKO mice fed normal chow diet have demonstrated reduced atherosclerotic lesion and necrotic lipid core, compared to apoE$^{-/-}$ mice at 25 or 40 weeks of age. However, the reduction in necrotic core size does not fully account for the reduction in atherosclerotic lesion size for DKO mice. The observation that the reduction in necrotic core accounts for approximately 35% of the reduction in the lesion size, implies that other anti-atherogenic cellular factors may contribute to the remaining ~65% reduction of lesion in DKO mice. Although a significant difference was not observed between apoE$^{-/-}$ and DKO mice lesion size at 15 weeks of age, the results demonstrated a trend towards the reduction in the atherosclerotic lesion size in DKO mice. The statistically insignificant difference in lesion size between apoE$^{-/-}$ and DKO mice was perhaps because of lack of power of the statistical test due to small n-values (n=3 for DKO or apoE$^{-/-}$ groups). This observation may also indicate that the difference in lesion development does not occur at the very early stages of atherosclerosis. TDAG51 may

promote apoptosis only in advanced atherosclerotic lesion when combined with other pro-atherogenic factors found only in advanced lesions.

Interestingly, our findings that the knockout of a pro-apoptotic ER stress inducible gene decreases lesion size in apoE$^{-/-}$ mouse model have recently been reproduced independently by Thorp *et al.* (2009). The authors have demonstrated that deficiency of CHOP in apoE$^{-/-}$ or LDLR$^{-/-}$ mice reduces atherosclerotic lesion size in advanced atherosclerosis. Importantly, CHOP and TDAG51 are two known ER stress-induced pro-apoptotic genes that are involved in atherosclerosis (Hossain *et al.*, 2003; Thorp *et al.*, 2009). Overall, the pro-apoptotic function of TDAG51 may not be the only contributory factor for the reduction of atherosclerotic lesion size observed in DKO mice. It is possible that there may be decreased recruitment of macrophages within the atherosclerotic lesions and/or increased migration of macrophages from the lesions. Nonetheless, our findings demonstrate that the loss of TDAG51 significantly attenuates atherosclerotic lesion development in DKO mice fed a normal chow diet.

In our earlier studies, we have reported that TDAG51 promotes detachment mediated-PCD in endothelial cells (Hossain *et al.*, 2003). Also, we have demonstrated that pro-atherogenic molecules, including homocysteine and peroxynitrite, cause endothelial injury and significantly upregulate the expression of the pro-apoptotic gene TDAG51 in endothelial cells (Hossain *et al.*, 2003; Dickhout *et al.*, 2005). Based on these findings, it is conceivable that the deficiency of TDAG51 may directly decrease endothelial injury, leading to reduced vessel wall inflammation. Less endothelial injury may decrease the inflammatory response by decreasing monocyte adhesion and leukocyte

infiltration. Recruitment and adhesion of monocytes are believed to be the initial proinflammatory response upon endothelial injury (Ross 1993). We have not documented any difference in endothelial function in the aortic root of DKO mice, compared to apoE$^{-/-}$ mice. Therefore, additional studies are required to further address whether TDAG51 plays any role in endothelial cell function and/or injury in the atherogenic process. However, our preliminary findings have demonstrated increased expression of peroxiredoxin 1 (Prdx 1) in TDAG51$^{-/-}$ MEFs (Edward and Austin: unpublished results). Importantly, Prdx 1 was upregulated within endothelial cells of atherosclerotic lesions from DKO mice, compared to apoE$^{-/-}$ mice **(Figure 48)**. Earlier studies have demonstrated that Prdx 1, an antioxidant protein, prevents excessive endothelial activation and early atherosclerosis (Kisucka *et al.*, 2008). Mice deficient in Prdx 1 showed increased leukocytes rolling per min, compared to C57 control mice. Further, Prdx 1$^{-/-}$/apoE$^{-/-}$ mice developed larger atherosclerotic lesions, compared to apoE$^{-/-}$ mice. DKO mice deficient in endothelial specific TDAG51 would explain whether TDAG51-mediated endothelial dysfunction contributes to atherogenesis. Also, it will be interesting to examine monocyte binding to endothelial cell surface in TDAG51$^{-/-}$ mice.

Alternatively, the attenuation of atherosclerosis in DKO mice can further be explained by the observation that the athero-protective molecule PPAR-γ is upregulated in TDAG51$^{-/-}$ MEFs, compared to wildtype MEFs. Earlier studies have shown that PPAR-γ promotes the efflux of cholesterol within lesion-resident macrophages (Chawla *et al.*, 2001; Castrillo and Tontonoz 2004). Atherosclerotic mice treated with PPAR-γ ligands promoted the reduction of atherosclerotic lesion (Jiang *et al.*, 1998; Collins *et al.*,

2001; Chen *et al.*, 2001). Interestingly, we have demonstrated a marked increase in PPAR-γ mRNA levels in TDAG51$^{-/-}$ MEFs, compared to wildtype control MEFs (in collaboration with Dr. John Capone). Reintroduction of TDAG51 into TDAG51$^{-/-}$ MEFs reduced the expression of PPAR-γ to wildtype levels. Consistent with this, we have observed an increased nuclear localization of PPAR-γ within atherosclerotic lesions from DKO mice, compared to apoE$^{-/-}$ mice fed control diets **(Figure 49)**.

The decreased atherosclerotic lesion in DKO may perhaps be the direct effect from increased efflux of macrophage cholesterol through scavenger receptor class B type 1 (SRB-1), ABCA1 or LXRα protein (Chawla *et al.*, 2001; Li *et al.*, 2004). ApoE deficiency contributes to the impaired clearance of chylomicron, VLDL and LDL remnants. We, however, have not observed any increase in plasma lipid levels. The findings are consistent with previously reported studies targeting proteins involved in macrophage cholesterol efflux. Conditional knockout of macrophage PPAR-γ presented an enhancement of atherosclerosis in LDLR$^{-/-}$ mice but did not demonstrate any difference in the plasma lipid levels (Babaev *et al.*, 2005). Also, peritoneal macrophages from these mice demonstrated decreased uptake of oxidized LDL and presented no change in cholesterol efflux or inflammatory cytokine expression. Importantly, cholesterol efflux from macrophages contributes to very small percentage (~ 0.1%) of total plasma lipids, and therefore, the enzymatic assays may not be as sensitive to detect the difference in plasma lipid levels. Our preliminary results show that loss of TDAG51 increases cholesterol efflux from peritoneal macrophages (in collaboration with Dr. Bernado Trigatti of McMaster University). However, we do not have the data to explain

the effect on oxLDL uptake or the expression of inflammatory markers from the loss of TDAG51 in peritoneal macrophages. Future studies are required to further elucidate the role of PPAR-γ in the attenuation of atherosclerosis in DKO mice.

Interestingly, DKO mice presented with hepatic steatosis – a possible pathological change from increased PPAR-γ expression. Numerous studies have reported an association between non-alcholic fatty liver disease (NAFLD; hepatic steatosis) and atherosclerosis (Völzke *et al.*, 2005; Targher and Arcaro 2007; Loria *et al.*, 2008; Sookoian and Pirola 2008). An epidemiological study by Völzke *et al.* (2005) has shown that individuals with fatty liver are 76.8% more likely to develop carotid plaques than those without fatty liver. Persons with hepatic steatosis were more likely to have other atherosclerotic risk factors, including hypertension, diabetes and obesity, than those without hepatic steatosis, this may explain the increased risk of CVD. Further, overexpression of PPAR-γ can result in the development of adipogenic hepatic steatosis (Yu *et al.*, 2003). It is also possible that liver scavenger receptors, including SRB-1, hepatic lipase or LDLR may facilitate the increased lipid uptake in the liver of DKO mice. Since hepatic triglyceride levels were increased in DKO mice, it is conceivable that increased hepatic PPAR-γ from the loss of TDAG51 may induce uptake and/or *de novo* lipid synthesis in DKO mice.

In summary, we have demonstrated that the gene TDAG51 contributes to the development and progression of atherosclerosis. Future studies are needed to demonstrate the exact mechanism(s) by which loss of TDAG51 contributes to attenuated atherosclerosis in apoE$^{-/-}$ mice.

CHAPTER 4: Role of TDAG51 in cell migration and its potential relevance to wound healing and atherosclerosis

4.1 Introduction

In previous chapters, we established that TDAG51 is a novel mediator of atherosclerosis and leads to endothelial cell death through a mechanism of detachment-mediated PCD referred to as anoikis (Hossain *et al.*, 2003). In these studies, we have investigated its role in other pathological effects such as wound healing and fibrosis.

We earlier have demonstrated through indirect immunofluorescence that endogenous TDAG51 co-localizes with focal adhesion kinase (FAK) (Hossain *et al.*, 2003), a protein found within focal adhesions (FAs). FAs are critical for anchoring cells to the extracellular matrix and are protein complexes on the plasma membrane that interact with the actin cytoskeleton of the cells, transmembrane proteins (such as integerins) on the cell surface and the extracellular matrix (Wozniak *et al.*, 2004; Romer *et al.*, 2006). FAs have been found to be dynamic complexes subject to assembly and disassembly depending on cellular signaling, cell proliferation and cell migration. Therefore, FAs are believed to be critical modulators of cell function. Given that overexpression of TDAG51 promotes detachment-mediated PCD and that TDAG51 co-localizes with FAK (Hossain *et al.*, 2003), it was hypothesized that the deficiency of TDAG51 enhances cell adhesion, and therefore, may affect actin cytoskeletal organization, cell migration and/or proliferation.

To better understand the role of TDAG51 in cell migration and proliferation, MEFs deficient in TDAG51 were derived from TDAG51$^{-/-}$ mice and compared to wild type MEFs. TDAG51$^{-/-}$ MEFs showed increased migration following monolayer disruption or in response to chemotaxis on fibronectin-coated Boyden chambers. In addition, loss of TDAG51 promotes the proliferation of MEFs. TDAG51-mediated migration and proliferation can be blocked by treating TDAG51$^{-/-}$ MEFs with active β_1-integrin inhibitory antibody. β_1-integrins are important for attachment and binding to fibronectin on the ECM (Brakebusch and Fässler 2005). In terms of a cellular phenotype, migratory TDAG51$^{-/-}$ MEFs have distinct filopodial and lamellipodial extensions, compared to migratory wild type MEFs. Laser scanning confocal microscopy demonstrated a significant increase in F-actin stress fibers as well as increased distribution of vinculin within the lamellipodial protrusions of TDAG51$^{-/-}$ MEFs. Importantly, reintroduction of TDAG51 into TDAG51$^{-/-}$ MEFs reversed these phenotypic changes. Collectively, our findings suggest that the functional loss of TDAG51 affects cell migration and proliferation through modifying focal adhesion complex assembly and cytoskeletal rearrangement.

Since fibroblast migration is believed to play a critical role in wound closure (McAnulty 2007), we examined the potential role of TDAG51 in dorsal skin wound healing process. We observed an *in vivo* association between loss of TDAG51 and skin wound healing process. Contrary to our findings in MEFs, skin wounds within TDAG51$^{-/-}$ mice appeared to heal slower than those in C57 control mice. This may be due to an impaired differentiation of fibroblasts into myofibroblasts in TDAG51$^{-/-}$ mice. Earlier

studies have shown that MEFs can differentiate into either adipocytes or myofibroblasts and the course of this differentiation process has been demonstrated to be dependent upon PPAR-γ stimulation/levels (Burgess *et al.*, 2005; McAnulty 2007). In addition, studies have demonstrated that upregulation of PPAR-γ can inhibit differentiation of fibroblasts into myofibroblasts (Hinz *et al.*, 2007). Interestingly, we have observed an increased expression of PPAR-γ and an impaired differentiation of myofibroblasts in TDAG51$^{-/-}$ MEFs, compared to wildtype MEFs. Given that myofibroblasts are essential for the wound contraction process, it is possible that defects in myofibroblast differentiation may thus contribute to the slower healing process observed in TDAG51$^{-/-}$ mice.

Furthermore, myofibroblasts are important in chronic inflammatory process throughout the body since they produce components of extracellular matrix (ECM) such as collagen (Hinz *et al.*, 2007). It is believed that collagen contributes mechanical strength and stability to tissues, and plays a critical role in stabilizing the development of atherosclerotic lesions (Shah *et al.*, 1995). Since cellular mechanism(s) involving skin wound healing and fibrosis are similar, it can be proposed that TDAG51 may have a role in fibrosis. Importantly, migration of fibroblasts and its subsequent deposition of ECM are hallmark features for both pathological processes (Wynn 2008). Although we have not documented the presence of fibrosis in DKO mice, it can be speculated that impaired myofibroblast differentiation could possibly affect atherosclerotic lesion size observed in DKO mice. Fibrosis is more prevalent in human atherosclerosis, compared to that in our apoE$^{-/-}$ mouse model, since human atherosclerotic lesions are acellular or fibrotic (Wynn 2007). Human blood vessels are elastic and are believed to provide a low resistance path

for blood supply to target organs (Greenwald 2007). In response to acute inflammation, the injured vessels are repaired rapidly and this is beneficial. However, persistent injury from cardiovascular risk factors can contribute to the chronic inflammatory state, leading to a sustained production of growth factors, proteolytic enzymes, angiogenic factors and fibrogenic molecules (Wynn 2008). This process facilitates the replacement of injured cells with connective tissues that may further stimulate the deposition of ECM components, thereby resulting in vascular remodeling and fibrosis. Importantly, fibrotic vessels are rigid, calcified and may be less able to absorb the forces generated by the pulse then normal elastic vessels This may predispose unstable lesion to rupture. Taken together, our current findings demonstrate that TDAG51 is involved in both atherosclerosis and wound healing. Future experiments, however, are essential to determine whether TDAG51 is associated with fibrosis.

In this chapter, I will provide novel evidence that TDAG51 is a critical gene in the pathogenesis of both wound healing and atherosclerosis perhaps through its influence on fibroblast gene expression and differentiation state.

4.2 Materials and Methods

4.2.1 Immunoblot analysis

Mouse embryonic fibroblasts (MEFs) were isolated as described in **section 2.2.2.15**. Total cell lysates from wildtype and TDAG51$^{-/-}$ MEFs were solublized in 4X SDS-PAGE sample buffer. Equivalent amounts of protein lysate were separated by electrophoresis on SDS-polyacrylamide gels under reducing conditions as described previously (Laemmli 1970). Immunoblot analysis was then performed as described in **section 2.2.2.8**.

4.2.2 Indirect immunofluorescence: Cell culture

To determine the status of vinculin and F-actin, wild type and TDAG51$^{-/-}$ MEFs were grown on fibronectin-coated (10 μg/mL) coverslips, washed in 1X PBS and fixed in cold 4% paraformaldehyde at 4°C. Cells were then washed in 1X PBS, permeablized in 0.025% Triton X-100 (1X PBS) for 10 min on ice, and blocked for 30 min in blocking buffer (3% BSA in 1X PBS). Following the blocking procedure, a mouse monoclonal antibody against vinculin diluted in blocking buffer (1:50) was added and incubated for 1 h. The coverslips were next washed in 1X PBS and incubated with Alexa^{TM} 488- or 594-conjugated goat anti mouse secondary antibody diluted in blocking buffer (1:100) to detect vinculin binding sites. Cells stained with normal serum or secondary only were used to normalize for non-specific immunofluorescence and considered as a negative control. Following 30 min of incubation with secondary antibody, the coverslips were washed in 1X PBS and were incubated for 30 min with FITC conjugated phalloidin or

rodamine conjugated pholloidin. The coverslips were then washed in 1X PBS and in H_2O, respectively. The coverslips were next mounted onto slides using PermaFluor mounting medium. Immunofluorescence was examined by epifluorescence microscopy using a Zeiss Axioskop 2 microscope. Images were captured using CCD color video camera (Sony, Tokyo, Japan) and image analysis/archival software (Northern Exposure; Empix Inc., Mississauga, ON).

4.2.3 Laser scanning confocal microscopy: Cell culture

MEFs were grown on fibronectin-coated (10 μg/mL) coverslips for laser scanning confocal microscopy to determine co-localization of vinculin and F-actin in wild type, TDAG51$^{-/-}$ and TDAG51$^{-/-}$ cells reconstituted with TDAG51 (tdko_recon). As described in **section 4.2.2**, coverslips were incubated with the anti-vinculin monoclonal antibody (1:50) and phalloidin conjugated to fluorphore targeting filamentous actin (1:100). Goat anti-mouse secondary antibody conjugated to alexa 488 (Molecular Probes, Eugene, OR) (1:100) was used to detect vinculin binding sites. Images were collected on a Zeiss LSM 510 confocal microscope (North York, ON, CA) as described before (Hossain *et al.*, 2003). Images were merged to determine vinculin and F-actin co-localization.

4.2.4 Calcium phosphate transfection and retroviral infection into MEFs

293T cells (3 x 10^6 cells per 100 mm dish) were seeded in DMEM media (10% FBS; 1% Glutamine solution; 1% Pen/Strep; 2% v/v of sterile 17.5 w/v glucose solution) and calcium phosphate transfection was performed as described previously (Tang *et al.*,

2001). In brief, plasmids (10 μg VSV, 10 μg GP and 10 μg pBabe retroviral plasmid with or without the open reading frame of the human TDAG51 gene) were added to a 12 mL falcon tube containing ddH_2O (up to 500 μL) and 50 μL of $CaCl_2$ (2.5 M). Five hundred microliters of 2X HEBS solution (pH 7.35) was then slowly added to the solution. After vortexing for 20 sec, the mixture was incubated at room temperature for 20-30 min and then added drop wise to the 293T cells. Twelve hours later, fresh DMEM media was added to the transfected 293T cells and the cells were allowed to grow.

After forty-eight hours, medium containing viral particles was harvested and filtered using a 10-15 mL syringe containing a 0.25-0.45 μm filter to remove cellular debris. The media was then centrifuged at 50,000 x g for 1.5 h to pellet the viral particles. After discarding the supernatant, the pelletted viral particles were resuspended into the desired volume of media containing polybrene (1 μg/mL). The media containing the viral particles was then used to infect target cells, that is, C57 control and $TDAG51^{-/-}$ MEFs. Two hours later, fresh media was added to the infected cells. After 48 h, fresh media was added and the infected cells were grown for 7-10 days in selection media containing purimycin (1.5 μg/mL). In addition, total cell lysates were collected from these stable cell lines and were subject to immunoblot analysis as described in **section 4.2.2** using an antibody against TDAG51 to determine TDAG51 protein expression.

4.2.5 Cell migration assays

4.2.5.1 Wounding experiments

Wildtype C57 and TDAG51$^{-/-}$ MEFs were plated onto glass coverslips coated overnight with 10 μg/mL fibronectin. Cells were allowed to grow to near confluence in 10% FBS DMEM and then wounded with a 1 ml plastic pipette tip introducing a disruption into the monolayer. After washing the cells with 1X PBS, fresh media was added to assess the rate at which the MEFs from wild type or TDAG51$^{-/-}$ mice could migrate into the denuded area. As described in **section 4.2.2**, cells were fixed in 4% paraformaldehyde, stained for F-actin or DAPI, and imaged at the site of the wound to determine the extent of filling at 0, 3, 8, 16 and 30 hrs.

4.2.5.2 Boyden chambers

To quantify the rate of migration, equal numbers ($1x10^5$ cells) of C57, TDAG51$^{+/-}$ or TDAG51$^{-/-}$ MEFs were plated onto fibronectin-coated Boyden chambers. In brief, cells were cultured in the upper chamber with 1% FBS and incubated at 37°C to allow the cells to attach. Two hours later, DMEM media containing 10% FBS was placed in the bottom chamber in order to initiate migration of the cells from the upper chamber. Within 6 h, fresh media was added to maintain the concentration gradient. Following overnight incubation, the cells were washed in 1X PBS and were fixed in 2% paraformaldehyde for 30 min at room temperature. The cells were again washed in 1X PBS and stained with DAPI solution for 10 min at room temperature. After removing the cells from the upper chamber using kimwipes, the membranes facing the bottom chamber were mounted into slides. The number of cells migrating through the membrane into the lower side of the chamber was counted. The data represent the number of cells (stained

by DAPI) that were counted in sampling grids from the lower side of the membrane and are given as mean ± SEM. These data were taken from 5 replicate wells for each cell type.

4.2.6 Cell proliferation assays:

4.2.6.1 Thymidine incorporation

To examine DNA synthesis, C57 control, TDAG51$^{+/-}$ or TDAG51$^{-/-}$ MEFs (5000 or 15000 cells per well) were seeded onto fibronectin-coated 96 well plates. Following overnight incubation, 1 μCi of [^{3}H]-thymidine was added to the medium of each well and allowed to incorporate into DNA for 4 h. The cells were then placed at -80°C to block further incorporation. After thawing the plates, the cells were harvested by transferring them into the filter paper. The radiolabelled DNA was then quantified using a Beckman LS 6000LL β-counter (Beckman Instruments, Fullerton, CA).

4.2.6.2 Quantitative assessment using a phosphorimager

Cell proliferation was also assessed utilizing a semi-automated system of cell counting with ethidium bromide (ETB) based fluorescent nuclear labelling and quantification on a Typhoon 9410 imager (Amersham) with laser excitation at 532 nm and signal collected through a 610 nm BP30 filter. C57 wild type, TDAG51$^{-/-}$ or TDAG51$^{-/-}$ MEFs reconstituted with TDAG51 (tdko_recon) using the pBabe retroviral system were grown on 24-well plates coated overnight with 10 μg/mL fibronectin. After seeding at 1x10^{4} cells/mL, cells were allowed to attach overnight, washed in 1X PBS and fresh medium

(10% FBS DMEM) was added. The cells were fixed at 0, 24 or 48 hrs with 0.1% paraformaldehyde, permeablized with 0.1% Triton-X, stained for 5 min with 5 μg/mL ETB in PBS, washed 3X in PBS, and placed in 65% glycerol in PBS for imaging on the Typhoon imager. Cell number was calculated by subtracting background and by quantifying the volume intensity of ETB fluorescence using ImageQuant software (Molecular Dynamics) as previously (Dickhout *et al.*, 2005). Fluorescence intensity was fit to cell number by scaling through the ratio of fluorescence to cell number emitted from a known number of cells.

Since active β_1-integrin binding to the fibronectin matrix is a critical component of fibroblast mobility, the rat anti-mouse CD29 monoclonal antibody (β_1-integrin antibody 9EG7 clone) was also used as an inhibitory antibody to determine if the increased rate of migration found in the TDAG51$^{-/-}$ MEFs accounted for their increased proliferation rate. C57 wild type and TDAG51$^{-/-}$ MEFs were seeded at $1x10^4$ cells/mL in 24-well plate coated with 10 μg/mL fibronectin. Once cells had attached to the matrix, the medium was changed to 10% FBS DMEM with or without 1:100 dilution of integrin β_1 chain antibody clone 9EG7. Cells were fixed for ETB fluorescent quantification procedure at times 0, 24 or 48 hrs as described previously (Dickhout *et al.*, 2005).

4.2.7 Flow cytometry analysis

Flow cytometry was used to determine the percentage of active β-integrin binding sites on the cell surface of C57 wild type vs TDAG51$^{-/-}$ MEFs. To measure cell surface β_1-integrin, cells were plated onto T25 flask to grow near confluency. The cells were first

dissociated from T25 flask and were then pipetted to become single cell suspensions, that is, to reduce cell clumping. Following addition of complete media, cells were spun down and resuspended in 1X Hanks solution containing 2% FBS. The cells were centrifuged at ~ 200 x g and the pellet was incubated with or without rat anti-mouse CD29 monoclonal antibody (antibody against active β_1-integrin clone 9EG7; 1:50). After 40 min of incubation on ice, the cells were washed in 1X Hanks solution (2% FBS). The cells were then incubated with secondary antibody (anti rat conjugated alexa 488; 1:200) against β_1-integrin for 30 min in ice and dark. Following washing in 1X Hanks solution (2% FBS), the cells were fixed in 1% paraformaldehyde for 30 min at room temperature. The cells were then filtered and analyzed by flow cytometry to obtain geometric mean value.

To assess total β_1-integrin, the cells were collected using cell dissociation buffer, fixed with 1% paraformaldehyde, and permeablized with 0.025% Triton X-100. The cells were then stained with or without rat anti-mouse CD29 monoclonal antibody (β_1-integrin antibody) as described earlier. After filtering, the cells were analyzed by flow cytometry and the geometric mean value was obtained. The cell surface active β_1-integrin was measured by using geometric mean value and the following equation:

% cell surface active β_1-integrin

= (geometric mean for cell surface active β_1-integrin / geometric mean for total β_1-integrin) X 100%

4.2.8 Statistical analysis

All experimental values are presented as mean ± standard deviation. Comparison between the means was performed using the unpaired student's *t*-test. ANOVA was used for multiple comparisons among the means. For all analyses, $P<0.05$ was considered statistically significant.

4.3 Results

4.3.1 Characterization of TDAG51 protein expression in MEFs

C57 control or TDAG51$^{-/-}$ MEFs were derived from C57BL/6 or TDAG51$^{-/-}$ mice, respectively. Western blotting indicated that there was undetectable level of TDAG51 protein expression in TDAG51$^{-/-}$ MEFs whereas C57 control MEFs retained TDAG51 protein expression (**Figure 50**). Using pBabe retroviral vector system, overexpression or reintroduction of TDAG51 into C57 or TDAG51$^{-/-}$ MEFs, respectively, was achieved as shown in purimycin selected stable cell lines expressing TDAG51 by Western blotting (**Figure 50**).

4.3.2 Effect of TDAG51 deficiency on migration and proliferation of MEFs

In earlier studies, we demonstrated that TDAG51 promotes detachment-mediated PCD and also co-localizes with FAC (Hossain *et al.*, 2003). Based on these findings, we investigated whether the loss of TDAG51 could affect cell adhesion, cell migration and/or proliferation. The images obtained from wounded monolayers of wild type control or TDAG51$^{-/-}$ MEFs indicate that TDAG51$^{-/-}$ MEFs show a time-dependent and increased rate of migration into the denuded area, compared to C57 control MEFs (**Figure 51**). By 30 h, TDAG51$^{-/-}$ MEFs showed a complete migration into the wounded area under the microscope.

To support this qualitative observation, Boyden chamber experiments were performed to obtain quantitative results. These experiments demonstrated a greater number of TDAG51$^{-/-}$ MEFs (130 $\pm$ 14.4 cells) migrating via chemotaxis from 1% FBS

Figure 50: Re-introduction of TDAG51 protein into TDAG51$^{-/-}$ MEFs.

MEFs derived from C57 control or TDAG51$^{-/-}$ mice were cultured in DMEM media. Stable cell lines were generated as described in the experimental procedures using the pBabe retroviral system. Following collection of cell lysates, immunoblot analysis was performed to confirm the authenticity of the generated cell lines. In brief, total protein lysates (40 μg/lane) were subjected to immunoblot analysis using antibodies against TDAG51 or β-actin. The figure demonstrates similar levels of TDAG51 protein between C57 control MEFs {untreated (U) or pBabe vector (pB) treated} and TDAG51$^{-/-}$ MEFs {infected with the retrovirus pBabe-TDAG51 construct (pB-TD)}.

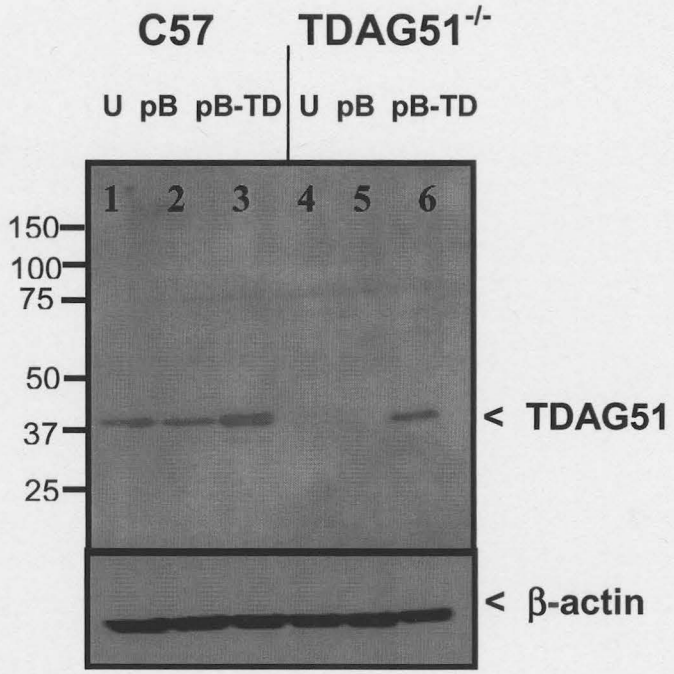
C57
TDAG51-/-
U pB pB-TD U pB pB-TD
1 2 3 4 5 6
150
100
75
50
37
25
< TDAG51
< β-actin

Figure 51: Time-dependent migration of TDAG51$^{-/-}$ MEFs following wounding

MEFs derived from wildtype (TDAG51$^{+/+}$) or TDAG51$^{-/-}$ mice were plated onto glass coverslips coated overnight with 10 µg/mL fibronectin. When the cells were near confluence, the cell layer was wounded with a 1 mL plastic pipette tip introducing a disruption into the monolayer. After washing the cells with 1X PBS, fresh media was added and the cells were allowed to migrate into the denuded area. The cells were then fixed at 0, 3, 8, 16 and 30 hrs, stained with DAPI and the image was captured at the site of the wound.

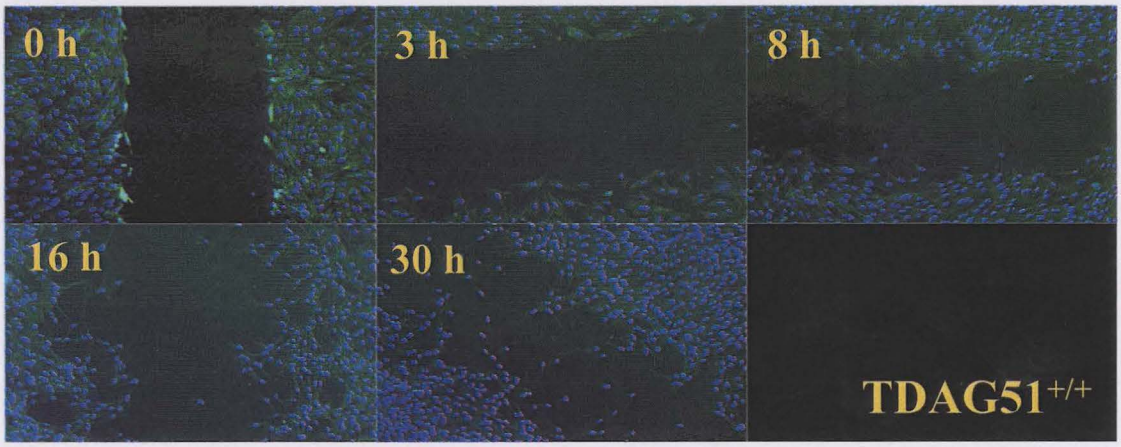
0 h
3 h
8 h
16 h
30 h
TDAG51+/+

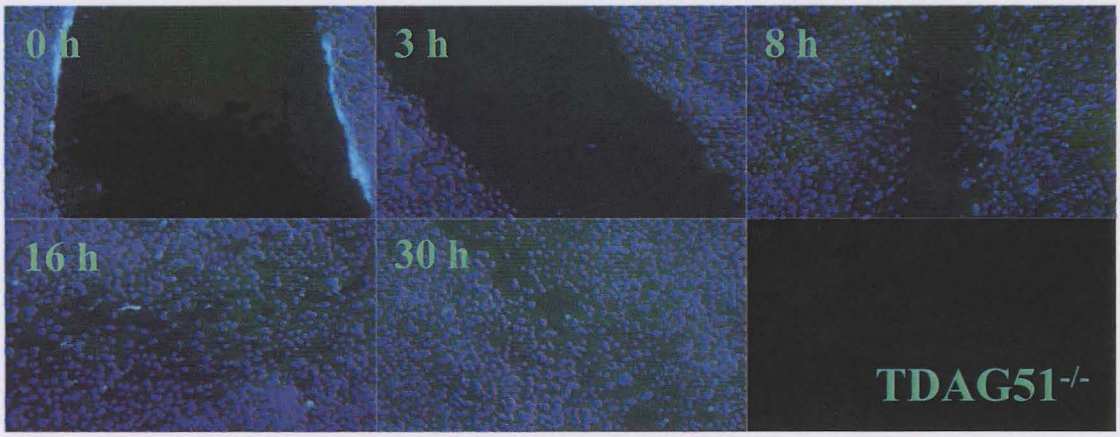
0 h
3 h
8 h
16 h
30 h
TDAG51-/-

to 10% FBS containing DMEM than C57 control (90 ± 12.7 cells) or TDAG51$^{+/-}$ (91 ± 10.3 cells) MEFs **(Figure 52)**.

Since migration and proliferation can occur together (Carragher and Frame 2004), the effect from the loss of TDAG51 on cell proliferation was also assessed. TDAG51$^{-/-}$ MEFs showed a significant (P<0.05) 2 to 3-fold increase rate in [^{3}H]-thymidine incorporation, compared to wild type C57 control or TDAG51$^{+/-}$ MEFs after a 4 h pulse **(Figure 53)**. This indicates that a greater percentage of TDAG51$^{-/-}$ MEFs were actively proliferating than C57 control or TDAG51$^{+/-}$ MEFs. In addition, ETB based fluorescent nuclear labelling technique as described in the experimental procedures was used to determine if this increased rate of DNA synthesis was reflected in enhanced cell number after a given period of time. After plating at low density (1x10^4 cells/mL), TDAG51$^{-/-}$ MEFs proliferated at an exponential phase by 48 h, compared to C57 control MEFs **(Figure 54)**. The results demonstrate an increase DNA synthesis in TDAG51$^{-/-}$ MEFs. Further, reintroduction of TDAG51 gene (td_recon) into TDAG51$^{-/-}$ MEFs significantly (P<0.05) decreased cell growth and number at 48 h, compared to TDAG51$^{-/-}$ MEFs **(Figure 54)**. This finding indicates a direct effect of TDAG51 gene on MEF proliferation rate.

Changes in cell adhesion are important contributor of cell migration. Earlier studies have reported that contact inhibition contributes to increased expression of TDAG51 in a mouse fetal fibroblast cell line, c3H10T1/2 (Gos *et al.*, 2005). We therefore examined the morphology of plated MEFs with or without TDAG51. Our findings demonstrated that TDAG51$^{-/-}$ MEFs have different morphology and distinct cell-

Figure 52: Loss of TDAG51 gene increases rate of migration in MEFs.

Wildtype and TDAG51$^{-/-}$ MEFs were grown on Boyden Chamber, as described in the experimental procedures. The experiments demonstrated a significant increase in the migration of TDAG51$^{-/-}$ MEFs (130±14.4 cells), migrating via chemotaxis from 1% FBS to 10% FBS containing DMEM, compared to wildtype control (90±12.7 cells) or TDAG51$^{+/-}$ (91±10.3 cells) MEFs. The result is statistically significant ($P<0.05$) as shown by the asterisk.

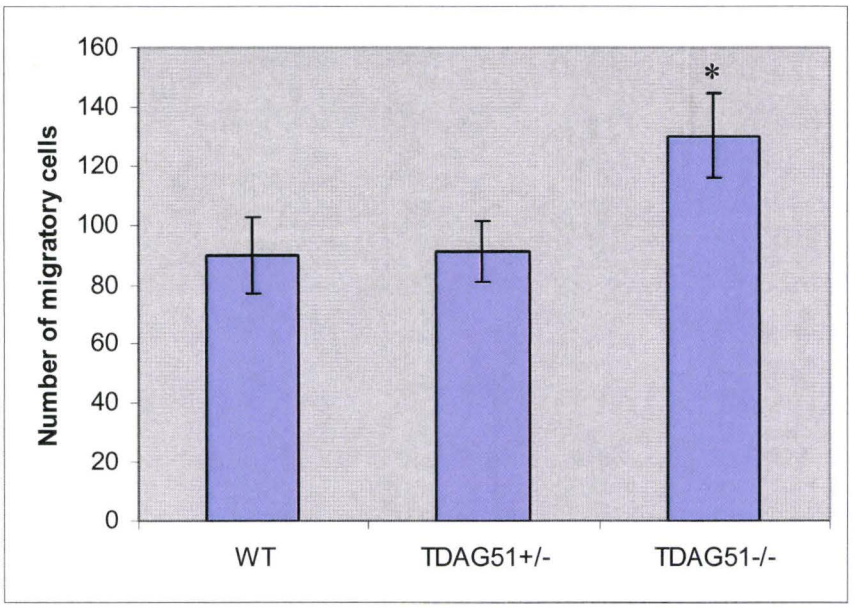
Number of migratory cells
160
140
120
100
80
60
40
20
0
*
WT
TDAG51+/-
TDAG51-/-

Figure 53: Loss of TDAG51 gene promotes MEF proliferation.

Wildtype, TDAG51$^{+/-}$ or TDAG51$^{-/-}$ MEFs {5,000 (A) or 15,000 (B) cells per well} were grown in 96 well plate as described in the experimental procedures. Cell lysates from TDAG51$^{-/-}$ MEFs displayed a 2 to 3-fold greater beta particle emission as measured in counts per minute (CPM) following 4 h of pulse incubation with [^{3}H]-thymidine, compared to wildtype C57 control or TDAG51$^{+/-}$ MEFs. The results are statistically significant (P<0.05) as shown by the asterisk.

A

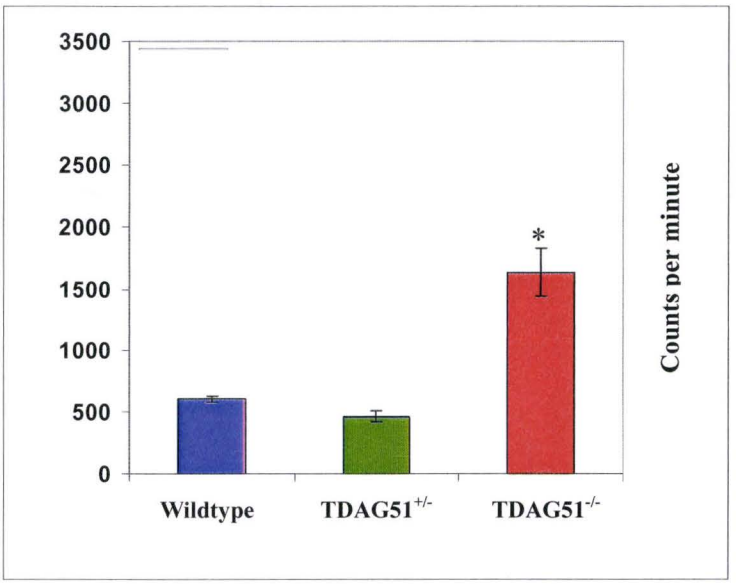

H^3-Thymidine incorporation, 5000 cells/well

B

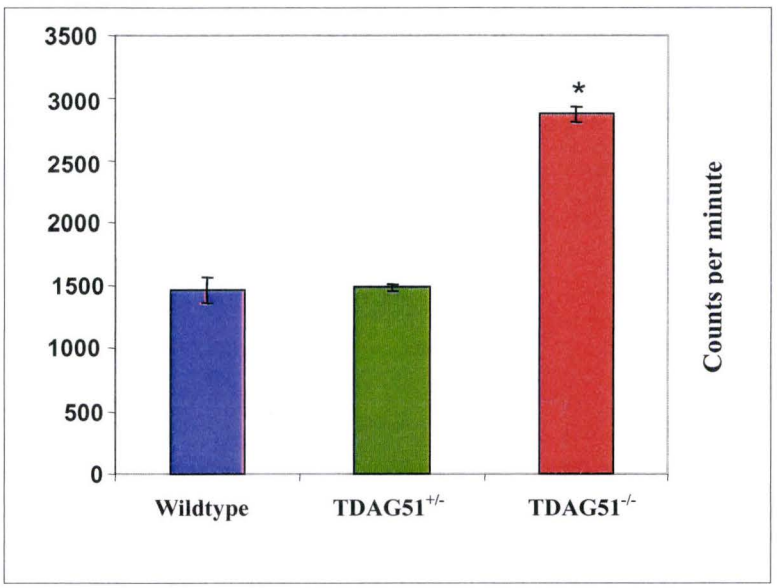

H^3-Thymidine incorporation, 15000 cells/well

Figure 54: Loss of TDAG51 gene increases rate of MEF proliferation.

Wildtype control or TDAG51$^{-/-}$ MEFs were grown as described in the experimental procedures. **(A)** Ethidium bromide (ETB) fluorescence obtained from C57 wildtype, TDAG51$^{-/-}$ or TDAG51$^{-/-}$ reconstituted with TDAG51 using pBabe retroviral vector system (tdko_recon). **(B)** Quantification of ETB fluorescence mapped to cell number obtained from wildtype, TDAG51$^{-/-}$ and td_recon MEFs. The data presents significantly ($P<0.05$) greater cell number of TDAG51$^{-/-}$ MEFs, compared to wildtype or td_recon MEFs at 48hrs.

A

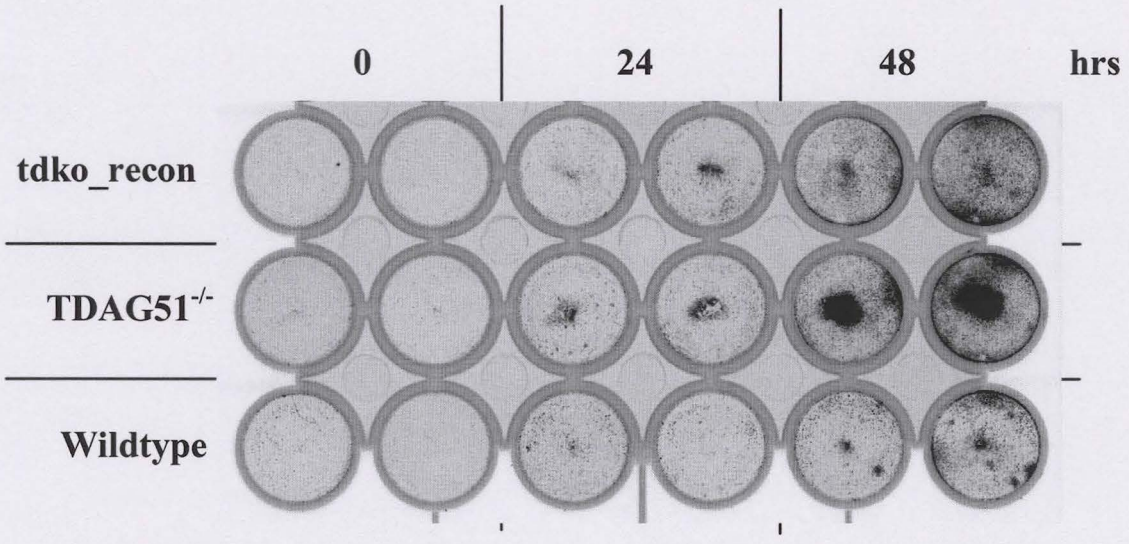
0
24
48
hrs
tdko_recon
TDAG51-/-
Wildtype

B

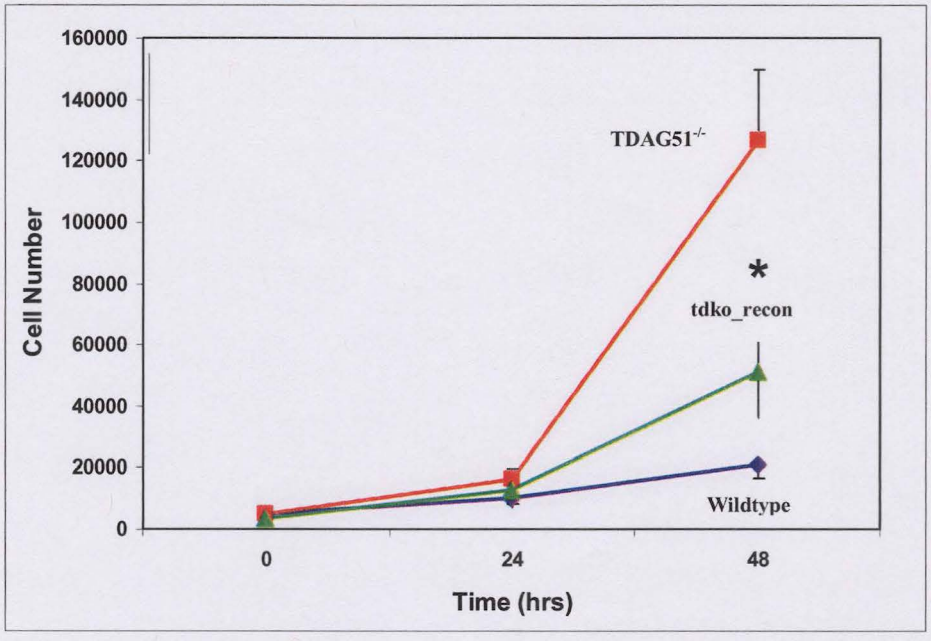
160000
140000
120000
100000
80000
60000
40000
20000
0
Cell Number
TDAG51-/-
*
tdko_recon
Wildtype
0
24
48
Time (hrs)

cell contacts, compared to wildtype MEFs **(Figure 55)**. Reintroduction of TDAG51 into TDAG51$^{-/-}$ MEFs normalizes the cell distribution pattern similar to wildtype MEFs.

4.3.3 Effect of TDAG51 deficiency on the phenotype of migratory MEFs

Using a Laser Scanning Confocal Microscope, images were captured at the site of the wound to investigate the phenotype of migratory wildtype or TDAG51$^{-/-}$ MEFs. Migrating TDAG51$^{-/-}$ MEFs showed distinct filopodial and lamellipodial extensions, compared to wildtype MEFs **(Figure 56)**. Interestingly, re-introduction of TDAG51 into TDAG51$^{-/-}$ MEFs reversed the phenotype similar to that observed for migratory wildtype MEFs. The expression of FACs in migratory cells was assessed by staining for vinculin, a marker of FAC assembly. The status of stress fiber (F-actin) was also examined. Confocal laser scanning microscopy showed that vinculin containing focal adhesions appeared mainly on the leading edge of the cells adjacent to the wound **(Figure 56A)**. The migratory cells from TDAG51$^{-/-}$ MEFs appeared to contain more prominent vinculin containing focal adhesions than wild type at the leading edges of the migratory cells **(Figure 56A)**. The migratory cells from TDAG51$^{-/-}$ MEFs also contain increased stress fibers, compared to wildtype MEFs **(Figure 56B)**. Reintroduction of TDAG51 into the TDAG51$^{-/-}$ MEFs converted the phenotype back to wildtype **(Figure 56A and 56B, tdko_recon)**. It is possible that the greater density of vinculin containing focal adhesions in the TDAG51$^{-/-}$ MEFs, combined with their increased interaction with F-actin filaments, enhances cell migration in the TDAG51$^{-/-}$ MEFs.

Figure 55: Morphological differences in MEFs with or without TDAG51

Wildtype control or TDAG51$^{-/-}$ MEFs were plated onto glass coverslips coated with 10 μg/mL fibronectin. Using pBabe retroviral vector system, TDAG51$^{-/-}$ MEFs reconstituted with TDAG51 (tdko_recon) were grown as described above. Forty eight hours after plating, the cells were washed with 1X PBS and fixed with paraformaldehyde. The image was then taken. The figure presents that the morphology of the confluent TDAG51$^{-/-}$ MEFs is different, compared to wildtype control MEFs.

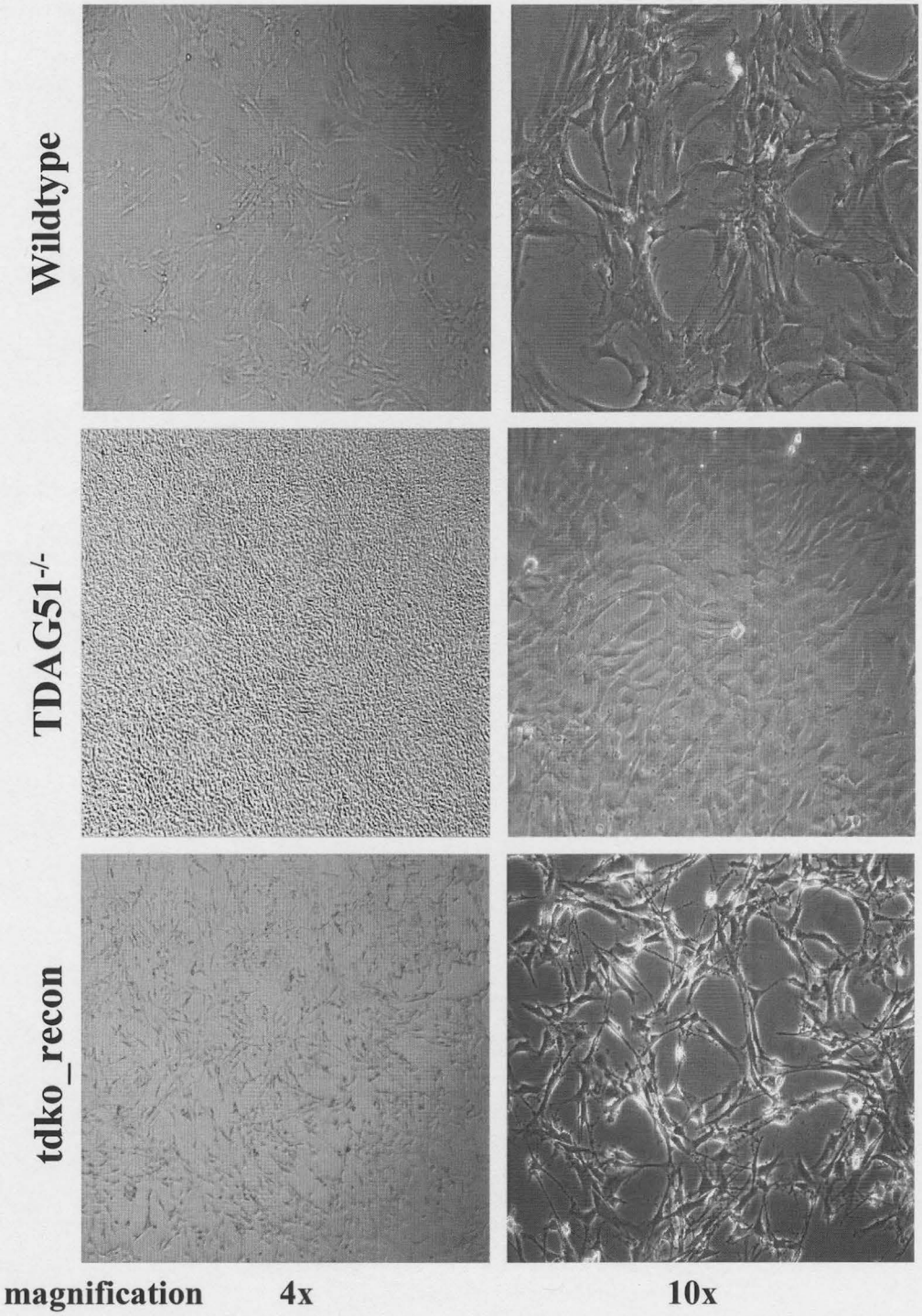
Wildtype
TDAG51-/-
tdko_recon
magnification
4x
10x

Figure 56: Co-localization of vinculin and F-actin in migratory MEFs.

Wildtype control, TDAG51$^{-/-}$ or reconstituted TDAG51 (tdko_recon) MEFs were grown to confluence on fibronectin-coated (10 μg/mL) coverslips. A wound in the monolayer was caused by dragging a 1 mL pipette tip across the bottom of the plate to disrupt the cell layer. Cells were labeled for vinculin (green) **(A)** and F-actin filaments (red) **(B)** and imaged 3hrs after injury (direction of migration, arrows). Images were collected on a Zeiss LSM 510 confocal microscope with 1 μm optical section depth to determine the co-localization of vinculin and F-actin **(merged image C)**. The results demonstrate that migratory TDAG51$^{-/-}$ MEFs have distinct filopodial and lamellipodial extensions, compared to wildtype or tdko_recon MEFs. Bar represents 10 μm.

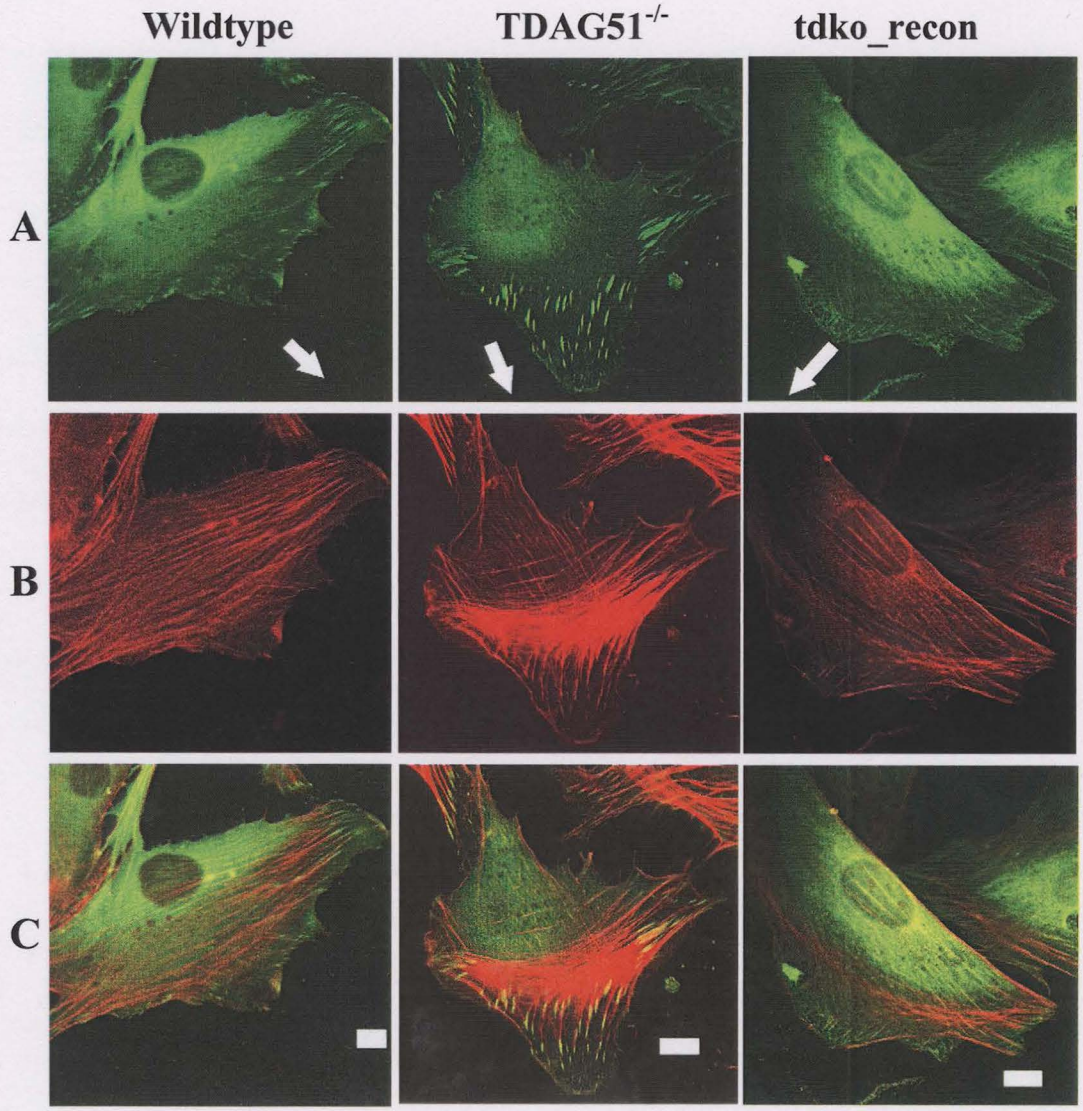
Wildtype
TDAG51-/-
tdko_recon
A
B
C

4.3.4 Assessing the status of β_1 integrin in the MEFs

Migratory cells are believed to express an increased number of active β_1 integrin on the cell surface (Carragher and Frame 2004). Binding of active β_1 integrin to its receptor, fibronectin, facilitates cell adhesion and migration. We therefore investigated the expression of active β_1-integrin on the cell surface of wildtype or TDAG51$^{-/-}$ MEFs. The results demonstrated that TDAG51$^{-/-}$ MEFs expressed a higher percentage of active β_1-integrin on the cell surface (52%), compared to wild type C57 control MEFs (39%) **(Figure 57)**. Following inhibition of the active site of β_1-integrin with the 9EG7 inhibitory antibody, TDAG51$^{-/-}$ MEFs grown on a fibronectin matrix demonstrated a decrease in proliferation **(Figure 58)**. This decrease in the rate of proliferation occurred mainly in the exponential phase of cells grown at 48 h after plating from a low density. The β_1-integrin inhibitory antibody (9EG7) had little effect on the growth of C57 wild type MEFs. The effect of 9EG7 inhibitory antibody on TDAG51$^{-/-}$ MEFs was to normalize the pattern of growth to that observed for the wild type MEFs **(Figure 58)**.

4.3.5 Examining the expression of genes that are involved in cell migration and atherosclerosis from the loss of TDAG51

Following isolation of mRNA from C57 wild type and TDAG51$^{-/-}$ MEFs, we performed affymetrix microarray analysis and compared the expression of 39,000 transcripts in wild type and TDAG51$^{-/-}$ MEFs. Approximately, 34 genes were found to be induced at the arbitrary cut off level of 4-fold (Table 3). Interestingly, we observed several genes involved in cell migration and atherosclerosis that were upregulated in TDAG51$^{-/-}$ MEFs,

Figure 57: TDAG51$^{-/-}$ MEFs express increased cell surface active β_1-integrin.

Wild type control or TDAG51$^{-/-}$ MEFs were grown to near confluence in T25 flask as described in the experimental procedures. Following trypsinization, the cells were stained with an antibody against active β_1-integrin (9EG7) to measure the cell surface β_1-integrin. The fluorescence was measured using flow cytometry after staining with secondary antibody. To measure the total β_1-integrin, cells were permeabilized and stained with 9EG7 antibody. The figure from the flow cytometry analysis shows the distribution of both cell types. Based on geometric mean analysis, TDAG51$^{-/-}$MEFs demonstrate increased percentage of cell surface β_1-integrin within total amount of β_1-integrin, compared to wild type MEFs.

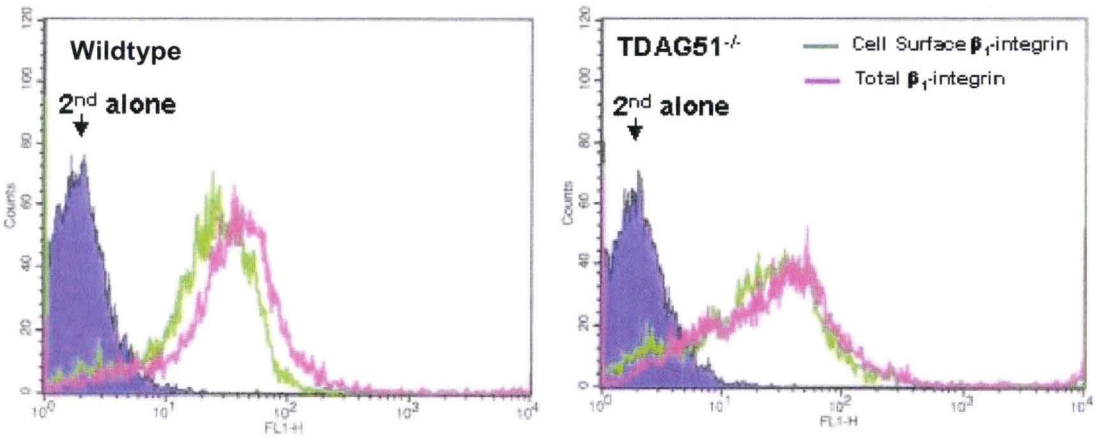
Wildtype
2nd alone
Counts
FL1-H
TDAG51-/-
2nd alone
Cell Surface β1-integrin
Total β1-integrin
Counts
FL1-H

Figure 58: β_1-integrin antibody (9EG7) inhibits the proliferation of TDAG51$^{-/-}$ MEFs.

Wildtype or TDAG51$^{-/-}$ MEFs ($1x10^4$ cells/mL) were grown as described in the experimental procedures. **(A)** Ethidium bromide (ETB) fluorescence obtained from C57 wildtype and TDAG51$^{-/-}$ MEFs with or without β_1-integrin antibody. **(B)** Quantification of ETB fluorescence was mapped to cell number obtained from wildtype and TDAG51$^{-/-}$ MEFs with or without β_1-integrin antibody. Graph B shows the inhibitory effect on the proliferation of MEFs from the incubation with β_1-integrin antibody. The results demonstrate that the effect on proliferation is more prominent in TDAG51$^{-/-}$ MEFs. The result is statistically significant ($P<0.05$) as shown by the asterisk.

A

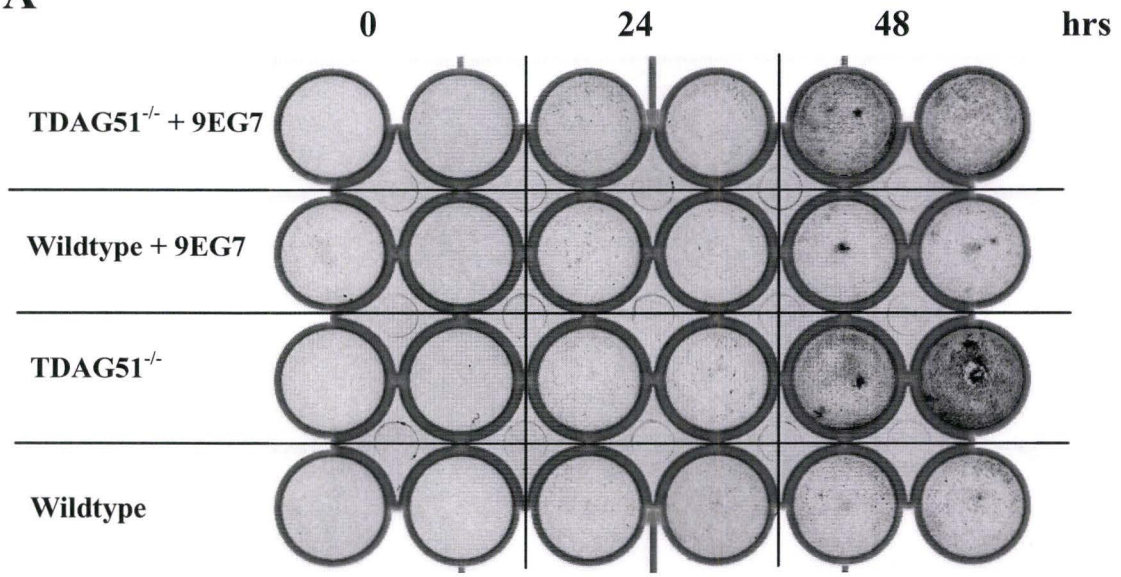
0
24
48
hrs
TDAG51-/- + 9EG7
Wildtype + 9EG7
TDAG51-/-
Wildtype

B

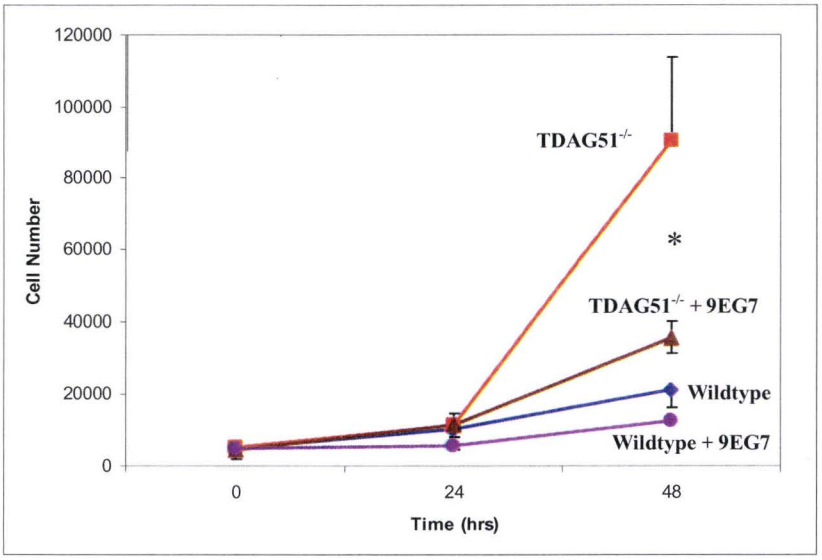
120000
100000
80000
60000
40000
20000
0
Cell Number
0
24
48
Time (hrs)
TDAG51-/-
*
TDAG51-/- + 9EG7
Wildtype
Wildtype + 9EG7

compared to wildtype MEFs. Ones that show highest upregulation include PPAR-γ (29-fold), Bcl2 (78.7-fold), decorin (34.2-fold), astrotactin 2 (57-fold) and Claudin 1 (26-fold).

4.3.6 Effect of fibroblast migration on wound healing ability in TDAG51$^{-/-}$ mice

Since loss of TDAG51 promotes migration and proliferation of MEFs, we hypothesized that TDAG51$^{-/-}$ mice enhance wound healing. Earlier studies have demonstrated that migration of fibroblasts plays a major role in repairing wounds (McAnulty 2007). However, the results showed that skin wound healing ability in TDAG51$^{-/-}$ mice is less efficient or slower, compared to C57 control mice **(Figures 59 & 60)**. To explain this observation, we examined whether there is any difference in the formation of FACs in C57 control and TDAG51$^{-/-}$ MEFs. The protein pattern identified from the mass spectrometry analysis of wild type MEFs was consistent with mature FACs (in collaboration with Dr. Christopher McCulloch of University of Toronto; **Table 4**). However, mass spectrometry analysis from TDAG51$^{-/-}$ MEFs revealed a more immature FACs.

Figure 59: Loss of TDAG51 delays skin wound healing in mice.

Mice were generated and then skin wound healing experiment was performed with the help of Dr. Jeff Dickhout. C57Bl/6 (n=10, 1 female and 9 males) and TDAG51$^{-/-}$ (n=8, 5 females and 3 males) mice of 30-32-weeks old were generated at the Henderson animal care facility. The experiment was performed under gas inhalation anesthesia (Isoflourane/oxygen mixture). A 1 cm incisional wound was made in the dorsum of the mouse with standard surgical scalpel. The wound was a full thickness wound through all layers of the dermis and epidermis and was closed with a single surgical suture and allowed to heal for periods of 2, 8 or 11-day. Wound healing in TDAG51-/- mice was compared to that in C57Bl/6 wild type mice by imaging the wounds through a Leica surgical microscope on days 2, 8 and 11. Image analysis of wounded area was performed from the resulting images with Image J software. The figure demonstrates scar formation in normal C57Bl/6 wildtype mice versus mice lacking the gene TDAG51. Mice lacking TDAG51 showed delayed dorsal skin wound healing and decreased scar formation at days 8 and 11 in comparison to control C57Bl/6 wildtype mice.

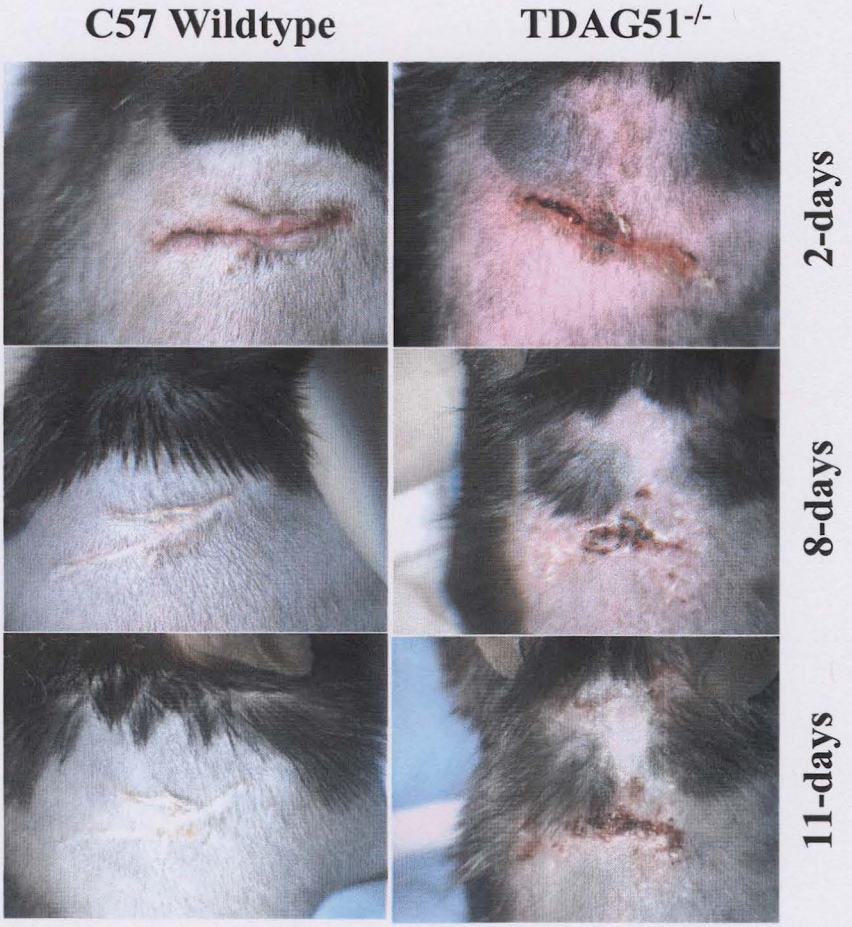
C57 Wildtype
TDAG51-/-
2-days
8-days
11-days

Figure 60: Quantitative measurement of wound area in mice with or without TDAG51.

C57Bl/6 (n=10, 1 female and 9 males) and TDAG51$^{-/-}$ (n=8, 5 females and 3 males) mice of 30-32-weeks old was generated at the Henderson animal care facility. The experiment was performed with the help of Dr. Jeff Dickhout as described in the legend of Figure 59. Image analysis of wounded area was performed from the resulting images with Image J software where region of wound was selected and quantified. The figure demonstrates the quantification of total wound area in C57Bl/6 wildtype mice versus TDAG51 lacking mice. Mice lacking the gene TDAG51 showed a statistically significant increase in wound area ($p<0.05$) at the 8 and 11 day time points versus normal C57Bl/6 wildtype controls (C57). Statistical comparison was performed with student's unpaired Two-tailed T-test.

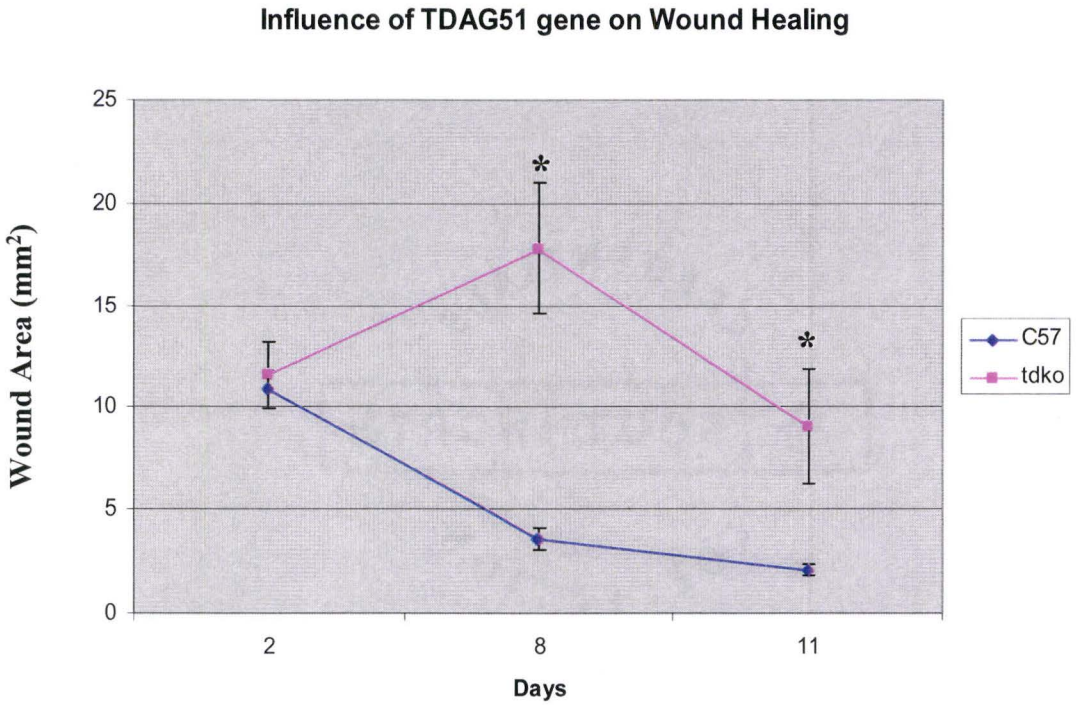
Influence of TDAG51 gene on Wound Healing
Wound Area (mm2)
25
20
15
10
5
0
2
8
11
Days
*
*
C57
tdko

Table 4: Tandem mass spectrometry analysis of MEFs.

C57 control and TDAG51$^{-/-}$ MEFs were grown in fibroblast growth media. Type I collagen coated iron beads were used to interact with the focal adhesion complex of TDAG51$^{-/-}$ and C57 control MEFs. Magnetic force was utilized to separate the beads from the cells and the proteins attached to the beads were subjected to tandem mass spectometry analysis. Herein, the table compares the genes that were present within focal adhesion complex of TDAG51$^{-/-}$ and C57 control MEFs during mass spec.

C57 MEFs	TDAG51$^{-/-}$ MEFs
	25kDA nuclear protein
Annexin A2	annexin A1
BC007171	
Caldesfmon 1	
cell division cycle 10 homolog	
Col1a2 protein (procollagen type1)	
DEAD box 1	dead-box RNA helicase
DNA segment, Chr 3, ERATO Doi 194, expressed	
eukaryotic translation elongation factor 1 a	
fibronectin	
fibulin 2	G kinase anchoring protein 1
hepatoma derived growth factor related protein 2	GPI-anchored membrane protein 1
Heterogeneous nuclear ribonucleo A0	heterogeneous nuclear ribonucleoprotein A0 iso 2
Heterogeneous nuclear ribonucleo A1	
High mobility group nucleosomal binding domain 1	
High mobility group nucleosomal binding domain 2	
Hist1h2bc	hist1h2bc
Hmga2	histone 1; histone 2
Hnrpa3 protein	Hnrpa 3 protein
Lamin A	JC7
Lysyl oxidase	
microtubule-associated protein 4	
moesin	
Myosin IC	non-POU-domain-containing octamer binding protein
Nucleolin	nucleolin
Nucleophosmin 1	nucleoplasmin 3
poly ADP-ribose polymerase 3	Poly A binding protein nuclear 1
Ribosomal protein L6	
ribosome receptor isoform mRRp47	
RNA binding motif protein 3	RNA binding motif protein 3
S100 calcium binding protein A10	
Sept9 protein	
serpine1 mRNA binding protein 1	
similar polyadenylation specific factor 6	similar to histone, H3
small acidic protein	similar to splicing factor SRP20
Vimentin	THO complex 4

4.4 Discussion

Vascular repair is a common mechanism in response to injuries by cardiovascular risk factors. Acute injuries are repaired rapidly but recurrent injuries result in a chronic inflammatory state. A number of cells, including endothelial cells, smooth muscle cells (SMC) and fibroblasts, are involved in vascular remodelling. Migration and proliferation of SMCs are important during transition from moderate to advanced atherosclerosis. Although the functions of SMCs and endothelial cells are well defined during vascular remodelling, relatively little is known regarding fibroblast migration in this process (Haurani and Pagano 2007). Furthermore, the underlying cellular components that induce migration and differentiation of fibroblasts as well as contribute to the pathogenesis of vascular disease are incompletely understood.

In our earlier studies, we demonstrated that TDAG51 induces detachment-mediated PCD and co-localizes with FAK (Hossain *et al.*, 2003). We therefore investigated whether the functional deficiency of TDAG51 affects cytoskeletal organization, cell migration and/or proliferation of MEFs. Our major findings can be explained here. **First**, loss of TDAG51 promotes migration and proliferation of MEFs in a time-dependent manner. **Second**, TDAG51$^{-/-}$ migratory MEFs present distinct filopodial and lamellipodial extensions, compared to wild type MEFs. **Third**, cell proliferation is mediated in part through β_1-integrin given that active β_1-integrin antibody significantly inhibits migration and proliferation in TDAG51$^{-/-}$ MEFs. **Fourth**, TDAG51 is also a critical molecule in cell differentiation since the deficiency of TDAG51 impairs

the differentiation of myofibroblasts, leading to slower dorsal skin wound healing in mice (Dickhout and Austin; unpublished results).

Although our earlier findings have demonstrated a causal association between TDAG51 and atherosclerosis, we do not have any direct evidence to link cell migration and atherosclerosis from the loss of TDAG51. The significance of cell migration can be explained in regard to reduced atherosclerotic lesions observed in DKO mice. It is possible that deficiency of TDAG51 in apoE$^{-/-}$ mice promotes migration of inflammatory cells, such as macrophages and T-cells, from the atherosclerotic lesions, thus decreasing inflammation and lesion progression. It can further be speculated that migratory macrophages carrying LDL or VLDL can be taken up by the liver, contributing to fatty liver but attenuated atherosclerosis as we have observed in DKO mice. In support of this, Yamashita *et al.* (2002) reported that prevention of monocyte/macrophage infiltration into atherogenesis by propagermanium, a suppressor of monocyte/macrophage infiltration, reduces atheroslcerosis in apoE$^{-/-}$ mice. Furthermore, Seki *et al.* (2005) reported that overexpression of PPAR-γ inhibits the recruitment and migration of macrophages and SMCs in the intima, leading to reduced intimal thickening observed in hypercholesterolemic rabbits. In brief, regulated migration of atherogenic cells can have significant affect on the development of atherosclerotic lesions.

Compared to macrophages, fibroblasts are rarely found in early atherosclerotic lesions. As the lesions progress to the advanced stage, chronic inflammatory conditions facilitate migration of fibroblasts to replace injured cells. Importantly, migratory fibroblasts deposit components of extracellular matrix (ECM), such as collagen, into the

intima of atherosclerotic artery to form a fibrous cap. Collagen maintains the mechanical strength of lesions and plays a major role in the stability of atherosclerotic lesions (Shah *et al.*, 1995). Studies have demonstrated that myofibroblasts can be generated from three primary sources, including adventitial fibroblasts, bone marrow-derived mesenchymal progenitor and smooth muscle cells (SMCs) (Hinz *et al.*, 2007; Bellini and Mattoli 2007; Michel *et al.*, 2009). Adventitial fibroblasts play a critical role in response to injury since they can migrate, proliferate and differentiate into myofibroblasts and secrete procollagen-1 (Michel *et al.*, 2009). In response to ballon injury, it has been reported that myofibroblast proliferation was greater within the adventitia, leading to an increased collagen turnover and matrix metalloproteinase expression (Strauss *et al.*, 1996). Studies have demonstrated that fibrocytes, bone marrow-derived mesenchymal progenitors, can differentiate into myofibroblasts and can migrate into the wound sites (Bucala *et al.*, 1994; Abe *et al.*, 2001; Mori *et al.*, 2005; Haudek *et al.*, 2006). Further, recent studies suggest that dedifferentiated smooth muscle cells can convert into potential myofibroblasts by the observation that myofibroblasts can develop the capacity of producing a long-lasting tension regulated at the level of Rho/Rho kinase-mediated inhibition of myosin light chain phosphatase, compared to that observed in SMCs (Hao *et al.*, 2006; Tomasek *et al.*, 2006).

Interestingly, affymatrix microarray analysis has revealed an upregulation of atheroprotective molecule PPAR-γ in the TDAG51$^{-/-}$ MEFs. Earlier studies have demonstrated that increased expression of PPAR-γ can impair differentiation of myofibroblasts through inhibition of transforming growth factor β_1 (TGF-β_1) signaling

(Burgess *et al.*, 2005). This inhibitory function of PPAR-γ can potentially result in less fibrosis and a less rigid blood vessel wall since there will be less deposition of collagen. Although we have not observed fibrosis in DKO mice, we have demonstrated an impaired myofibroblast differentiation in TDAG51$^{-/-}$ MEFs (Dickhout *et al.*; unpublished results). Also, atherosclerotic vessels in humans are fundamentally different from mice and are much more fibrotic (Wynn 2007). In mice, fibrosis allows the lesions to become more stable due to formation of fibrous cap and the size of the necrotic core determines whether the lesions will progress into prothrombotic state. As for human, years of repeated injuries from risk factors cause the replacement of elastin with collagen. Rigid and calcified blood vessels thus become prone to rupture. Herein, it is important to mention one of our recent observation associating TDAG51 and fibrosis. Our preliminary findings demonstrate that TDAG51$^{-/-}$ mice appeared to present less fibrosis from acute lung injury, compared to C57 control mice.

Furthermore, microarray analysis demonstrated an increased expression of decorin in the TDAG51$^{-/-}$ MEFs. Decorin is a small ECM matrix proteoglycan that can regulate cell proliferation and/or migration (Comalada *et al.*, 2003; Kresse and Schonherr 2001). Decorin can also inhibit TGF-β_1 signaling by forming complexes, leading to an impairment of myofibroblast differentiation (Jahanyar *et al.*, 2007). Importantly, earlier studies demonstrated that overexpression of decorin reduces inflammation and attenuates atherosclerotic lesion progression in apoE$^{-/-}$ mice (Al Haj Zen *et al.*, 2006). Since increased decorin expression is observed in TDAG51$^{-/-}$ MEFs, it is possible that TDAG51 is a negative regulator of decorin. Increased decorin can inhibit TGF-β signalling in

DKO mice, leading to decreased atherosclerotic lesions. However, the mechanisms by which loss of TDAG51 contribute to the upregulation of decorin in MEFs remains to be explained. Collectively, fibroblast migration may not have a direct effect on the attenuation of atherosclerosis observed in DKO mice since fibroblast migration is believed to occur at advanced stages of atherosclerosis. Other atherogenic cells, including monocytes, macrophages, lymphocytes and smooth muscle cells, are involved in all stages of atherosclerosis. Therefore, recruitment, migration and differentiation of these cells into lesions can have profound impact on the development and progression of atherosclerotic lesions.

In addition to the athero-protective properties of TDAG51, we speculated that TDAG51 may have a role in wound healing. Since loss of TDAG51 promotes migration of fibroblasts and differentiated myofibroblast can play a critical role in wound closure process, it was hypothesized that dorsal skin wound in TDAG51$^{-/-}$ mice would heal faster than that in C57 control mice. Interestingly, in contrast to our assumption, loss of TDAG51 significantly slows down skin wound healing ability in mice, compared to C57 control mice. Delayed wound healing was in part due to an impaired myofibroblast differentiation in TDAG51$^{-/-}$ mice. This has been supported by recent observations that TDAG51$^{-/-}$ MEFs treated with TGF-β_1 did not differentiate into myofibroblasts (Dickhout *et al.*; unpublished results). Following treatment with TGF-β_1, TDAG51$^{-/-}$ MEFs also demonstrate decreased SMAD2 phosphorylation. Earlier studies have shown that activation of TGF-β_1 differentiates fibroblasts and increases collagen synthesis through phosphorylation of SMAD2/3 (Kuratomi *et al.*, 2005; Brown *et al.*, 2007).

Furthermore, we have observed through protein profiling from mass spectrometry that TDAG51$^{-/-}$ MEFs displayed fewer proteins assocaited with focal adhesion complexes, compared to wild type MEFs. Earlier studies have demonstrated that mechanical force increases myofibroblast differentiation with more mature focal adhesion complexes (Wang *et al.*, 2003). In support of this, migratory TDAG51$^{-/-}$ MEFs had distinct filopodial and lamellipodial extensions, compared wildtype MEFs, suggesting that TDAG51$^{-/-}$ fibroblasts are not attaching well to the fibronectin coated matrix. Thus, impaired wound healing in the TDAG51$^{-/-}$ mice likely results from impaired adherence of fibroblast and lack of subsequent myofibroblast differentiation. It is also possible that normal contact inhibition is suppressed in TDAG51$^{-/-}$ MEFs, suggesting that deficiency of TDAG51 may contribute to impaired adherence of fibroblasts. The underlying mechanisms by which enhanced fibroblast migration reduces wound healing in TDAG51$^{-/-}$ mice remains to be explained.

Taken together, loss of TDAG51 promotes the migration and proliferation of fibroblasts through interaction between β_1-integrin and fibronectin on the ECM. Increased fibroblast migration may have a significant affect on atherosclerosis and wound healing. However, future studies are needed to explain the in-dept mechanisms by which loss of TDAG51 impairs myofibroblast differentiation and thus contributes to the pathogenesis of atherosclerosis and wound healing. Importantly, this will further allow us to investigate whether TDAG51 is involved in the pathogenesis of fibrosis.

CHAPTER 5: Concluding discussion and future directions

5.1 Concluding remarks

This research project was initiated to identify gene(s) that were responsive to the cardiovascular risk factor, homocysteine, using mRNA differential display technique. As a result, I have identified TDAG51 as a homocysteine-responsive gene. Further, we demonstrated that TDAG51 is an ER stress-induced pro-apoptotic gene in cultured endothelial cells and is associated with the development of atherosclerosis in HHcy (Hossain *et al.*, 2003). Subsequently, we have established a causal association of TDAG51 in the development and progression of atherosclerosis given that loss of TDAG51 attenuates the progression of atherosclerosis in apoE$^{-/-}$ mice fed a normal chow diet. Although we have not established a definitive mechanism for the reduction of lesion size in DKO mice, several mechanisms have been proposed in this thesis. **First**, since TDAG51 is a pro-apoptotic gene, it is conceivable that the deficiency of TDAG51 may reduce apoptosis of cells relevant to atherosclerosis leading to reduced lesion size in DKO mice. This has been demonstrated by the statistically significant reduction in necrotic core size of the atherosclerotic lesions and the contribution of this reduction to the overall reduction in lesion size. In support of this, Thorp *et al.* (2009) have recently demonstrated reduced atherosclerotic lesion size in apoE$^{-/-}$ or LDLR$^{-/-}$ mice lacking CHOP, an ER-stress response pro-apoptotic gene. **Second**, since overexpression of TDAG51 promotes detachment-mediated PCD in endothelial cells, loss of TDAG51 may

decrease endothelial dysfunction and apoptosis resulting in reduced inflammation and lesion size in DKO mice. **Third**, since there is increased expression of PPAR-γ in TDAG51$^{-/-}$ MEFs, it is possible that deficiency of TDAG51 may attenuate the development and progression of atherosclerosis in DKO mice through a mechanism involving PPAR-γ. It has been reported that PPAR-γ has both anti-atherogenic and anti-inflammatory properties (Lehrke and Lazar 2005). **Fourth**, given that loss of TDAG51 promotes cell migration and proliferation in MEFs, it is possible that there may be an increased migration of macrophages from the lesions, thus contributing to attenuated atherosclerosis in DKO mice.

The most significant finding of my research is that TDAG51 is a novel gene involved in the development and progression of atherosclerosis. The attenuation of atherosclerosis from the loss of the pro-apoptotic gene TDAG51 is in contrast to the previously reported studies involving deficiency of cell cycle and pro-apoptotic genes, including p53, Bax or Rb. Studies have implicated that the deficiency of macrophage specific p53, Bax or Rb enhances atherosclerotic lesion development (Guevara *et al.*, 1999; Liu *et al.*, 2004; Boesten *et al.*, 2006). Loss of macrophage specific p38α MAPK in apoE$^{-/-}$ mice, however, does not affect lesion development, even though deficiency of p38α MAPK promotes macrophage apoptosis and plaque necrosis in advanced lesions (Seimon *et al.*, 2009). Since p38α MAPK has both pro- and anti-apoptotic function depending on the stimulus (DeVries-Seimon *et al.*, 2005; Park *et al.*, 2002; Wang *et al.*, 2007), it is possible that p38α MAPK plays a crucial role in suppressing ER stress-induced macrophage apoptosis in advanced atherosclerosis. Further, p38α MAPK may

not be a crucial molecule in regulating atherosclerotic lesion size. Interestingly, Thorp *et al.* (2009) have recently demonstrated that functional deficiency of CHOP in apoE$^{-/-}$ or LDLR$^{-/-}$ mice results in reduced atherosclerotic lesion sizes. Like TDAG51, studies have demonstrated that CHOP is an ER stress-induced pro-apoptotic gene and promotes apoptosis in cells relevant to atherosclerosis (Seimon and Tabas 2008).

The ability of TDAG51 to decrease atherosclerotic lesion development may not be solely due to its pro-apoptotic characteristics. Since reduction in necrotic core size does not fully account for the reduction in lesion size, we have proposed involvement of other factors for the attenuation of atherosclerotic lesion observed in DKO mice. Additional factor(s), such as PPAR-γ, may be associated with the reduction of lesion in DKO mice, given that PPAR-γ is atheroprotective and that its expression is increased in TDAG51$^{-/-}$ MEFs. Importantly, PPAR-γ influence cholesterol efflux and our preliminary results demonstrate an increased cholesterol efflux in TDAG51$^{-/-}$ peritoneal macrophages (unpublished results). Future studies, however, are essential to elucidate the underlying mechanism(s) by which functional loss of TDAG51 contributes to the reduction of atherosclerotic lesions in DKO mice.

My findings further suggest that TDAG51 can be an important target for anti-atherogenic therapy. During the last-two decades, statins have been successful in the management of cardiovascular disease. However, despite the use of statins as a first order therapy against atherosclerosis, significant morbidity and mortality still occurs. Identifying drugs and/or small molecules that suppress the expression/activity of TDAG51 may allow the opportunity to explore whether TDAG51 can potentially be a

relevant therapeutic target for the treatment of cardiovascular disease, especially clinical complications such as myocardial infarction.

In addition to its atheroprotective properties, we demonstrated that TDAG51 is a critical molecule during wound healing. We observed that the dorsal skin wounds do not close efficiently in TDAG51$^{-/-}$ mice, compared to those in C57 mice. This delayed wound healing in TDAG51$^{-/-}$ mice may in part be from an impaired differentiation of myofibroblasts. Studies have shown that myofibroblasts play very important role in wound healing, especially during contraction of wounds (Hinz *et al.*, 2007). Further, it has been suggested that PPAR-γ mediates the differentiation of fibroblasts into myofibroblasts through a cross talk influence of TGF-β1 signaling pathway. Our observation that TDAG51$^{-/-}$ MEFs have increased PPAR-γ expression and have reduced TGF-β1 mediated SMAD2 phosphorylation, may further explain the impaired myofibroblast differentiation from the loss of TDAG51. The underlying mechanism(s), however, remain to be explained how functional loss of TDAG51 delays wound healing.

In this thesis, I have presented data suggesting that TDAG51 is a novel mediator of atherosclerosis. During the progression of atherosclerosis, migration of SMCs from media is well documented (Ross 1999; Lusis 2000; Glass and Witztum 2001). Subsequent proliferation of SMCs and their collagen deposition facilitates the formation of fibrous cap. Studies have suggested that fibroblasts also migrate into the moderate or advanced atherosclerotic lesions and differentiated into myofibroblasts that then release ECM components to generate fibrous networks, providing lesion stability (Hinz *et al.*, 2007). Although we have demonstrated an association between TDAG51 and skin

wound healing, we have not observed fibrosis in apoE$^{-/-}$ or DKO mice. Interestingly, our recent observation demonstrates that TDAG51$^{-/-}$ mice are protective from acute lung injury-induced fibrosis, compared to C57 mice. Herein, it is important to mention that mice and human atherosclerosis are fundamentally different, especially at the advanced stage. Fibrosis is believed to provide stability in mouse atherosclerotic lesions, including apoE$^{-/-}$ or other atherogenic mouse models (Libby *et al.*, 1996; Rosenfeld *et al.*, 2002). However, fibrosis is more prevalent in humans and can cause blood vessels to become more rigid as well as promoting lesion calcification. Over time, rigid and calcified vessels become prone to rupture, thus leading to thrombosis. Collectively, our findings demonstrate that TDAG51 is involved in the pathogenesis of both atherosclerosis and skin wound healing, however, future studies are required to suggest a definite involvement of TDAG51 with fibrosis.

5.2 Future directions

Future *in vitro* and *in vivo* studies are essential to further understand the function of TDAG51 and to investigate the mechanism(s) by which loss of TDAG51 attenuates atherosclerosis and impairs the wound healing process.

5.2.1 Specific objective 1: To further determine the effect from transplantation of TDAG51$^{-/-}$ hematopoietic cells on atherosclerotic lesion development

Although loss of TDAG51 attenuates atherosclerotic lesion development in apoE$^{-/-}$ mice, it is not understood whether this is a systemic or lesion specific effect. Bone marrow transplantation experiments can be performed to explain whether attenuated

atherosclerosis observed in DKO mice is due to the deficiency of TDAG51 in hematopoietic cells, including macrophages and lymphocytes. Bone marrows from apoE$^{-/-}$ and DKO mice can be isolated as described earlier (Covey *et al.*, 2003). Irradiated ten-week old female apoE$^{-/-}$ mice should then be injected with fresh bone marrows isolated from either apoE$^{-/-}$ or DKO mice of similar age. Genotype of recipients and donors should be confirmed by PCR. By 24-36 weeks, the recipient mice should be sacrificed to analyze the lesion size. This experiment will definitely explain us whether the atheroprotective effect of TDAG51 deficiency involves hematopoietic cells.

5.2.2 Specific objective 2: To examine TDAG51 as a potential therapeutic target for the treatment of cardiovascular disease

In this thesis, I have demonstrated that TDAG51 is causally associated with the development and progression of atherosclerosis. High throughput screening approach of biomolecules can be utilized to identify molecules that suppress the expression/activity of TDAG51. Insulin growth factor or PBA can be used to express increased or decreased expression of TDAG51 in NIH3T3 cell lines, respectively (Toyoshima *et al.*, 2004; Özcan *et al.*, 2006). Stable cell lines expressing TDAG51 reporter construct can be generated to examine the induction or suppression of TDAG51 expression by the biomolecules during high throughput screening process. Following identification of several potential compounds, pharmacokinetics and pharmacodynamics studies can be performed in mice to define the safety and doses of the compounds. A few of the potential compounds can then be tested on apoE$^{-/-}$ mice to demonstrate attenuated atherosclerosis during lesion progression. If any of the compounds are successful in

preclinical studies, the drug(s) can be tested in clinical trials to assess the safety and efficacy in human subjects following approval from FDA.

5.2.3 Specific objective 3: To further define the functional domain(s) of TDAG51 that mediate apoptosis and cell migration

TDAG51 has distinct regions within the open reading frame (ORF), including polyglutamin (QQ) stretch, proline-glutamine (PQ)/prolin-histidine (PH) rich repeats, pleckstrin homology (PH) domain. Studies have demonstrated that proteins with QQ, PQ or PH repeats can act as a transcriptional regulator and/or activator, and can thus contribute to PCD and other cellular processes (Han *et al.*, 1989; McNabb and Courtney, 1992; Cai *et al.*, 1994; Li *et al.*, 1995; Park *el al.*, 1996). Herein, generation of a series of mutants within ORF (as described in figure 20) will facilitate to explain the region(s) that contribute to PCD and cell migration/proliferation. In addition, TDAG51 also have nuclear localization signal (NLS) and nuclear export signal (NES). Generation of mutants by disrupting NLS or NES will further define whether TDAG51 is a nuclear protein shuttling between cytosol and nucleus. Importantly, it will allow us to understand whether retention of TDAG51 within cytosol will affect the cellular processes, such as apoptosis and/or cell migration.

5.2.4 Specific objective 4: To examine the relationship among ER stress, TDAG51 expression, PCD and atherosclerosis

We earlier demonstrated that TDAG51 is an ER stress-inducible pro-apoptotic gene and its transcriptional activation is dependent on the phosphorylation of eIF2α (Hossain *et al.*, 2003). To further define the UPR pathways that regulate TDAG51 expression, transient

transfection experiments could be performed using plasmid encoding wildtype, mutant or constitutively active forms of eIF2α. Constitutively active form of eIF2α should increase TDAG51 expression and PCD. Since eIF2α phosphorylation activates other ER stress-inducible pro-apoptotic gene GADD153, it will be interesting to see whether overexpression of TDAG51 promotes PCD in GADD153$^{-/-}$ cells. These experiments should further clarify which UPR pathways directly mediate TDAG51 expression. In addition, studies have shown that chemical chaperones, 4-phenyl butyric acid (PBA), can reduce ER stress (Özcan *et al.*, 2006). Given that loss of TDAG51 attenuate atherosclerosis in apoE$^{-/-}$ mice, a future experiment can be designed to address whether PBA treatment reduces TDAG51 expression in cells relevant to atherosclerosis, leading to the attenuation of atherosclerosis in apoE$^{-/-}$ and DKO mice.

5.2.5 Specific objective 5: To further investigate how TDAG51 modulates the expression of PPAR-γ and its downstream targets

Using Affymatrix microarray analysis and real time PCR, we demonstrated that loss of TDAG51 induces expression of PPAR-γ and several of its downstream targets in MEFs. Further, reintroduction of TDAG51 into TDAG51$^{-/-}$ MEFs reverses the effect on PPAR-γ expression, suggesting that TDAG51 is a potential negative regulator of PPAR-γ. Using PPAR-responsive reporter assay system, transient transfection experiment can be performed on wildtype and TDAG51$^{-/-}$ MEFs to examine the effect on PPAR-γ targets in presence or absence of PPAR-γ specific agonists and antagonists. Herein, real time PCR should allow us to reconfirm our findings in microarray analysis. To investigate whether PPAR-γ is regulated at transcriptional or translational level, co-transfection experiment

can be performed using reporter gene linked to PPAR-γ promoter together with TDAG51 expression plasmids. If PPAR-γ promoter activity is responsive from exogenous TDAG51 in wildtype and TDAG51$^{-/-}$ MEFs, additional experiments such as DNA/protein binding assays can be performed to identify the nature of regulation. In addition, an *in vivo* experiment can be designed to address whether attenuated atherosclerosis observed in DKO mice requires PPAR-γ. Treatment of apoE$^{-/-}$ or DKO mice with PPAR-γ agonists should further reduce atherosclerotic lesion size since PPAR-γ agonists activate the expression of PPAR-γ. Alternatively, PPAR-γ antagonists should enhance the atherosclerotic lesion size in apoE$^{-/-}$ or DKO mice.

5.2.6 Specific objective 6: To examine whether TDAG51 has role in macrophage apoptosis, migration, or foam cell formation

To further understand about the underlying mechanisms by which atherosclerosis is attenuated in DKO mice, a number of future *in vitro* experiments should focus attention into the role of TDAG51 in macrophages. Peritoneal macrophages from wildtype and TDAG51$^{-/-}$ mice can be isolated and treated with the inducers of apoptosis to explain whether loss of TDAG51 protects or enhances apoptosis of macrophages. Further, peritoneal macrophage migration experiments can be performed using Boyden Chamber as described in section 4.2.5.2. Number of migratory cells from plated wildtype and TDAG51$^{-/-}$ macrophages can then be counted and compared. This experiment should explain whether migration of macrophages from the atherosclerotic lesions occurs in DKO mice. In addition, since the atherosclerotic lesion size is attenuated in DKO mice, it will be interesting to examine whether TDAG51$^{-/-}$ mice macrophages accumulate less

acetylated LDL and show enhanced cholesterol efflux, compared to macrophages from C57 wildtype control mice. Macrophage foam cell formation can also be measured by the uptake of acetylated lipoproteins by peritoneal macrophages (Brown *et al.*, 1979). Cholesterol loading and efflux assay can be performed as described previously (Chawla *et al.*, 2001).

5.2.7 Specific objective 7: To further investigate the role of TDAG51 in wound healing

We observed that loss of TDAG51 delays skin wound healing process, perhaps through a mechanism involving impaired myofibroblast differentiation. Re-introduction of TDAG51 should therefore decrease wound healing time. Retroviral or adenoviral vectors encoding TDAG51 expression plasmids can be applied to the fresh skin wounds of wildtype and TDAG51$^{-/-}$ mice. The healing process can be observed up to 12 days and the images can then be compared. If TDAG51 has a direct involvement with skin wound healing, reintroduction of TDAG51 should rectify the delay. Alternatively, high throughput screen may allow for the identification of molecules that increase the expression of TDAG51. Skin wounds of wildtype mice can also be treated with some of these molecules. If skin wound healing time is faster, this can further suggest a direct involvement of TDAG51. Importantly, the compound(s) can further be investigated to see whether there is a therapeutic potential for wound healing treatment, especially in the reduction of scar formation.

5.2.8 Specific objective 8: To assess whether TDAG51 is involved in fibrosis

We earlier have shown that TDAG51 is a mediator of atherosclerosis (Hossain *et al.*, 2003). Further, our recent findings demonstrated that loss of TDAG51 promotes fibroblast migration and delays skin wound healing in mice. Since fibroblast migration is a hallmark feature during skin wound healing and fibrosis, we speculate that TDAG51 may have role in fibrosis. To address this issue, bleomycin-induced pulmonary fibrosis can be introduced in wildtype and TDAG51$^{-/-}$ mice as described earlier (Hattori *et al.*, 2000). If TDAG51 deficiency decreases fibrosis, we would expect a reduced pulmonary fibrosis in TDAG51$^{-/-}$ mice, compared to wildtype mice. In addition, it can be examined whether exogenous TDAG51 accelerates the healing within injured area of lung in wildtype mice following infection with retroviral expression plasmids encoding TDAG51 ORF. To further test the association between TDAG51 and fibrosis, wildtype and TDAG51$^{-/-}$ mice can be treated with PPAR-γ agonist such as rosiglitazone. Since studies have shown that rosiglitazone abrogates pulmonary fibrosis (Burgess *et al.*, 2005; Wu *et al.*, 2009), these experiments should demonstrate whether TDAG51 is associated with the pathogenesis of fibrosis.

CHAPTER 6: References

6.0 References

Abbondanzo SJ, Gadi I, Stewart CL (1993). Derivation of embryonic stem cell lines. Methods Enzymol. 225: 803-23.

Abe R, Donnelly SC, Peng T, Bucala R, Metz CN (2001). Peripheral blood fibrocytes: differentiation pathway and migration to wound sites. J Immunol 166: 7556–7562.

Aji W, Ravalli S, Szabolcs M, Jiang XC, Sciacca RR, Michler RE, Cannon PJ (1997). L-arginine prevents xanthoma development and inhibits atherosclerosis in LDL receptor knockout mice. Circulation 95(2): 430-7.

Al Haj Zen A, Caligiuri G, Sainz J, Lemitre M, Demerens C, Lafont A (2006). Decorin overexpression reduces atherosclerosis development in apolipoprotein E-deficient mice. Atherosclerosis. 187(1): 31-9.

Alnemri ES, Livingston DJ, Nicholson DW, Salvesen G, Thornberry NA, Wong WW, and Yuan J (1996). Human ICE/CED-3 protease nomenclature. Cell 87: 171.

Anderson KM, Castelli WP, Levy D (1987). Cholesterol and mortality. 30 years of follow-up from the Framingham study. JAMA 257(16): 2176-80.

Antonsson B, Conti F, Ciavatta A, Montessuit S, Lewis S, Martinou I, Bernasconi L, Bernard A, Mermod JJ, Mazzei G, Maundrell K, Gambale F, Sadoul R, Martinou JC. (1997). Inhibition of Bax channel-forming activity by Bcl-2. Science 277: 370-72.

Arad Y, Newstein D, Cadet F, Roth M, Guerci AD (2001). Association of multiple risk factors and insulin resistance with increased prevalence of asymptomatic coronary artery disease by an electron-beam computed tomographic study. Arterioscler Thromb Vasc Biol. 21(12): 2051-8.

Ardissino D, Merlini PA, Ariens R, Coppola R, Bramucci E, Mannucci PM (1997). Tissue-factor antigen and activity in human coronary atherosclerotic plaques. Lancet 349(9054): 769-71.

Arruda VR, von Zuben PM, Chiaparini LC, Annichino-Bizzacchi JM, Costa FF (1997). The mutation Ala677→Val in the methylene tetrahydrofolate reductase gene: a risk factor for arterial disease and venous thrombosis. Thromb Haemost 77: 818-21.

Ashkenazi A, and Dixit VM (1998). Death receptors: signaling and modulation. Science 281: 1305-08.

Ashwell JD, Cunningham RE, Noguchi PD, Hernandez D (1987). Cell growth cycle block of T cell hybridomas upon activation with antigen. J Exp Med. 165(1): 173-94.

Assmann G, Cullen P, Jossa F, Lewis B, and Mancini M (1999). Coronary heart disease: reducing the risk. Arterioscl Thromb Vasc Biol 19: 1819-24.

Attwell S, Roskelley C, and Dedhar S (2000). The integrin-linked kinase (ILK) suppresses anoikis. Oncogene 19: 3811-15.

Azumi H, Inoue N, Takeshita S, Rikitake Y, Kawashima S, Hayashi Y, Itoh H, Yokoyama M (1999). Expression of NADH/NADPH oxidase p22phox in human coronary arteries. Circulation 100: 1494-98.

Babaev VR, Yancey PG, Ryzhov SV, Kon V, Breyer MD, Magnuson MA, Fazio S, Linton MF (2005). Conditional knockout of macrophage PPARgamma increases atherosclerosis in C57BL/6 and low-density lipoprotein receptor-deficient mice. Arterioscler Thromb Vasc Biol. 25(8): 1647-53.

Bachelder RE, Wendt MA, Fujita N, Tsuruo T, and Mercurio AM (2001). The cleavage of Akt/protein kinase B by death receptor signaling is an important event in detachment-induced apoptosis. J Biol Chem 276: 34702-07.

Ballard-Barbash R, Callaway CW (1987). Marine fish oils: role in prevention of coronary artery disease. Mayo Clin Proc 62(2): 113-18.

Ball RY, Stowers EC, Burton JH, Cary NR, Skepper JN, Mitchinson MJ (1995). Evidence that the death of macrophage foam cells contributes to the lipid core of atheroma. Atherosclerosis 114(1): 45-54.

Barbato JC, Catanescu O, Murray K, DiBello PM, Jacobsen DW (2007). Targeting of metallothionein by L-homocysteine: a novel mechanism for disruption of zinc and redox homeostasis. Arterioscler Thromb Vasc Biol. 27(1): 49-54.

Bellini A and Mattoli S (2007). The role of the fibrocyte, a bone marrow-derived mesenchymal progenitor, in reactive and reparative fibroses. Lab Invest 87(9): 858-70.

Bennet MR (1999). Apoptosis of vascular smooth muscle cells in vascular remodeling and atherosclerotic plaque rupture. Cardiovascular Res 41: 361-68.

Bierman EL (1992). George Lyman Duff Memorial Lecture. Atherogenesis in diabetes. Arterioscler Thromb 12(6): 647-56.

Boers GHJ (1997). Hyperhomocysteinemia as a Risk factor for Arterial and Venous Disease. A Review of Evidence and Relevance. Thrombosis and Haemostasis 78(1): 520-22.

Boesten LS, Zadelaar AS, van Nieuwkoop A, Hu L, Jonkers J, van de Water B, Gijbels MJ, van der Made I, de Winther MP, Havekes LM, van Vlijmen BJ (2006). Macrophage retinoblastoma deficiency leads to enhanced atherosclerosis development in ApoE-deficient mice. FASEB J. 20(7): 953-5.

Bønaa KH, Njølstad I, Ueland PM, Schirmer H, Tverdal A, Steigen T, Wang H, Nordrehaug JE, Arnesen E, Rasmussen K; NORVIT Trial Investigators (2006). Homocysteine lowering and cardiovascular events after acute myocardial infarction. N Engl J Med. 354(15): 1578-88.

Bostom AG, Carpenter MA, Kusek JW, Hunsicker LG, Pfeffer MA, Levey AS, Jacques PF, McKenney J; FAVORIT Investigators (2006). Rationale and design of the Folic Acid for Vascular Outcome Reduction In Transplantation (FAVORIT) trial. Am Heart J. 152(3): 448. e1-7.

Boushey CJ, Beresford SA, Omenn GS, Motulsky AG (1995). A quantitative assessment of plasma homocysteine as a risk factor for vascular disease: probable benefits of increasing folic acid intakes. JAMA 274: 1049-57.

Brakebusch C, Fässler R (2005). beta 1 integrin function in vivo: adhesion, migration and more. Cancer Metastasis Rev. 2005 Sep;24(3):403-11.

Brattström L, Israelsson B, Lindgärd F, and Hultberg B (1988). Higher total plasma homocysteine in vitamin B_{12} deficiency than in heterozygosity for homocystinuria due to cystathionine β-synthase deficiency. Metabolism 37: 175-78.

Breslow JL (1993). Transgenic mouse models of lipoprotein metabolism and atherosclerosis. Proc Natl Acad Sci USA 90(18): 8314-18.

Breslow JL (1996). Mouse models of atherosclerosis. Science 272(5262): 685-88.

Brown KA, Pietenpol JA, Moses HL (2007). A tale of two proteins: differential roles and regulation of Smad2 and Smad3 in TGF-beta signaling. J Cell Biochem 101 (1): 9-33.

Brown MS, and Goldstein JL (1986). A receptor-mediated pathway for cholesterol homeostasis. Science 232(4746): 34-47.

Brown MS and Goldstein JL. Lipoprotein receptors: therapeutic implications. J Hypertens Suppl 1990; 8: S33-6.

Brown MS and Goldstein JL (1999). A proteolytic pathway that controls the cholesterol content of membranes, cells, and blood. Proc Natl Acad Sci 96: 11041-48.

Brown MS, Goldstein JL, Krieger M, Ho YK, Anderson RG (1979). Reversible accumulation of cholesteryl esters in macrophages incubated with acetylated lipoproteins. J Cell Biol 82(3): 597-613.

Brunner T, Mogil RJ, LaFace D, Yoo NJ, Mahboubi A, Echeverri F, Martin SJ, Force WR, Lynch DH, Ware CF, et al. (1995). Cell-autonomous Fas (CD95)/Fas-ligand interaction mediates activation-induced apoptosis in T-cell hybridomas. Nature 373(6513): 441-4.

Bucala R, Spiegel LA, Chesney J, Hogan M, Cerami A (1994). Circulating fibrocytes define a new leukocyte subpopulation that mediates tissue repair. Mol Med 1:71–81.

Burgess HA, Daugherty LE, Thatcher TH, Lakatos HF, Ray DM, Redonnet M, Phipps RP, Sime PJ (2005). PPARgamma agonists inhibit TGF-beta induced pulmonary myofibroblast differentiation and collagen production: implications for therapy of lung fibrosis. Am J Physiol Lung Cell Mol Physiol 288(6): L1146-53.

Busse R, Mulsch A, Fleming I, Hecker M (1993). Mechanisms of nitric oxide release from the vascular endothelium. Circulation 87: V18-V25.

Butz LW, du Vigneaud V (1932). The formation of a homologue of cysteine by the decomposition of methionine. J Biol Chem 99: 135-42.

Cai J, Lan Y, Appel L, and Weir M (1994). Dissection of the Drosophila paired protein: functional requirements for conserved motifs. Mech Dev 47: 139-50.

Cai Y, Zhang C, Nawa T, Aso T, Tanaka M, Oshiro S, Ichijo H, and Kitajima S (2000). Homocysteine-responsive ATF3 gene expression in human vascular endothelial cells: activation of c-Jun NH_2-terminal kinase and promoter response element. Blood 96: 2140-48.

Carragher NO and Frame MC (2004). Focal adhesion and actin dynamics: a place where kinases and proteases meet to promote invasion. Trends in Cell Bio. 14: 241-49.

Carson NAJ, Neil DW (1962). Metabolic abnormalities detected in a survey of mentally backward individuals in northern Ireland. Arch Dis Child 137: 505-13.

Casciola-Rosen L, Rosen A, Petri M, Schlissel M (1996). Surface blebs on apoptotic cells are sites of enhanced procoagulation activity: implication for coagulation events and antigenic spread in systemic lupus erythematosus. Proc Natl Acad Sci USA 93: 1624-29.

Castrillo A, Tontonoz P (2004). PPARs in atherosclerosis: the clot thickens. J Clin Invest. 114(11): 1538-40.

Cattaneo M (1999). Hyperhomocysteinemia, atherosclerosis and thrombosis. Thromb Haemost 81: 165-76.

Chambers JC, McGregor A, Jean-Marie J, Obeid OA, Kooner JS (1999). Demonstration of rapid onset vascular endothelial dysfunction after hyperhomocysteinemia: an effect reversible with vitamin C therapy. Circulation 99: 1156-60.

Chappell DC, Varner SE, Nerem RM, Medford RM, Alexander RW (1998). Oscillatory shear stress stimulates adhesion molecule expression in cultured human endothelium. Circ Res. 82: 532-39.

Chawla A, Boisvert WA, Lee CH, Laffitte BA, Barak Y, Joseph SB, Liao D, Nagy L, Edwards PA, Curtiss LK, Evans RM, Tontonoz P (2001). A PPAR gamma-LXR-ABCA1 pathway in macrophages is involved in cholesterol efflux and atherogenesis. Mol Cell. 7(1): 161-71.

Chen C, Holkos ME, Surowiec SM, Conklin BS, Lin PH, Lumsden AB (2000). Effects of homocysteine on smooth muscle cell proliferation in both cell culture and artery perfusion culture models. J Surg Res 88: 26-33.

Chen Z, Ishibashi S, Perrey S, Osuga Ji, Gotoda T, Kitamine T, Tamura Y, Okazaki H, Yahagi N, Iizuka Y, Shionoiri F, Ohashi K, Harada K, Shimano H, Nagai R, Yamada N (2001). Troglitazone inhibits atherosclerosis in apolipoprotein E-knockout mice: pleiotropic effects on CD36 expression and HDL. Arterioscler Thromb Vasc Biol. 21(3): 372-7.

Chen Z, Karaplis AC, Ackerman SL, Pogribny IP, Melnyk S, Lussier-Cacan S, Chen MF, Pai A, John SMW, Smith RS, Bottiglieri T, Bagley P, Selhub J, Rudnicki MA, James J, and Rosen R (2001). Mice deficient in methylenetetrahydrofolate reductase exhibit hyperhomocysteinemia and decreased methylation capacity, with neuropathology and aortic lipid deposition. Hum Mol Genet 10(5): 433-43.

Chinetti G, Lestavel S, Bocher V, Remaley AT, Neve B, Torra IP, Teissier E, Minnich A, Jaye M, Duverger N, Brewer HB, Fruchart JC, Clavey V, Staels B (2001). PPAR-alpha and PPAR-gamma activators induce cholesterol removal from human macrophage foam cells through stimulation of the ABCA1 pathway. Nat Med. 7(1): 53-58.

Christen WG, and Ridker PM (2000). Blood levels of homocysteine and atherosclerotic vascular disease. Curr Atheroscler Rep 2(3): 194-99.

Clarke R, Daly L, Robinson K, Naughten E, Cahalane S, Fowler B, and Graham I (1991). Hyperhomocysteinemia: an independent risk factor for vascular disease. N Engl J Med 324: 1149-55.

Colgan SM, Austin RC (2007). Homocysteinylation of metallothionein impairs intracellular redox homeostasis: the enemy within! Arterioscler Thromb Vasc Biol. 27(1): 8-11.

Colgan SM, Tang D, Werstuck GH, Austin RC (2007). Endoplasmic reticulum stress causes the activation of sterol regulatory element binding protein-2. Int J Biochem Cell Biol. 39(10): 1843-51.

Collins AR, Meehan WP, Kintscher U, Jackson S, Wakino S, Noh G, Palinski W, Hsueh WA, Law RE (2001). Troglitazone inhibits formation of early atherosclerotic lesions in diabetic and nondiabetic low density lipoprotein receptor-deficient mice. Arterioscler Thromb Vasc Biol. 2001 Mar;21(3):365-71.

Collins RG, Velji R, Guevara NV, Hicks MJ, Chan L, and Beaudet AL (2000). P-selectin or intercellular adhesion molecule (ICAM)-1 deficiency substantially protects against atherosclerosis in apolipoprotein E-deficient mice. J Exp Med 191: 189-94.

Collins T and Cybulsky MI (2001). NF-κB: pivotal mediator or innocent bystander in atherogenesis? J Clin Invest 107(3): 255-64.

Comalada M, Cardó M, Xaus J, Valledor AF, Lloberas J, Ventura F, Celada A (2003). Decorin reverses the repressive effect of autocrine-produced TGF-beta on mouse macrophage activation. J Immunol 170(9): 4450-6.

Corti R, Hutter R, Badimon JJ, Fuster V (2004). Evolving concepts in the triad of atherosclerosis, inflammation and thrombosis. J Thromb Thrombolysis. 17(1): 35-44.

Covey SD, Krieger M, Wang W, Penman M, Trigatti BL (2003). Scavenger receptor class B type I-mediated protection against atherosclerosis in LDL receptor-negative mice involves its expression in bone marrow-derived cells. Arterioscler Thromb Vasc Biol. 2003 Sep 1;23(9):1589-94.

Dai G, Kaazempur-Mofrad MR, Natarajan S, Zhang Y, Vaughn S, Blackman BR, Kamm RD, Garcia-Cardena G, Gimbrone MA Jr (2004). Distinct endothelial phenotypes evoked by arterial waveforms derived from atherosclerosis-susceptible and -resistant regions of human vasculature. Proc Natl Acad Sci U S A 101(41): 14871-6.

Daugherty A (2002). Mouse models of atherosclerosis. Am J Med Sci 323(1): 3-10.

Davies MJ. A macro and micro view of coronary vascular insult in ischemic heart disease. Circulation. 1990; 82 (suppl II): 38-46.

Davies MJ, and Woolf N (1993). Atherosclerosis: what is it and why does it occur? Br Heart J 69(supplement): S3-S11.

Davies PF (1986). Vascular cell interactions with special reference to the pathogenesis of atherosclerosis. Lab Invest 55(1): 5-24.

Davingnon J and Ganz P. Role of endothelial dysfunction in atherosclerosis. Circulation. 2004. 109 (Suppl III): 27-32.

Dayal S, Arning E, Bottiglieri T, Böger RH, Sigmund CD, Faraci FM, Lentz SR (2004). Cerebral vascular dysfunction mediated by superoxide in hyperhomocysteinemic mice. Stroke 35(8): 1957-62.

de Koning A.B.L., Werstuck G H., Zhou J., Austin R.C (2003). Hyperhomocysteinemia and its role in the development of atherosclerosis. Clinical Biochemistry 36 : 431-41.

Deloughery TG, Evans A, Sadeghi A *et al.* (1996). Common mutation in methylenetetrahydrofolate reductase: correlation with homocysteine metabolism and late-onset vascular disease. Circulation 94: 3074-78.

den Heijer M, Koster T, Blom HJ, Bos GM, Briet E, Reitsma PH, Vandenbroucke JP, and Rosendaal FP (1996). Hyperhomocysteinemia as a risk factor for deep-vein thrombosis. N Engl J Med 334: 759-62.

Devries-Seimon T, Li Y, Yao PM, Stone E, Wang Y, Davis RJ, Flavell R, Tabas I (2005). Cholesterol-induced macrophage apoptosis requires ER stress pathways and engagement of the type A scavenger receptor. J Cell Biol. 171(1): 61-73.

Dhein J, Walczak H, Bäumler C, Debatin KM, Krammer PH (1995). Autocrine T-cell suicide mediated by APO-1/(Fas/CD95). Nature 373(6513): 438-41.

Dickhout JG, Basseri S, Austin RC (2008). Macrophage function and its impact on atherosclerotic lesion composition, progression, and stability: the good, the bad, and the ugly. Arterioscler Thromb Vasc Biol 28(8): 1413-5.

Dickhout JG, Hossain GS, Pozza LM, Zhou J, Lhoták S, Austin RC (2005). Peroxynitrite causes endoplasmic reticulum stress and apoptosis in human vascular endothelium: implications in atherogenesis. Arterioscler Thromb Vasc Biol.: 25(12): 2623-29.

Dickhout JG, Sood SK, Austin RC (2007). Role of endoplasmic reticulum calcium disequilibria in the mechanism of homocysteine-induced ER stress. Antioxid Redox Signal. 9(11): 1863-73.

Dong Z, Chapman S, Brown A, Frenette P, Hynes R, and Wagner D (1998). The combined role of P- and E-selectins in atherosclerosis. J Clin Invest 102: 145-52.

Drobnik J, Dabrowski R, Szczepanowska A, Giernat L, Lorene J. Response of aorta connective tissue matrix to injury caused by vasopressin-induced hypertension or hypercholesterolemia. J Physiol Pharmacol 2000; 51: 521-33.

Duan J, Murohara T, Ikeda T, Sasaki KI, Shintani S, Akita T, Shimada T, Imaizumi T (2000). Hyperhomocysteinemia impairs angiogenesis in response to hindlimb ischemia. Arterioscler Thromb Vasc Biol 20(12): 2579-85.

Dudman NP, Hicks C, Wang J, Wilcken DE (1991). Human arterial endothelial cell detachment in vitro: its promotion by homocysteine and cysteine. Atherosclerosis 91: 77-83.

du Vigneaud V, Ressler C, Rachele JR (1952). The biological synthesis of "labile methyl group". Science 112: 267-71.

Earnshaw WC, Martins LM, and Kaufmann SH (1999). Mammalian caspases: structure, activation, substrates, and functions during apoptosis. Annu Rev Biochem 68: 383-424.

Eikelboom JW, Lonn E, Genest J, Hankey G, and Yusuf S (1999). Homocyst(e)ine and cardiovascular disease: a critical review of the epidemiologic evidence. Ann Intern Med 131: 363-75.

Fadok VA, Voelker DR, Campbell PA, Cohen JJ, Bratton DL, Henson PM (1992). Exposure of phosphatidylserine on the surface of apoptotic lymphocytes triggers specific recognition and removal by macrophages. J Immunol 148(7): 2207-16.

Faggiotto A, Ross R. Studies of hypercholesterolemia in the nonhuman primate. II. Fatty streak conversion to fibrous plaque. Arteriosclerosis 1984; 4: 341-56.

Faggiotto A, Ross R, Harker L (1984). Studies of hypercholesterolemia in the nonhuman primate. I. Changes that lead to fatty streak formation. Arteriosclerosis 4(4): 323-40.

Feng B, Yao PM, Li Y, Devlin CM, Zhang D, Harding HP, Sweeney M, Rong JX, Kuriakose G, Fisher EA, Marks AR, Ron D, Tabas I (2003). The endoplasmic reticulum is the site of cholesterol-induced cytotoxicity in macrophages. Nat Cell Biol 5(9): 781-92.

Foody JM, Shah R, Galusha D, Masoudi FA, Havranek EP, Krumholz HM. Statins and mortality among elderly patients hospitalized with heart failure. Circulation. 2006 Feb 28;113(8):1086-92.

Frank D, Mendelsohn CL, Ciccone E, Sevensson K, Ohlsson R, Tycko B (1999). A novel pleckstrin homology-related gene family defined by *Ipl/Tssc3, TDAG51, and Tih1*: tissue-specific expression, chromosomal location, and parental imprinting. Mammalian Genome 10: 1150-59.

Frei B, Stocker R, Ames BN (1988). Antioxidant defenses and lipid peroxidation in human blood plasma. Proc Natl Acad Sci USA 85(24): 9748-52.

Frisch SM, and Francis H (1994). Disruption of epithelial cell-matrix interactions induces apoptosis. J Cell Biol 124: 619-26.

Frisch SM, and Screaton RA (2001). Anoikis mechanism. Curr Opin Cell Biol 13: 555-62.

Frohlich J, Dobiasova M, Lear S, Lee KW (2001). The role of risk factors in the development of atherosclerosis. Crit Rev Clin Lab Sci. 38(5): 401-40.

Frosst P, Blom HJ, Milos R, Goyette P, Sheppard CA, Matthews RG, Boers GJH, den Heijer M, Kluijtmans LAJ, van den Heuvel LP, Rozen R (1995). A candidate genetic risk factor for vascular disease: a common mutation in methylenetetrahydrofolate reductase. Nature Gen 10: 111-13.

Frostegård J, Ulfgren AK, Nyberg P, Hedin U, Swedenborg J, Andersson U, Hansson GK (1999). Cytokine expression in advanced human atherosclerotic plaques: dominance of pro-inflammatory (Th1) and macrophage-stimulating cytokines. Atherosclerosis 145(1): 33-43.

Fryer RH, Wilson BD, Gubler DB, Fitzgerald LA, Rodgers GM (1993). Homocysteine, a risk factor for premature vascular disease and thrombosis, induces tissue factor activity in endothelial cells. Arterioscler Thromb Vasc Bio 13(9): 1327-33.

Fujio Y, and Walsh K (1999). Akt mediates cytoprotection of endothelial cells by vascular endothelial growth factor in an anchorage-dependent manner. J Biol Chem 274: 16349-54.

Fuster V (1994). Mechanisms leading to myocardial infarction: insight from studies of vascular biology. Circulation 90: 2126-46.

Gerritsen T, Vaughn JG, Waisman HA (1962). The identification of homocysteine in the urine. Biochem Biophys Res Commun 9: 493.

Gerrity RG (1981). The role of the monocyte in atherosclerosis. I. Transition of blood – borne monocytes into foam cells in fatty lesions. Am J Pathol 103: 181-190.

Gerrity RG, Goss JA, Soby L (1985). Control of monocyte recruitment by chemotactic factor(s) in lesion-prone areas of swine aorta. Arteriosclerosis 5(1): 55-66.

Gibson JB, Carson NA, Neil DW (1964). Pathological findings in homocystinuria. J Clin Pathol 17: 427-37.

Girgis S, Suh JR, Jolivet J, Stover PJ (1997). 5-Formyltetrahydrofolate regulates homocysteine remethylation in human neuroblastoma. J Biol Chem 272(8): 4729-34.

Glagov S, Zarins C, Giddens DP, Ku DN (1988). Hemodynamics and atherosclerosis. Insights and perspectives gained from studies of human arteries. Arch Patho Lab Med 112(10): 1018-31.

Glass CK, and Witztum JL (2001). Atherosclerosis: the road ahead. Cell 104: 503-16.

Goldstein JL and Brown MS (1974). Binding and degradation of low density lipoproteins by cultured human fibroblasts. Comparison of cells from a normal subject and from a patient with homozygous familial hypercholesterolemia. J Biol Chem 249: 5153-62.

Goldstein JL, and Brown MS (1977). The low density lipoprotein pathway and its relation to atherosclerosis. Ann. Reveiw Biochem 46: 897-930.

Gomes I, Xiong W, Miki T, and Rosner MR (1999). A proline- and glutamine-rich protein promotes apoptosis in neuronal cells. J Neurochem 73: 612-22.

Gosling J, Slaymaker S, Gu L, Tseng S, Zlot CH, Young SG, Rollins BJ, and Charo IF (1999). MCP-1 deficiency reduces susceptibility to atherosclerosis in mice that overexpress human apolipoprotein B. J Clin Invest. 103: 773-78.

Gos M, Miloszewska J, Swoboda P, Trembacz H, Skierski J and Janik P (2005). Cellular quiescence induced by contact inhibition or serum withdrawal in C3H10T1/2 cells. Cell Prolif. 38: 107-16.

Green DR, Mahboubi A, Nishioka W, Oja S, Echeverri F, Shi Y, Glynn J, Yang Y, Ashwell J, Bissonnette R (1994). Promotion and inhibition of activation-induced apoptosis in T-cell hybridomas by oncogenes and related signals. Immunol Rev. 142: 321-42.

Greenwald SE (2007). Ageing of the conduit arteries. J Pathol. 211(2): 157-72.

Gross A, MoDonnell JM, Korsmeyer SJ (1999). BCL-2 family members and the mitochondria in apoptosis. Genes Dev 13(15): 1899-911.

Guevara NV, Kim HS, Antonova EI, and Chan L (1999). The absence of p53 accelerates atherosclerosis by increasing cell proliferation in vivo. Nat Med 5(3): 335-39.

Gu L, Okada Y, Clinton SK, Gerard C, Sukhova GK, Libby P, and Rollins BJ (1998). Absence of monocyte chemoattractant protein-1 reduces atherosclerosis in low density lipoprotein deficient mice. Mol Cell 2: 275-81.

Gupta S, Pablo AM, Jiang X, Wang N, Tall AR, Schindler C (1997). IFN-γ potentiates atherosclerosis in apoE knock-out mice. J Clin Invest. 99: 2752-61.

Hatai T, Matsuzawa A, Inoshita S, Mochida Y, Kuroda T, Sakamaki K, Kuida K, Yonehara S, Ichijo H, Takeda K (2000). Execution of apoptosis signal-regulating kinase 1 (ASK1)-induced apoptosis by the mitochondria-dependent caspase activation. J Biol Chem. 275(34): 26576-81.

Hattori N, Degen JL, Sisson TH, Liu H, Moore BB, Pandrangi RG, Simon RH, Drew AF (2000). Bleomycin-induced pulmonary fibrosis in fibrinogen-null mice. J Clin Invest. 106(11): 1341-50.

Hajjar KA (1993). Homocysteine-induced modulation of tissue plasminogen activator binding to its endothelial cell receptor. J Clin Invest 91: 2873-79.

Hajjar KA, Mauri L, Jacovina AT, Zhong FM, Mirza UA, Padovan JC, Chait BT (1998). Tissue plasminogen activator binding to the annexin II tail domain: direct modulation by homocysteine. J Biol Chem 273: 9987-93.

Han K, Levine MS, and Manley JL (1989). Synergistic activation and repression of transcription by Drosophila homeobox proteins. Cell 56: 573-83.

Han KH, Han KO, Green SR, and Quehenberger O (1999). Expression of the monocyte chemoattractant protein-1 receptor CCR2 is increased in hypercholesterolemia: differential effects of plasma lipoproteins on monocyte function. J Lipid Res 40: 1053-63.

Hansson GK, Robertson AK, Söderberg-Nauclér C (2006). Inflammation and atherosclerosis. Annu Rev Pathol. 1: 297-329.

Hao H, Gabbiani G, Camenzind E, Bacchetta M, Virmani R, Bochaton-Piallat ML (2006). Phenotypic modulation of intima and media smooth muscle cells in fatal cases of coronary artery lesion. Arterioscler Thromb Vasc Biol. 26: 326–332.

Harding HP, Zhang Y, Bertolotti A, Zeng H, Ron D (2000). Perk is essential for translational regulation and cell survival during the unfolded protein response. Mol Cell 5(5): 897-904.

Harding HP, Zhang Y, Zeng H, Novoa I, Lu PD, Calfon M, Sadri N, Yun C, Popko B, Paules R, Stojdl DF, Bell JC, Hettmann T, Leiden JM, Ron D (2003). An integrated stress response regulates amino acid metabolism and resistance to oxidative stress. Mol Cell. 11(3): 619-33.

Harding HP, Zeng H, Zhang Y, Jungries R, Chung P, Plesken H, Sabatini DD, and Ron D (2001). Diabetes mellitus and exocrine pancreatic dysfunction in *perk-/-* mice reveals a role for translational control in secretory cell survival. Mol Cell 7: 1153-63.

Harding HP, Zhang Y, Ron D (1999). Protein translation and folding are coupled by an endoplasmic-reticulum-resident kinase. Nature 397(6716): 271-4.

Harker LA, Slichter SJ, Scott CR, Ross R (1974). Homocysteinemia. Vascular injury and arterial thrombosis. N Engl J Med 291: 537-43.

Haudek SB, Xia Y, Huebener P, Lee JM, Carlson S, Crawford JR, Pilling D, Gomer RH, Trial J, Frangogiannis NG, Entman ML (2006). Bone marrow-derived fibroblast precursors mediate ischemic cardiomyopathy in mice. Proc Natl Acad Sci USA 103: 18284–18289.

Haurani MJ, Pagano PJ (2007). Adventitial fibroblast reactive oxygen species as autacrine and paracrine mediators of remodeling: bellwether for vascular disease? Cardiovasc Res. 75(4): 679-89.

Hayashida N, Inouye S, Fujimoto M, Tanaka Y, Izu H, Takaki E, Ichikawa H, Rho J and Nakai A (2006). A novel HSF1-mediated death pathway that is suppressed by heat shock proteins. The EMBO J. 25(20): 4773-83.

Hegyi L, Skepper JN, Cary NR, and Mitchison MJ (1996). Foam cell apoptosis and the development of the lipid core of human atherosclerosis. J Pathol 180: 423-42.

Helft G, Worthley SG, Fuster V, Zaman AG, Schechter C, Osende JI, Rodriguez OJ, Fayad ZA, Fallon JT, Badimon JJ (2001). Atherosclerotic aortic component quantification by noninvasive magnetic resonance imaging: an in vivo study in rabbits. J Am Coll Cardiol. 37(4): 1149-54.

Hengartner MO (2000). The biochemistry of apoptosis. Nature 407: 769-76.

Hinz B, Phan SH, Thannickal VJ, Galli A, Bochaton-Piallat ML, Gabbiani G (2007). The myofibroblast: one function, multiple origins. Am J Pathol. 170(6): 1807-16.

Hinz T, Flindt S, Marx A, Janssen O, and Kabelitz D (2001). Inhibition of protein synthesis by the T cell receptor-inducible human TDAG51 gene product. Cellular Signalling 13: 345-52.

Hitomi J, Katayama T, Eguchi Y, Kudo T, Taniguchi M, Koyama Y, Manabe T, Yamagishi S, Bando Y, Imaizumi K, Tsujimoto Y, Tohyama M (2004). Involvement of caspase-4 in endoplasmic reticulum stress-induced apoptosis and Abeta-induced cell death. J Cell Biol. 165(3): 347-56.

Hladovec J, Sommerova Z, and Pisarikova A (1997). Homocysteinemia and endothelial damage after methionine load. Thromb Res 88: 361-64.

Hofmann MA, Lalla E, Lu Y, Gleason MR, Wolf BM, Tanji N, Ferran LJ, Kohl B, Rao V, Kisiel W, Stern DM, and Schimidt AM (2001). Hyperhomocysteinemia enhances vascular inflammation and accelerates atherosclerosis in a murine model. J Clin Invest 107: 675-83.

Horton JD, Shimano H, Hamilton RL, Brown MS, and Goldstein JL (1999). Disruption of LDL receptor gene in transgenic SREBP-1a mice unmasks hyperlipidemia resulting from production of lipid-rich VLDL. J Clin Invest 103(7): 1067-76.

Hossain GS, Van Thienen JV, Werstuck GH, Zhou J, Sood SK, Dickhout JG, De Koning AB, Tang D, Wu D, Falk E, Poddar R, Jacobsen DW, Zhang K, Kaufman RJ, Austin RC (2003). TDAG51 is induced by homocysteine, promotes detachment-mediated programmed cell death and contributes to the development of atherosclerosis in hyperhomocysteinemia. J Biol Chem 278(32): 30317-27.

Huang RFS, Huang SM, Lin BS, Wei JS, and Liu TZ (2001). Homocysteine thiolactone induces apoptotic DNA damage mediated by increased intracellular hydrogen peroxide and caspase 3 activation in HL-60 cells. Life Sci 68: 2799-811.

Ignatowski AC. Influence of animal food on the organism of rabbits. S Peterb Izviest Imp Voyenmo-Med. Akad 1908; 16: 154-73.

Iiyama K, Hajra L, Iiyama M, Li H, DiChiara M, Medoff BD, Cybulsky MI (1999). Patterns of vascular cell adhesion molecule-1 and intercellular adhesion molecule-1 expression in rabbit and mouse atherosclerotic lesions and at sites predisposed to lesion formation. Circ Res. 85: 199-207.

Ishibashi S, Brown MS, Goldstein JL, Gerard RD, Hammer RE, Herz J (1993). Hypercholesterolemia in low density lipoprotein receptor knockout mice and its reversal by adenovirus-mediated gene delivery. J Clin Invest 92: 883-93.

Ishibashi S, Herz J, Maeda N, Goldstein JL, Brown MS (1994). The two-receptor model of lipoprotein clearance: tests of the hypothesis in "knockout" mice lacking the low density lipoprotein receptor, apolipoprotein E, or both proteins. Proc Natl Acad Sci U S A. 91(10): 4431-5.

Isner JM, Kearney M, Bortman S, and Passeri J (1995). Apoptosis in human atherosclerosis and restenosis. Circulation 91: 2703-11.

Izu H, Inouye S, Fujimoto M, Shiraishi K, Naito K, Nakai A (2004). Heat shock transcription factor 1 is involved in quality-control mechanisms in male germ cells. Biol Reprod. 70(1):18-24.

Jacobsen DW (2001). Cellular mechanism of homocysteine pathogenesis in atherosclerosis. In Homocysteine in Heath and Disease. R Carmel and DW Jacobsen, editors. Cambridge University Press, Cambridge, UK, pp 425-40.

Jacobsen DW (2000). Hyperhomocysteinemia and oxidative stress. Time for a reality check? Arterioscler Thromb Vasc Biol 20: 1182-84.

Jaffe EA, Nachman RL, Becker CG, Minick CR (1973). Culture of human endothelial cells derived from umbilical veins. J Clin Invest 53: 2745-56.

Jahanyar J, Joyce DL, Southard RE, Loebe M, Noon GP, Koerner MM, Torre-Amione G, Youker KA (2007). Decorin-mediated transforming growth factor-beta inhibition ameliorates adverse cardiac remodeling. J Heart Lung Transplant. 26(1): 34-40.

Jakubowski H (1997). Metabolism of homocysteine thiolactone in human cell cultures: possible mechanism for pathological consequences of elevated homocysteine levels. J Biol Chem 272: 1935-42.

Jia L, and Furchgott RF (1993). Inhibition by sulphydryl compounds of vascular relaxation induced by nitric oxide and endothelium derived relaxing factor. J Pharmacol Exp Ther 267: 371-78.

Jiang C, Ting AT, Seed B (1998). PPAR-gamma agonists inhibit production of monocyte inflammatory cytokines. Nature. 391(6662): 82-6.

Jinlian L, Yingbin Z, Chunbo W (2007). p38 MAPK in regulating cellular responses to ultraviolet radiation. J Biomed Sci. 14(3): 303-12.

Johnson JL, Baker AH, Oka K, Chan L, Newby AC, Jackson CL, George SJ (2006). Suppression of atherosclerotic plaque progression and instability by tissue inhibitor of metalloproteinase-2: involvement of macrophage migration and apoptosis. Circulation 113(20): 2435-44.

Joo JH, Liao G, Collins JB, Grissom SF, Jetten AM (2007). Farnesol-induced apoptosis in human lung carcinoma cells is coupled to the endoplasmic reticulum stress response. Cancer Res. 67(16): 7929-36.

Ju ST, Panka DJ, Cui H, Ettinger R, el-Khatib M, Sherr DH, Stanger BZ, Marshak-Rothstein A (1995). Fas(CD95)/FasL interactions required for programmed cell death after T-cell activation. Nature 373(6513): 444-8.

Jurgensmeier JM, Xie Z, Deveraux Q, Ellerby L, Bredesen D, and Reed JC (1998). Bax directly induces release of cytochrome c from isolated mitochondria. Proc Natl Acad Sci USA 95: 4997-5002.

Kalinina N, Agrotis A, Tararak E, Antropova Y, Kanellakis P, Ilyinskaya O, Quinn MT, Smirnov V, Bobik A. Cytochrome b558-dependent NAD(P)H oxidase-phox units in smooth muscle and macrophages of atherosclerotic lesions. Arter Thromb Vasc Biol 2002; 22: 2037-43.

Kammoun HL, Chabanon H, Hainault I, Luquet S, Magnan C, Koike T, Ferré P, Foufelle F (2009). GRP78 expression inhibits insulin and ER stress-induced SREBP-1c activation and reduces hepatic steatosis in mice. J Clin Invest. 119(5): 1201-15.

Kane JP and Havel RJ (1989). Disorders of the biogenesis and secretion of lipoproteins containing the B apolipoproteins. In the Metabolic basis of inherited disease. CR Scriver, AR Beauder, WS Sly, D Valle, JB Stanbury, JB Wyngnarden and DS Frederickson, editor. McGraw-Hill, New York. 1139-64.

Kang SS, Wang PWK, and Noursis M (1987). Homocyst(e)inemia due to folate deficiency. Metabolism 36: 458-62.

Kaufman RJ (2002). Orchestrating the unfolded protein response in health and disease. J Clin Invest. 110(10): 1389-98.

Kim R, Emi M, Tanabe K, Murakami S (2006). Role of the unfolded protein response in cell death. Apoptosis 11(1): 5-13.

Kisucka J, Chauhan AK, Patten IS, Yesilaltay A, Neumann C, Van Etten RA, Krieger M, Wagner DD (2008). Peroxiredoxin1 prevents excessive endothelial activation and early atherosclerosis. Circ Res. 103(6): 598-605.

Klucken J, Büchler C, Orsó E, Kaminski WE, Porsch-Ozcürümez M, Liebisch G, Kapinsky M, Diederich W, Drobnik W, Dean M, Allikmets R, Schmitz G (2000). $ABCG_1$ (ABC8), the human homolog of the Drosophila white gene, is a regulator of macrophage cholesterol and phospholipids transport. Proc Natl Acad Sci USA 97: 817-22.

Kockx MM, Demeyer GRY, Muhring J, Bult H, Bultinck J, and Herman AG (1996). Distribution of cell replication and apoptosis in atherosclerotic plaques of cholesterol-fed rabbits. Atherosclerosis 120: 115-24.

Kokame K, Agarwala KL, Kato H, and Miyata T (2000). Herp, a new ubiquitin-like membrane protein induced by endoplasmic reticulum stress. J Biol Chem 275: 32846-53.

Kokame K, Kato H, and Miyata T (1996). Homocysteine-respondent genes in vascular endothelial cells identified by differential display analysis: GRP78 and novel genes. J Biol Chem 271: 29659-65.

Kolodgie FD, Narula J, Burke AP, Haider N, Farb A, Hui-Liang Y, Smialek J, Virmani R (2000). Localization of apoptotic macrophages at the site of plaque rupture in sudden coronary death. Am J Pathol 157: 1259-68.

Kothakota S, Azuma T, Reinhard C, Klippel A, Tang J, Chu K, McGarry TJ, Kirschner MW, Koths K, Kwiatkowski DJ, and Williams LT (1997). Caspase-3-generated fragment of gelsolin: effector of morphological change in apoptosis. Science 278: 294-98.

Kresse H, Schönherr E (2001). Proteoglycans of the extracellular matrix and growth control. J Cell Physiol. 189(3): 266-74.

Kuhlencordt PJ, Gyurko R, Han F, Scherrer-Crosbie M, Aretz TH, Hajjar R, Picard MH, Huang PL. Accelerated atherosclerosis, aortic aneurysm formation, and ischemic heart disease in apolipoprotein E/endothelial nitric oxide synthase double-knockout mice. Circulation. 2001 Jul 24;104(4): 448-54.

Kuratomi G, Komuro A, Goto K, Shinozaki M, Miyazawa K, Miyazono K, Imamura T (2005). NEDD4-2 (neural precursor cell expressed, developmentally down-regulated 4-2) negatively regulates TGF-beta (transforming growth factor-beta) signalling by inducing ubiquitin-mediated degradation of Smad2 and TGF-beta type I receptor. Biochem J. 386(Pt 3): 461-70.

Kuske MDA, and Johnson JP (2000). Assignment of the human PHLDA1 gene to chromosome 12q15 by radiation hybrid mapping. Cytogenet Cell Genet 89: 1.

Laakso M, Lehto S (1998). Epidemiology of risk factors for cardiovascular disease in diabetes and impaired glucose tolerance. Atherosclerosis 137 Suppl:S65-73.

Ladiges WC, Knoblaugh SE, Morton JF, Korth MJ, Sopher BL, Baskin CR, MacAuley A, Goodman AG, LeBoeuf RC, Katze MG (2005). Pancreatic beta-cell failure and diabetes in mice with a deletion mutation of the endoplasmic reticulum molecular chaperone gene P58IPK. Diabetes 54(4): 1074-81.

Laemmli UK (1970). Cleavage of structural proteins during the assembly of the head of bacteriophage T4. Nature 227: 680-85.

Lambie DG, Johnson RH (1985). Drugs and folate metabolism. Drugs 30: 145-55.

Lang D, Kredan MB, Moat SJ, Hussain SA, Powell CA, Bellamy MF, Powers HJ, and Lewis MJ (2000). Homocysteine-induced inhibition of endothelium-dependent relaxation in rabbit aorta: role for superoxide anions. Arterioscler Thromb Vasc Biol 20(2): 422-27.

Lavillette D, Maurice M, Roche C, Russell SJ, Sitbon M, and Cosset FL (1998). A proline-rich motif downstream of the receptor binding domain modulates conformation and fusogenicity of murine retroviral envelopes. J Virol 72: 9955-65.

Lazebnik YA, Kaufmann SH, Desnoyers S, Poirier GG, and Earnshaw WC (1994). Cleavage of poly(ADP-ribose) polymerase by a proteinase with properties like ICE. Nature 371: 346-47.

Lee MP, and Feinberg AP (1998). Genomics Imprinting of a Human Apoptosis Gene Homologue, *TSSC3*. Cancer Res 58: 1052-56.

Lee AH, Iwakoshi NN, Glimcher LH (2003). XBP-1 regulates a subset of endoplasmic reticulum resident chaperone genes in the unfolded protein response. Mol Cell Biol. 23(21): 7448-59.

Lee MP, Reeves C, Schmitt A, Su K, Connors TD, Hu R-J, Brandenburg S, Lee MJ, Miller G, and Feinberg AP (1998). Somatic mutation of *TSSC5*, a novel imprinted gene from human chromosome 11p15.5. Cancer Res 58: 4155-59.

Lee RT, and Libby P (1997). The unstable atheroma. Arterioscler Thromb Vasc Biol 17: 1859-67.

Lehrke M, and Lazar MA (2005). The many faces of PPARgamma. Cell 123(6): 993-99.

Lentz SR (2005). Mechanisms of homocysteine-induced atherothrombosis. J Thromb Haemost. 3(8): 1646-54.

Lentz SR, Piegors DJ, Malinow RM, and Heistad DD (2001). Supplementation of atherogenic diet with B vitamins does not prevent atherosclerosis or vascular dysfunction in monkeys. Circulation 103(7): 1006-11.

Lentz SR, and Sadler JE (1991). Inhibition of thrombomodulin surface expression and protein C activation by arterial and venous endothelial cells. Blood 75: 895-901.

Lentz SR, Sobey CG, Piegors DJ, Bhopatkar MY, Faraci FM, Malinow MR, Heistad DD (1996). Vascular dysfunction in monkeys with diet-induced hyperhomocysteinemia. J Clin Invest 98: 24-29.

Liang SH, Clarke MF (1999). The nuclear import of p53 is determined by the presence of a basic domain and its relative position to the nuclear localization signal. Oncogene 18(12): 2163-6.

Libby P. Current concept of the pathogenesis of the acute coronary syndromes. Circulation. 2001; 104: 365-72.

Libby P. Inflammation in atherosclerosis. Nature. 2002; 420:868-74.

Libby P, Ridker PM and Maseri A. Inflammation and atherosclerosis. Circulation. 2002; 105: 1135-43.

Li AC, Binder CJ, Gutierrez A, Brown KK, Plotkin CR, Pattison JW, Valledor AF, Davis RA, Willson TM, Witztum JL, Palinski W, Glass CK (2004). Differential inhibition of macrophage foam-cell formation and atherosclerosis in mice by PPARalpha, beta/delta, and gamma. J Clin Invest. 114(11): 1564-76.

Li AC, Glass CK (2004). PPAR- and LXR-dependent pathways controlling lipid metabolism and the development of atherosclerosis. J Lipid Res. 45(12): 2161-73.

Li H, Zhu H, Xu CJ, and Yuan J (1998). Cleavage of BID by caspase 8 mediates the mitochondrial damage in the Fas pathway of apoptosis. Cell 94: 491-501.

Li P, Allen H, Banerjee S, Franklin S, Herzog L, Johnston C, McDowell J, Paskind M, Rodman L, Salfeld J, Towne E, Tracey D, Wardwell S, Wei FY, Wong W, Kamen R, and Seshadri T (1995). Mice deficient in IL-1beta-converting enzyme are defective in production of mature IL-1beta and resistant to endotoxic shock. Cell 80: 401-11.

Li P, Nijhawan D, Budihardjo I, Srinivasula SM, Ahmad M, Alnemri ES, and Wang X (1997). Cytochrome c and dATP-dependent formation of apaf-1/caspase-9 complex initiates an apoptotic protease cascade. Cell 91: 479-89.

Linton MF, Farese RV Jr, Chiesa G, Grass DS, Chin P, Hammer RE, Hobbs HH, Young SG (1993). Transgenic mice expressing high plasma concentrations of human apolipoprotein B100 and lipoprotein$_a$. J Clin Invest 92: 3029-37.

Linton MF, Fazio S (2003). Macrophages, inflammation, and atherosclerosis. Int J Obes Relat Metab Disord. Suppl 3:S35-40.

Liu J, Thewke DP, Su YR, Linton MF, Fazio S, Sinensky MS (2005). Reduced macrophage apoptosis is associated with accelerated atherosclerosis in low-density lipoprotein receptor-null mice. Arterioscler Thromb Vasc Biol. 25(1): 174-9.

Liu X, Kim CN, Yang J, Jemmerson R, and Wang X (1996). Induction of apoptotic program in cell-free extracts: requirement for dATP and cytochrome c. Cell 86: 147-57.

Liu ZG, Smith SW, McLaughlin KA, Schwartz LM, Osborne BA (1994). Apoptotic signals delivered through the T-cell receptor of a T-cell hybrid require the immediate-early gene nur77. Nature 367(6460): 281-4.

Lonn E, Yusuf S, Arnold MJ, Sheridan P, Pogue J, Micks M, McQueen MJ, Probstfield J, Fodor G, Held C, Genest J Jr; Heart Outcomes Prevention Evaluation (HOPE) 2 Investigators (2006). Homocysteine lowering with folic acid and B vitamins in vascular disease. N Engl J Med. 354(15): 1567-77.

Loria P, Lonardo A, Targher G (2008). Is liver fat detrimental to vessels?: intersections in the pathogenesis of NAFLD and atherosclerosis. Clin Sci (Lond). 115(1): 1-12.

Loscalzo J (1996). The oxidative stress of hyperhomocyst(e)inemia. J Clin Invest 98: 5-7.

Luo X, Budihardjo I, Zou H, Slaughter C, and Wang X (1998). Bid, a Bcl-2 interacting protein, mediates cytochrome c release from mitochondria in response to activation of cell surface death receptors. Cell 94: 481-90.

Lusis AJ (2000). Atherosclerosis. Nature 407: 233-41.

Lutgens E, Gorelik L, Daemen MJ, de Muinck ED, Grewal IS, Koteliansky VE, Flavell RA (1999). Requirement for CD154 in the progression of atherosclerosis. Nat Med. 5: 1313-16.

Ma K, Vattem KM, Wek RC (2002). Dimerization and release of molecular chaperone inhibition facilitate activation of eukaryotic initiation factor-2 kinase in response to endoplasmic reticulum stress. J Biol Chem. 277(21): 18728-35.

Mach F, Schönbeck U, Sukhova GK, Atkinson E, Libby P (1998). Reduction of atherosclerosis in mice by inhibition of CD40 signalling. Nature. 394: 200-03.

Maffucci T, Falasca M (2001). Specificity in pleckstrin homology (PH) domain membrane targeting: a role for a phosphoinositide-protein co-operative mechanism. FEBS Letters 506: 173-79.

Mahley RW (1988). Apolipoprotein E: cholesterol transport protein with expanding role in cell biology. Science 240: 622-30.

Majors A, Ehrhart LA, Pezacka EH (1997). Homocysteine as a risk factor for vascular disease. Enhanced collagen production and accumulation by smooth muscle cells. Arterioscler Thromb Vasc Biol 17: 2074-81.

Malinow MR, Bostom AG, and Krauss RM (1999). Homocyst(e)ine, diet, and cardiovascular diseases- a statement for healthcare professionals from the Nutrition Committee, American Heart Association. Circulation 99: 178-82.

Malinow MR, Nieto FJ, Szklo M, Chambless LE, Bond G (1993). Carotid artery intimal-medial wall thickening and plasma homocyst(e)ine in asymptomatic adults. The Atherosclerosis Risk in Communities Study. Circulation 87(4): 1107-13.

Martin SJ, Finucane DM, Amarante-Mendes GP, O'Brien GA, Green DR (1997). Phosphatidylserine externalization during CD95-induced apoptosis of cells and cytoplasts requires ICE/CED-3 protease activity. J Biol Chem 271(46): 28753-6.

Masucci-Magoulas L, Goldberg IJ, Bisgaier CL, Serajuddin H, Francone OL, Breslow JL, Tall AR (1997). A mouse model with features of familial combined hyperlipidemia. Science 275: 391-94.

Masuda J, Ross R (1990). Atherogenesis during low level hypercholesterolemia in the nonhuman primate. II. Fatty streak conversion to fibrous plaque. Arteriosclerosis 10(2): 164-77.

Masuda J, Ross R (1990). Atherogenesis during low level hypercholesterolemia in the nonhuman primate. I. Fatty streak formation. Arteriosclerosis 10(2): 178-87.

Maytin EV, Ubeda M, Lin JC, and Habener JF (2001). Stress-inducible transcription factor CHOP/gadd153 induces apoptosis in mammalian cells via p38 kinase-dependent and -independent mechanisms. Exp Cell Res 267: 193-204.

McAnulty RJ (2007). Fibroblasts and myofibroblasts: their source, function and role in disease. Int J Biochem Cell Biol 39(4): 666-71.

McCullough KD, Martindale JL, Klotz LO, Aw TY, and Holbrook NJ (2001). Gadd153 sensitizes cells to endoplasmic reticulum stress by down-regulating Bcl2 and perturbing the cellular redox state. Mol Cell Biol 21: 1249-59.

McCully KS (1969). Vascular pathology of homocysteinemia: implication for the pathogenesis of arteriosclerosis. Am J Pathol 56: 111-28.

McCully KS (1996). Homocysteine and vascular disease. Nat Med 2: 386-89.

McNabb DS, and Courtney RJ (1992). Analysis of the UL36 open reading frame encoding the large tegument protein (ICP1/2) of herpes simplex virus type 1. J Virol 66: 7581-84.

Mehta JL, Bursac Z, Hauer-Jensen M, Fort C, Fink LM (2006). Comparison of mortality rates in statin users versus nonstatin users in a United States veteran population. Am J Cardiol. 98(7): 923-8.

Meredith JE, Fazeli JB, and Schwartz MA (1993). The extracellular matrix as a cell survival factor. Mol Biol Cell 4: 953-61.

Michel JB, Thaunat O, Houard X, Meilhac O, Caligiuri G, Nicoletti A (2007). Topological determinants and consequences of adventitial responses to arterial wall injury. Arterioscler Thromb Vasc Biol. 27(6): 1259-68.

Miura M, Zhu H, Rotello R, Hartwieg EA, and Yuan J (1993). Induction of apoptosis in fibroblasts by IL-1β-converting enzyme, a mammalian homolog of the *C. elegans* cell death gene *ced-3*. Cell 75: 653-60.

Mori L, Bellini A, Stacey MA, Schmidt M, Mattoli S (2005). Fibrocytes contribute to the myofibroblast population in wounded skin and originate from the bone marrow. Exp Cell Res 304: 81–90.

Morimoto RI (1998). Regulation of the heat shock transcriptional response: cross talk between a family of heat shock factors, molecular chaperones, and negative regulators. Genes Dev. 12(24): 3788-96.

Mosharov E, Cranford MR, Banerjee R (2000). The quantitatively important relationship between homocysteine metabolism and glutathione synthesis by the transsulfuration pathway and its regulation by redox changes. Biochemistry 39: 13005-11.

Moulian N, Truffault F, Gaudry-Talamain YM, Serraf A, and Berrih-Aknin S (2001). *In vivo* and *in vitro* apoptosis of human thymocytes are associated with nitrotyrosine formation. Blood 97: 3521-30.

Mrhova O, Hladovec J, Urbanova D (1988). Metabolic changes in the arterial wall and endothelial injury in experimental methioninemia. Cor Vasa 30: 73-79.

Mudd SH, Finkelstein JD, Irreverre F, Laster L (1964). Homocystinuria: an enzymatic defect. Science 143: 1443-45.

Mudd SH, Finkelstein JD, Refsum H, Ueland PM, Malinow MR, Lentz SR, Jacobsen DW, Brattström L, Wilcken B, Wilcken DEL, Blom HJ, Stabler SP, Allen RH, Selhub J, Rosenberg IH (2000). Homocysteine and its disulfide derivatives: a suggestion consensus terminology. Arterioscler Thromb Vasc Biol 20: 1704-06.

Mudd SH, Levy HL, Skovby F (1995). Disorders of transsulfuration. In: The Metabolic and Molecular Bases of Inherited Disease. Scriver CR, Beaudet AL, Sly WS, Valle D, Stanbury JB, Wyngarden JB, Fredrickson DS (eds). New York: McGraw-Hill, pp 1279-327.

Mudd SH, Skovby F, Levy HL, Pettigrew KD, Wilcken B, Pyeritz RE, Andria G, Boers GHJ, Bromberg IL, Cerone R, Flower B, Grobe H, Schmidt H, Schweitzer L (1985). The natural history of homocystinuria due to cystathionine β-synthase deficiency. Am J Hum Genet 37: 1-31.

Munro JM, and Cotran RS (1988). The pathogenesis of atherosclerosis: atherogenesis and inflammation. Lab Invest 58(3): 249-61.

Munro JM, van der Walt JD, Munro CS, Chalmers JA, Cox EL (1987). An immunohistochemical analysis of human aortic fatty streaks. Human Pathol. 18: 375-80.

Muzio M, Stockwell BR, Stennicke HR, Salvesen GS, and Dixit VM (1998). An induced proximity model for caspase-8 activation. J Biol Chem 273: 2926-30.

Nagai MA, Fregnani JH, Netto MM, Brentani MM, Soares FA (2007). Down-regulation of PHLDA1 gene expression is associated with breast cancer progression. Breast Cancer Res Treat. 106(1): 49-56.

Nagata S and Goldstein P (1995). The Fas death factor. Science 267: 1449-56.

Nakagawa T, Zhu H, Morishima N, Li E, Xu J, Yankner BA, and Yuan J (2000). Caspase-12 mediates endoplasmic-reticulum-specific apoptosis and cytotoxicity by amyloid-β. Nature 403: 98-103.

Nakashima Y, Plump AS, Raines EW, Breslow IL, Ross R. ApoE-deficient mice develop lesions of all phages of atherosclerosis throughout the arterial tree. Arterioscler Thromb 1994; 14: 133-40.

Naughton ER, Yap S, Mayne PD (1998). Newborn screening for homocystinuria: Irish and world experience. Eur J Pediatr 157(Suppl 2): S84-S87.

Navab M, Berliner JA, Watson AD, Hama SY, Territo MC, Lusis AJ, Shih DM, Van Lenten BJ, Frank JS, Demer LL, Edwards PA, Fogelman AM (1996). The Yin and Yang of oxidation in the development of the fatty streak. A review based on the 1994 George Lyman Duff Memorial Lecture. Arterioscler Thromb Vasc Biol 16(7): 831-42.

Neef R, Kuske MA, Prols E, Johnson JP (2002). Identification of the human PHLDA1/TDAG51 gene: down-regulation in metastatic melanoma contributes to apoptosis resistance and growth deregulation. Cancer Res 62(20):5920-9.

Nilsson J (1993). Cytokines and smooth muscle cells in atherosclerosis. Cardiovascular Res. 27: 1184-90.

Nishio E, and Watanabe Y (1997). Homocysteine as a modulator of platelet-derived growth factor action in vascular smooth muscle cells: a possible role for hydrogen peroxide. Br J Pharmacol 122: 269-74.

Nishitoh H, Matsuzawa A, Tobiume K, Saegusa K, Takeda K, Inoue K, Hori S, Kakizuka A, Ichijo H (2002). ASK1 is essential for endoplasmic reticulum stress-induced neuronal cell death triggered by expanded polyglutamine repeats. Genes Dev. 16(11): 1345-55.

Nonaka H, Tsujino T, Watari Y, Emoto N, and Yokoyama M (2001). Taurine prevents the decrease in expression and secretion of extracellular superoxide dismutase induced by homocysteine. Amelioration of homocysteine-induced endoplasmic reticulum stress by taurine. Circulation 104: 1165-70.

Ohashi R, Mu H, Yao Q and Chen C (2004). Cellular and molecular mechanisms of atherosclerosis with mouse models. Trends Cardiovasc Med 14: 187-190.

Outinen PA, Sood SK, Liaw PCY, Sarge KD, Maeda N, Hirsh J, Ribau J, Podor TJ, Weitz JI and Austin RC (1998). Characterization of the stress-inducing effects of homocysteine. Biochem J 332: 213-21.

Outinen PA, Sood SK, Pfeifer SI, Pamidi S, Podor TJ, Weitz JI and Austin RC (1999). Homocysteine-induced endoplasmic reticulum stress and growth arrest leads to specific changes in gene expression in human vascular endothelial cells. Blood 94(3): 959-67.

Ozcan U, Yilmaz E, Ozcan L, Furuhashi M, Vaillancourt E, Smith RO, Görgün CZ, Hotamisligil GS (2006). Chemical chaperones reduce ER stress and restore glucose homeostasis in a mouse model of type 2 diabetes. Science 313(5790): 1137-40.

Pahl HL, Sester M, Burgert HG, and Baeuerle PA (1996). Activation of transcription factor NF-kappaB by the adenovirus E3/19K protein requires its ER retention. J Cell Biol 132(4): 511-22.

Paigen B, Morrow A, Brandon C, Mitchell D, Holmes P (1985). Variation in susceptibility to atherosclerosis among inbred strains of mice. Atherosclerosis 57: 65-73.

Paigen B, Plump AS, Rubin EM (1994). The mouse as a model for human cardiovascular disease and hyperlipidemia. Curr Opin Lipidol 5: 258-64.

Park JM, Greten FR, Li ZW, Karin M (2002). Macrophage apoptosis by anthrax lethal factor through p38 MAP kinase inhibition. Science 297(5589): 2048-51.

Park CG, Lee SY, Kandala G, Lee SY, and Choi Y (1996). A novel gene product that couples TCR signalling to Fas(CD95) expression in activation-induced cell death. Immunity 4: 583-91.

Paz-Miguel JE, Flores R, Sanchez-Velasco P, Ocejo-Vinyals G, de Diego JE, de Rego JL, and Leyva-Cobian F (1999). Reactive oxygen intermediates during programmed cell death and induced in the thymus of the Ts(17^{16})65Dn mouse, a murine model for human Down's syndrome. J Immunol 163: 5399-410.

Pei G, Powers DD, Lentz BR (1993). Specific contribution of different phospholipid surfaces to the activation of prothrombin by the fully assembled prothrombinase. J Biol Chem 268: 3226-33.

Parsell DA, Lindquist S (1993). The function of heat-shock proteins in stress tolerance: degradation and reactivation of damaged proteins. Annu Rev Genet. 27: 437-96.

Plump AS, Smith JD, Hayek T, Aalto-Setala K, Walsh A, Verstuyft JG, Rubin EM, Breslow JL (1992). Severe hypercholesterolemia and atherosclerosis in apolipoprotein E-deficient mice created by homologous recombination in ES cells. Cell 71: 343-53.

Poddar R, Sivasubramanian N, Dibello PM, Robinson K, and Jacobsen D (2001). Homocysteine induces expression and secretion of monocyte chemoattractant protein-1 and interleukin-8 in human aortic endothelial cells: implications for vascular disease. Circulation 103(22): 2717-23.

Purcell-Huynh DA, Farese RV Jr, Johnson DF, Flynn LM, Pierotti V, Newland DL, Linton MF, Sanan DA, Young SG (1995). Transgenic mice expressing high levels of

human apolipoprotein B develop severe atherosclerotic lesions in response to a high-fat diet. J Clin Invest 95: 2246-57.

Puthalakath H, Villunger A, O'Reilly LA, Beaumont JG, Coultas L, Cheney RE, Huang DCS, and Strasser A (2001). Bfm: a proapoptotic BH3-only protein regulated by interaction with the myosin v actin motor complex, activated by anoikis. Science 293: 1829-32.

Qian N, Frank D, O'Keefe D, Dao D, Zhao L, Yuan L, Qing W, Keating M, Walsh C, and Tycko B (1997). The *IPL* gene on chromosome 11p15.5 is imprinted in humans and mice and is similar to *TDAG51*, implicated in Fas expression and apoptosis. Hum Mol Genet 6(12): 2021-29.

Rajavashisth TB, Andalibi A, Territo MC, Berliner JA, Navab M, Fogelman AM, Lusis AJ (1990). Induction of endothelial cell expression of granulocyte and macrophage colony-stimulating factors by modified low-density lipoproteins. Nature 344: 254-57.

Rao RV, Castro-Obregon S, Frankowski H, Schuler M, Stoka V, del Rio G, Bredesen DE, Ellerby HM (2002). Coupling endoplasmic reticulum stress to the cell death program. An Apaf-1-independent intrinsic pathway. J Biol Chem. 277(24): 21836-42.

Rao RV, Hermel E, Castro-Obregon S, del Rio G, Ellerby LM, Ellerby HM, and Bredesen DE (2001). Coupling endoplasmic reticulum stress to the cell death program. Mechanism of caspase activation. J Biol Chem 276: 33869-74.

Rao RV, Peel A, Logvinova A, del Rio G, Hermel E, Yokota T, Goldsmith PC, Ellerby LM, Ellerby HM, Bredesen DE (2002). Coupling endoplasmic reticulum stress to the cell death program: role of the ER chaperone GRP78. FEBS Lett. 514(2-3): 122-8.

Ray JG, Kearon C, Yi Q, Sheridan P, Lonn E; Heart Outcomes Prevention Evaluation 2 (HOPE-2) Investigators (2007). Homocysteine-lowering therapy and risk for venous thromboembolism: a randomized trial. Ann Intern Med. 146(11): 761-7.

Reddick RL, Zhang SH, Maeda N. Atherosclerosis in mice lacking apoE: evaluation of lesional development and progression. Arterioscler Thromb 1994; 14: 141-47.

Reddy PH, Stockburger E, Gillevet P, and Tagle DA (1997). Mapping and characterization of novel $(CAG)_n$ repeat cDNAs from adult human brain derived by the oligo capture method. Genomics 46: 174-82.

Rees MW, Rodgers GM (1993). Homocysteinemia: association of a metabolic disorder with vascular disease and thrombosis. Thromb Res 71: 337-59.

Refsum H, Ueland PM, Nygård O, and Vollset SE (1998). Homocysteine and cardiovascular disease. Annu Rev Med 49: 31-62.

Reiter CD, Teng RJ, Beckman JS. Superoxide reacts with nitric oxide to nitrate tyrosine at physiological pH via peroxinitrite. J Biol Chem. 2000. 275: 32460-66.

Rho J, Gong S, Kim N, and Choi Y (2001). TDAG51 is not essential for Fas/CD95 regulation and apoptosis in vivo. Mol Cell Biol 21(24): 8365-70.

Ridker PM, Hennekens B, Roitman-Johnson B, Stampfer MJ and Allen J. Plasma concentrations of soluble intercellular adhesion molecule-1 and risks of future myocardial infarction in apparently healthy men. Lancet 1998; 351: 88-92.

Robinson K, Arheart K, Refsum H, Brattstrom L, Boers G, Ueland P, Rubba P, Palma-Reis R, Meleady R, Daly L, Witteman J, Graham I (1998). Low circulating folate and vitamin B6 concentrations: risk factors for stroke, peripheral vascular disease, and coronary artery disease. European COMAC Group. Circulation 97(5): 437-43.

Robinson K, Mayer EL, Miller DP, Green R, van Lente F, Gupta A, Kottke-Marchant K, Savon SR, Selhub J, Nissen SE *et al.* (1995). Hyperhomocysteinemia and low pyridoxal phosphate. Circulation 92: 2825-30.

Romer LH, Birukov KG, Garcia JG (2006). Focal adhesions: paradigm for a signaling nexus. Circ Res. 98(5): 606-16.

Ron D (2002). Translational control in the endoplasmic reticulum stress response. J Clin Invest. 110(10): 1383-8.

Ron D, and Habener JF (1992). CHOP, a novel developmentally regulated nuclear protein that dimerizes with transcription factors C/EBP and LAP and functions as a dominant negative inhibitor of gene transcription. Genes Dev 6: 439-53.

Roselaar SE, Kakkanathu PX, Daugherty A. Lymphocyte populations in atherosclerotic lesions of apoE$^{-/-}$ and LDL receptor$^{-/-}$ mice. Decreasing density with disease progression. Arterioscler Thromb Vasc Biol 1996; 16: 1013-8.

Rosenblatt DS, Copper BA (1990). Inherited disorders of vitamin-B_{12} utilization. BioEassys 12: 331-34.

Rosenfeld ME, Palinski W, Yla-Herttuala S, Carew TE (1990). Macrophages, endothelial cells, and lipoprotein oxidation in the pathogenesis of atherosclerosis. Toxicol Path 18(4 Pt 1): 560-71.

Rosenfeld ME, Tsukada T, Chait A, Bierman EL, Gown AM, Ross R (1987). Fatty streak expansion and maturation in Watanabe Heritable Hyperlipemic and comparably hypercholesterolemic fat-fed rabbits. Arteriosclerosis 7(1): 24-34.

Rosen R (1996). Molecular genetics of methylenetetrahydrofolate reductase deficiency. J Inherit Metab Dis 19: 589-94.

Ross R (1993). The pathogenesis of atherosclerosis: a perspective for the 1990s. Nature 362: 801-09.

Ross R (1999). Atherosclerosis - an inflammatory disease. N Engl J Med 340(2): 115-26.

Rye KA, Clay MA, Barter PJ (1999). Remodelling of high density lipoproteins by plasma factors. Atherosclerosis 145(2): 227-38.

Saleh M, Mathison JC, Wolinski MK, Bensinger SJ, Fitzgerald P, Dorin N, Ulevitch RJ, Green DR, Nicholson DW (2006). Enhanced bacterial clearance and sepsis resistance in caspase-12-deficient mice. Nature 440:1064-68.

Scheuner D, Song B, McEwen E, Liu C, Laybutt R, Gillespie P, Saunders T, Bonner-Weir S, Kaufman RJ (2001). Translational control is required for the unfolded protein response and in vivo glucose homeostasis. Mol Cell. 7(6): 1165-76.

Schröder M, Kaufman RJ (2005). ER stress and the unfolded protein response. Mutat Res. 569(1-2): 29-63.

Schönbeck U, Mach F, Sukhova GK, Murphy C, Bonnefoy JY, Fabunmi RP, Libby P (1997). Regulation of matrix metalloproteinase expression in human vascular smooth muscle cells by T lymphocytes: a role for CD40 signalling in plaque rupture. Circ Res. 81: 448-54.

Schwienbacher C, Angioni A, Scelfo R, Veronese A, Calin GA, Massazza G, Hatada I, Barbanti-Brodano G, and Negrine M (2000). Abnormal RNA expression of 11p15 imprinted genes and kidney developmental genes in Wilms' Tumor. Cancer Res 60: 1521-25.

Schwienbacher C, Sabbioni S, Campi M, Veronese A, Bernardi G, Menegatti A, Hatada L, Mukai T, Ohashi H, Barbanti-Brodano G, Croce CM, and Negrini M (1998). Transcriptional map of 170 kb at chromosome 11p15.5: identification and mutational analysis of the *BWR1A* gene reveals the presence of mutations in tumor samples. Proc Natl Acad Sci USA 95: 3873-78.

Seimon T, Tabas I (2009). Mechanisms and consequences of macrophage apoptosis in atherosclerosis. J Lipid Res. 50 Suppl:S382-7.

Seimon TA, Wang Y, Han S, Senokuchi T, Schrijvers DM, Kuriakose G, Tall AR, Tabas IA (2009). Macrophage deficiency of p38alpha MAPK promotes apoptosis and plaque necrosis in advanced atherosclerotic lesions in mice. J Clin Invest.119(4): 886-98.

Selhub J, Jacques PF, Bostom AG, D'Agostino RB, Wilson PW, Belanger AJ, O'Leary DH, Wolf PA, Schaefer EJ, Rosenberg IH (1995). Association between plasma homocysteine concentrations and extracranial carotid-artery stenosis. N Engl J Med 332(5): 286-91.

Selhub J, Jacques PF, Wilson PW, Rush D, and Rosenberg IH (1993). Vitamin status and intake as primary determinants of homocysteinemia in an elderly population. JAMA 270(22): 2693-98.

Seki N, Bujo H, Jiang M, Shibasaki M, Takahashi K, Hashimoto N, Saito Y (2005). A potent activator of PPARalpha and gamma reduces the vascular cell recruitment and inhibits the intimal thickning in hypercholesterolemic rabbits. Atherosclerosis 178(1): 1-7.

Seshiah PN, Kereiakes DJ, Vasudevan SS, Lopes N, Su BY, Flavahan NA, Goldschmidt-Clermont PJ (2002). Activated monocytes induce smooth muscle cell death: role of macrophage colony-stimulating factor and cell contact. Circulation 105(2): 174-80.

Shah PK, Falk E, Badimon JJ, Fernandez-Qrtiz A, Mailhac A, Villareal-Levy G, Fallon JT, Regnstrom J, Fuster V (1995). Human monocyte-derived macrophages induce collagen breakdown in fibrous caps of atherosclerotic plaques: potential role of matrix-degrading metalloproteinases and implications for plaque rupture. Circulation 92: 1565-69.

Shen X, Zhang K, Kaufman RJ (2004). The unfolded protein response--a stress signaling pathway of the endoplasmic reticulum. J Chem Neuroanat. 28(1-2): 79-92.

Sherman MY and Goldberg AL (2001). Cellular defenses against unfolded proteins: a cell biologist thinks about neurodegenerative diseases. Neuron 29(1): 15-32.

Shih DM, Welch C, Lusis AJ (1995). New insights into atherosclerosis from studies with mouse models. Mol Med Today 1: 364-72.

Shi Y, Glynn JM, Guilbert LJ, Cotter TG, Bissonnette RP, Green DR (1992). Role for c-myc in activation-induced apoptotic cell death in T cell hybridomas. Science 257(5067): 212-4.

Shi Y, Vattem KM, Sood R, An J, Liang J, Stramm L, Wek RC (1998). Identification and characterization of pancreatic eukaryotic initiation factor 2 alpha-subunit kinase, PEK, involved in translational control. Mol Cell Biol. 18(12): 7499-509.

Smith JD, Trogan E, Ginsberg M, Grigaux C, Tian J, Miyata M (1995). Decreased atherosclerosis in mice deficient in both macrophage colony-stimulating factor (op) and apolipoprotein E. Proc Natl Acad Sci USA. 92: 8264-68.

Smithies O, and Maeda N (1995). Gene targeting approaches to complex genetic diseases: atherosclerosis and essential hypertension. Proc Natl Acad Sci U S A 92(12): 5266-72.

Sookoian S, Pirola CJ (2008). Non-alcoholic fatty liver disease is strongly associated with carotid atherosclerosis: a systematic review. J Hepatol. 49(4): 600-7.

Sorescu D, Weiss D, Lassègue B, Clempus RE, Szöcs K, Sorescu GP, Valppu L, Quinn MT, Lambeth JD, Vega JD, Taylor WR, Griendling KK (2002). Superoxide production and expression of nox family proteins in human atherosclerosis. Circulation 105: 1429-35.

Sprent J, Webb SR (1995). Intrathymic and extrathymic clonal deletion of T cells. Curr Opin Immunol 7: 196-205.

Stabler SP, Marcell PD, Podell ER, Allen RH, Savage DG, and Lidenbaum J (1988). Elevation of total homocysteine in the serum of patients with cobalamine or folate deficiency detected by capillary gas chromatography-mass spectrometry. J Clin Invest 81: 466-74.

Stamler JS, Osborne JA, Jaraki O, Rabbani LE, Mullins M, Singel D, Loscalzo J (1993). Adverse vascular effects of homocysteine are modulated by endothelium derived relaxing factor and related oxides of nitrogen. J Clin Invest 91: 308-18.

Stampfer MJ, Malinow MR, Willett WC, Newcomer LM, Upson B, Ullmann D, Tishler PV, Hennekens CH (1992). A propective study of plasma homocyst(e)ine and risk of myocardial infarction in US physicians. JAMA 268: 877-81.

Starkebaum G, and Harlan JM (1986). Endothelial cell injury due to copper-catalyzed hydrogen peroxide generation from homocysteine. J Clin Invest 77: 1370-76.

Stary HC (1989). Evolution and progression of atherosclerotic lesions in coronary arteries of children and young adults. Atherosclerosis 9(1 Suppl): I19-32.

Stary HC, Blankenhorn DH, Chandler AB, Glagov S, Insull W Jr, Richardson M, Rosenfeld ME, Schaffer SA, Schwartz CJ, Wagner WD, *et al.* (1992). A definition of the intima of human arteries and of its atherosclerosis-prone regions. A report from the Committee on Vascular Lesions of the Council on Arteriosclerosis, American Heart Association. Arterioscler Thromb 12(1): 120-34.

Stary HC, Blankenhorn DH, Chandler AB, Glagov S, Insull W Jr, Richardson M, Rosenfeld ME, Schaffer SA, Schwartz CJ, Wagner WD, *et al.*, (1992). A definition of the intima of human arteries and of its atherosclerosis-prone regions. A report from the Committee on Vascular Lesions of the Council on Arteriosclerosis, American Heart Association. Circulation 85(1): 391-405.

Stary HC, Chandler AB, Glagov S (1994). A definition of initial, fatty streak, and intermediate lesions of atherosclerosis: a report from the Committee on Vascular Lesions of the Council on Arteriosclerosis, American Heart Association. Circulation 89: 2462-78.

Stenmark KR, Bouchey D, Nemenoff R, Dempsey EC, Das M (2000). Hypoxia-induced pulmonary vascular remodeling: contribution of the adventitial fibroblasts. Physiol Res 49(5): 503-17.

Steinberg D (1991). Antioxidants and atherosclerosis. A current assessment. Circulation 84(3): 1420-25.

Steinberg D, and Witztum JL (1999). Lipoproteins, Lipoprotein, Oxidation, and Atherosclerosis, KR Chien, ed. (Philadelphia: WB Sanders Co.).

Steinbrecher UP, Zhang HF, Lougheed M (1990). Role of oxidatively modified LDL in atherosclerosis. Free Radical Biol Med 9(2): 155-68.

Stoll G and Bendszus M (2006). Inflammation and atherosclerosis: Novel insights into plaque formation and destabilization. Stroke 37: 1923-32.

Strauss BH, Robinson R, Batchelor WB, Chisholm RJ, Ravi G, Natarajan MK, Logan RA, Mehta SR, Levy DE, Ezrin AM, Keeley FW (1996). In vivo collagen turnover following experimental balloon angioplasty injury and the role of matrix metalloproteinases. Circ Res. 79: 541–550.

Sucu N, Unlu A, Tamer L, Aytacoglu B, Ercan B, Dikmengil M, Atik U (2003). 3-Nitrotyrosine in atherosclerotic blood vessels. Clin Chem Lab Med. 41: 23-25.

Tang D, Okada H, Ruland J, Liu L, Stambolic V, Mak TW, Ingram AJ (2001). Akt is activated in response to an apoptotic signal. J Biol Chem. 276(32): 30461-6.

Targher G, Arcaro G (2007). Non-alcoholic fatty liver disease and increased risk of cardiovascular disease. Atherosclerosis 191(2): 235-40.

Tedgui A, and Mallat Z (2001). Apoptosis as a determinant of atherosclerosis. Thromb Haemost 86: 420-26.

Thompson JS (1969). Atheromata in an in-bred strain of mice. J Atheroscler Res 10: 113-22.

Thronberry NA, and Lazebnik Y (1998). Caspases: enemises within. Science 281: 1312.

Thorp E, Kuriakose G, Shah YM, Gonzalez FJ, Tabas I (2007). Pioglitazone increases macrophage apoptosis and plaque necrosis in advanced atherosclerotic lesions of nondiabetic low-density lipoprotein receptor-null mice. Circulation 116(19): 2182-90.

Thorp E, Li G, Seimon TA, Kuriakose G, Ron D, Tabas I (2009). Reduced apoptosis and plaque necrosis in advanced atherosclerotic lesions of Apoe-/- and Ldlr-/- mice lacking CHOP. Cell Metab 9(5): 474-81.

Toborek M, Kopieczna-Grzebieniak E, Drozdz M, Wieczorek M (1995). Increased lipid peroxidation as a mechanism of methionine-induced atherosclerosis in rabbits. Atherosclerosis 115: 217-24.

Tomasek JJ, Vaughan MB, Kropp BP, Gabbiani G, Martin MD, Haaksma CJ, Hinz B (2006). Contraction of myofibroblasts in granulation tissue is dependent on Rho/Rho kinase/myosin light chain phosphatase activity. Wound Repair Regen. 14(3): 313-20.

Toschi V, Gallo G, Lettino M, Fallon JT, Gertz SD, Fernandez-Oritz A, Cheserbo JH, Badimon L, Nemerson Y, Fuster V, Badimon JJ (1997). Tissue factor modulates thrombogenecity of human atherosclerotic plaques. Circulation 95: 594-99.

Toyoshima Y, Karas M, Yakar S, Dupont J, Lee Helman, LeRoith D (2004). TDAG51 mediates the effects of insulin-like growth factor I (IGF-I) on cell survival. J Biol Chem. 279(24):25898-904.

Trigatti B, Rayburn H, Viñals M, Braun A, Miettinen H, Penman M, Hertz M, Schrenzel M, Amigo L, Rigotti A, Krieger M (1999). Influence of the high density lipoprotein receptor SR-BI on reproductive and cardiovascular pathophysiology. Proc Natl Acad Sci U S A. 96(16): 9322-7.

Trigatti B, Covey S, Rizvi A (2004). Scavenger receptor class B type I in high-density lipoprotein metabolism, atherosclerosis and heart disease: lessons from gene-targeted mice. Biochem Soc Trans. 32(Pt 1): 116-20.

Trigatti B, Rigotti A, Krieger M (2000). The role of the high-density lipoprotein receptor SR-B1 in cholesterol metabolism. Curr Opin Lipidol 11: 123-31.

Tsai JC, Perrella MA, Yoshizumi M, Hsieh CM, Haber E, Schlegel R, and Lee ME (1994). Promotion of vascular smooth muscle cell growth by homocysteine: a link to atherosclerosis. Proc Natl Acad Sci USA 91: 6369-73.

Ubbink JB, van der Merwe A, Delport R, Allen RH, Stabler SP, Riezler R, Vermaak WJ (1996). The effect of a sub-normal vitamin B_6 status on homocysteine metabolism. J Clin Invest 98: 177-84.

Ucker DS, Ashwell JD, Nickas G (1989). Activation-driven T cell death. I. Requirements for de novo transcription and translation and association with genome fragmentation. J Immunol. 143(11): 3461-9.

Ueland PM and Refsum H (1989). Plasma homocysteine, a risk factor for vascular disease: plasma levels in health, disease and drug therapy. J Lab Clin Med 114: 473-501.

Ueland PM, Refsum H, Beresford SA, Vollset SE (2000). The controversy over homocysteine and cardiovascular risk. Am J Clin Nutr 72(2): 324-32.

Ueland PM, Refsum H, and Brattström (1992). Plasma homocysteine and cardiovascular disease. In: Francis RB Jr, ed. Atherosclerotic cardiovascular disease, homoeostasis, and endothelial dysfucntion. New York: Mercel Dekker. pp 183-236.

Ueland PM, Refsum H, Stabler SP, Malinow MR, Andersson A, Allen RH (1993). Total homocysteine in plasma or serum: methods and clinical applications. Clin Chem 39: 1764-79.

Upchurch GR, Welch GN, Fabian AJ, Freedman JE, Johnson JL, Keaney JF, and Loscalzo J (1997). Homocyst(e)ine decrease bioavailable nitric oxide by a mechanism involving glutathione peroxidase. J Biol Chem 272: 17012-17.

Urano F, Wang X, Bertolotti A, Zhang Y, Chung P, Harding HP, and Ron D (2000). Coupling of stress in the ER to activation of JNK protein kinases by transmembrane protein kinase IRE1. Science 287(5453): 664-66.

Vanhoutte PM (1997). Endothelial dysfunction and atherosclerosis. Eur Heart J. 18 Suppl E: E19-29.

van Vlijmen BJ, Gerritsen G, Franken AL, Boesten LS, Kockx MM, Gijbels MJ, Vierboom MP, van Eck M, van De Water B, van Berkel TJ, Havekes LM (2001). Macrophage p53 deficiency leads to enhanced atherosclerosis in APOE*3-Leiden transgenic mice. Circ Res. 88(8): 780-6.

Vaux DL and Korsmeyer SJ (1999). Cell death in development. Cell 96: 245-54.

Vergès B (2004). Clinical interest of PPARs ligands. Diabetes Metab. 30(1): 7-12

Vitvitsky V, Dayal S, Stabler S, Zhou Y, Wang H, Lentz SR, Banerjee R (2004). Perturbations in homocysteine-linked redox homeostasis in a murine model for hyperhomocysteinemia. Am J Physiol Regul Integr Comp Physiol. 287(1): R39-46.

Vollset SE, Refsum H, Nygärd O, Ueland PM (2001). Lifestyle factors associated with hyperhomocysteinemia. In Homocysteine in Heath and Disease. R Carmel and DW Jacobsen, editors. Cambridge University Press, Cambridge, UK, pp 341-55.

Volzke H, Robinson DM, Kleine V, Deutscher R, Hoffmann W, Ludemann J, Schminke U, Kessler C, John U (2005). Hepatic steatosis is associated with an increased risk of carotid atherosclerosis. World J Gastroenterol. 11(12): 1848-53.

Voutilainen S, Morrow JD, Roberts LJ 2nd, Alfthan G, Alho H, Nyyssonen K, Salonen JT (1999). Enhanced in vivo lipid peroxidation at elevated plasma total homocysteine levels. Arterioscler Thromb Vasc Biol 19: 1263-66.

Wang H, Jiang X, Yang F, Gaubatz JW, Ma L, Magera MJ, Yang X, Berger PB, Durante W, Pownall HJ, Schafer AI (2003). Hyperhomocysteinemia accelerates atherosclerosis in cystathionine beta-synthase and apolipoprotein E double knock-out mice with and without dietary perturbation. Blood 101(10): 3901-7.

Wang J, Chen H, Seth A, McCulloch CA (2003). Mechanical force regulation of myofibroblast differentiation in cardiac fibroblasts. Am J Physiol Heart Circ Physiol 285(5): H1871-81.

Wang R, Zhang L, Yin D, Mufson RA, and Shi Y (1998). Protein Kinase C regulates Fas (CD95/APO-1) expression. J Immunology 161: 2201-07.

Watanabe M, Osada J, Aratani Y, Kluckman K, Reddick R, Malinow MR, Maeda N (1995). Mice deficient in cystathionine beta-synthase: animal models for mild and severe homocyst(e)inemia. Proc Natl Acad Sci 92(5): 1585-89.

Welch GN, and Loscalzo J (1998). Homocysteine and atherothrombosis. N Engl J Med 338: 1042-50.

Welihinda AA, Tirasophon W, and Kaufman RJ (1999). The cellular response to protein misfolding in the endoplasmic reticulum. Gene Expr 7: 293-300.

Werder EA, Curtins HCH, Tancredi F, Anders PW, and Proder A (1966). Homocystinuria. Helv Paediatr Acta 21: 1-18.

Weiss N, Heydrick S, Zhang YY, Bierl C, Cap A, and Loscalzo J (2002). Cellular redox state and endothelial dysfunction in mildly hyperhomocysteinemic cystathionine beta-synthase-deficient mice. Arterioscler Thromb Vasc Biol 22(1): 34-41.

Werstuck GH, Lentz SR, Dayal S, Hossain GS, Sood SK, Shi YY, Zhou J, Maeda N, Krisans SK, Malinow MR, and Austin RC (2001). Homocysteine-induced endoplasmic reticulum stress causes dysregulation of the cholesterol and triglyceride biosynthetic pathways. J Clin Invest 107: 1263-73.

Wilcken DEL and Dudman NPB (1992). In: Molecular Genetics of Coronary Artery Disease. Candidate Genes and Process in Atherosclerosis. Monograms in Human Genetics. Lusis AJ, Rotter JI, and Sparkes RS (Eds.) Basel, Karger 14: 311.

Wilcken DEL, Gupta VJ, and Reddy SG (1980). Accumulation of sulphur-containing amino acids including cysteine-homocysteine in patients on maintenance haemodialysis. Clin Sci 58: 427-30.

Wilcken DEL, Reddy SG, Gupta VJ (1983). Homocysteinemia, ischemic heart disease, and the carrier state for homocystinuria. Metabolism 32: 363-70.

Wilcken DE, and Wilcken B (1976). The pathogenesis of coronary artery disease. A possible role for methionine metabolism. J Clin Invest 57: 1079-82.

Wissler RW, and Vesselinovich D (1983). Atherosclerosis-relationship to coronary blood flow. Am J Cardiol 52(2): 2A-7A.

Witting PK, Pettersson K, Ostlund-Lindqvist AM, Westerlund C, Eriksson AW, Stocker R (1999). Inhibition by a coantioxidant of aortic lipoprotein lipid peroxidation and atherosclerosis in apolipoprotein E and low density lipoprotein receptor gene double knockout mice. FASEB J. 13(6): 667-75.

Wolter KG, Hsu Y, Smith CL, Nechushtan A, Xi X, and Youle RJ (1997). Movement of Bax from the cytosol to mitochondria during apoptosis. J Cell Biol 139: 1281-92.

Wong WL, Brostrom MA, Kuznetsov G, Gmitter-Yellen D, and Brostrom CO (1993). Inhibition of protein synthesis and early protein processing by thapsigargin in cultured cells. Biochem J 289: 71-79.

Woronicz JD, Calnan B, Ngo V, Winoto A (1994). Requirement for the orphan steroid receptor Nur77 in apoptosis of T-cell hybridomas. Nature 367(6460): 277-81.

Wozniak MA, Modzelewska K, Kwong L, Keely PJ (2004). Focal adhesion regulation of cell behavior. Biochim Biophys Acta. 1692(2-3): 103-19.

Wu M, Melichian DS, Chang E, Warner-Blankenship M, Ghosh AK, Varga J (2009). Rosiglitazone abrogates bleomycin-induced scleroderma and blocks profibrotic responses through peroxisome proliferator-activated receptor-gamma. Am J Pathol 174(2): 519-33.

Wyllie AH, Kerr JF, and Currie AR (1980). Cell death: the significance of apoptosis. Int Rev Cytol 68: 251-306.

Wynn TA (2008). Cellular and molecular mechanisms of fibrosis. J Pathol 214(2): 199-210.

Yamaguchi S, Ishihara H, Tamura A, Yamada T, Takahashi R, Takei D, Katagiri H, Oka Y (2004). Endoplasmic reticulum stress and N-glycosylation modulate expression of WFS1 protein. Biochem Biophys Res Commun. 325(1): 250-6.

Yamashita T, Kawashima S, Ozaki M, Namiki M, Inoue N, Hirata K, Yokoyama M (2002). Propagermanium reduces atherosclerosis in apolipoprotein E knockout mice via inhibition of macrophage infiltration. Arterioscler Thromb Vasc Biol 22(6): 969-74.

Yan W, Frank CL, Korth MJ, Sopher BL, Novoa I, Ron D, Katze MG (2002). Control of PERK eIF2alpha kinase activity by the endoplasmic reticulum stress-induced molecular chaperone P58IPK. Proc Natl Acad Sci U S A 99(25): 15920-5.

Yang Y, Merćep M, Ware CF, Ashwell JD (1995). Fas and activation-induced Fas ligand mediate apoptosis of T cell hybridomas: inhibition of Fas ligand expression by retinoic acid and glucocorticoids. J Exp Med. 181(5): 1673-82.

Yang LK, Wong KC, Wu MY, Liao SL, Kuo CS, Huang RF (2007). Correlations between folate, B12, homocysteine levels, and radiological markers of neuropathology in elderly post-stroke patients. J Am Coll Nutr. 26(3): 272-8.

Yazdanbakhsh K, Choi JW, Li Y, Lau LF, Choi Y (1995). Cyclosporin A blocks apoptosis by inhibiting the DNA binding activity of the transcription factor Nur77. Proc Natl Acad Sci U S A. 92(2): 437-41.

Ye J, Rawson RB, Komuro R, Chen X, Davé UP, Prywes R, Brown MS, and Goldstein JL (2000). ER stress induces cleavage of membrane-bound ATF6 by the same proteases that process SREBPs. Mol Cell 6: 1355-64.

Yla-Herttuala S, Palinski W, Rosenfeld ME, Parthasarathy S, Carew TE, Butler S, Witztum JL, Steinberg D (1989). Evidence for the presence of oxidatively modified low density lipoprotein in atherosclerotic lesions of rabbit and man. J Clin Invest 84(4): 1086-95.

Yoshida H, Matsui T, Yamamoto A, Okada T, Mori K (2001). XBP1 mRNA is induced by ATF6 and spliced by IRE1 in response to ER stress to produce a highly active transcription factor. Cell 107(7): 881-91.

Yokote K, Kobayashi K, Saito Y (2006). The role of Smad3-dependent TGF-beta signal in vascular response to injury. Trends Cardiovasc Med. 16(7): 240-5.

Young JC, Agashe VR, Siegers K, Hartl FU (2004). Pathways of chaperone-mediated protein folding in the cytosol. Nat Rev Mol Cell Biol. 5(10): 781-91.

Young SG. Recent progress in understanding apolipoprotein B. Circulation 1990. 82: 1574-94.

Yu S, Matsusue K, Kashireddy P, Cao WQ, Yeldandi V, Yeldandi AV, Rao MS, Gonzalez FJ, Reddy JK (2003). Adipocyte-specific gene expression and adipogenic steatosis in the mouse liver due to peroxisome proliferator-activated receptor gamma1 (PPARgamma1) overexpression. J Biol Chem. 278(1): 498-505.

Yusuf S, Dagenais G, Pogue J, Bosch J, and Sleight P (2000). Vitamin E supplementation and cardiovascular events in high-risk patients. The Heart Prevention Evaluation Study Investigators. N Engl J Med 342: 154-60.

Yusuf S, Hawken S, Ounpuu S, Dans T, Avezum A, Lanas F, McQueen M, Budaj A, Pais P, Varigos J, Lisheng L; INTERHEART Study Investigators (2004). Effect of potentially modifiable risk factors associated with myocardial infarction in 52 countries (the INTERHEART study): case-control study. Lancet 364(9438): 937-52.

Zappacosta B, Mordente A, Persichilli S, Minucci A, Carlino P, Martorana GE, Giardina B, and De Sole P (2001). Is homocysteine a pro-oxidant? Free Radic Res 35(5): 499-505.

Zhang C, Cai Y, Adachi MT, Oshiro S, Aso T, Kaufman RJ, and Kitajama S (2001). Homocysteine induces programmed cell death in human vascular endothelial cells through activation of the unfolded protein response. J Biol Chem 276: 35867-74.

Zhang L, Chawla A (2004). Role of PPARgamma in macrophage biology and atherosclerosis. Trends Endocrinol Metab. 15(10): 500-5.

Zhou J, Lhotak S, Hilditch BA, and Austin RC (2004). Activation of the unfolded protein response occurs at all stages of atherosclerotic lesion development in apolipoprotein E-deficient mice. Circulation 111(14):1814-21.

Zhou J, Møller J, Danielsen CC, Bentzon J, Ravn HB, Austin RC, and Falk E (2001). Hyperhomocysteinemia promotes the development of collagen-rich and stable plaques in apoE-deficient mice. Arterioscler Thromb Vasc Biol 21: 1470-76.

Zhou J, Moller J, Ritskes-Hoitinga M, Larsen ML, Austin RC, Falk E (2003). Effects of vitamin supplementation and hyperhomocysteinemia on atherosclerosis in apoE-deficient mice. Atherosclerosis 168(2): 255-62.

Zhou J, Werstuck GH, Lhoták S, Shi YY, Tedesco V, Trigatti B, Dickhout J, Majors AK, DiBello PM, Jacobsen DW, Austin RC (2008). Hyperhomocysteinemia induced by methionine supplementation does not independently cause atherosclerosis in C57BL/6J mice. FASEB J. 22(7): 2569-78.

Zhou J, Werstuck GH, Lhotak S, de Koning AB, Sood SK, Hossain GS, Moller J, Ritskes-Hoitinga M, Falk E, Dayal S, Lentz SR, Austin RC (2004). Association of multiple cellular stress pathways with accelerated atherosclerosis in hyperhomocysteinemic apolipoprotein E-deficient mice. Circulation 110(2): 207-13.

Zinszner H, Kuroda M, Wang XZ, Batchvarova N, Lightfoot RT, Remotti H, Stevens JL, and Ron D (1998). CHOP is implicated in programmed cell death in response to impaired function of the endoplasmic reticulum. Genes Dev 12: 982-95.